DETERMINATION OF THE MOLECULAR MOBILTY AND OXYGEN PERMEABILITY IN AMORPHOUS PROTEIN FILMS

by

THOMAS J. NACK

A Dissertation submitted to the

Graduate School-New Brunswick

Rutgers, The State University of New Jersey

in partial fulfillment of the requirements

for the degree of

Doctor of Philosophy

Graduate Program in Department of Food Science

Written under the direction of

Dr. Richard Ludescher

and approved by

_____

_____

_____

_____

_____

New Brunswick, New Jersey

January, 2008

ABSTRACT OF THE DISSERTATION

Determination of Molecular Mobility and Oxygen Permeability in Amorphous

Protein Films

by THOMAS J. NACK

Dissertation Director: Dr. Richard Ludescher

In food systems, the amorphous solid is a metastable region subject to chemical, physical, and biological deterioration influenced by chemical structure and composition, environmental factors, and molecular mobility.   Molecular mobility is thought to determine the rates of physiochemical changes occurring during food processing and storage.   Temperature affects the motion of molecules, and therefore, the stability and quality of amorphous solids.   To understand the events that occur at the macroscopic level in foods, we must first understand the events that take place at the molecular level. Phosphorescence can be used to monitor the distribution of molecular mobility and oxygen permeability in heterogeneous foods, providing the molecular detail necessary to connect food quality and stability to molecular structure, molecular mobility, and oxygen permeability.

In initial studies, erythrosin B was embedded into model protein systems (BSA and gelatin), and phosphorescence techniques such as lifetime and emission energy were

used to determine the molecular mobility and oxygen permeability as a function of temperature. Next, studies were performed on a more complicated model system of BSA and sugars, followed by a progression to the simple food systems of gelatin and dried collagen sausage casings. Finally, a method was developed to study actual sausages stuffed into erythrosin B doped collagen sausage casings via an external fiber optic coupler from the fluorescence spectrophotometer.

The matrices studied showed a positive correlation between molecular mobility and oxygen permeability, and also, dynamic site heterogeneity. The addition of sucrose and trehalose to amorphous BSA films greatly reduced oxygen permeability. Gelatin showed a significantly lower molecular mobility (higher rigidity) as compared to BSA and collagen casings, and collagen casings were the least permeable to oxygen. Dried collagen casings became more heterogeneous and permeable to oxygen with aging. Measurements on sausages stuffed into erythrosin B doped casings demonstrated that this technique was very sensitive to oxygen quenching under different types of packaging and storage conditions. This was the first time phosphorescent techniques have been applied to actual food products in this manor, and future research will involve optimizing this technique by correlating the phosphorescent measurements to food quality and stability.

ACKNOWLEDGEMENTS

TABLE OF CONTENTS

CHAPTER 6: CONCLUSIONS FROM THE MODEL SYSTEMS.

CHAPTER 7: THE DEVELOPMENT OF A PHOSPHORESCENT TECHNIQUE TO STUDY SAUSAGES STUFFED INTO ERYTHROSIN B DOPED COLLAGEN CASINGS.

LIST OF TABLES AND FIGURES

Table or Figure	Page

Chapter 1: Introduction.

Molecular Mobility

Most foods exist in a metastable or non-equilibrium (amorphous) state; therefore focus should be on kinetic rather than thermodynamic approaches to understand, predict, and control their properties. Molecular mobility is a suitable kinetic approach because it is related to the diffusion-limited events in foods (Fennema, 1996). Molecular mobility has been studied in great detail in aqueous solutions. Reduction of the molecular mobility in aqueous spin-labeled proteins can be attributed to a decrease in the solution temperature, increasing the viscosity of the solution, and/or binding ligands to the protein molecule (Nicholov et al., 1995; Sochava et al., 1985). Recently, research within the food and pharmaceutical industries has been focusing on molecular mobility within amorphous systems (as reviewed by Yoshioka and Aso (2007), Hill et al. (2005), and Champion et al. (2000)). Protein molecular mobility is less fully characterized and understood in the solid state. Besides the obvious effect of slowing overall translational and rotational motion, dehydration also hinders internal modes of vibrational motion important for biological function (Rupley and Careri, 1991). Fully hydrated proteins in solvents or crystals undergo a dynamical transition (T_d) at ~200 K (recently reviewed in Hill et al. (2005)) that has been identified as a polymer glass transition. Below T_d, protein motions are limited to harmonic vibrations of bonded atoms, while above T_d, anharmonic collective vibrations of non-bonded atoms are activated. These collective motions appear to be required for conformational change, including perhaps denaturation, and biological activity. Although T_d increases upon dehydration in some proteins (Hill et

al., 2005; Tsai et al., 2000), it uncertain what is the general influence of dehydration is on T_d, and the role that T_d plays in the matrix dynamics of amorphous, proteinaceous solids.

Recent studies have demonstrated that the phosphorescence emission spectrum and intensity decay from the xanthene probe erythrosin B (Ery B) dispersed in thin films composed of amorphous gelatin (Lukasik and Ludescher, 2006a, b; Simon-Lukasik and Ludescher, 2004), sugars (Pravinata et al., 2005; Shirke and Ludescher, 2005; You and Ludescher, 2006), and globular proteins (Nack and Ludescher, 2006; Sundaresan and Ludescher, 2007) are sensitive to specific modes of molecular mobility within the amorphous solid. Phosphorescence techniques are capable of monitoring nano-scale manipulations, which have the possibility of converging new technologies into the classical scientific disciplines leading to major impacts within raw material sourcing for food processing and our understanding of how food ingredients affect human physiology (Shelke, 2006). In addition, since oxygen is a contact quencher of the excited triplet state, phosphorescence can also be used as a sensitive indicator of oxygen diffusion within the amorphous solid (Lu, 2001; Nack and Ludescher, 2006; Simon-Lukasik and Ludescher, 2004; Sundaresan and Ludescher, 2007).

Molecular mobility is sensitive to environmental variables such as temperature, relative humidity, pressure, water activity, and solute concentration. Temperature dependence, in particular, can be used to obtain a measure of the expected molecular mobility over extended periods of time for the purpose of establishing expiration dates (Shamblin et al., 1999). The molecular mobility of the structural components in amorphous foods can be thought of as the phenomenon responsible for macroscopic physical, chemical, and sensory qualities of these foods (Figure I-1). The rates of the

degradative processes occurring in amorphous foods are sensitive to the specific biomolecules involved in the process, the states of the local configurations, and the different modes of motion involved.   Research on molecular mobility in the amorphous and rubbery states is required to recognize the complex connections existing between molecular structure and molecular mobility. Such connections are necessary to predict, control, and manipulate the quality of amorphous solid foods (Ludescher et al., 2001).

Why study amorphous solids?

Most low moisture foods and food ingredients are classified as amorphous solids. Examples of such foods include candies, pasta, jerky, frozen meats, and crackers. Amorphous solids are formed during physical processes such as rapid cooling of melts, drying of solutions (Zallen, 1998), or other destructive processing that prevent the formation of the regular crystalline lattice (Ludescher et al., 2001; Zallen, 1998).   The same intrinsic steric constraints that control crystallization also facilitate the formation of amorphous solids.   It has been proposed that proteins have evolved to avoid crystallization because crystallization compromises the viability of the cell (Doye et al., 2004). The physical properties of amorphous solid proteins are important for the texture of protein-containing foods (Slade et al., 1989), the stability of pharmaceuticals (Hill et al., 2005), the viability of seeds and spores (Buitink and Leprince, 2004), and the permeability of edible films (Krochta and DeMulder-Johnston, 1997). These physical properties are largely influenced on the molecular level by the three-dimensional structure (conformation) of the solid state protein and the mobility of the protein and its component parts within the amorphous matrix (Nack and Ludescher, 2006).

Zallen (1998) stated that nearly all materials can be in the amorphous state if they are cooled fast enough and far enough. Fast enough meaning that the matrix must be brought below the glass transition temperature (T_g) faster than the time required for crystallization, and far enough meaning that the matrix must be taken to a temperature below T_g (refer to Figure I-2 for a phase diagram). Amorphous solids differ from crystalline solids in that amorphous solids are metastable, disordered and irregular in molecular structure, have local minimum energy configurations, usually exhibit a T_g, and participate in vibrational, rotational, and translation molecular motions. On the contrary, crystalline solids are at thermodynamic equilibrium, are highly ordered in molecular structure, have a global minimum energy conformation, exhibit a melting transition, and participate in only vibrational molecular motions. Amorphous solids can be thought of as having short range local order, while crystalline solids have long range global order (Zallen, 1998). At low temperatures amorphous solids are hard and brittle, and at higher temperatures soft and flexible (Pravinata et al., 2005), while avoiding complete loss of structure as in the melt of a crystal lattice.

Molecular Mobility and T_g

Molecular mobility modulates physical properties, such as texture, and chemical processes, such as reaction rate, crystallization rate, and diffusion of solutes. T_g is thought to be the index temperature for food stability and to demonstrate the effect of water plasticization on the glassy state. While it is belived that T_g can be used to predict and control the macroscopic physical properties and stability of foods, we propose that one must focus on what is happening at the molecular level (Ludescher et al., 2001). T_g represents the translational motion associated with individual molecules in the matrix.

Below T_g the glassy solids are rigid because the molecules are only participating in vibrational and limited rotational motions, and above T_g, in the rubbery state, amorphous solids show flow due to translational motion (Figure I-3). Zallen (1998) has theorized that in order to understand complex amorphous matrices, focus should be drawn to the translational mobility of individual molecules in the continuous amorphous phase.

T_g has an important relationship with the stability of diffusion limited properties of foods (Fennema, 1996) and macroscopic food quality, but future work may reveal that T_g reflects more of an effect rather than a cause (Ludescher et al., 2001). T_g should not be used to predict stability for certain diffusion limited reactions because they occur at temperatures below T_g. Examples of these reactions include the Maillard reaction, sugar bloom in chocolate, caking in foods during drying, staling of breads, moisture migration, enzymatic activity, collapse of structure, and hydrolysis (Champion et al., 2000; Fennema, 1996). Sub-T_g relaxations and physical ageing are processes that show we can not neglect sub-T_g molecular mobility. A direct example of this lies in the loss of crispness observed in cereal products, which is not a consequence of T_g, but rather caused by the molecular motions due to the reorganization in the glassy state as shown by dielectric spectroscopy (Champion et al., 2000). Yoshioka (1997) also demonstrated that freeze dried protein stability is more closely related to molecular mobility than to T_g in amorphous pharmaceuticals.

Dynamic transitions have been observed below T_g in synthetic polymers showing localized vibrational motions of the molecules (McCrum et al., 1991). Although these transitions have been observed in synthetic polymers, very little research has been devoted to similar studies in more complex matrices such as foods. These studies have

the potential to provide information on chemical reactivity, molecular diffusion, texture, crystallization, and other quality attributes important in food systems (Ludescher et al., 2001).

Focusing on the macroscopic changes that occur at T_g overlooks the importance of structural heterogeneity in modulating the physical and chemical properties in foods. Amorphous foods are structurally complex (containing proteins, carbohydrates, and lipids in many different proportions) with structural elements of different length scales ranging from nanometers to centimeters, which can be in many different states (glassy, rubbery, crystalline, or liquid) even at uniform temperature and water activity (Ludescher et al., 2001). Each region has different local molecular mobilities, which in turn influence macroscopic food parameters such as quality, texture, and stability.

Protein Motions

Proteins are dynamic flexible polymers in which thermally driven random motions modulate all aspects of their structure (Ludescher, 1990). These motions include bond vibrations, side chain rotations, surface loops wiggling, domain flexing at connecting bonds, and the entire structure fluctuating to assemble the most stable structure. Proteins are large asymmetric molecules having many possible modes of motion (Figure I-4). Asymmetric molecules have three modes of translational motion and three modes of rotational motion (about the three mutually perpendicular axes) and 3N-6 modes of vibrational mobility where N is the number of atoms in the molecule (Castellan, 1983). Amorphous glasses may participate in all three modes of motion depending on the temperature. Considering the vibrational motions alone in a small protein (N<2000), we have an estimated 6000 modes of motion. It should be noted that

in very rigid glasses the translational and rotational motions, and even some of the vibrational motions, are slowed by molecular interactions, due to the lower free volume in the matrix. If the temperature is increased and the matrix is in a rubbery state, the translational and rotational motions can be cooperatively activated by thermal motion (Ludescher et al., 2001). Vibrations may have a small effect on the overall molecular mobility of an amorphous matrix, but will have consequences in modulating the local matrix mobility, such as the reorientation of side chain hydroxyl, amino, and carboxyl groups on the surface of proteins, and may also couple with larger scale global mobility (Yoshioka and Aso, 2007)

Oxygen Permeability

The aging of polymeric films includes both chemical and physical processes that occur in the matrix after exposure to environmental conditions over a period of time (Anker et al., 2001). The diffusion of oxygen molecules (Guillet, 1985) and temperature are factors that determine the aging of many materials. Increased oxygen permeation leads to increases in vitamin degradation, lipid oxidation, and other oxidative reactions that may lead to degradation in food systems (Anker et al., 2001). Oxygen permeability in amorphous protein films increases dramatically with relative humidity (McHugh and Krochta, 1994; Simon-Lukasik and Ludescher, 2004) and temperature (Nack and Ludescher, 2006; Smiddy et al., 2002; Sundaresan and Ludescher, 2007). The mechanism of the mobility of oxygen in small disordered amorphous matrices is of great interest, and luminescence techniques are the preferred method to study microscopic mobility of oxygen (Korolev et al., 1995).

Gas permeability is an important characteristic for edible films and amorphous foods. Proteins and polysaccharides are thought to be excellent oxygen barriers due to their low solubility and tightly packed and ordered hydrogen bonded network (McHugh and Krochta, 1994). The ease of mass transfer essentially determines the film's barrier properties (refer to Figure I-5 for a schematic). Oxygen permeability (P) is related to its diffusion coefficient (D) and solubility (S) by the equation P=DS. Several techniques are used for direct determination of the diffusion coefficient, but they are usually quite complicated. The permeability of O_2 and CO_2 through packaging material is traditionally measured using the double chamber gas transmission cell. Such methods have been employed to assess the permeabilities of several types of edible films from polysaccharide, protein, and/or lipidic sources (Gontard et al., 1996). Diffusion measurements through freestanding films via the gas transmission cell are appropriate for packaging applications and edible films if the conditions are altered on each side of the film to represent the food surface and the desired environmental conditions. The gas transmission cell, on the other hand, can not be used as a direct measurement of diffusion through edible films in direct contact with food products (Simon-Lukasik and Ludescher, 2004). This research introduces an innovative and noninvasive spectroscopic technique to measure O_2 permeability of amorphous foods and edible films applied directly to food surfaces.

Edible Protein Films

Edible films can be used to improve food quality, extend shelf life, or to add some other beneficial functional property (Fennema, 1996). The study of edible protein films is a logical application of research in the food materials science area and the subject of

many novel analytical techniques in the field of food technology (Cuq et al., 1995b). Edible films are amorphous in nature and can be composed of proteins, carbohydrates, lipids, and/or synthetic material in various combinations. The structure of the matrix is not only controlled by the film forming treatment (usually heat or pressure), but also depends on environmental factors such as pH, ionic strength, types of ions, and protein conformation (Lefevre et al., 2005). Protein films often contain plasticizers to add flexibility, thus the macroscopic functional properties of edible films are controlled by molecular mobility in the rubbery state (Anker et al., 2001). Despite this, edible protein films still have the appropriate mechanical properties and low permeabilities for oxygen and water to serve as effective barriers in food systems (Krochta and DeMulder-Johnston, 1997).

Edible films are typically applied on food surfaces or between food layers to prevent moisture, gas, and lipid migration between the food and the environment or different food internal components (Erdohan and Turhan, 2005) (Figure I-6). Edible protein films are used on many food products such as meats, fruits, and confectionary snack foods (Krochta and DeMulder-Johnston, 1997), and as the primary component in pharmaceutical capsules and tablets (Wood, 1977). In food products, edible films extend the shelf life and preserve quality by inhibiting the migration of aroma, flavors, moisture, and oxygen (Lefevre et al., 2005). These films act as ingredient carriers (encapsulation) and improve the overall macrostructural integrity of the food product (Krochta and DeMulder-Johnston, 1997). Gelatin films in particular have been used as glues and adhesives (Jones, 1977), oxygen barriers, mold retardants, antioxidant carriers, and frying oil barriers (Krochta and DeMulder-Johnston, 1997).

Due to the aforementioned functionality of edible protein films, it is easy to understand why it is such a popular area of research. Many studies focus on the film's macroscopic barrier and mechanical properties such as water vapor and oxygen permeability, tensile strength, elasticity, elongation, and apparent modulus. These traditional mechanical and barrier properties in films composed of wheat gluten (Gontard et al., 1993), whey (Simelane and Ustunol, 2005), soy (Wan et al., 2005), casein (Frinault et al., 1997), and water soluble fish proteins (Bourtoom et al., 2006; Cuq et al., 1995a) have been evaluated with traditional methods such as texture analysis and direct measurements of permeability. Some studies have used analytical methods to better understand the microstructural environments of protein films and to provide a qualitative capacity of the traditional methods using atomic force microscopy (Lent et al., 1998), calorimetry (Sirotkin and Korolev, 2005), transmission electron microscopy (Anker et al., 2000), transmission infrared spectroscopy (Lefevre et al., 2005), scanning and transmission electron microscopy (Frinault et al., 1997), and Fourier transform infrared (FTIR) spectroscopy (Mangavel et al., 2001; Sirotkin and Korolev, 2005). Overall, there has been very few, if any, studies looking at the underlying molecular mobility and the possible effects on barrier and mechanical properties, other than measurements of T_g (Anker et al., 2001; Sobral et al., 2002; Vanin et al., 2005).

Protein Conformation

There is very limited data available about the molecular events occurring during film formation, especially during dehydration. Protein conformation in the solid state appears to be largely dependent upon the method of preparation. In the case of procedures such as lyophilization and spray drying that involve temperature extremes

(either cold or hot) it appears that proteins may often lose their native conformation (Dong et al., 1995; Heller et al., 1997). Mere dehydration *per se*, however, does not appear to induce significant loss of native structure (Kachalova et al., 1991), and it is in this manner that we prepare our films. Clearly, the numerous proteins within seed, spores, and whole organisms can withstand significant dehydration without permanent loss of native conformation.

Hypothesis and Research Model

The general hypothesis is that to understand the macroscopic and microscopic properties of foods, one must first understand the molecular mobility and oxygen permeability in these complex systems. It has previously been shown that molecular mobility can be monitored using Ery B in many simple model amorphous systems such as sucrose (Pravinata et al., 2005; You and Ludescher, 2006; Zunic et al., 2003), gelatin (Lukasik and Ludescher, 2006b), bovine serum albumin (Nack and Ludescher, 2006), β-lactoglobulin (Sundaresan and Ludescher, 2007), and glucose, maltose and maltotriose (Shirke and Ludescher, 2005). The same luminescent techniques will be utilized to examine more complex model systems and commercially available sausage casings.

Luminescence Spectroscopy and Molecular Mobility

Luminescence spectroscopy, including fluorescence and phosphorescence, is an appropriate method to study the subtle microstructural elements that underlie molecular behavior in heterogeneous materials (Lakowicz, 1999). Luminescence provides direct information about the rotation of the luminescent probe, as well as indirect information regarding the molecular mobility and oxygen quenching of the microenvironment directly surrounding the probe (Ludescher et al., 2001) in a non-invasive manor. The time scale

of such mobility measurements depends on the excited state emission lifetime (τ). Fluorescence emission from the excited state occurs on the nanosecond timescale, where phosphorescence emission from the triplet state ranges from the microsecond to second timescales. Therefore, phosphorescence is better suited to monitor the slower motions characteristic of the rubbery and glassy states (Ludescher et al., 2001), as well as the oxygen quenching of the triplet state due to molecular collisions.

Information about molecular mobility is gained through measurements of emission energy (frequency), intensity, time resolved decay, and polarization of well characterized luminescent chromophores (probes). Luminescent chromophores can also serve as "molecular reporters" providing information on conformational changes, hydrophobicity, ligand binding, and other various environmental effects (Slavic, 1994; Strasburg and Ludescher, 1995) due to changes in temperature, pressure, or relative humidity. These well characterized chromophores or probes act as reporters of the structure, physical and chemical properties, and the general dynamics of the surrounding environment (Slavic, 1994). From this luminescent data, it is possible to better understand the molecular processes in food products.

Phosphorescence is especially useful for studying molecular mobility on the microsecond to millisecond and longer timescales by monitoring the local environment of the triplet probe. These timescales correspond to the modes of local and segmental motions observed in solid phase proteins (Ludescher, 1990). Triplet probes vary greatly due to differences in structure, with lifetime values ranging from microseconds to seconds. This provides information that is suitable for glassy matrixes with very limited motions, and also matrices in the rubbery or melt state where the molecules are more

mobile. Tryptophan, for example, demonstrates the wide range of applications for a single phosphorescent probe, as it has been used to monitor internal molecular mobility of both aqueous proteins (Schauerte et al., 1997), and also solid state proteins (Shah and Ludescher, 1993; Zunic et al., 2003).

Introduction to Photophysics

Luminescence spectroscopy is one of the most promising techniques in the biological, chemical, pharmaceutical, and medical fields for the beginning of the 21st century. Fluorescence spectrophotometers have been forecast to be the fastest growing market in molecular spectroscopy, with biological research being its most important area of study. Along with the recent explosion of new video and imaging markets, luminescence applications are reaching even greater numbers (Slavic, 1994). See Figure I-7 for a schematic of a luminescence spectrophotometer. It appears that the explosion of fluorescence based analytical techniques is due to the fact that they are noninvasive, very sensitive, and relatively easy to use. Computer software companies were well aware of the trends in luminescence spectroscopy, and have written user friendly programs for data analysis, imaging, and modeling.

Fluorescence and phosphorescence analysis are widely used analytical techniques in the food industry, but have not yet been applied for novel applications in problem solving related to food quality and stability. These techniques can be used to complement other physical methods commonly used in the food industry, offering a more thorough understanding of the food matrix on the molecular level. Molecular mobility, which is critical in understanding and controlling quality and stability factors in food products, can be successfully studied using these luminescent techniques (Lukasik,

2005). Luminescence from a probe is fully characterized by its intensity, energy, and polarization (Strasburg and Ludescher, 1995). Each of these signals provides details related to the molecular mobility of the probe or its immediate surrounding environment (Lakowicz, 1999; Ludescher, 1990) (Figure I-8). In this project, these novel techniques are used to better understand the molecular process in various amorphous solids.

Once the quantum values and lifetimes are acquired, it is possible to use photophysical equations to calculate rate constants for the excited state processes (Hurtubise, 1997). The Jablonski energy level diagram is depicted in Figure I-9. It summarizes the various photophysical events occurring during luminescence, including the radiative and non-radiative processes that collectively depopulate the excited singlet and triplet states of a luminescent probe. S_0 represents the singlet ground state (where most molecules are at room temperature), and S_1 and T_1 represent the singlet and triplet excited states, respectively. Emission from the singlet state to the ground state is termed fluorescence rate (k_{RF}), and phosphorescence rate (k_{RP}) is the emission from the triplet to the ground state, both being radiative processes (solid lines). The non-radiative processes are depicted with dashed lines in Figure I-9 for ease of understanding. k_{SIC} is the non-radiative rate of internal conversion from the excited singlet state to the ground state and k_{TS0} is the non-radiative rate of intersystem crossing from the excited triplet state to the ground state. k_{ST} is the rate of intersystem crossing from the excited singlet to the excited triplet state involving a forbidden electron spin flip, which is kinetically slow but thermodynamically favorable, and k_{TS1} is the rate of reverse, thermally activated intersystem crossing from the excited triplet to the excited singlet state. The rate of quenching the triplet state by oxygen, $k_Q[O_2]$, is the product of the quenching constant

rate k_Q and the oxygen concentration $[O_2]$, and this value is easily calculated from the difference in lifetime values under oxy and anoxic conditions. The non-radiative processes that depopulate the triplet state (k_{TS1}, k_{TS0}, and $k_Q[O_2]$) are of great interest, because they give molecular information about the processes within the matrix.

Emission Intensity

Emission intensity is directly proportional to the quantum yield (ϕ), which is the ratio of photons emitted to photons absorbed. It can be thought of as the probability that a molecule will emit a photon following excitation. As shown in Figure I-9, there are several de-excitation pathways available for the excited chromophores reflected in the quantum yield. The quantum yield for fluorescence (ϕ_F) is a ratio of the rate of fluorescence to the sum of all the other de-excitation processes from the singlet state (Hurtubise, 1990; Lakowicz, 1999):

$$\phi_F = \frac{k_{RF}}{k_{RF} + k_{SIC} + k_{ST} + k_Q[O_2]} \qquad (1)$$

In the absence of a quencher in the local environment, mainly oxygen, the equation can be simplified to:

$$\phi_F = \frac{k_{RF}}{k_{RF} + k_{SIC} + k_{ST}} \qquad (2)$$

The quantum yield for phosphorescence emission (ϕ_P), includes a term to describe the probability that the triplet state will be generated (ϕ_T) from the excited singlet state and also that the emission will occur from the triplet state (q_P) (Hurtubise, 1990).

$$\phi_P = \phi_T q_P = \{\frac{k_{ST}}{k_{RF} + k_{SIC} + k_{ST} + k_Q[O_2]}\} \{\frac{k_{RP}}{k_{RP} + k_{TS0} + k_{TS} + k_Q[O_2]}\} \; (3)$$

In the absence of oxygen, Equation 3 simplifies to:

$$\phi_P = \{\frac{k_{ST}}{k_{RF} + k_{SIC} + k_{ST}}\} \{\frac{k_{RP}}{k_{RP} + k_{TS0} + k_{TS1}}\} \tag{4}$$

The quantum yield for delayed fluorescence (ϕ_{DF}) in the absence of oxygen is the product of the quantum yield of fluorescence and the probabilities of the intersystem crossing from S_1 to T_1 and also from T_1 back to S_1 (Duchowicz et al., 1998)

$$\phi_{DF} = \phi_F \{\frac{k_{ST}}{k_{RF} + k_{SIC} + k_{ST}}\} \{\frac{k_{TS1}}{k_{RP} + k_{TS0} + k_{TS1}}\} \tag{5}$$

By comparing the emission intensities of delayed fluorescence (I_{DF}) and phosphorescence (I_P), it is possible to obtain information about the rate constants for intersystem crossing, k_{TS1}. k_F and k_P are the total decay rates for deexcitation of the singlet and triplet state, respectively.

$$\frac{I_{DF}}{I_P} = \frac{\phi_F \{\frac{k_{ST}}{k_F}\} \{\frac{k_{TS1}}{k_P}\}}{\{\frac{k_{ST}}{k_F}\} \{\frac{k_{RP}}{k_P}\}} = \phi_F \frac{k_{TS1}}{k_{RP}} \tag{6}$$

This ratio is highly temperature dependant due to the additional energy required to go from the T_1 to S_1 energy level, and can be described by the following equation where ΔE_{TS} is the effective energy gap between the triplet and singlet states:

$$\frac{I_{DF}}{I_P} = \phi_F \frac{k_{TS1}}{k_{RP}} = \{\frac{\phi_F}{k_{RP}}\} k_{TS1}^{\ 0} \exp(-\frac{\Delta E_{TS}}{RT}) \tag{7}$$

The slope of a Van't Hoff plot of the natural log of the ratio of delayed fluorescence (I_{DF}) to phosphorescence (I_P) intensity versus inverse temperature provides a measure of ΔE_{TS} (Duchowicz et al., 1998):

$$d[\ln(I_{DF}/I_P)]/d(1/T) = -\Delta E_{TS}/R \tag{8}$$

Rate constants k_{RF}, k_{RP}, and k_{ST1} are fixed by the molecular structure of the chromophores and are not influenced by environmental conditions (Turro, 1991), thus an increase in non-radiative decay will result in lower luminescence intensity.

Phosphorescence intensity decays in amorphous solids are often non-exponential and a stretched exponential decay function, the Kohlrausch-Williams-Watts (KWW) decay model, has been shown to be appropriate to describe the wide distribution of relaxation times (Champion et al., 2000) for the molecular processes that depopulate excited states in tissues (Lee et al., 2001), crystalline solids (Chen, 2003), super cooled liquids (Richert, 1997), concentrated BSA solutions (Brownsey et al., 2003), and amorphous solids (Nack and Ludescher, 2006; Pravinata et al., 2005):

$$I(t) = I_0 \exp[-(t/\tau)^\beta] + c \tag{9}$$

Where $I(t)$ is the intensity as a function of time following pulsed excitation, I_0 is the initial intensity at time zero, τ is the KWW lifetime, and β is the stretching exponent which characterizes the distribution of the decay times (Richert and Heuer, 1997). All data were analyzed using the program Igor (Wavemetrics, Inc., Lake Oswego, OR).

The phosphorescence lifetime is the inverse sum of the rate constants associated with the various processes that depopulate the excited triplet state.

$$\tau^{-1} = k_P = k_{RP} + k_{TS1} + k_{TS0} + k_Q[O_2] \tag{10}$$

This equation can be used to calculate k_{TS0}, the rate of collisional quenching to the ground state, if k_{RP}, k_{TS1}, and $k_Q[O_2]$ are known. k_{TS0} provides a measure of molecular mobility because it monitors the interactions between the probe and the environment (the rate at which probe energy is dissipated from the excited state to the surrounding matrix). Under anoxic conditions $k_Q[O_2]$, the rate of oxygen quenching, is zero. k_{RP}, the radiative

decay rate of the triplet state, is 41 s^{-1} for erythrosin B (Duchowicz et al., 1998; Lettinga et al., 2000). k_{TS1}, the rate of reverse intersystem crossing from the excited triplet state to the excited singlet state, depends on ΔE_{TS}, the energy gap between S_1 and T_1 (Simon-Lukasik and Ludescher, 2004).

$$k_{TS1}(T) = k^o_{TS1} \exp(-\Delta E_{TS}/RT) \qquad\qquad (11)$$

Literature values of k^o_{TS1} for Ery B vary from 0.3 x 10^7 s^{-1} in ethanol and 6.5 x 10^7 s^{-1} in water (Duchowicz et al., 1998) to 111 x 10^7 s^{-1} in solid polyvinyl alcohol (Lettinga et al., 2000), and thus provide little guidance. We estimated the maximum possible value for k$^o_{TS1}$ in each matrix where k$^o_{TS1}$ cannot result in values for k$_{TS0}$(T) that decrease with increasing temperature. This procedure thus estimated the minimum possible values for k$_{TS0}$(T).

In summary, phosphorescence lifetime measurements can provide a direct measurement of the collisional quenching rate (k$_{TS0}$) of the probe and the surrounding matrix. Also, a comparison of lifetime measurements in oxic and anoxic conditions provides a direct measurement of oxygen quenching k$_Q$[O$_2$], which is related to the permeability of the matrix to oxygen.

Emission Energy

Absorption and emission are distributed over a large range of energies, and the energetic transitions are sensitive to the dipolar interactions between the polar chromophore and the immediate environment (Ludescher et al., 2001). Absorption of light is accompanied by the transition of the molecule from the ground state to the excited state, with this transition occurring on the order of 10^{-15} s (Ludescher et al., 2001; Slavic, 1994). The molecule then relaxes within the excited state (10^{-12} s) and eventually returns

to the ground state (10^{-8} s for fluorescence) (Hurtubise, 1997; Slavic, 1994). When the molecule is excited it has a different electronic configuration, and it can be stabilized by dipolar relaxations in the local matrix (Demchenko, 1988) resulting in a dramatic effect on the emission energy. Dipolar relaxation only influences the emission energy if it is on the same time scale as the excited lifetime, making the slower process of phosphorescence (10^{-6} to 1 s) more desirable for studies of amorphous solids. In amorphous rubbery and glassy matrices the solvent relaxation is slow ($\sim 10^{-6}$ s or slower) due to limited molecular mobility, and emission does not occur from the excited state while fully surrounded by a relaxed solvent shell, but rather from a non-equilibrium state undergoing relaxation (Ludescher et al., 2001) (Figure I-10).

Probe Information

Luminescent probes should have a high absorption coefficient, a high quantum yield (Slavic, 1994), should be site specific, and sensitive to the molecular environment. Phosphorescent probes can directly monitor the rigidity of the local environment (Strambini and Gonnelli, 1985), and this environment can be the interior or surface of a protein (Shah and Ludescher, 1995). Dye molecules are the most sensitive reporters because of their extended π-electron system, strong dispersion interaction with the environment, very high quantum yields, and their range of long wavelength absorption bands that often lie within the range easily accessible via laser spectroscopy (Lesch et al., 2004). Our studies are best conducted with a phosphorescent probe. Ery B satisfies all of the previously mentioned requirements and also yields a phosphorescence emission time scale of 10^{-5} to 10^{-3} s corresponding to molecular motions in glassy environments, and has been shown to be a very sensitive oxygen sensor (Lam et al., 2001). Ery B (tetra-

iodofluorescein, FD & C red 3, or cherry red) is perhaps the most widely used phosphorescent probe to assess the molecular mobility of water soluble membrane bound proteins due to its large extinction coefficient and high phosphorescence quantum yield (Pravinata et al., 2005). The phosphorescent nature of Ery B is attributed to the xanthene ring with four iodine molecules (Figure I-11). Phosphorescence from the triplet state of the luminescent probe Ery B can provide information about the subsequent relaxations, oxygen permeability, and dynamic site heterogeneity in the BSA, BSA/sugar, gelatin, and collagen matrixes, due to its site specificity and high sensitivity.

Research Objectives

Objective 1: Develop phosphorescent techniques to measure the structural and dynamic heterogeneity in model BSA films, and apply these techniques to determine the molecular mobility and oxygen permeability as a function of temperature in the matrix.

Objective 2: Monitor the molecular mobility and oxygen permeability in more complicated amorphous systems composed of protein and sugar mixtures.

Objective 3: Analyze the molecular mobility, oxygen permeability, and dynamic site heterogeneity in gelatin films as a function of temperature.

Objective 4: Analyze the molecular mobility and oxygen permeability and dynamic site heterogeneity in dried collagen sausage casings as a function of temperature.

Objective 5: Develop a phosphorescent technique using Ery B to evaluate rigidity, heterogeneity, and oxygen permeability in actual sausages stuffed into Ery B doped collagen casings.

Summary

   This project aimed to first prove the effectiveness of phosphorescent techniques in regards to monitoring molecular mobility, oxygen permeability, and dynamic site heterogeneity, and then to devise a method to adapt this technique from model systems to actual food products.

Chapter 1 Figures
Figure I-1: A schematic model for the role that environmental variables, molecular and microscopic structure, and molecular mobility play in modulating food quality.

Food Quality Attributes
(Physical properties, Chemical reactivity, Organoleptic appeal, etc)

Molecular Mobility   **Molecular & Microscopic Structure**
(Vibrational, Rotational,   *(Functional groups, MW,*
Translational)   *Colloidal Structure, etc)*

Environmental Variables
(T, P, aw, [Salt], etc)
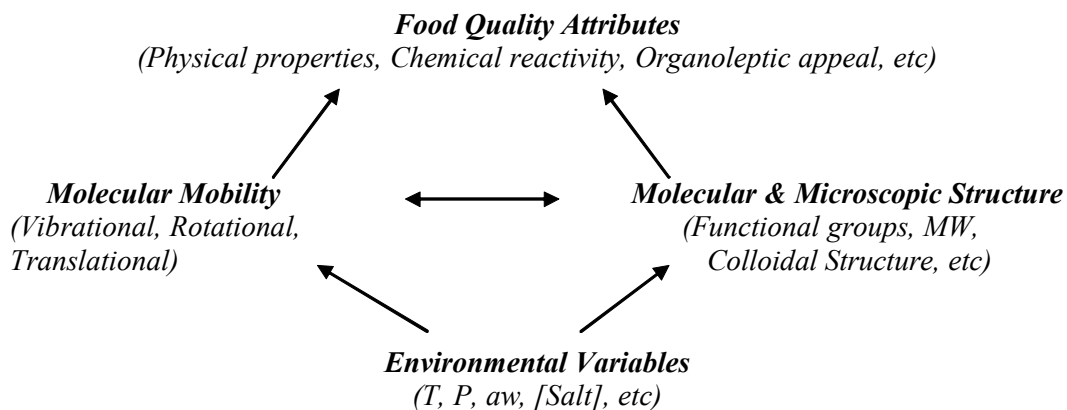
Reproduced from Ludescher et al. (2001)

Figure I-2: A schematic representation of molar volume or enthalpy for a substance as a function of temperature in the crystalline, liquid, and amorphous states. T_m is the melting temperature, T_g the glass transition temperature, and T_K the Kauzmann temperature, or the "ideal" T_g.
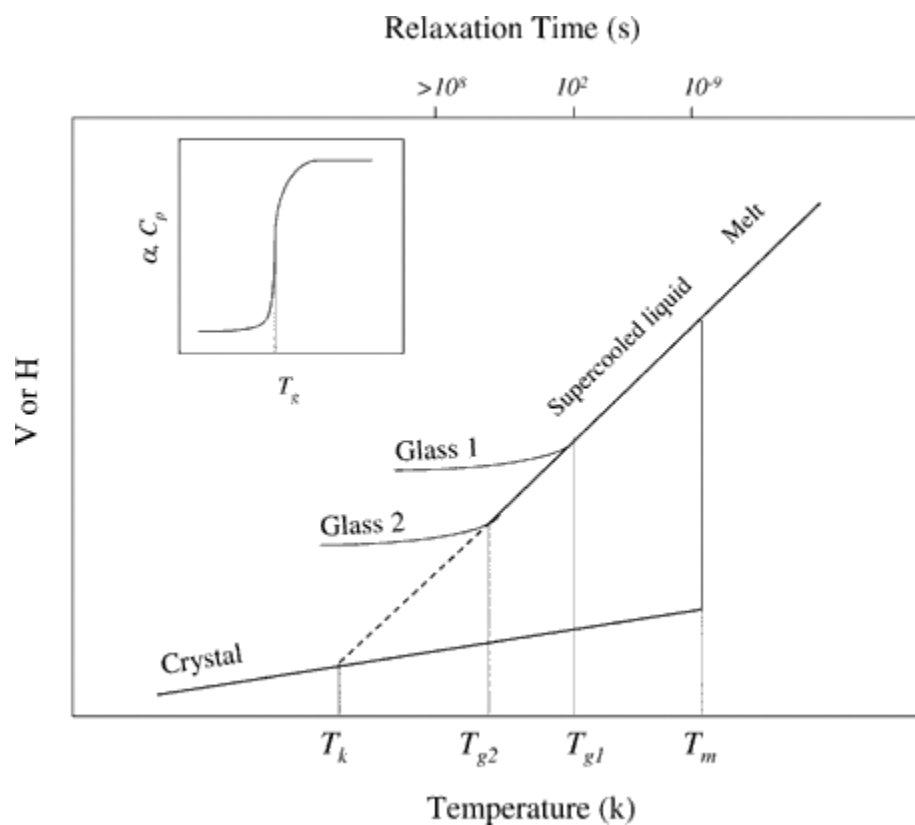
Reproduced from Hill et al. (2005)

Figure I-3: Macromolecular dynamic transitions. Inset diagrams depict the different molecular motions associated with each dynamic transition. The glass transition (Tg) involves a change in the protein or polymer backbone (translational motions), and the lower temperature motions (β and γ) involve side change motions.
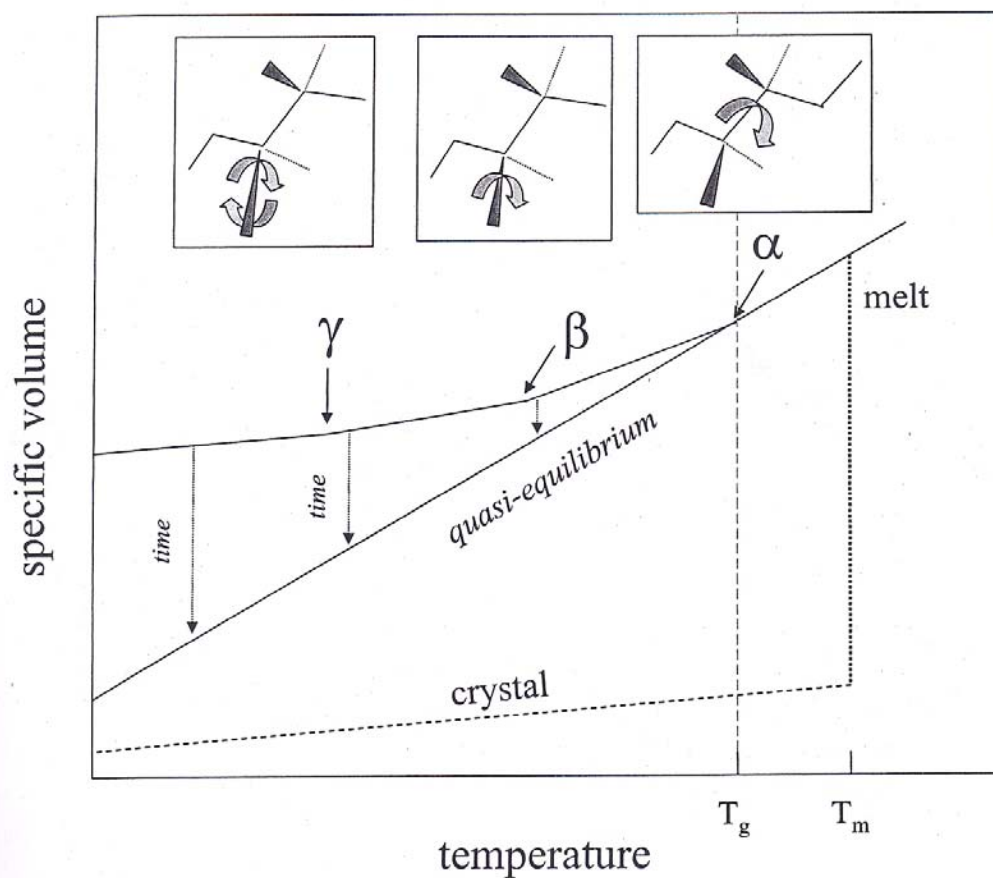
Reproduced from Lukasik (2005) and modified from Hill and Tant (1998)

Figure I-4: Time scales and associated modes of motion in protein solution.

Time Scale	Dynamic Event
Picosecond (10^{-12} s)	Bond vibrations, rotational motions of water, side chain motions
Nanosecond (10^{-9} s)	Segmental motions (small proteins) Rotational motions (small proteins)
Microsecond (10^{-6} s)	Segmental motions (large proteins) Rotational motions (large/asymetric proteins) Flexing of filamentous proteins
Millisecond (10^{-3} s)	Conformational changes Enzyme turnover
Seconds (s)	Protein denaturation, unfolding

Adopted from Hill et al. (2005) and Ludescher et al. (2001)

Figure I-5: Schematic of gas permeability.
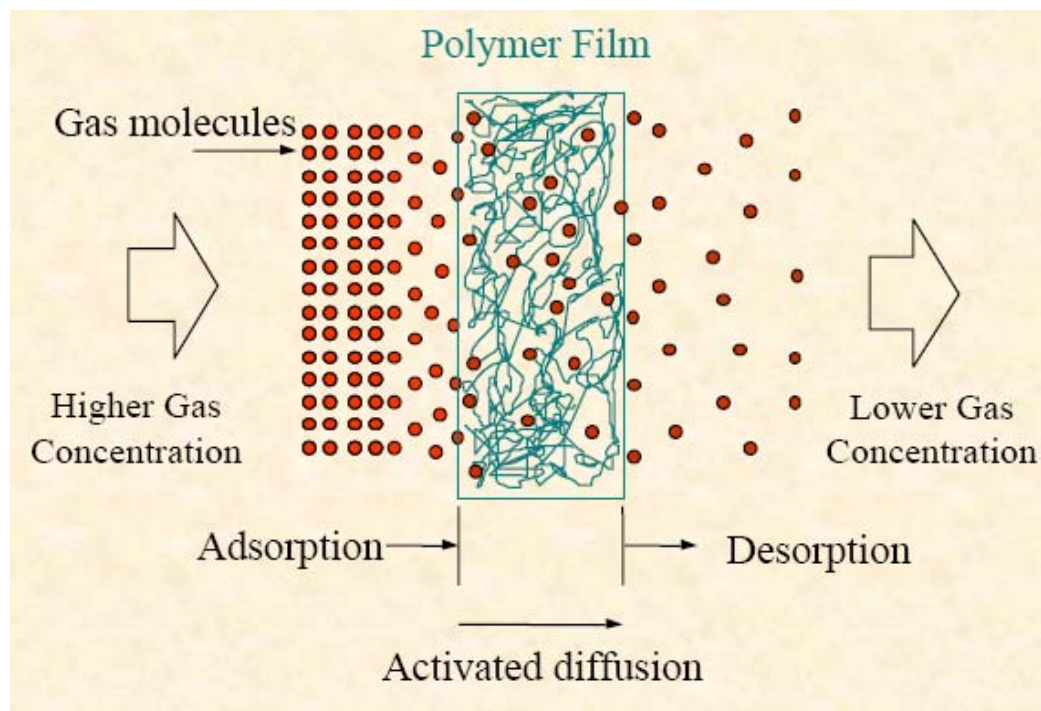
Taken with permission from Dr. Kit Yam's "Shelf-life" course notes (2005).

Figure I-6: Various processes taking place through edible films over time.
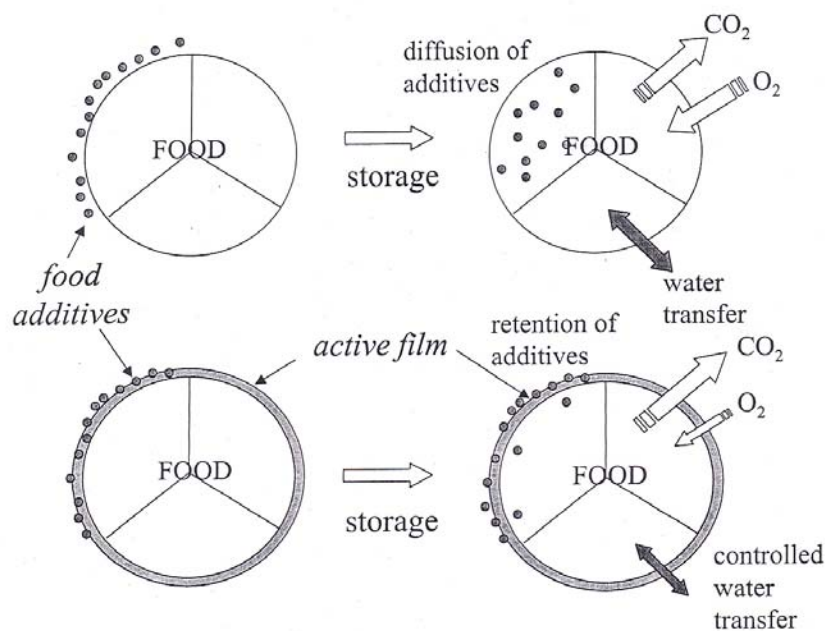
Reproduced from Lukasik (2005), initially modified from Cuq et al. (1995b)

Figure I-7: This figure shows the standard set-up for a fluorescence spectrophotometer. Many variations exist, but the main components are orientated in this manner. Light from a source passes through the excitation monochromator at the desired slit or bandpass and the light is then absorbed by the sample at the desired wavelength. Next, the various relaxation processes take place and the sample emits a photon which passes through the emission monochromator, also set at the desired slit or bandpass. The detector converts photon counts to an electric signal, and finally the data is collected and displayed through various software programs.
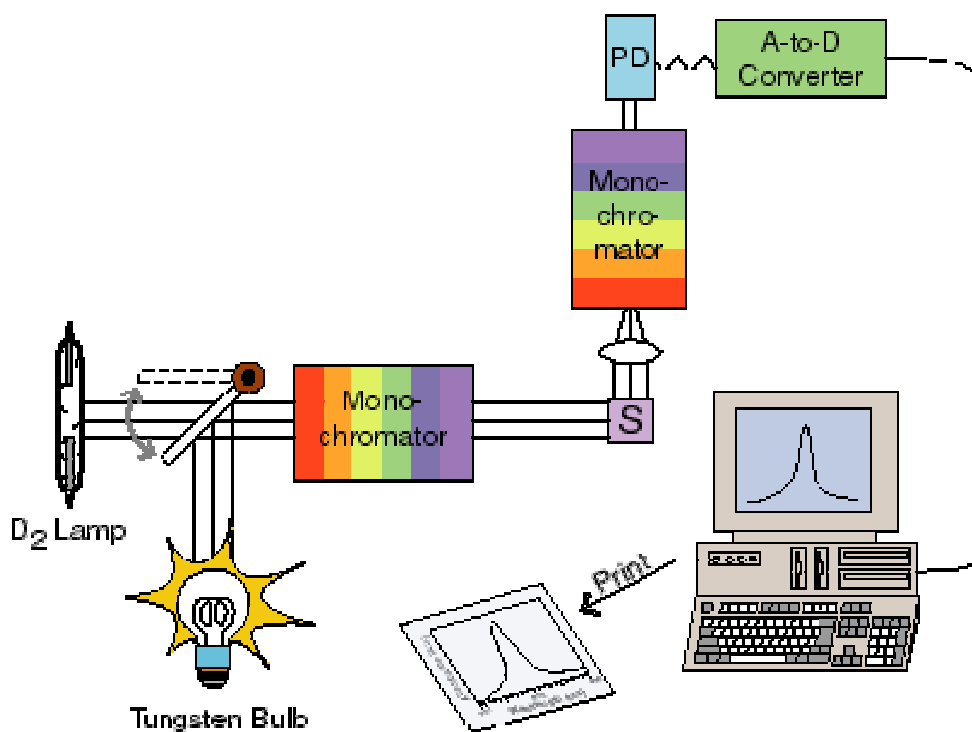
Figure I-8: Sensitivity of luminescence to molecular mobility.

Luminescent Variable	Photphysical Mechanism	Types of Experiments	Type of Probe Mobility Measured	Measure of Matrix Mobility
Intensity	Quenching of the excited state by vibrational coupling to the ground state (non-radiative quenching)	Measurement of the probe lifetime or emission energy	Vibrational motions	Matrix viscosity and free volume
	Quenching of the excited state by collisions with quencher molecules in the matrix such as O_2 ($k_Q[O_2]$)	Measurement of the probe intensity or lifetime as a function of the concentration of quenching species (O_2)	Translational mobility (permeation)	Translational mobility or the permeation of the quencher
Energy	Dipolar relaxation of the matrix/solvent around the excited state chromophore	Measurement of the excitation and emission spectra (shape, FWHM, and peak frequency)	None	Matrix/solvent relaxation dynamics

Adopted with modification from Ludescher et al. (2001) and Lukasik (2005)

Figure 9: Jablonski diagram of the various photophysical processes.
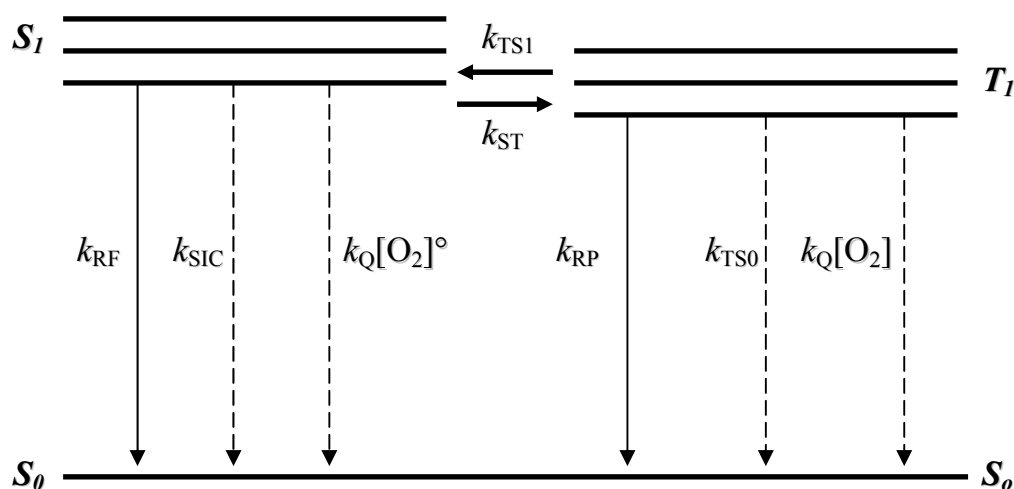
Modified from Simon-Lukasik and Ludescher (2004)

Energy levels

S_0 Ground State

S_1 Excited singlet state

T_1 Excited triplet state

Radiative rate constants

k_{RF} Rate for fluorescence emission

k_{RP} Rate for phosphorescence emission

Non-radiative rate constants

k_{ST} Rate of intersystem crossing from the singlet to the triplet state

k_{TS1} Rate of intersystem crossing from the triplet to the singlet state

k_{SIC} Rate of internal conversion from the S_1 state to the S_0 state

k_{TS0} Rate of intersystem crossing between the T_1 and S_0 state

$k_Q[O_2]$ Rate of collisional quenching due to oxygen

Figure I-10: Energy level diagram illustrating the effect of dipolar relaxation on the relative energies of the ground and excited states of a luminescent probe. The vertical dimension represents energy of the electronic state while the horizontal axis reflects the passage of time.
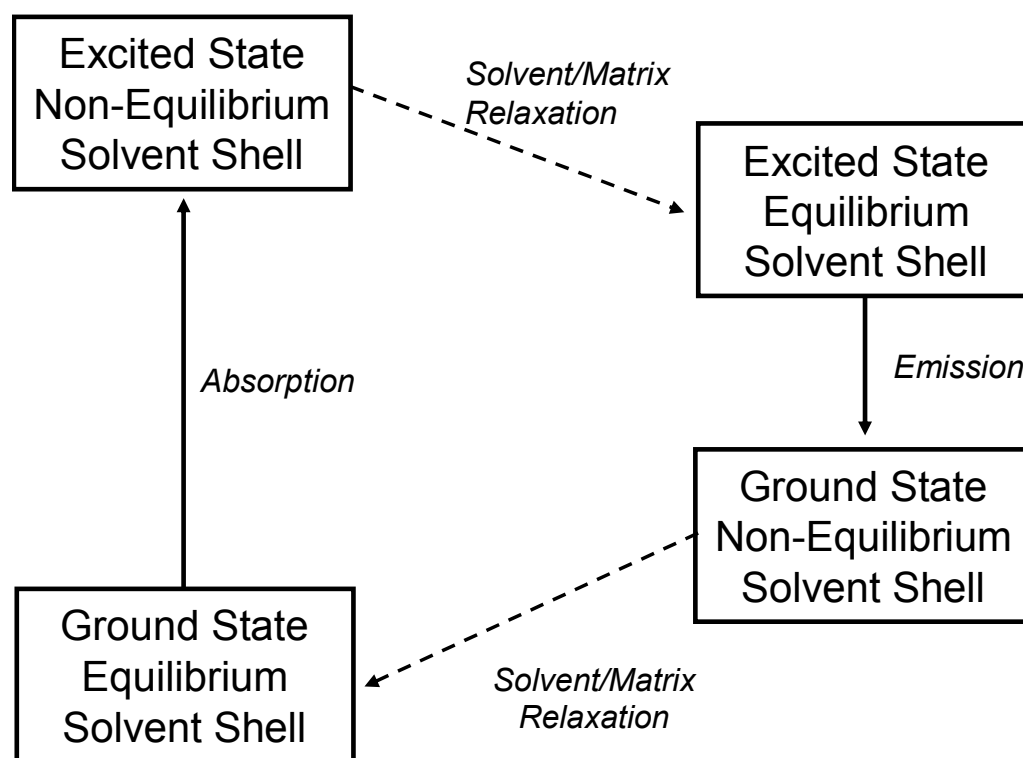
Reproduced from Ludescher et al. (2001)

Figure I-11: Structure of erythrosin B.
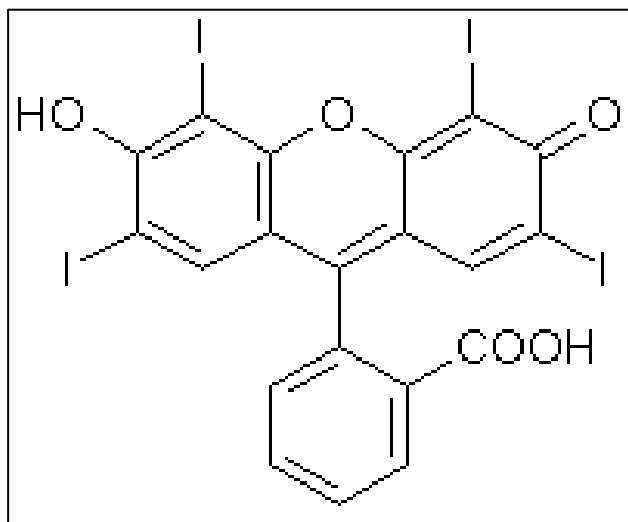
Chapter 1 References

Anker, M., Stading, M., and Hermansson, A. M. (2000). Relationship between the microstructure and the mechanical and barrier properties of whey protein films. *Journal of Agricultural and Food Chemistry* **48**, 3806-3816.

Anker, M., Stading, M., and Hermansson, A. M. (2001). Aging of whey protein films and the effect on mechanical and barrier properties. *Journal of Agricultural and Food Chemistry* **49**, 989-995.

Bourtoom, T., Chinnan, M. S., Jantawat, P., and Sanguandeekul, R. (2006). Effect of Plasticizer Type and Concentration on the Properties of Edible Film from Water-Soluble Fish Proteins in Surimi Wash-Water. *Food Science and Technology International* **12**, 119-126.

Brownsey, G. J., Noel, T. R., Parker, R., and Ring, S. G. (2003). The Glass Transition Behavior of the Globular Protein Bovine Serum Albumin. *Biophys. J.* **85**, 3943-3950.

Buitink, J., and Leprince, O. (2004). Glass formation in plant anhydrobiotes: survival in the dry state. *Cryobiology* **48**, 215-228.

Castellan, G. W. (1983). "Physical Chemistry," Third/Ed. The Benjamin / Cummings Publishing Company, Inc, Menlo Park.

Champion, D., Le Meste, M., and Simatos, D. (2000). Towards an improved understanding of glass transition and relaxations in foods: molecular mobility in the glass transition range. *Trends in Food Science & Technology* **11**, 41-55.

Chen, R. (2003). Apparent stretched-exponential luminescence decay in crystalline solids. *Journal of Luminescence* **102-103**, 510-518.

Cuq, B., Aymard, C., Cuq, J.-L., and Guilbert, S. (1995a). Edible packaging films based on fish myofibrillar proteins: Formation and functional properties. *Journal of Food Science* **60**, 1369-1374.

Cuq, B., Gontard, N., and Guilbert, S. (1995b). Edible films and coatings as active layers. *In* "Active Food Packaging" (M. L. Rooney, ed.). Blackie Academic and Prefessional, New York.

Demchenko, A. P. (1988). Site-selective excitation: a new dimension in protein and membrane spectroscopy. *Trends in Biochemical Sciences* **13**, 374-377.

Dong, A. C., Prestrelski, S. J., Allison, S. D., and Carpenter, J. F. (1995). Infrared Spectroscopic Studies of Lyophilization-Induced and Temperature-Induced Protein Aggregation. *Journal of Pharmaceutical Sciences* **84**, 415-424.

Doye, J. P. K., Louis, A. A., and Vendruscolo, M. (2004). Inhibition of protein crystallization by evolutionary negative design. *Physical Biology* **1**, P9-P13.

Duchowicz, R., Ferrer, M. L., and Acuna, A. U. (1998). Kinetic Spectroscopy of Erythrosin Phosphorescence and Delayed Fluorescence in Aqueous Solution at Room Temperature. *Photochemistry and Photobiology* **68**, 494-501.

Erdohan, Z. O., and Turhan, K. N. (2005). Barrier and mechanical properties of methyicellulose-whey protein films. *Packaging Technology and Science* **18**, 295-302.

Fennema, O. R. (1996). Food Chemistry. (O. R. Fennema, ed.), pp. 17-94. Marcel Dekker, Inc., New York.

Frinault, A., Gallant, D. J., Bouchet, B., and Dumont, J. P. (1997). Preparation of Casein Films by a Modified Wet Spinning Process. *Journal of Food Science* **62**, 744-747.

Gontard, N., Guilbert, S., and Cuq, J.-L. (1993). Water and Glycerol as Plasticizers Affect Mechanical and Vapor Barrier Properites of and Edible Wheat Gluten Film. *Journal of Food Science* **58**, 206-211.

Gontard, N., Thibault, R., Cuq, B., and Guilbert, S. (1996). Influence of relative humidity and film composition on oxygen and carbon dioxide permeabilities of edible films. *Journal of Agricultural and Food Chemistry* **44**, 1064-1069.

Guillet, J. (1985). "Polymer photophysics and photochemistry : an introduction to the study of photoprocesses in macromolecules," Cambridge University Press, New York.

Heller, M. C., Carpenter, J. F., and Randolph, T. W. (1997). Manipulation of lyophilization-induced phase separation: Implications for pharmaceutical proteins. *Biotechnology Progress* **13**, 590-596.

Hill, A. J., and Tant, M. R. (1998). The Structure and Properties of Glassy Polymers: An Overview. *In* "Stucture and Properties of Glassy Ploymers" (M. R. Tant and A. J. Hill, eds.). American Chmicial Society Washington D.C.

Hill, J. J., Shalaev, E. Y., and Zografi, G. (2005). Thermodynamic and dynamic factors involved in the stability of native protein structure in amorphous solids in relation to levels of hydration. *Journal of Pharmaceutical Sciences* **94**, 1636-1667.

Hurtubise, R. J. (1990). "Phosphorimetry: Theory, Instumentation and Applications," VCH Publishers, Inc., New York.

Hurtubise, R. J. (1997). Solid-matrix luminescence analysis: photophysics, physicochemical interactions and applications. *Analytica Chimica Acta* **351**, 1-22.

Jones, N. R. (1977). Use of gelatin in edible products. *In* "The science and technology of gelatin" (A. G. Ward and A. Courts, eds.), pp. 366-394. Academic Press, New York.

Kachalova, G. S., Morozov, V. N., Morozova, T., Myachin, E. T., Vagin, A. A., Strokopytov, B. V., and Nekrasov, Y. V. (1991). Comparison of structures of wet and dry hen egg-white lysozyme molecule at 1.8 A resolution. *FEBS Lett.* **284**, 91-94.

Korolev, V. V., Bolotsky, V. V., Shokhirev, N. V., Krissinel, E. B., Bagryansky, V. A., and Bazhin, N. M. (1995). Diffusion of Molecular-Oxygen in Glassy Matrices, Studied by Luminescence Quenching. *Chemical Physics* **196**, 317-325.

Krochta, J. M., and DeMulder-Johnston, C. (1997). Edible and biodegradable polymer films: Challenges and opportunities. *Food Technology* **51**, 61-74.

Lakowicz, J. R. (1999). "Principles of fluorescence spectroscopy," Second/Ed. Kluwer Academic/Plenum Press, New York.

Lam, S. K., Chan, M. A., and Lo, D. (2001). Characterization of phosphorescence oxygen sensor based on erythrosin B in sol-gel silica in wide pressure and temperature ranges. *Sensors and Actuators B: Chemical* **73**, 135-141.

Lee, K. C. B., Siegel, J., Webb, S. E. D., Leveque-Fort, S., Cole, M. J., Jones, R., Dowling, K., Lever, M. J., and French, P. M. W. (2001). Application of the Stretched Exponential Function to Fluorescence Lifetime Imaging. *Biophys. J.* **81**, 1265-1274.

Lefevre, T., Subirade, M., and Pezolet, M. (2005). Molecular description of the formation and structure of plasticized globular protein films. *Biomacromolecules* **6**, 3209-3219.

Lent, L. E., Vanasupa, L. S., and Tong, P. S. (1998). Whey Protein Edible Film Structures Determined by Atomic Force Microscope. *Journal of Food Science* **63**, 824-827.

Lesch, H., Schlichter, J., Friedrich, J., and Vanderkooi, J. M. (2004). Molecular Probes: What Is the Range of Their Interaction with the Environment? *Biophys. J.* **86**, 467-472.

Lettinga, M. P., Zuilhof, H., and van Zandvoort, M. A. M. J. (2000). Phosphorescence and fluorescence characterization of fluorescein derivatives immobilized in various polymer matrices. *Physical Chemistry Chemical Physics* **2**, 3697-3707.

Lu, X., Manner, I., Winnik, M.A. (2001). Oxygen diffusion in polymer films for luminescence barometry application. *New Trends in Fluorescence Spectoscopy*, 229-256.

Ludescher, R. D. (1990). Molecular dynamics of food proteins: experimental techniques and observations. *Trends in Food Science & Technology* **1**, 145-149.

Ludescher, R. D., Shah, N. K., McCaul, C. P., and Simon, K. V. (2001). Beyond Tg: optical luminescence measurements of molecular mobility in amorphous solid foods. *Food Hydrocolloids* **15**, 331-339.

Lukasik, K. V. (2005). Luminescent Probes of Structural and Dynamic Heterogeneity in Gelatin, Rutgers University, New Brunswick.

Lukasik, K. V., and Ludescher, R. D. (2006a). Effect of plasticizer on dynamic site heterogeneity in cold-cast gelatin films. *Food Hydrocolloids* **20**, 88-95.

Lukasik, K. V., and Ludescher, R. D. (2006b). Molecular mobility in water and glycerol plasticized cold- and hot-cast gelatin films. *Food Hydrocolloids* **20**, 96-105.

Mangavel, C., Barbot, J., Popineau, Y., and Gueguen, J. (2001). Evolution of wheat gliadins conformation during film formation: A Fourier transform infrared study. *Journal of Agricultural and Food Chemistry* **49**, 867-872.

McCrum, N. G., Read, B. E., and Williams, G. (1991). "Anelastic and dielectric effects in ploymer solids," Dover Publications, New York.

McHugh, T. H., and Krochta, J. M. (1994). Sorbitol- vs Glycerol-Plasticized Whey Protein Edible Films: Integrated Oxygen Permeability and Tensile Property Evaluation. *Journal of Agricultural and Food Chemistry* **42**, 841-845.

Nack, T. J., and Ludescher, R. (2006). Molecular Mobility and Oxygen Permeability in Amorphous Bovine Serum Albumin Films. *Food Biophysics* **In Press**.

Nicholov, R., Veregin, R. P. N., and DiCosmo, F. (1995). Conformational changes of bovine serum albumin as a consequence of adsorption mimicked by freezing molecular motion. *Colloids and Surfaces B: Biointerfaces* **4**, 45-54.

Pravinata, L. C., You, Y., and Ludescher, R. D. (2005). Erythrosin B Phosphorescence Monitors Molecular Mobility and Dynamic Site Heterogeneity in Amorphous Sucrose. *Biophys. J.* **88**, 3551-3561.

Richert, R. (1997). Evidence for dynamic heterogeneity near T-g from the time-resolved inhomogeneous broadening of optical line shapes. *Journal of Physical Chemistry B* **101**, 6323-6326.

Richert, R., and Heuer, A. (1997). Rate-memory and dynamic heterogeneity of first-order reactions in a polymer matrix. *Macromolecules* **30**, 4038-4041.

Rupley, J. A., and Careri, G. (1991). Protein hydration and function. *Adv. Protein Chem.* **41**, 37-172.

Schauerte, J. A., Steel, D. G., and Gafni, A. (1997). Time-resolved room temperature tryptophan phosphorescence in proteins. *Fluorescence Spectroscopy* **278**, 49-71.

Shah, N. K., and Ludescher, R. D. (1993). Influence of hydration on the internal dynamics of hen egg white lysozyme in the dry state. *Photochemistry and Photobiology* **58**, 169-174.

Shah, N. K., and Ludescher, R. D. (1995). Phosphorescence Probes of the Glassy State in Amorphous Sucrose. *Biotechnology Progress* **11**, 540-544.

Shamblin, S. L., Tang, X., Chang, L., Hancock, B. C., and Pikal, M. J. (1999). Characterization of the Time Scales of Molecular Motion in Pharmaceutically Important Glasses. *J. Phys. Chem. B* **103**, 4113-4121.

Shelke, K. (2006). Tiny, Invisible, Ingredients. *Food Processing*, 42-45.

Shirke, S., and Ludescher, R. D. (2005). Molecular mobility and the glass transition in amorphous glucose, maltose, and maltotriose. *Carbohydrate Research* **340**, 2654-2660.

Simelane, S., and Ustunol, Z. (2005). Mechanical Properties of Heat-cured Whey Protein–based Edible Films Compared with Collagen Casings under Sausage Manufacturing Conditions. *Journal of Food Science* **70**, E131-134.

Simon-Lukasik, K. V., and Ludescher, R. D. (2004). Erythrosin B phosphorescence as a probe of oxygen diffusion in amorphous gelatin films. *Food Hydrocolloids* **18**, 621-630.

Sirotkin, V. A., and Korolev, D. V. (2005). Effect of acetonitrile on the hydration of human serum albumin films: a calorimetric and spectroscopic study. *Thermochimica Acta* **432**, 246-253.

Slade, L., Levine, H., and Finley, J. W. (1989). Protein-water interaction: Water as a plasticizer of gluten and other protein polymers. *In* "Protein Quality and the Effects of Processing" (R. D. Phillips and J. W. Finley, eds.), pp. 9-124. Marcel Dekker, Inc, New York.

Slavic, J. (1994). "Fluorescent probes in cellular and molecular biology," CRC Press, Inc., Boca Raton.

Smiddy, M., Papkovskaia, N., Papkovsky, D. B., and Kerry, J. P. (2002). Use of oxygen sensors for the non-destructive measurement of the oxygen content in modified atmosphere and vacuum packs of cooked chicken patties; impact of oxygen content on lipid oxidation. *Food Research International* **35**, 577-584.

Sobral, P. J. A., Monterrey-Q, E. S., and Habitante, A. M. Q. B. (2002). Glass transition study of Nile Tilapia myofibrillar protein films plasticized by glycerin and water. *Journal of Thermal Analysis and Calorimetry* **67**, 499-504.

Sochava, I. V., Belopolskaya, T. V., and Smirnova, O. I. (1985). DSC study of reversible and irreversible thermal denaturation of concentrated globular protein solutions. *Biophysical Chemistry* **22**, 323-336.

Strambini, G. B., and Gonnelli, M. (1985). The indole nucleus triplet-state lifetime and its dependence on solvent microviscosity. *Chemical Physics Letters* **115**, 196-200.

Strasburg, G. M., and Ludescher, R. D. (1995). Theory and Applications of Fluorescence Spectroscopy in Food Research. *Trends in Food Science & Technology* **6**, 69-75.

Sundaresan, K. V., and Ludescher, R. D. (2007). Molecular mobility and oxygen permeability in amorphous Beta-lactoglobulin films. *Food Hydrocolloids* **In Press**.

Tsai, A. M., Neumann, D. A., and Bell, L. N. (2000). Molecular dynamics of solid-state lysozyme as affected by glycerol and water: A neutron scattering study. *Biophysical Journal* **79**, 2728-2732.

Turro, N. J. (1991). "Modern Molecular Photochemistry," University Science Books, Sausalito.

Vanin, F. M., Sobral, P. J. A., Menegalli, F. C., Carvalho, R. A., and Habitante, A. M. Q. B. (2005). Effects of plasticizers and their concentrations on thermal and functional properties of gelatin-based films. *Food Hydrocolloids* **19**, 899-907.

Wan, V. C.-H., Kim, M. S., and Lee, S.-Y. (2005). Water vapor permeability and mechanical properties of soy protein isolate edible films composed of different plasticizer combinations. *Journal of Food Science* **70**, E387-E391.

Wood, P. D. (1977). Technical and pharmaceutical uses of gelatin. *In* "The science and technology of gelatin" (A. G. Ward and A. Courts, eds.), pp. 414-437. Academic Press, New York.

Yam, Kit. *Shelf Life Course Notes*. Food Science Department. Rutgers University. 2006.

Yoshioka, S., Aso, Y., and Kojima, S. (1997). Dependence of the molecular mobility and protein stability of freeze-dried gamma-globulin formulations on the molecular weight of dextran. *Pharmaceutical Research* **14**, 736-741.

Yoshioka, S., and Aso, Y. (2007). Correlations between molecular mobility and chemical stability during storage of amorphous pharmaceuticals. *Journal of Pharmaceutical Sciences* **96**, 960-981.

You, Y. M., and Ludescher, R. D. (2006). Phosphorescence of erythrosin B as a robust probe of molecular mobility in amorphous solid sucrose. *Applied Spectroscopy* **60**, 813-819.

Zallen, R. (1998). "The physics of amorphous solids," John Wiley & Sons, Inc., New York.

Zunic, A., Pravinata, L., and Ludescher, R. D. (2003). Tryptophan phosphorescence is sensitive to molecular mobility and oxygen diffusion in glassy sugars. *Biophysical Journal* **84**, 287a-287a.

Chapter 2: Molecular Mobility and Oxygen Permeability in Amorphous Bovine Serum Albumin Films[1].

Introduction

The physical properties of amorphous solid proteins are important for the texture of protein-containing foods (Slade et al., 1989), the stability of pharmaceuticals (Hill et al., 2005; Yoshioka and Aso, 2007), the viability of seeds and spores (Buitink and Leprince, 2004), and the permeability of edible films (Krochta and DeMulder-Johnston, 1997). These physical properties are largely influenced on the molecular level by the three-dimensional structure (conformation) of the protein in the solid state and the mobility of the protein and its component parts within the amorphous matrix.

Protein conformation in the solid state appears to be largely dependent upon the method of preparation. In the case of procedures such as lyophilization and spray drying that involve extreme temperatures it appears that proteins may often lose native conformation (Dong et al., 1995; Heller et al., 1997). Dehydration alone, however, does not appear to induce significant loss of native structure (Kachalova et al., 1991). Clearly, the numerous proteins within seeds and spores and even whole organisms can withstand significant dehydration without permanent loss of native conformation.

Protein molecular mobility is less fully characterized in the solid state. Besides the obvious effect of slowing overall translational and rotational motion, dehydration also hinders internal modes of vibrational motion important for biological function (Rupley and Careri, 1991). Fully hydrated proteins in solvents or in crystals undergo a dynamical transition (T_d) at ~200 K (recently reviewed in Hill et al. (2005)) that has been identified

---

[1] Content in this section was published in *Food Biophysics* (2006) **1**, 151-162. Some portions are included *verbatim*.

with the polymer glass transition. Below T_d, protein motions are limited to harmonic vibrations of bonded atoms while above T_d anharmonic, collective vibrations of non-bonded atoms are activated. These collective motions appear to be required for conformational change (including perhaps denaturation) and biological activity. Although T_d increases upon dehydration in some proteins (Tsai et al., 2000), the general influence of dehydration on T_d is uncertain, as is the role that T_d plays in influencing the matrix dynamics of amorphous, proteinaceous solids.

We have recently demonstrated that the phosphorescence emission spectrum and intensity decay from the xanthene probe erythrosin B (tetra-iodo fluorescein) dispersed in thin films composed of amorphous gelatin (Simon-Lukasik and Ludescher, 2004; Lukasik and Ludescher, 2006a, b) and sugars (Pravinata et al., 2005; Shirke and Ludescher, 2005; You and Ludescher, 2006) are sensitive to specific modes of molecular mobility within the amorphous solid. In addition, since oxygen is a contact quencher of the excited triplet state, phosphorescence can also be used as a sensitive indicator of oxygen diffusion within the amorphous solid (Simon-Lukasik and Ludescher, 2004; Lu, 2001). Here, we use phosphorescence from erythrosin B dispersed in the matrix to study the molecular mobility and oxygen permeability within amorphous solid films made from pure native bovine serum albumin. These data further characterize the intrinsic molecular mobility within an amorphous solid protein and provide insight into the role that molecular mobility within the protein matrix plays in modulating the permeability of oxygen.

Materials and Methods

Preparation of Samples

Purified bovine serum albumin (BSA) was obtained from Sigma Chemical Company (St Louis, MO) and used as received. In order to define and minimize the presence of counter ions, BSA was dissolved in distilled deionized water at 20 mg/ml, placed in a cellulose dialysis tube having a 12-14 kDa molecular weight cutoff (Spectrum, Houston, TX), dialyzed against 0.1 M potassium chloride for at least 36 hours with frequent changes of buffer, and then dialyzed extensively against distilled deionized water. All dialysis was carried out at room temperature. The solution was then filter sterilized through a 0.2 μm Acrodisc® filter (Pall Gellman Laboratory, Ann Arbor, MI). The concentration of the protein after dialysis was determined by absorbance at 280 nm using a molar absorptivity of 4.3 x 10^{-4} $M^{-1}cm^{-1}$ (Fasman, 1989).

A 10 mg/ml stock solution of erythrosin B free acid (Ery B) (Molecular Probes, Inc., Eugene, OR) was prepared in *N, N*-dimethlyformamide (DMF) (Sigma-Aldrich, Milwaukee, WI). DMF has negligible effects on the spectroscopic properties of the probe in amorphous sucrose at a variety of concentrations (Pravinata et al., 2005). This concentration was selected to simplify the addition of the probe to the BSA solution, and the solvent was selected for probe stability during long term storage. The probe was added to the BSA solution at a molar ratio of 1:10 (Ery B:BSA). At this concentration it was determined that the Ery B does not aggregate, existing only as individual molecules monitoring the molecular mobility of the protein (You and Ludescher, 2006). Garland and Moore (1979) demonstrated that BSA binds Ery B via phosphorescence techniques

(emission peak wavelength shift), although the specific binding sites are unknown since the crystal structure for BSA has not been determined.

The Ery B:BSA films were made by pipetting 15 μL of the solution onto quartz slides (13 mm x 30 mm x 0.6 mm) (NSG Precision Cells, Farmingdale, NY) and spreading the solution over an area approximately 15 mm x 10 mm. Before use, to improve the surface activity for spreading the BSA solutions, the slides were soaked in Alconox soap, washed with double distilled water, and rinsed with ethanol. After spreading, the slides were dried under constant flow of air for 30 minutes, allowing the films to set, and then transferred to a desiccator over phosphorus pentoxide for at least one week. The slides were stored at 23.0 ± 1 ℃, protected from light to prevent any photobleaching of the Ery B, and desiccant was refreshed as needed to maintain a relative humidity close to 0%.

Phosphorescence Measurements

To prevent oxygen quenching of the triplet state, a virtually oxygen free nitrogen stream was generated by passing high purity nitrogen through a Supelco carrier gas purifier (Bellfonte, PA). This gas line was routed into the sample compartment and directly into the quartz fluorescence cuvette that held the slide. The cuvette was capped with a lid having inlet and outlet ports for the gas line, so all experiments were done at constant pressure. The cuvette was flushed for at least 30 minutes to ensure that oxygen was eliminated. The sample compartment was jacketed, and dry air was used to prevent condensation on the cuvette faces when experimental conditions were below room temperature.

Measurements were made on a Cary Eclipse fluorescence spectrophotometer (Varian Instruments, Walnut Creek, CA) equipped with a temperature controller and multi-cell holder. This instrument, which collects in analog mode, uses a high intensity pulsed lamp, and a time delay was used to avoid any fluorescence during the lamp pulse. Phosphorescence and delayed fluorescence emission scans were collected over the range from 535-800 nm with an excitation wavelength of 525 nm. The excitation and emission monochromators were both set at 10 nm bandpass. Each data point (collected at 1 nm intervals with a 0.1 s averaging time) was collected from a single flash with a 0.2 ms delay, 0.5 ms gate time, and 4.0 ms total decay time. Excitation scans were collected using the same electronic parameters over the range of 400-600 nm with a 688 nm emission wavelength and both monochromators set at 10 nm.

Lifetime measurements were collected under air or under a nitrogen purge, and the following experimental parameters were the same in both instances. Samples were excited at 540 nm and the emission was measured at 685 nm with a 20 nm bandpass for both excitation and emission monochromators. Each time-resolved decay transient was the average of 40 cycles, and for each cycle data were collected from a single flash with a delay of 0.1 ms, a 0.02 ms gate time, and 4.0 ms total decay time. All experiments were done in triplicate at least, and the standard deviation of the averages was calculated to validate reproducibility. For the lifetime experiments a temperature range of $-20°$ to $110º$ C was used, and temperature was increased at ten degree increments with a 15 minute delay between readings. The phosphorescence lifetime was exactly reversible during heating and subsequent cooling cycles indicating that the sample was indeed completely deoxygenated in the presence of nitrogen since softening of the matrix at

higher temperature would have allowed oxygen to enter or escape from the matrix, thus altering the lifetime.

Intensity decays were collected as a function of emission wavelength over the emission range from 660-720 nm at 10 nm increments with an excitation wavelength of 540 nm. The temperature range was 0-100°C and the excitation and emission bandwidth were 20 nm and 10 nm, respectively, with a delay time of 0.1 ms, gate time of 0.01 ms, and a total decay time of 4.0 ms.

Data Analysis

The emission spectra were analyzed by fitting both the delayed fluorescence and the phosphorescence to a lognormal function.

$$I(\nu) = I_0 \exp\{-\ln(2)[\ln(1+2b(\nu-\nu_P)/\Delta)/b]^2\} \tag{1}$$

In this equation, I_0 is the maximum intensity value of the emission spectra, ν_P is the frequency in cm^{-1} of the emission maximum, Δ is the line width parameter, and b is the asymmetry parameter. The bandwidth of the emission, the full width at half maximum (Γ), is related to b and Δ.

$$\Gamma = \Delta \sinh(b)/b \tag{2}$$

Emission spectra were fit using the program Igor (Wavemetrics, Inc., Lake Oswego, OR). We also analyzed some data by fitting with the program Nfit (Island Products, Galveston, TX), to make sure that the results agreed in both fitting programs.

The phosphorescence time-resolved emission spectra collected as a function of delay time and temperature used an excitation wavelength of 540 nm and emission from 620-780 nm. Emission spectra were collected with delay times of 0.1, 0.6, 1.1, 1.6, and 2.1 ms after the lamp flash. The data were analyzed using Equations 1 and 2.

Phosphorescence lifetimes were determined by nonlinear least-squares analysis with the statistical programs Igor and Nfit. Fits were judged satisfactory if the r^2 values were in the range of 0.995-1.0 and the modified residuals ((data − fit)/data$^{1/2}$) varied randomly about zero. Data were analyzed using a stretched exponential, or Kohlrausch-Williams-Watts (KWW), decay model, which has been shown to be appropriate to describe the wide distribution of relaxation times (Champion et al., 2000; Yoshioka and Aso, 2007) for the molecular processes that depopulate excited states in tissues (Lee et al., 2001), crystalline solids (Chen, 2003), super cooled liquids (Richert, 1997), and amorphous solids (Pravinata et al., 2005):

$$I(t) = I(0) \exp[-(t/\tau)^\beta] + c \qquad (3)$$

Where I(t) is the intensity as a function of time following pulsed excitation, I(0) is the initial intensity at time zero, τ is the KWW lifetime, and β is the stretching exponent which characterizes the distribution of the decay times (Richert and Heuer, 1997). Further explanation of the parameters of the stretched exponential equation is provided in the results section.

The phosphorescence lifetime is the inverse sum of the rate constants associated with the various processes that depopulate the excited triplet state.

$$\tau^{-1} = k_P = k_{RP} + k_{TS1} + k_{TS0} + k_Q[O_2] \qquad (4)$$

This equation can be used to calculate k_{TS0}, the rate of collisional quenching to the ground state, if k_{RP}, k_{TS1}, and $k_Q[O_2]$ are known. Under anoxic conditions $k_Q[O_2]$, the rate of oxygen quenching, is zero; k_{RP}, the radiative decay rate of the triplet state, is 41 s^{-1} for Ery B (Duchowicz et al., 1998; Lettinga et al., 2000); k_{TS1}, the rate of reverse intersystem

crossing from the excited triplet state to the excited singlet state, depends on ΔE_{TS}, the energy gap between S_1 and T_1 (Simon-Lukasik and Ludescher, 2004):

$$k_{TS1}(T) = k^o_{TS1} \exp(-\Delta E_{TS}/RT) \tag{5}$$

The slope of a Van't Hoff plot of the natural log of the ratio of delayed fluorescence (I_{DF}) to phosphorescence (I_P) intensity versus inverse temperature provides a measure of ΔE_{TS} (Duchowicz et al., 1998):

$$d[\ln(I_{DF}/I_P)]/d(1/T) = -\Delta E_{TS}/R \tag{6}$$

(where $R = 8.314$ J K^{-1} mol^{-1}). Literature values of k^o_{TS1} for erythrosin B vary from 0.3 x 10^7 s^{-1} in ethanol and 6.5 x 10^7 s^{-1} in water (Duchowicz et al., 1998) to 111 x 10^7 s^{-1} in solid polyvinyl alcohol (Lettinga et al., 2000), and thus provide little guidance. We estimated the maximum possible value for k^o_{TS1} in BSA films (= 4.4 x 10^7 s^{-1}) by assuming that $k_{TS1}(T)$ (calculated using equation 5 with $\Delta E_{TS} = 32.88$ kJ mol^{-1}; see results) cannot result in values for $k_{TS0}(T)$ that decrease with temperature. This procedure thus estimated the minimum possible values for $k_{TS0}(T)$.

Results

Delayed Emission Spectra.

The delayed emission spectra of Ery B (tetra-iodo fluorescein) in amorphous thin films of BSA at a mole ratio of 1 Ery B:10 BSA have emission maxima at ~557 nm and ~685 nm (Figure II-1). The longer wavelength band is phosphorescence from the excited triplet state (T_1) while the shorter wavelength band is delayed fluorescence from the excited singlet state (S_1) that has been repopulated from the triplet state by thermally activated reverse intersystem crossing (Parker, 1968). Delayed emission spectra were collected over the temperature range from 0 to 100ºC. As the temperature increased, the

phosphorescence intensity (I_P) decreased and the delayed fluorescence intensity (I_{DF}) increased as expected for a thermally activated process. The value for ΔE_{TS}, the energy gap between the T_1 and S_1 states, was calculated from the slope of a Van't Hoff plot of $\ln(I_{DF}/I_P)$ versus $1/T$ (Equation 6, Materials and Methods) using values for the intensity of delayed fluorescence (I_{DF}) and phosphorescence (I_P) determined from a fit of the spectra to a sum of two lognormal functions (Equation 1). This value, 32.9 ± 0.5 kJ mol^{-1}, was significantly smaller than the values in water (36.9 ± 0.6 kJ mol^{-1}) or 66 wt % aqueous sucrose (36.9 ± 0.1 kJ mol^{-1}) (Pravinata et al., 2005) and in polyvinyl alcohol (41.2 ± 0.4 kJ mol^{-1}) (Lettinga et al., 2000), similar to the values in amorphous sucrose (31.6 ± 0.4 kJ mol^{-1}) (Pravinata et al., 2005) and maltose (32.7 ± 1.1 kJ mol^{-1}) (Shirke et al., 2005), and larger than the value in ethanol (28.5 ± 2.5 kJ mol^{-1}) (Duchowicz et al., 1998), indicating that solvent or matrix properties modulate the singlet-triplet energy gap of Ery B.

The phosphorescence emission band shifted to longer wavelength (lower energy) with increasing temperature. The peak emission energy ν_P and bandwidth Γ_P (full width at half maximum) of phosphorescence were determined by fitting the emission bands to a lognormal function (Equation 1, Materials and Methods); these parameters are plotted versus temperature in Figure II-2. The phosphorescence emission energy decreased monotonically with temperature from 0 to 90°C and the slight increase seen at 100°C may be an artifact of analysis due to the low emission intensity. The decrease in emission energy was gradual and linear at temperatures below and steeper and linear at temperatures above ~50°C. The decrease in emission energy reflects an increase with temperature in the extent of matrix dipolar relaxation around the excited triplet state prior to emission (Lakowicz, 1999; Stratt and Maroncelli, 1996). The bandwidth (Γ_P)

increased linearly and gradually with temperature up to ~60ºC and quite dramatically at higher temperatures. The large increase in spectral bandwidth reflects a corresponding increase in the extent of inhomogeneous broadening of the emission spectrum (Nemkovich, 1991) due to an increase in the width of the distribution of energetically distinct matrix environments in the BSA film. Similar trends have been seen in amorphous sucrose (Pravinata et al., 2005), maltose (Shirke et al., 2005), and lactose (Shirke, 2005) around their glass transition temperatures. Both the decrease in emission frequency and the increase in bandwidth thus provide indications that the protein matrix softened around 50-60°C.

Phosphorescence Intensity Decays.

Phosphorescence intensity decay transients of Ery B in BSA films at 0°C equilibrated against nitrogen (–O_2) and against air (+O_2) are plotted in Figure II-3a along with fits using a stretched exponential decay model (Equation 3, Materials and Methods). The residuals for these fits, Figure II-3b, varied randomly about zero indicating that the stretched exponential function provided a satisfactory fit. All intensity decays in BSA collected as a function of temperature from 0 to 100°C were well analyzed using a stretched exponential decay model; the same model was used to fit Ery B phosphorescence intensity decays in amorphous solids composed of sucrose (Pravinata et al., 2005), maltose and maltitol (Shirke et al., 2005a, b), glucose and maltotriose (Shirke and Ludescher, 2005c), and gelatin (Simon-Lukasik and Ludescher, 2004; Lukasik and Ludescher, 2006a, b).

The physically meaningful parameters in this decay model are the Kohlraush-Williams-Watts (KWW) lifetime τ (Williams and Watts, 1970) and the stretching

exponent β (Pravinata et al., 2005; Lindsey and Patterson, 1980). The stretched exponential function, which is considered appropriate for fitting the complex relaxation processes that depopulate the excited triplet state in the millisecond timeframe in amorphous materials (Richert, 1997), models the decay as an asymmetric distribution of lifetimes with peak value approximately equal to τ whose breadth increases dramatically as β decreases from 1 to 0 (Lindsey and Patterson, 1980). These parameters, which depend on the matrix and the temperature (Chen, 2003), provide a measure of the environmental diversity of the ensemble of excited chromophores.

The KWW lifetimes and stretching exponents of Ery B in BSA films in the presence and absence of oxygen are plotted as a function of temperature from −20 to 110°C in Figures II-4a and II-4b, respectively. At 20ºC, the lifetime in the absence of oxygen was 0.58 ms, which is higher than the lifetime of 0.42 ms reported for Ery B bound to aqueous BSA at 20°C (Ferrer et al., 2001). Below 0°C, the lifetimes were indistinguishable in films equilibrated against nitrogen and against air. At 0°C and above, however, the lifetimes were significantly lower in the presence of oxygen. Over the temperature interval from 0 to 100ºC, the lifetimes decreased gradually in nitrogen and more steeply in air. The decrease in lifetime with temperature in nitrogen reflects an increase in k_P, the rate of non-radiative decay of the excited T_1 state, due to increases in the rate of reverse intersystem crossing (k_{TS1}) to the excited S_1 state, and of rate of intersystem crossing (k_{TS0}) to the ground state S_0 due to collisional quenching (Equation 4, Materials and Methods). The lower lifetimes when oxygen is present are due to the additional collisional quenching by oxygen ($k_Q[O_2]$).

The temperature dependence of k_{TS0}, calculated as described in Materials and Methods, is plotted in an Arrhenius format in Figure II-5a. The magnitude of k_{TS0} reflects both internal factors related to the manner in which the excited T_1 state of Ery B is vibrationally coupled to the S_0 ground state as well as external factors apparently related to the way in which the ground state vibrational energy can dissipate from the excited probe into the surrounding matrix (Fischer et al., 2002). Because the efficiency of this vibrational coupling is related to the overall mobility of the matrix (Strambini and Gonnelli, 1985), the magnitude of k_{TS0} provides a measure of matrix mobility. The value of k_{TS0} was ~1600 s^{-1} at low temperature (−10 to 0°C). Since k_{TS0} was also ~1600 s^{-1} at comparably low temperatures in glassy sucrose (Pravinata et al., 2005), maltose and maltitol (Shirke et al., 2005a, b), and lactose and lactitol (Shirke, 2005a), this value may represent the basal level of non-radiative decay due to coupling of the internal probe vibrations with the vibrational modes in the glassy matrix. The magnitude of k_{TS0} increased gradually and linearly at low temperature and more dramatically at high temperature. Linear fits of the Arrhenius plot at low temperature (0-60°C) and high temperature (70-110°C) had r^2 values of 0.911 and 0.843, respectively, and gave activation energies of 1.4 kJ mol^{-1} at low and 7.9 kJ mol^{-1} at high temperature. The break in the Arrhenius plot, indicating a dynamic transition, occurred at 68°C (calculated from the intersection of the linear fits at low and high temperatures).

The rate constant for quenching the triplet state by oxygen ($k_Q[O_2]$), calculated from the difference in inverse lifetime in air and in nitrogen (Equation 4, Materials and Methods), is also plotted in a Arrhenius fashion in Figure II-5a. The value of $k_Q[O_2]$ was essentially 0 s^{-1} below 0°C and increased dramatically above this temperature. A linear

fit to the data had $r^2 = 0.986$ and gave an activation energy of 29.9 kJ mol^{-1}. Despite the dramatically different activation energies characterizing the collisional and oxygen quenching rates, the near linear dependence of the oxygen quenching rate ($k_Q[O_2]$) on the non-radiative quenching rate (k_{TS0}) is evident in the plot of $k_Q[O_2]$ versus k_{TS0} in Figure II-5b. Except for a single errant datum, the magnitude of $k_Q[O_2]$ varied directly and linearly with k_{TS0} over ~3 orders of magnitude.

The magnitude of the stretching exponent β also varied with temperature in films equilibrated against nitrogen and against air (Figure II-4b). The value of β was constant at ~0.88 in both nitrogen and air over the temperature range from −20 to 10°C and decreased above this temperature. Above 30°C, β was lower in films equilibrated against air than in films equilibrated against nitrogen with the difference generally increasing with an increase in temperature. Since β is a measure of the breadth of the distribution of lifetimes required to fit the intensity decay (Lindsey and Patterson, 1980), the decay kinetics of Ery B in BSA films thus became more heterogeneous with increasing temperature and in the presence of oxygen. Similar trends of β with temperature have been seen for this probe in amorphous sucrose (Pravinata et al., 2005), maltose and maltitol (Shirke et al., 2005), and lactose and lactitol (Shirke, 2005) and for other optical probes in poly-ethylene terphthalate (Teyssedre et al., 2001).

Time-resolved Emission Spectra

Standard techniques to monitor the rate of dipolar relaxation involve direct measurement of the emission spectra as a function of time following excitation (Lakowicz, 1999). For Ery B in BSA films, the phosphorescence emission shifted to higher energy as a function of delay time following excitation (Figure II-6). Such

behavior, which cannot be explained by a homogenous dipolar relaxation model (Demchenko, 2002), has also been seen for Ery B phosphorescence in thin films of amorphous sugars (Shirke et al., 2005) and gelatin (Lukasik and Ludescher, 2006a). In those samples, the behavior was interpreted in terms of a heterogeneous emission model in which Ery B probes reside in distinct sites within the matrix, such that sites with higher emission energy have longer lifetimes (Pravinata et al., 2005).

Phosphorescence intensity decay transients were collected at emission wavelengths ranging from 660 to 720 nm over the temperature range from 0 to 100ºC to test whether a comparable spectral model applies to BSA films. Decay transients at all wavelengths and temperatures were well analyzed by a stretched exponential model. The lifetimes and stretching exponents at each temperature are plotted versus wavelength in Figure II-7a. The lifetime decreased systematically with increasing emission wavelength at all temperatures up to ~60ºC, whereas at higher temperatures the lifetime was either approximately constant with wavelength or exhibited a maximum near the Ery B emission peak at ~685 nm. These trends are essentially the same as those reported in thin films of amorphous sugars (Pravinata et al., 2005; Shirke et al., 2005)ʼ and gelatin (Lukasik and Ludescher, 2006a). In these systems, and in BSA films, the effect of site heterogeneity appeared to dominate over any red shift that may occur due to matrix relaxation around the excited triplet state (Pravinata et al., 2005).

The value of β also varied systematically with emission wavelength (Figure II-7b). The trend of lower β values at higher and lower wavelengths indicated that there was greater dynamic heterogeneity within the intensity decays collected at the red and blue edges of the emission spectrum.

The lifetime decreased with an increase in temperature at all emission wavelengths. The apparent activation energy (E_A) for deexcitation of the triplet state, calculated from the slope of a $\ln(k_{TS0})$ versus $1/T$ curve, also decreased systematically with an increase in emission wavelength at both low (0-20°C) and high (80-100°C) temperature (Figure II-8). Similar behavior has been seen for Ery B in sugars (Pravinata et al., 2005; Shirke et al., 2005a).

Discussion

We have recently shown that phosphorescence from erythrosin B provides information about matrix molecular mobility (Lukasik and Ludescher, 2006b; Pravinata et al., 2005; Shirke et al., 2005; Simon-Lukasik and Ludescher, 2004) and dynamic site heterogeneity (Lukasik and Ludescher, 2006a; Pravinata et al., 2005; Shirke et al., 2005a) in amorphous solid sugars (sucrose, maltose, and maltitol) and in solid gelatin. Ery B phosphorescence was found to be sensitive to both dipolar relaxation around the excited triplet state that lowers the emission energy, and to molecular collisions with the triplet state that lowers the emission intensity and lifetime. In addition, coupling between the rates of dipolar relaxation and molecular collisions within the dynamically complex amorphous matrix gives rise to long-lived dynamic site heterogeneity in which probes in rigid sites have both higher emission energy (slower dipolar relaxation) and longer lifetime (slower molecular collisions), while probes in mobile sites have both lower emission energy (faster dipolar relaxation) and shorter lifetime (faster molecular collisions). Similar phosphorescence behavior for Ery B dispersed within thin dry films of native bovine serum albumin indicates that amorphous BSA exhibits a similar pattern of molecular mobility.

Matrix Molecular Mobility

Because dipolar relaxation stabilizes the Ery B triplet state and lowers the emission energy (Richert, 2000; Stratt and Maroncelli, 1996), the decrease in peak energy with temperature provides direct evidence for an increase in the extent of dipolar relaxation, presumably due to an increase in the dipolar relaxation rate. For Ery B dispersed in a BSA film, dipolar relaxation is primarily due to reorientation of side chain hydroxyl, amino, and carboxyl groups on the surface of BSA. The increase in matrix mobility seen at ~50°C thus appears to reflect an increase in the ability of these groups to reorient around the Ery B triplet state.

Analysis of the photophysical properties of erythrosin (Duchowicz et al., 1998; Lettinga et al., 2000) indicates that the triplet state lifetime decreases with temperature due to thermal activation of the rates of both reverse intersystem crossing to the excited singlet state (k_{TS1}) and collisionally activated non-radiative decay to the ground singlet state (k_{TS0}). k_{TS0}, due to its sensitivity to collisions between matrix groups and the probe, provides an estimate of the overall matrix mobility. The magnitude of k_{TS0} for Ery B in BSA increased moderately at low and more dramatically at high temperature with a transition temperature of ~68°C. This temperature was very close to that detected by emission spectral changes. The activation energy for the motions associated with k_{TS0} was ~0.9 kJ mol^{-1} at low temperature and ~8 kJ mol^{-1} at high temperature. These activation energies are quite similar to those seen for Ery B in amorphous sugars in the glass and melt states, respectively (Pravinata et al., 2005; Shirke et al., 2005; Shirke and Ludescher, 2005), suggesting that comparable molecular motions caused quenching in both amorphous sugars and amorphous BSA. Collisional quenching in BSA thus also

appeared to involve local motions with small activation energy at temperatures below the softening transition and more delocalized, collective motions with larger activation energy at temperatures above the softening transition.

The systematic decrease in the magnitude of the stretching exponent β at higher temperatures indicated that the width of the lifetime distribution also increased with temperature. Some of this increase may be due to the increase in energetic heterogeneity discussed above, due to the dependence of k_{TS1} on the S_1-T_1 energy gap (Equation 5, Materials and Methods); however, given the small increase in bandwidth actually measured, this effect is expected to be minor. The increase in the lifetime distribution, hence, provides evidence for an increase in the distribution of dynamically distinct environments with a range of values for k_{TS0} at higher temperature.

Origin of Dynamical Transition.

Three spectroscopic measures of molecular mobility in BSA films, erythrosin emission energy, emission bandwidth, and emission lifetime, indicate that the protein undergoes a softening transition at ~60°C. There are two possible physical origins for this softening: protein denaturation or protein glass transition.

BSA in these dry films is most likely in the native or near-native conformation because films were prepared from solutions of native BSA at room temperature and because dehydration without freezing or heating steps typically does not lead to significant conformational changes (Hill et al., 2005). BSA in aqueous solution denatures in a two step process, with initial denaturation beginning around 57-60°C (Elysee-Collen and Lencki, 1997; Giacomelli and Norde, 2001; Michnik, 2003; Murayama and Tomida, 2004) and further unfolding occurring at 70-75°C (Michnik,

2003; Murayama and Tomida, 2004). The softening seen in BSA films could thus reflect the initial denaturation process seen in solution. Two lines of evidence, however, argue against this possibility. First, dry proteins are known to have significantly better thermostability than fully hydrated proteins in aqueous solution (Hill et al., 2005) with denaturation temperatures as much as 70°C (Hill et al., 2005). Second, the variation of emission lifetime in the BSA films was found to be reversible upon heating and cooling from 0 to 100°C (Figure II-9); such behavior is not expected for denaturation in the solid phase where entanglements are likely and because Michnik (2003) has demonstrated that thermal scans were not reversible above 60ºC even for aqueous BSA.

Fully hydrated globular proteins are known to undergo a dynamic transition (T_d) at temperatures near 200K. This transition involves a change from a regime where protein motions are dominated by small amplitude, harmonic vibrations of covalently bonded atoms to a regime where large scale, anharmonic, collective motions of non-bonded atoms are also activated (as reviewed in Hill et al. (2005)). This dynamic transition has many of the characteristics of a small molecule or polymer glass transition. Although there are no detailed investigations of how T_d is modulated by water in a manner comparable to how T_g is modulated in less structured polymers, it appears to increase considerably upon dehydration (Tsai et al., 2000). The softening transition seen in BSA at ~60°C may consequently correspond to a glass transition within the native BSA molecules in the film regardless of whether they are in the native state or not. This interpretation is supported by the extensive similarities noted above between the phosphorescence response of Ery B to the effect of heating in amorphous BSA and in amorphous sugars through their glass transition.

Oxygen Permeability

Since the oxygen quenching constant, $k_Q[O_2]$, is the product of terms proportional to both the rate of oxygen diffusion (k_Q) and the thermodynamics of oxygen solubility ($[O_2]$), it reflects the permeability of the protein matrix to oxygen (Simon-Lukasik and Ludescher, 2004). Although $k_Q[O_2]$ does appear to correlate with the permeability determined from the rate of outgassing of oxygen from a gelatin film (Simon-Lukasik and Ludescher, 2004) the exact relation between these properties is unknown in the BSA film, as we have not yet made direct measurements of oxygen transport.

Oxygen quenching was insignificant below 0°C suggesting that there was a threshold temperature for oxygen permeability through the BSA matrix. Above 0°C, however, $k_Q[O_2]$ increased dramatically with temperature with an activation energy of ~30 kJ mol^{-1}, significantly larger than that seen for the rate of collisional quenching, ~1.4 and ~8 kJ mol^{-1} at low and high temperature, respectively (or ~3.1 kJ mol^{-1} averaged over the entire temperature range). Thus, with activation energy ~10-fold larger, the molecular motions underlying oxygen permeability appear to involve significantly more delocalized collective motions of the protein matrix. In part, this difference must reflect the qualitatively different processes that are being monitored: k_{TS0} measures the coupling of vibrational motions in the probe with local vibrational motions in the protein matrix while $k_Q[O_2]$ measures the coupling of translational motion of an oxygen molecule with collective motions of the protein matrix. The linear dependence seen in Figure II-5b, however, provides evidence that the collective motions that facilitate oxygen permeability are modulated in some direct fashion by the modes of local molecular mobility measured by k_{TS0}.

Dynamic Site Heterogeneity

The emission spectra of Ery B in BSA films shifted to higher energy as a function of time following excitation, while the lifetimes decreased systematically with increasing emission wavelength. These data, which are inconsistent with a dipolar relaxation model in which emission spectra shift to lower energy as a function of time and lifetimes increase systematically with increasing emission wavelength (Pravinata et al., 2005; Stratt and Maroncelli, 1996), clearly indicate that probes with longer lifetimes have blue-shifted emission spectra and probes with shorter lifetimes have red-shifted emission spectra. We have interpreted this behavior in terms of a dynamic site heterogeneity model (Demchenko, 2002; Pravinata et al., 2005; Shirke et al., 2005) in which blue-shifted probes in rigid matrix sites have slower rates of both dipolar relaxation and collisional quenching, whereas red-shifted probes in mobile matrix sites have faster rates of both dipolar relaxation and collisional quenching. Because blue-shifted probes also have higher apparent activation energies for collisional quenching than red-shifted probes, the slower molecular mobility at rigid sites may reflect the collective motions of larger regions of the protein matrix.

Conclusions

We have used phosphorescence from the xanthene probe erythrosin B to characterize the molecular mobility and oxygen permeability as a function of temperature in amorphous solid bovine serum albumin films. Analysis of the emission spectrum using a lognormal fitting function provided information on how temperature modulates the emission peak frequency and bandwidth (full-width at half maximum). The peak frequency decreased gradually at low and more steeply at high temperature while the

bandwidth increased gradually at low and more steeply at high temperature, both changes indicating a softening of the protein matrix at ~60°C. Phosphorescence intensity decay transients were well fit using a stretched exponential decay function at all temperatures. Lifetimes decreased gradually at low and more steeply at high temperature. Arrhenius analysis of the rate constant for non-radiative collisional quenching indicated an increase in matrix softening at ~70°C. The oxygen quenching rate was calculated from a comparison of emission lifetimes in the presence and absence of oxygen. This rate varied linearly with the collisional quenching rate over nearly 3 orders of magnitude, suggesting that the more global motions that control oxygen translational diffusion are modulated by more local motions that influence collisional quenching of erythrosin. The emission spectrum shifted to higher energy as a function of time following excitation while the phosphorescence lifetime decreased with increasing emission wavelength; both behaviors provided strong evidence for distinct sites within the protein matrix varying in molecular mobility. These results enrich our molecular understanding of the intrinsic mobility of proteins within the amorphous solid phase, provide evidence for a dynamic transition within solid BSA, and provide insight into the molecular mechanisms controlling oxygen diffusion.

Chapter 2 Figures

Figure II-1. Delayed emission spectra of Ery B in amorphous BSA film as a function of temperature (excitation at 525 nm). The spectra were collected at 10°C intervals from 0 to 100°C (curves plotted from high to low intensity at 685 nm).
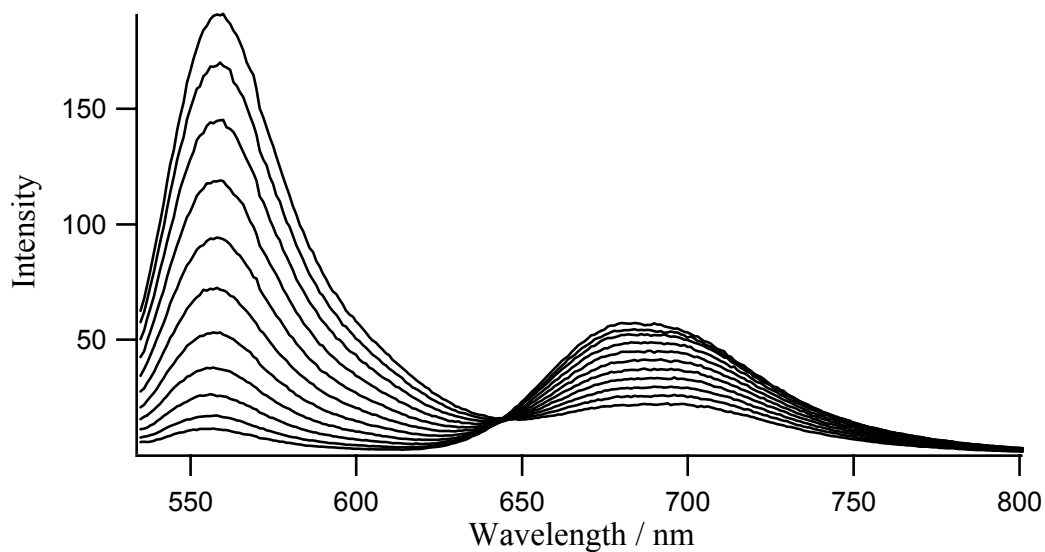
Figure II-2. Peak energy ν_P ($\blacklozenge$, left hand scale) and bandwidth (full-width half maximum) ($\blacksquare$, right hand scale) for phosphorescence emission from Ery B in amorphous BSA film as a function of temperature. The delayed emission spectra collected as a function of temperature (Figure 1) were analyzed as described in Materials and Methods using Equations 1 and 2.
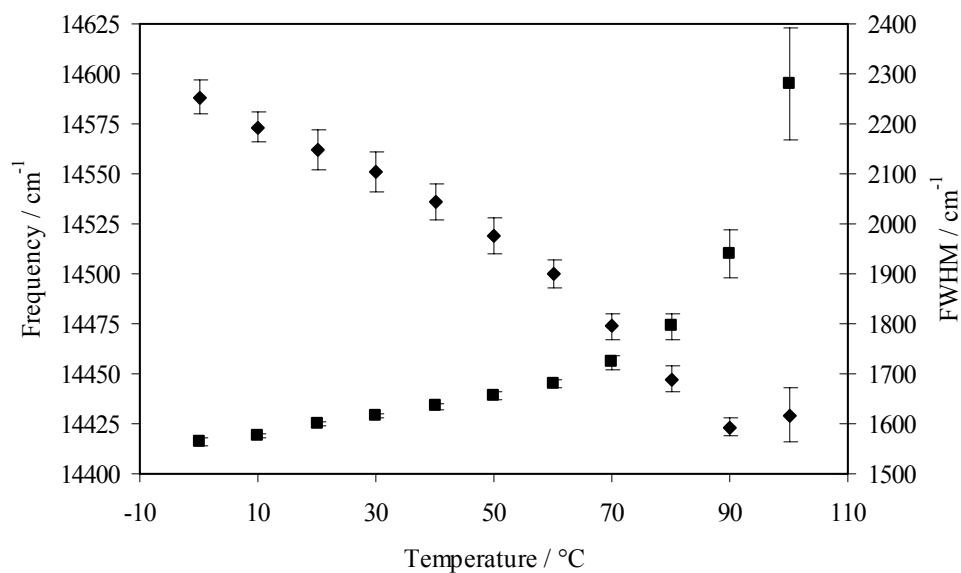
Figure II-3. (a) Normalized phosphorescence intensity decays ($I(t)/I(0)$) of Ery B in amorphous BSA film at 0 °C equilibrated against nitrogen (♦) and against air (■). The solid lines through the data are fits using a stretched exponential model (equation 3, Materials and Methods) with the following parameters: $\tau = 0.61$ ms and $\beta = 0.88$ for data in nitrogen and $\tau = 0.53$ ms and $\beta = 0.87$ for data in air. (b) A plot of the modified residuals $\{(\text{Data-Fit})/\text{Data}^{1/2}\}$ for these fits for the data in nitrogen (dotted line) and air (solid line).

a)
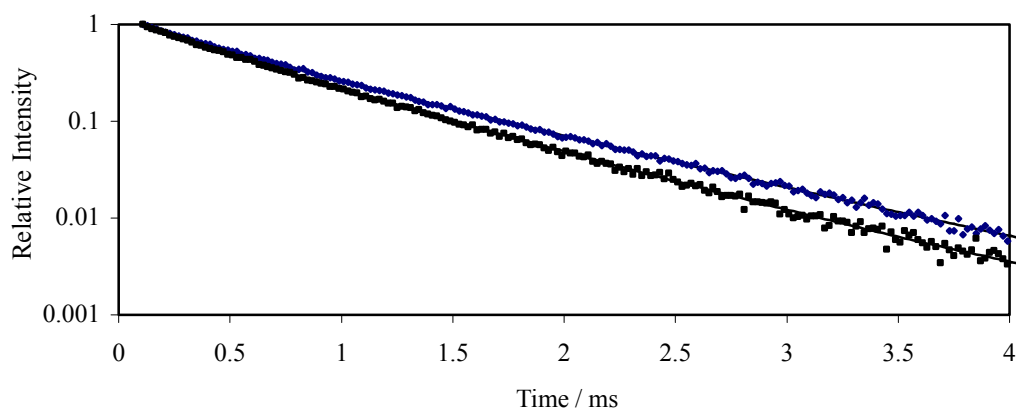
b)
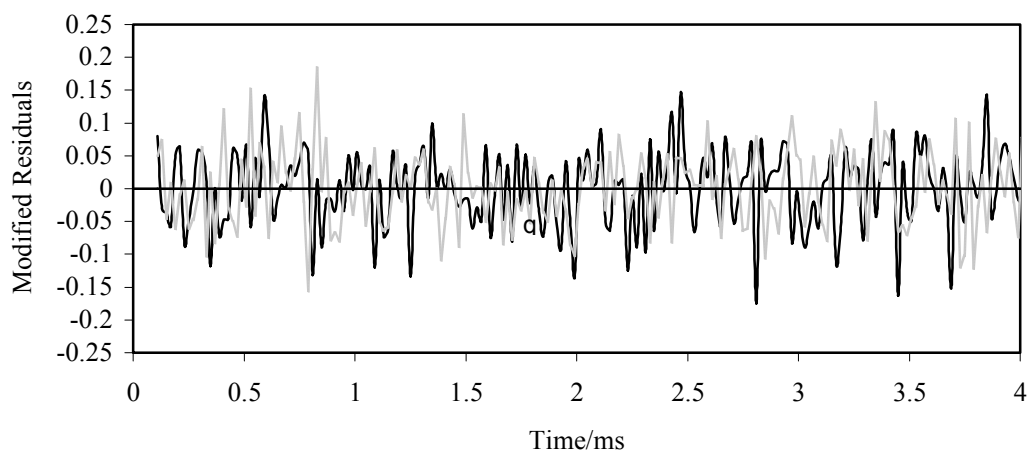
Figure II-4: Lifetimes τ (a) and stretching exponents β (b) from a stretched exponential model fit (Equation 3, Materials and Methods) to phosphorescence intensity decay data from Ery B in BSA films equilibrated against air (♦) and nitrogen (■).

a)
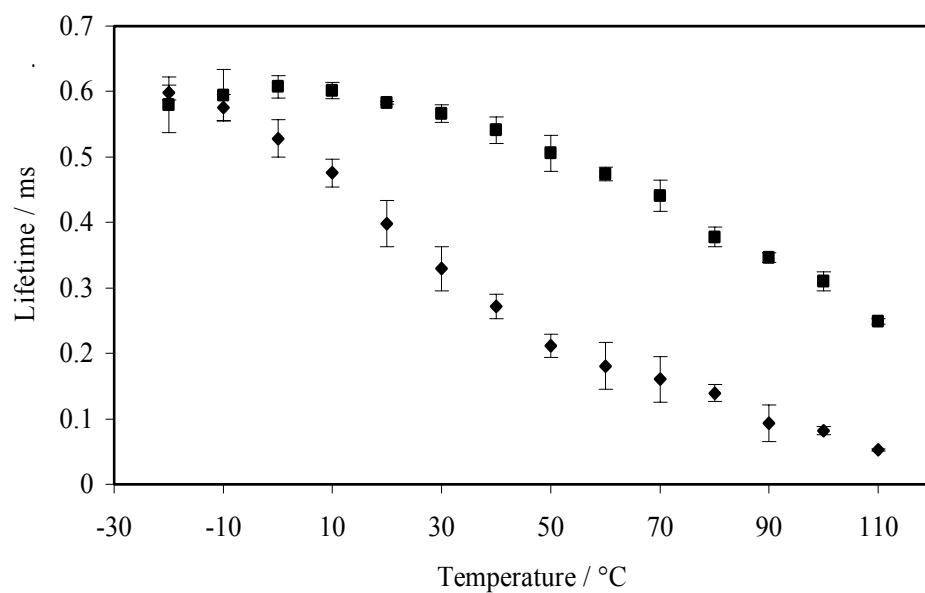
b)
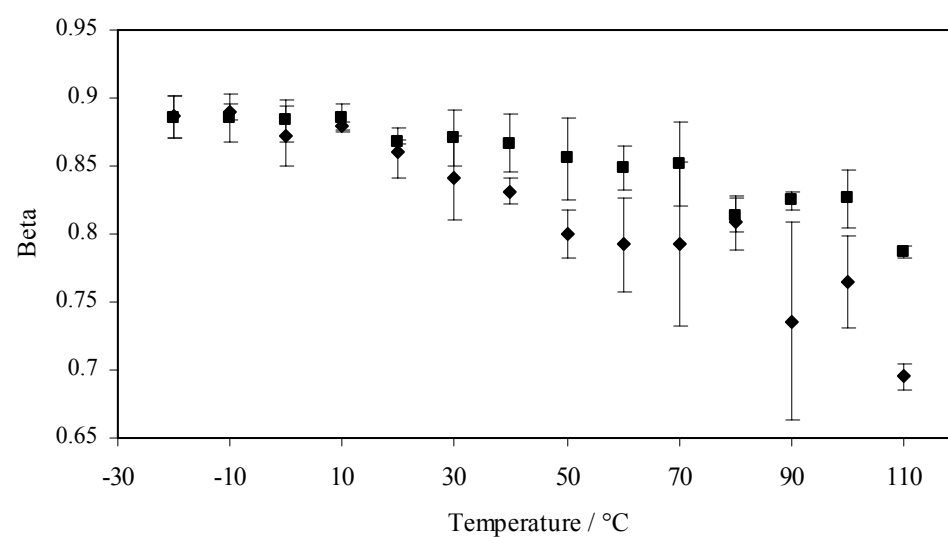
Figure II-5: (a) Arrhenius plot of the temperature dependence of the rates for non-radiative quenching k_{TS0} (■) and oxygen quenching $k_Q[O_2]$ (♦) calculated from the lifetime data in Figure II-4a (see text for details of calculations). (b) Plot of $k_Q[O_2]$ versus k_{TS0}; data from figure II-5a.

a)
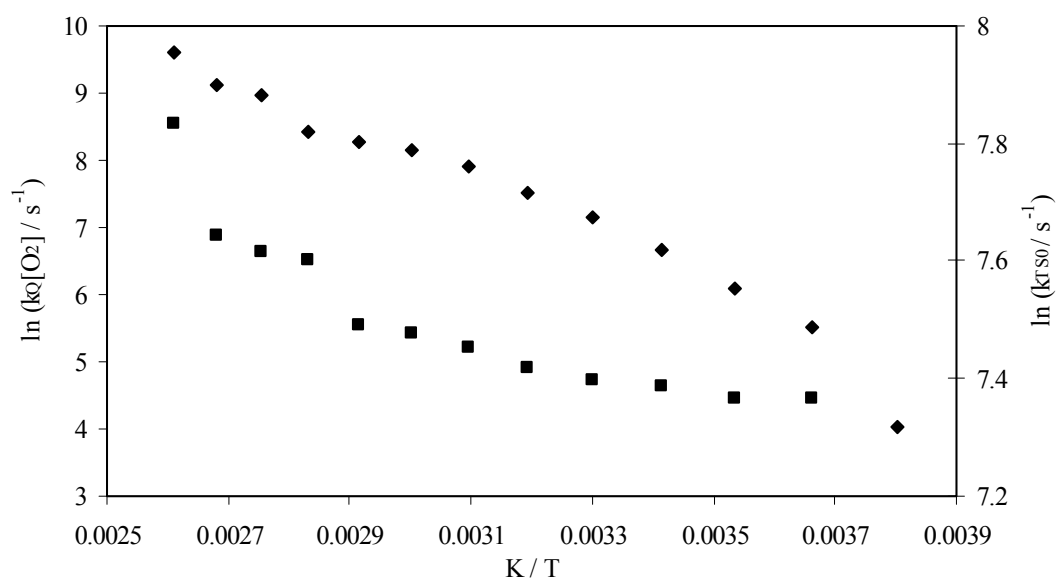
b)
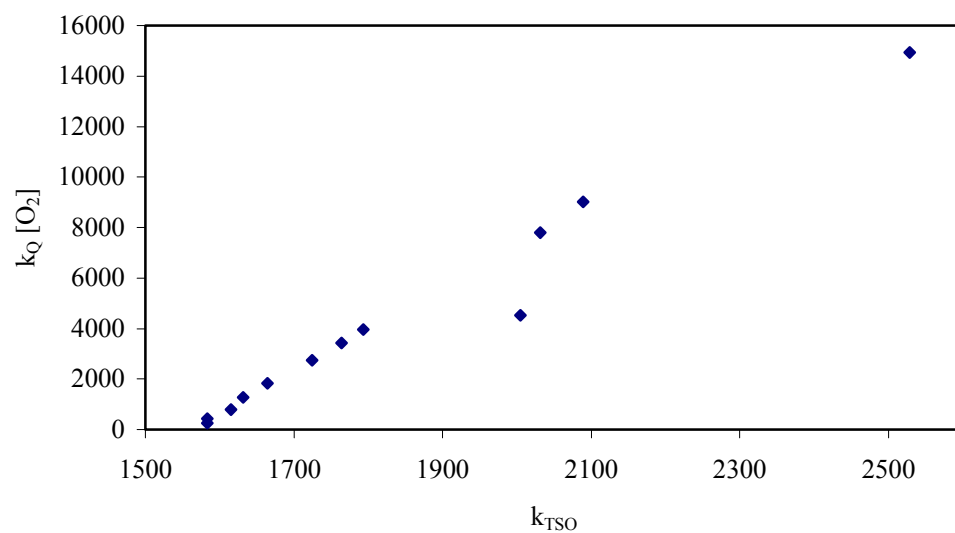
Figure II-6: Effect of delay time on the peak frequency of the phosphorescence emission spectra of Ery B in BSA films at 25ºC (■), 60ºC (▲), and 100ºC (♦) determined from time-resolved emission spectra; peak frequency was calculated from analysis of emission spectra using a lognormal function (Equation 1, Materials and Methods)
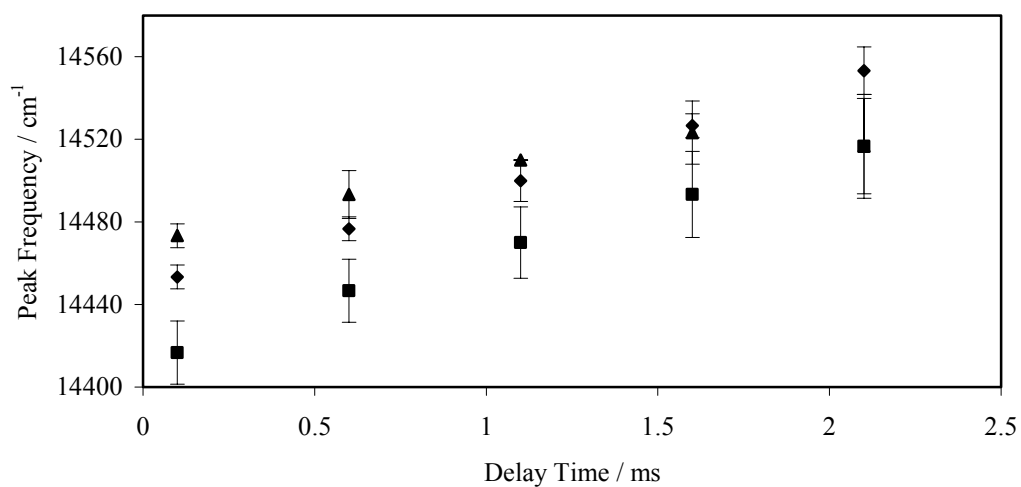
Figure II-7: Lifetimes (a) and stretching exponents (b) from a stretched exponential model fit (equation 3, Materials and Methods) to phosphorescence intensity decay data from Ery B in BSA films collected as a function of emission wavelength with excitation at 540 nm (films equilibrated against nitrogen).

a)
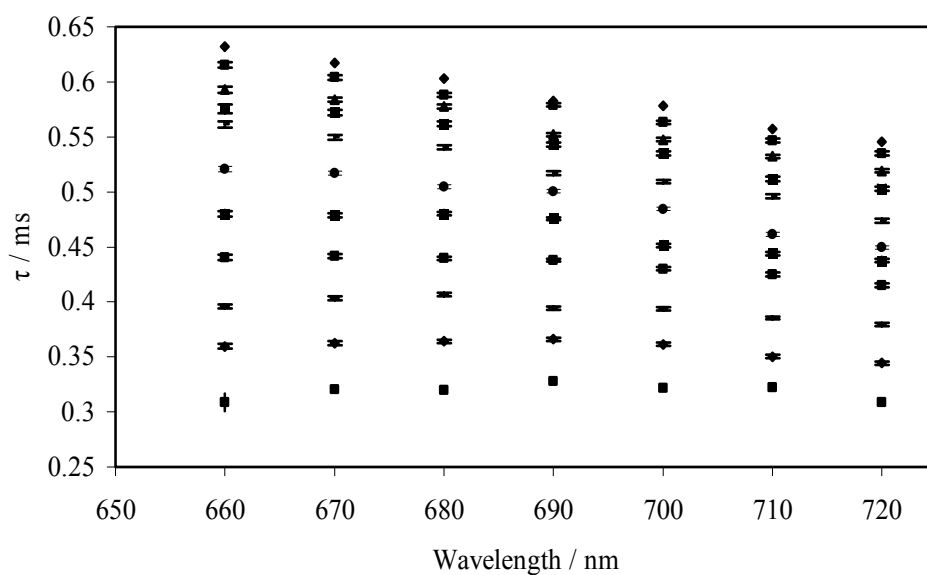
b)
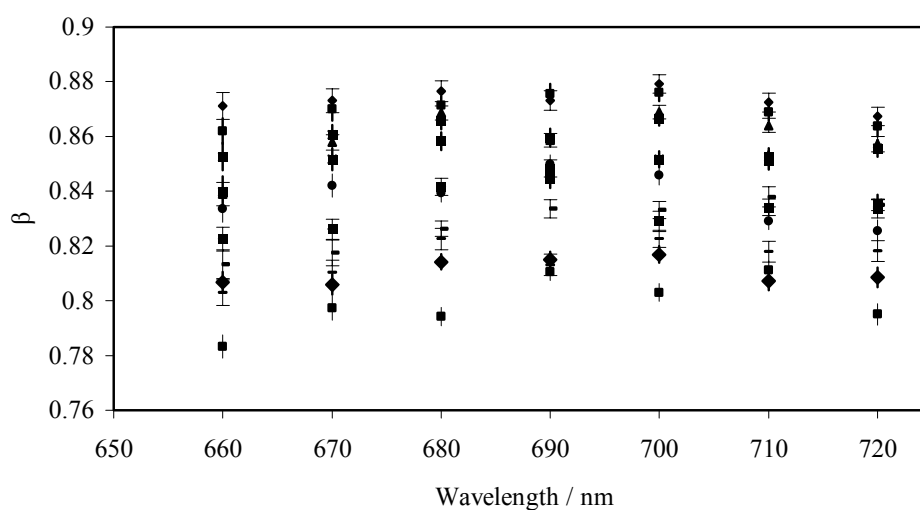
Figure II-8: Activation energies for the non-radiative decay k_{TS0} of Ery B in amorphous BSA at 0-20ºC (■) and at 80-100ºC (♦); the activation energies were calculated from an Arrhenius analysis of k_{TS0} data calculated from the lifetimes in Figure II-7a.
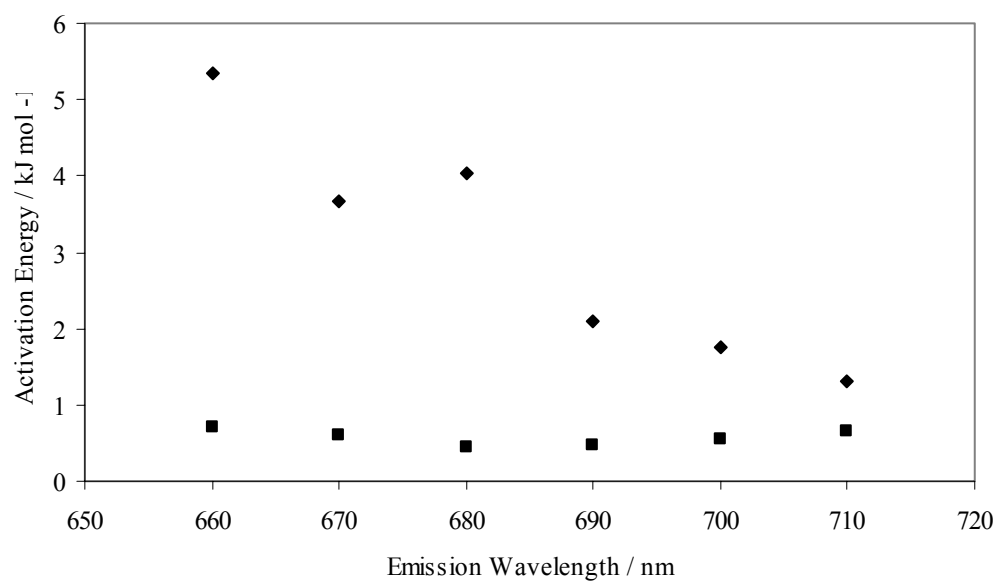
Figure II-9: The emission lifetime in the BSA films over a heating and cooling from 0 to 100°C.
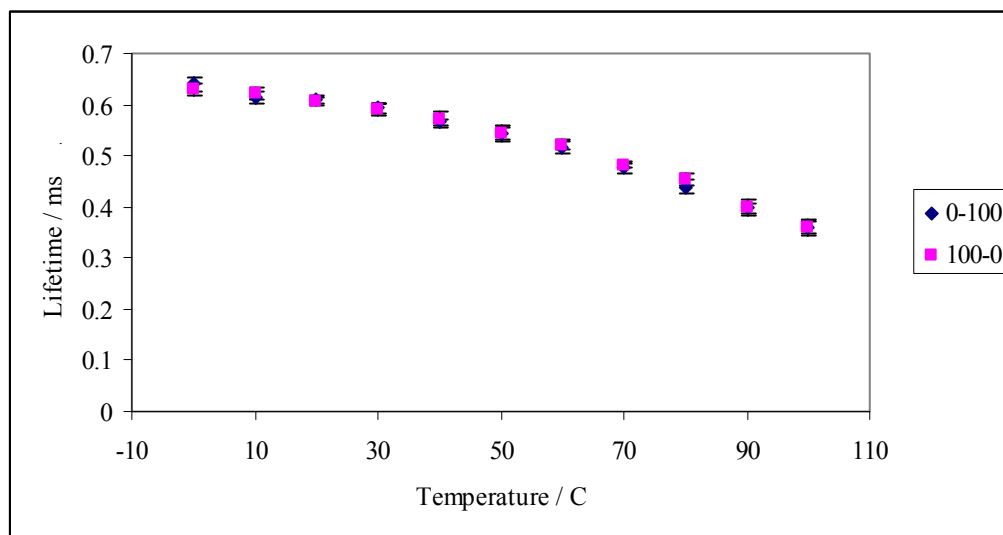
Chapter 2 References

Buitink, J., and Leprince, O. (2004). Glass formation in plant anhydrobiotes: survival in the dry state. *Cryobiology* **48**, 215-228.

Champion, D., Le Meste, M., and Simatos, D. (2000). Towards an improved understanding of glass transition and relaxations in foods: molecular mobility in the glass transition range. *Trends in Food Science & Technology* **11**, 41-55.

Chen, R. (2003). Apparent stretched-exponential luminescence decay in crystalline solids. *Journal of Luminescence* **102-103**, 510-518.

Demchenko, A. P. (2002). The red-edge effects: 30 years of exploration. *Luminescence*, 19-42.

Dong, A. C., Prestrelski, S. J., Allison, S. D., and Carpenter, J. F. (1995). Infrared Spectroscopic Studies of Lyophilization-Induced and Temperature-Induced Protein Aggregation. *Journal of Pharmaceutical Sciences* **84**, 415-424.

Duchowicz, R., Ferrer, M. L., and Acuna, A. U. (1998). Kinetic Spectroscopy of Erythrosin Phosphorescence and Delayed Fluorescence in Aqueous Solution at Room Temperature. *Photochemistry and Photobiology* **68**, 494-501.

Elysee-Collen, B., and Lencki, R. W. (1997). Effect of ethanol, ammonium sulfate, fatty acids, and temperature on the solution behavior of bovine serum albumin. *Biotechnology Progress* **13**, 849-856.

Fasman, G. D. (1989). "Practical Handbook of Biochemistry and Molecular Biology," CRC Press, Boca Ranton, FL.

Ferrer, M. L., Duchowicz, R., Carrasco, B., de la Torre, J. G., and Acuna, A. U. (2001). The Conformation of Serum Albumin in Solution: A Combined Phosphorescence Depolarization-Hydrodynamic Modeling Study. *Biophys. J.* **80**, 2422-2430.

Fischer, C. J., Gafni, A., Steel, D. G., and Schauerte, J. A. (2002). The triplet-state lifetime of indole in aqueous and viscous environments: Significance to the interpretation of room temperature phosphorescence in proteins. *Journal of the American Chemical Society* **124**, 10359-10366.

Garland, P. B. and Moore, C. H. (1979). Phosphorescence of Protein-Bound Eosin and Erythrosin. *Biochemical Journal* **183**, 561-572.

Giacomelli, C. E., and Norde, W. (2001). The Adsorption-Desorption Cycle. Reversibility of the BSA-Silica System. *Journal of Colloid and Interface Science* **233**, 234-240.

Heller, M. C., Carpenter, J. F., and Randolph, T. W. (1997). Manipulation of lyophilization-induced phase separation: Implications for pharmaceutical proteins. *Biotechnology Progress* **13**, 590-596.

Hill, J. J., Shalaev, E. Y., and Zografi, G. (2005). Thermodynamic and dynamic factors involved in the stability of native protein structure in amorphous solids in relation to levels of hydration. *Journal of Pharmaceutical Sciences* **94**, 1636-1667.

Kachalova, G. S., Morozov, V. N., Morozova, T., Myachin, E. T., Vagin, A. A., Strokopytov, B. V., and Nekrasov, Y. V. (1991). Comparison of structures of wet and dry hen egg-white lysozyme molecule at 1.8 A resolution. *FEBS Lett.* **284**, 91-94.

Krochta, J. M., and DeMulder-Johnston, C. (1997). Edible and biodegradable polymer films: Challenges and opportunities. *Food Technology* **51**, 61-74.

Lakowicz, J. R. (1999). "Principles of fluorescence spectroscopy," Second/Ed. Kluwer Academic/Plenum Press, New York.

Lam, S. K., Chan, M. A., and Lo, D. (2001). Characterization of phosphorescence oxygen sensor based on erythrosin B in sol-gel silica in wide pressure and temperature ranges. *Sensors and Actuators B: Chemical* **73**, 135-141.

Lee, K. C. B., Siegel, J., Webb, S. E. D., Leveque-Fort, S., Cole, M. J., Jones, R., Dowling, K., Lever, M. J., and French, P. M. W. (2001). Application of the Stretched Exponential Function to Fluorescence Lifetime Imaging. *Biophys. J.* **81**, 1265-1274.

Lettinga, M. P., Zuilhof, H., and van Zandvoort, M. A. M. J. (2000). Phosphorescence and fluorescence characterization of fluorescein derivatives immobilized in various polymer matrices. *Physical Chemistry Chemical Physics* **2**, 3697-3707.

Lindsey, C. P., and Patterson, G. D. (1980). Detailed comparision of the Williams-Watts and Cole-Davidson functions. *J. Chem. Phys.* **73**, 3348-3357.

Lu, X., Manner, I., Winnik, M.A. (2001). Oxygen diffusion in polymer films for luminescence barometry application. *New Trends in Fluorescence Spectoscopy*, 229-256.

Lukasik, K. V., and Ludescher, R. D. (2006a). Effect of plasticizer on dynamic site heterogeneity in cold-cast gelatin films. *Food Hydrocolloids* **20**, 88-95.

Lukasik, K. V., and Ludescher, R. D. (2006b). Molecular mobility in water and glycerol plasticized cold- and hot-cast gelatin films. *Food Hydrocolloids* **20**, 96-105.

Michnik, A. (2003). Thermal stability of bovine serum albumin DSC study. *Journal of Thermal Analysis and Calorimetry* **71**, 509-519.

Murayama, K., and Tomida, M. (2004). Heat-induced secondary structure and conformation change of bovine serum albumin investigated by Fourier transform infrared spectroscopy. *Biochemistry* **43**, 11526-11532.

Nemkovich, N. A., Rubinov, A. N., and Tomlin, V. I. (1991). "Inhomogeneous broadening of electric spectra of dye molecules in solutions," Plenum Press, New York.

Parker, C. A. (1968). "Photoluminescence of Solutions," Elsevier Publishing Company, Amsterdam.

Pravinata, L. C., You, Y., and Ludescher, R. D. (2005). Erythrosin B Phosphorescence Monitors Molecular Mobility and Dynamic Site Heterogeneity in Amorphous Sucrose. *Biophys. J.* **88**, 3551-3561.

Richert, R. (1997). Evidence for dynamic heterogeneity near T-g from the time-resolved inhomogeneous broadening of optical line shapes. *Journal of Physical Chemistry B* **101**, 6323-6326.

Richert, R. (2000). Triplet state solvation dynamics: Basics and applications. *Journal of Chemical Physics* **113**, 8404-8429.

Richert, R., and Heuer, A. (1997). Rate-memory and dynamic heterogeneity of first-order reactions in a polymer matrix. *Macromolecules* **30**, 4038-4041.

Rupley, J. A., and Careri, G. (1991). Protein hydration and function. *Adv. Protein Chem.* **41**, 37-172.

Shirke, S. (2005a). Molecular Mobility in Amorphous Sugars and Sugar Alcohols as Detected by Phosphorescence of Erythrosin B. M.S., Rutgers, The State University of New Jersey, New Brunswick.

Shirke, S., Takhistov, P., and Ludescher, R. D. (2005b). Molecular mobility in amorphous maltose and maltitol from phosphorescence of erythrosin B. *Journal of Physical Chemistry B* **109**, 16119-16126.

Shirke, S., and Ludescher, R. D. (2005c). Molecular Mobility and the Glass Transition in Amorphous Glucose, Maltose, and Maltotriose. *Carbohydrate Research* **340**, 2654-2660.

Simon-Lukasik, K. V., and Ludescher, R. D. (2004). Erythrosin B phosphorescence as a probe of oxygen diffusion in amorphous gelatin films. *Food Hydrocolloids* **18**, 621-630.

Slade, L., Levine, H., and Finley, J. W. (1989). Protein-water interaction: Water as a plasticizer of gluten and other protein polymers. *In* "Protein Quality and the Effects of Processing" (R. D. Phillips and J. W. Finley, eds.), pp. 9-124. Marcel Dekker, Inc, New York.

Strambini, G. B., and Gonnelli, M. (1985). The indole nucleus triplet-state lifetime and its dependence on solvent microviscosity. *Chemical Physics Letters* **115**, 196-200.

Stratt, R. M., and Maroncelli, M. (1996). Nonreactive dynamics in solution: The emerging molecular view of solvation dynamics and vibrational relaxation. *Journal of Physical Chemistry* **100**, 12981-12996.

Teyssedre, G., Menegotto, J., and Laurent, C. (2001). Temperature dependence of the photoluminescence in poly(ethylene terephthalate) films. *Polymer* **42**, 8207-8216.

Tsai, A. M., Neumann, D. A., and Bell, L. N. (2000). Molecular dynamics of solid-state lysozyme as affected by glycerol and water: A neutron scattering study. *Biophysical Journal* **79**, 2728-2732.

Williams, G., and Watts, D. C. (1970). Nonsymmetrical dielectric relaxation behavior arising from a simple empirical decay function. *Trans. Faraday Soc.* **66**, 80-85.

You, Y. M., and Ludescher, R. D. (2006). Phosphorescence of erythrosin B as a robust probe of molecular mobility in amorphous solid sucrose. *Applied Spectroscopy* **60**, 813-819.

Chapter 3: Oxygen Permeability and Stability of Sucrose/BSA and Trehalose/BSA Mixtures.

<u>*Introduction*</u>

Globular proteins are important in the food and pharmaceutical industries because of their unique functional attributes such as surface activity, enzyme catalysis, film formation, and structure stabilizing aspects. The expression of these functional attributes depends on the molecular structure, chemical environment, and processing history of the proteins (as reviewed by Baier and McClements (2001)). In the food industry, we also have to account for how other ingredients in complex food systems affect the functional attributes of the protein. Understanding protein functionality on the molecular level in food products is a very difficult task due to the compositional, structural, and dynamic complexity in foods, and because of the wide array of stresses introduced during processing (Baier and McClements, 2001). In this study, we employ a novel noninvasive technique using phosphorescence from erythrosin B as an indicator of the mobility, stability, dynamic heterogeneity, and oxygen permeability of the sugar/protein films at the molecular level. This more complicated sugar/protein model system is working towards that of an actual food product, which is the ultimate goal of our luminescent studies.

Sugars can serve as plasticizers, stabilizers, and/or protectants when added to protein solutions or solids (as reviewed by Kaushik and Bhat (2003)). The preserving properties of sugar molecules on proteins against denaturation and dehydration have been known for many years, and as a result sugar/protein mixtures are commonly used in food and pharmaceutical formulations (López-Díez and Bone, 2000). The addition of sugars

can alter the conformation and functional properties of proteins by binding directly to the protein surface, or indirectly, by altering protein structure and physiochemical properties (Baier and McClements, 2001). It is important to focus not only on the stabilizing and protecting effects of adding sugars to protein matrices, but also how the sugars influence protein functionality within the food system.

Sugars protect proteins against loss of activity, chemical and thermal denaturation, and sugars also stabilize native proteins during lyophilization and exposure to high temperatures when in solution. The nature of the interactions of macromolecules and sugars is not well understood, and many different theories have been proposed. One theory is that sugars protect proteins in solution because they are preferentially excluded from the proteins, leaving the protein preferentially hydrated, which in turn makes denaturation or unfolding unfavorable from a thermodynamic standpoint (Carpenter et al., 1988). This generalization is not applicable to proteins in the amorphous or dried states, due to the lack of water to hydrate the protein shell (Carpenter and Crowe, 1989). Carpenter and Crowe (1988) suggested that certain sugars may stabilize dried proteins by serving as a water substitute, when the hydration shell is removed. In this account, they demonstrated that hydrogen bonding occurred between the stabilizing sugar and the dried protein, and also that sugar binding was a prerequisite for preservation of protein structure during drying and rehydration (Carpenter and Crowe, 1988; Mazzobre et al., 1997). Another theory for preservation or stabilization, initially proposed by Green and Angel (1989) and Mazzobre et al. (1997), stated that sugars provide a glassy environment limiting the conformational flexibility of the protein, therefore, reducing the probability that it will unfold. This is supported by the fact that the effectiveness of preservation can

be correlated to the glass transition temperatures of the sugars. Belton and Gil (1994) proposed a mechanism involving the trapping of water on the protein surface in the complex formed by the protein and sugar mixture, but this is generally not widely accepted. Allison et al. (1999) showed through FTIR that the protection mechanism was due to direct hydrogen bonding between the protein and sugar, and not due to the entrapment of water at the protein surface. The extent of hydrogen bonding appears to determine the extent of stabilization, and the formation of an amorphous phase alone is not enough to maintain protein structure during dehydration (Allison et al., 1999). Crowe et al. (1998) have updated their previous theory by stating that hydrogen bonding along with the formation of a glassy matrix is essential for preservation. More research is needed in this area to fully understand what interactions truly control the stabilizing effect sugars have on dried proteins, and luminescent technologies, in respect to molecular mobility, are promising options.

Oxygen Permeability

The aging of polymeric films includes both chemical and physical processes that occur in the matrix after exposure to environmental conditions over a period of time (Anker et al., 2001). The diffusion of oxygen molecules (Guillet, 1985) and temperature are factors that determine the aging of many materials. Increased oxygen permeation may lead to degradation in food systems via microbial growth, enzymatic browning (Fennema, 1996), vitamin degradation, lipid oxidation, and other oxidative reactions (Anker et al., 2001). Oxygen permeability in amorphous protein films increases dramatically with relative humidity (McHugh and Krochta, 1994; Simon-Lukasik and Ludescher, 2004) and temperature (Nack and Ludescher, 2006). The mechanism of the

oxygen molecules' mobility in small disordered amorphous matrices is of great interest, and luminescence methods are the preferred method to study microscopic mobility of oxygen (Korolev et al., 1995). The following study focuses on understanding how the addition of sugars to a model amorphous protein film affects oxygen permeability.

The above discussion was general for sugar/protein stabilizing interactions. Sucrose was chosen because it is the most common food sugar, and there are many high sucrose-containing glassy foods, such as hard candies and cotton candy, similar to the sucrose model system studied in our lab. Trehalose was chosen for its excellent preservation properties and stabilizing effects on proteins in the amorphous and dry states. The molecular interactions of these sugars and protein are of great interest as preliminary model systems for dynamically complex foods, and this study monitors dipolar relaxations, intensity decays, heterogeneity, mobility, and oxygen permeability of these binary systems.

Materials and Methods

Preparation of Amorphous BSA and Sugar Films

Purified bovine serum albumin (BSA) was obtained from Sigma Chemical Company (St Louis, MO) and used as received. In order to define and minimize the presence of counter ions, BSA was dissolved in distilled deionized water at 20 mg/ml, placed in a cellulose dialysis tube having a 12-14 kDa molecular weight cutoff (Spectrum, Houston, TX), dialyzed against 0.1 M potassium chloride for at least 36 hours with frequent changes of buffer, and then dialyzed extensively against distilled deionized water. All dialysis was carried out at room temperature. The solution was then filter sterilized through a 0.2 μm Acrodisc® filter (Pall Gellman Laboratory, Ann Arbor, MI).

The concentration of the protein after dialysis was determined by absorbance at 280 nm using a molar absorptivity of $4.3 \times 10^{-4} \, M^{-1} cm^{-1}$ (Fasman, 1989).

A 10 mg/ml stock solution of erythrosin B free acid (Ery B) (Molecular Probes, Inc., Eugene, OR) was prepared in N, N-dimethlyformamide (DMF) (Sigma-Aldrich, Milwaukee, WI). DMF has shown negligible effects on the spectroscopic properties of the probe in amorphous sucrose at a variety of concentrations (Pravinata et al., 2005). This concentration was selected to simplify the addition of the probe to the BSA solution, and the solvent was selected for probe stability during long term storage. The probe was added to the BSA solution at a molar ratio of 1:10 (Ery B:BSA). At this concentration it was determined that Ery B does not aggregate, existing only as individual molecules monitoring the molecular mobility of the protein.

Sucrose and trehalose solutions were added to solutions of Ery B and BSA at mole ratios of 0.1:1 through 1000:1 (sugar : protein). The amorphous sucrose/BSA and trehalose/BSA films were made by pipetting 15 μL of the solution onto quartz slides (13 mm x 30 mm x 0.6 mm) (Wilmad Lab Glass, Buena, NJ) and spreading the solution over an area approximately 15 mm x 10 mm, similar to the methods of Hurtubise (1997). Before use, to improve the surface activity for spreading the solutions, the slides were soaked in Terg-A-Zyme, washed with Alconox, rinsed with distilled deionized water, and rinsed with ethanol. After spreading, the slides were dried under constant flow of air for 30 minutes, allowing the films to set, and then transferred to a desiccator over phosphorus pentoxide for at least one week (changing the phosphorous pentoxide as needed). Over phosphorous pentoxide the water activity in the desiccator was not greater than 0.01 (Sirotkin and Korolev, 2005). The slides were stored at 23 ± 1ºC protected from light to

prevent any photobleaching of the Ery B probe and desiccant was refreshed as needed to maintain a relative humidity close to 0%.

Probe Information

It is desirable for luminescent probes to have a high absorption coefficient, high quantum yield (Slavic, 1994), and they should be site specific and sensitive to the molecular environment. Phosphorescent probes can directly monitor the rigidity of the local environment (Strambini and Gonnelli, 1985), and this environment can be the interior or surface of a protein (Shah and Ludescher, 1995). Dye molecules are the most sensitive reporters because of their extended π-electron system, strong dispersion interaction with the surrounding environment, very high quantum yields, and their range of long wavelength absorption bands often lies within the range easily accessible to laser spectroscopy (Lesch et al., 2004). Our studies are best suited with a phosphorescent probe. Ery B satisfies all of the previously mentioned requirements and also yields a phosphorescence emission time scale of 10^{-5} to 10^{-3} s corresponding to molecular motions in glassy environments, and has been shown to be a very sensitive oxygen sensor (Lam et al., 2001; Nack and Ludescher, 2006; Sundaresan and Ludescher, 2007). Ery B (tetra-iodofluorescein, FD & C red 3, or cherry red) is perhaps the most widely used phosphorescent probe to assess the molecular mobility of water soluble and membrane bound proteins, due to its large extinction coefficient and high phosphorescence quantum yield (Pravinata et al., 2005). The phosphorescent nature of Ery B is due to the xanthene ring with four iodine molecules. Phosphorescence from the triplet state of the luminescent probe Ery B can provide information about the subsequent relaxations,

oxygen permeability, and dynamic site heterogeneity in the sugar/BSA matrices due to its site specificity and high sensitivity.

Phosphorescence Measurements

To prevent oxygen quenching of the triplet state, a virtually oxygen free nitrogen stream was generated by passing high purity nitrogen through a Supelco carrier gas purifier (Bellfonte, PA). This gas line was routed into the sample compartment and directly into the quartz fluorescence cuvette that held the slide. The cuvette was capped with a lid having inlet and outlet ports for the gas line, thus all experiments were done at constant pressure. The cuvette was flushed for at least 30 minutes to ensure that oxygen was eliminated. The sample compartment was jacketed, and dry air was used to prevent condensation on the slide and cuvette faces when experimental conditions were below room temperature.

Measurements were made on a Cary Eclipse fluorescence spectrophotometer (Varian Instruments, Walnut Creek, CA) equipped with a temperature controller and multi-cell holder. This instrument, which collects in analog mode, uses a high intensity pulsed lamp, and a time delay was used to avoid any fluorescence during the lamp pulse. Phosphorescence and delayed fluorescence emission scans were collected over the range from 535-800 nm with an excitation wavelength of 525 nm. The excitation and emission monochromators were both set at 10 nm band pass. Each data point (collected at 1 nm intervals with a 0.1 s averaging time) was collected from a single flash with a 0.2 ms delay, 0.5 ms gate time, and 4.0 ms total decay time. Excitation scans were collected using the same electronic parameters over the range of 400-600 nm with a 688 nm emission wavelength and both monochromators set at 10 nm.

Lifetime measurements were collected under air or under the nitrogen purge, and the following experimental parameters were the same in both instances. Samples were excited at 540 nm and the emission was measured at 685 nm with a 20 nm band pass for both excitation and emission monochromators. Each time-resolved decay was the average of 40 cycles, and for each cycle data was collected from a single flash with a delay of 0.1 ms, a 0.02 ms gate time, and 4.0 ms total decay time. All experiments were done in at least triplicate, and the standard deviation of the averages was calculated to validate reproducibility. All lifetime experiments were conducted over a temperature range of 0° to 100° C, and the temperature was increased at ten degree increments with a 15 minute delay between readings.

Data Analysis

The emission spectra were analyzed by fitting both the delayed fluorescence and the phosphorescence to a lognormal function.

$$I(\nu) = I_0 \exp\{-\ln(2)[\ln(1+2b(\nu-\nu_P)/\Delta)/b]^2\} \tag{1}$$

In this equation I_0, is the maximum intensity value of the emission spectra, ν_P is the frequency in cm^{-1} of the emission maximum, Δ is the line width parameter, and b is the asymmetry parameter. The bandwidth of the emission, the full width at half maximum (Γ), is related to b and Δ.

$$\Gamma = \Delta \sinh(b)/b \tag{2}$$

Emission spectra were fit using the program Igor (Wavemetrics, Inc., Lake Oswego, OR). We also analyzed some data by fitting with the program Nfit (Island Products, Galveston, TX), to ensure that the results agreed in both fitting programs.

Phosphorescence lifetimes were determined by nonlinear least-squares analysis with the statistical program Igor. Fits were judged satisfactory if the r^2 values were in the range of 0.995-1.0 and the modified residuals ((data – fit)/data$^{1/2}$) varied randomly about zero. Data was analyzed using a stretched exponential, or Kohlrausch-Williams-Watts (KWW), decay model. The stretched exponential model has been shown to be appropriate to describe the wide distribution of relaxation times (Champion et al., 2000) for the molecular process that depopulate excited states in tissues (Lee et al., 2001), crystalline solids (Chen, 2003), super cooled liquids (Richert, 1997), and amorphous protein solids (Nack and Ludescher, 2006; Simon-Lukasik and Ludescher, 2004; Sundaresan and Ludescher, 2007):

$$I(t) = I(0) \exp[-(t/\tau)^{\beta}] + c \tag{3}$$

Where $I(t)$ is the intensity as a function of time following pulsed excitation, $I(0)$ is the initial intensity at time zero, τ is the KWW lifetime, and β is the stretching exponent which characterizes the distribution of the decay times (Richert and Heuer, 1997). Further explanation of the parameters of the stretched exponential equation is provided in the results section.

The phosphorescence lifetime is the inverse sum of the rate constants associated with the various processes that depopulate the excited triplet state.

$$\tau^{-1} = k_P = k_{RP} + k_{TS1} + k_{TS0} + k_Q[O_2] \tag{4}$$

This equation can be used to calculate k_{TS0}, the rate of collisional quenching to the ground state, if k_{RP}, k_{TS1}, and $k_Q[O_2]$ are known. Under anoxic conditions $k_Q[O_2]$, the rate of oxygen quenching, is zero; k_{RP}, the radiative decay rate of the triplet state, is 41 s^{-1} for erythrosin B (Duchowicz et al., 1998; Lettinga et al., 2000); k_{TS1}, the rate of reverse

intersystem crossing from the excited triplet state to the excited singlet state, depends on

ΔE_{TS}, the energy gap between S_1 and T_1 (Simon-Lukasik and Ludescher, 2004):

$$k_{TS1}(T) = k^o_{TS1} \exp(-\Delta E_{TS}/RT) \tag{5}$$

The slope of a Van't Hoff plot (the natural log of the ratio of delayed fluorescence (I_{DF})

to phosphorescence (I_P) intensity versus inverse temperature) provides a measure of ΔE_{TS}

(Duchowicz et al., 1998):

$$d[\ln(I_{DF}/I_P)]/d(1/T) = -\Delta E_{TS}/R \tag{6}$$

(where R = 8.314 J K^{-1} mol^{-1}). Literature values of k^o_{TS1} for erythrosin B vary greatly

depending on the matrix in which the probe was embedded. Calculated values range

from 0.3 x 10^7 s^{-1} in ethanol and 6.5 x 10^7 s^{-1} in water (Duchowicz et al., 1998) to 111 x

10^7 s^{-1} in solid polyvinyl alcohol (Lettinga et al., 2000), demonstrating the large range of

values. The estimated maximum k^o_{TS1} values for Ery B in amorphous sucrose is 3.0 x 10^7

s^{-1} and 4.4 x 10^7 s^{-1} for amorphous BSA.   The estimated maximum possible values for

k^o_{TS1} in the different ratios of sugar to BSA films also varied greatly between ratios

(Table III-1). We assumed that $k_{TS1}(T)$ (calculate using equation 5 with ΔE_{TS} = 33.7 +/-

0.3 kJ mol^{-1} for the sucrose/BSA matrix and 33.5 +/- 0.4 kJ mol^{-1} in the trehalose/BSA

matrix) cannot result in values for $k_{TS0}(T)$ that decrease with temperature. This procedure

thus estimated the minimum possible values for $k_{TS0}(T)$.

Results

Delayed Emission Spectra

The delayed emission spectra for erythrosin B dispersed in the amorphous

sucrose/BSA and trehalose/BSA films as a function of temperature (Figures III-1a and

III-1b) showed similar trends as in an aqueous solution of Ery B (Duchowicz et al., 1998)

and the amorphous BSA matrix (Nack and Ludescher, 2006).   The emission maxima for the sucrose/BSA and the trehalose/BSA matrices are ~560 nm and ~680 nm for delayed fluorescence and phosphorescence, respectively.   The longer wavelength band corresponds to emission from the triplet state (T_1) and the shorter wavelength band is due to delayed fluorescence from the singlet state (S_1), which has been repopulated from the triplet state by the thermally activated process known as reverse intersystem crossing rate (k_{TS1}) (Parker, 1968).   The delayed fluorescence intensities increased with temperature due to the additional thermal energy available to overcome the energy gap between the excited triplet and singlet states (Figure I-9 in Chapter 1).   The delayed fluorescence intensity increase with temperature and the corresponding decrease in phosphorescence intensity occurred because the excited molecules are more likely to experience reverse intersystem crossing from the T_1 to the S_1 state at higher temperatures.

The values for ΔE_{TS} varied throughout the ratios of sugars to protein (Table III-2). $\Delta E_{TS,}$ the energy gap between the T_1 and S_1 states, was calculated from the slope of a Van't Hoff plot of ln (I_{DF}/I_P) vs. 1/T (Equation 6, Materials and Methods) using values for the intensity of delayed fluorescence (I_{DF}) and phosphorescence (I_P) which were determined from a fit of the spectra to a sum of two lognormal functions (Equation 1, Materials and Methods).   These values are shown in Tables III-2a and III-2b, for sucrose/BSA and trehalose/BSA, respectively.   The ΔE_{TS} values and standard deviations were entered into a Student T-Test, and the differences were deemed insignificant between the different ratios of sugar to protein in both the sucrose/BSA and trehalose/BSA matrices.   Consequently, the overall average of the different ratios for each sugar/BSA ratio was used when calculating k_{TS0} for each matrix.   The average

values were 33.7 +/- 0.3 kJ mol^{-1} for the sucrose/BSA matrix and 33.5 +/- 0.4 kJ mol^{-1} for

the trehalose/BSA matrix. These values compare to 32.88 +/- 0.5 kJ mol^{-1} for amorphous

BSA (Nack and Ludescher, 2006) and 31.6 +/- 0.4 kJ mol^{-1} for amorphous sucrose,

indicating that the combination of sugars and protein alter the singlet-triplet energy gap

of Ery B. For reference, the weight percent of sucrose and trehalose is shown in Tables

III-3a and III-3b, respectively.

Peak frequency (ν_P) along with the bandwidth (Γ) were determined by fitting the

emission bands to a lognormal function (Equation 1). Over the tested temperature range

of 0-90°C for the sucrose/BSA matrix the phosphorescence emission energy decreased in

a slightly biphasic manner with a break point around 60°C at all ratios except 1000:1.

The ν_P values ranged from 14680 cm^{-1} at 0°C to 14390 cm^{-1} at 90°C for the sucrose/BSA

matrices. A small change was observed in phosphorescence emission peak frequency

(ν_P) for the protein matrix at lower ratios of sucrose/BSA. For pure BSA and sucrose to

BSA ratios 1:1 and 10:1, the ν_P is essentially constant within error (Figures III-2a and III-

3a). There is a distinct increase in the phosphorescence peak frequency (ν_P) for Ery B

between the ratios of 10:1 and 30:1 sucrose/BSA over the 0-90°C temperature range

(Figures III-2a and III-3a).   The significant increase in ν_P is attributed to decreased

dipolar relaxations at the 30:1 and higher ratios, most likely attributed to slower

vibrational relaxations around the excited state prior to emission along with decreased

probe interactions with the matrix itself (Lakowicz, 1999). At ratios of sucrose/BSA

30:1, 60:1, and 100:1, ν_P is essentially constant, and then another increase was observed

at the 1000:1 ratio. As the ratio of sucrose to BSA increased, the matrix became more

rigid, and hence, surrounding molecules could not relax as easily as when the probe was in a more mobile environment.

The phosphorescence emission energy of the trehalose/BSA matrix followed a similar trend with temperature as observed in sucrose, being slightly biphasic in nature. The v_P values ranged from 14600 cm^{-1} at 0°C to 14415 cm^{-1} at 90°C. The trehalose/BSA matrix had lower frequency values throughout the temperature range (Figure III-2b and III-3b) when compared to the sucrose/BSA matrix. The v_P values in the trehalose/BSA matrix did not increase as a function of the ratio of trehalose to BSA (Figure III-3b) as seen in the sucrose/BSA films, and a distinct gap between trehalose/BSA ratios was not observed for the frequency values. The decrease in v_P at the 1000:1 ratio of trehalose to BSA might be linked to the fact that these samples exhibited noticable phase separation and partial crystallization. Taking into account the error bars of these data, the individual ratios do not seem to be significantly different.

The bandwidth (Γ), or full width at half maximum, for the sucrose/BSA matrices did not exhibit any significant differences between the different ratios of sucrose to BSA until 90°C (Figure III-4a). Although the different ratios were distinguishable at 90°C, a trend between ratios was not observed, with the 100:1 ratio having the highest Γ values and the pure BSA the lowest.

For the different ratios of trehalose to BSA, Γ values did not exhibit any significant differences until reaching 90°C (Figure III-4b). In both binary systems, lower ratios of sugar to BSA had lower Γ values. Γ increased gradually and linearly to ~60°C, and then the increase became more dramatic. The increase in bandwidth is related to an

increase in heterogeneity of the emission energy (Nemkovich, 1991) due to a larger distribution of energetically distinct matrix environments within the sugar/protein films.

Phosphorescence Intensity Decays

The stretched exponential function is appropriate for fitting complex relaxation processes that depopulate the excited triplet state in the millisecond timescales (Richert, 1997). It models the decay of the excited state as an asymmetric distribution of lifetimes (τ) which become more heterogeneous as the stretching exponent (β) decreases from 1 to 0 (1 being completely homogeneous) (Lindsey and Patterson, 1980). These parameters, KWW lifetime (Williams and Watts, 1970) and β (Lindsey and Patterson, 1980), are the physically meaningful aspects of the decay model, and they are highly sensitive to temperature and the molecular environment of the matrix (Chen, 2003; Nack and Ludescher, 2006).

The KWW lifetime values for Ery B in the sucrose/BSA matrix are shown under nitrogen conditions (Figure III-5a) and in the presence of oxygen (Figure III-5b), a known quencher of the triplet state. The lifetimes decreased approximately linearly under nitrogen conditions ranging from 0.69 ms at 0°C to 0.32 ms at 100°C. The decrease in lifetime values was due to an increase in the rate of nonradiative decay of the excited triplet state T_1, more specifically, increases in the rate of intersystem crossing back to the S_1 state (k_{TS1}) and the rate of nonradiative decay of the T_1 state, or collision quenching (k_{TS0}) (Equation 4, Materials and Methods). Lifetime values can be thought of as a measure of the rigidity of the matrix, and it was expected that the 1000:1 ratio of sucrose/BSA would have the highest τ values and the pure BSA matrix would have the lowest τ values. Under both nitrogen and in the presence of oxygen, this exact trend was

not observed, but the data were very close to the hypothesized outcomes. The sugar to protein ratios above 30:1 were among the most rigid (higher τ values), and the ratios below 30:1 were more mobile (lower τ values). Also, when taking into account the error bars, some of the ratios that were out of the expected order (either above or below the 30:1 ratio cutoff) were within error of the expected result.

Examining Figure III-5b, a distinct increase in τ for the ratios of sucrose to BSA above the 30:1 ratio was observed. At ratios of sugar to BSA below 30:1, oxygen was a very active quencher, with a rate constant ($k_Q[O_2]$), of the T_1 state of Ery B. At these ratios, oxygen seemed to penetrate the matrix, and the lifetime values were lower due to the additional collisions of the probe with oxygen molecules.

Plots of the lifetime values for the trehalose/BSA matrices were similar in shape to the sucrose/BSA curves, but did not follow any pattern based on the ratio of trehalose present (Figures III-6a and III-6b), and were slightly lower ranging from 0.63 ms at 0°C to 0.31 ms at 100°C. Under nitrogen conditions, the 1000:1 ratio had the lowest lifetime, and we believe this was because the 1000:1 samples showed partial crystallization when viewed through cross-polarizers, after the samples were equilibrated to the established testing conditions (water content ~0%). The other ratios didn't show a noticeable trend, and considering the error bars, there was not a significant difference among the ratios. The lifetime measurements in the presence of oxygen yielded similar trends to those observed in the sucrose/BSA matrix in the presence of oxygen, with the first significant increase in lifetime values with the addition of trehalose coming at a ratio of 300:1 instead of 30:1, which was observed in the sucrose/BSA matrix.

The stretching factor, or beta values (β), followed similar trends in regards to the ratio of sugars to protein, as observed in the lifetime values. As the beta values decrease, the matrix increases in heterogeneity; or another way to look at it is that there is a broader distribution of lifetimes from an increase in dynamically distinct areas within the matrix. In Figures III-7a and III-8a, the sucrose/BSA and trehalose/BSA values for β in the presence of nitrogen decreased slightly and linearly from ~0.89 to ~0.85 as temperature increased from 0°C to 100°C (excluding the 1000:1 trehalose/BSA data, for reasons discussed previously). This may not seem like a significant increase in the site heterogeneity of the matrices, but even very small decreases in the β values correlate to very large differences in the distribution of lifetimes (Lindsey and Patterson, 1980). In the presence of oxygen, the β values above the break point ratios (30:1 for sucrose/BSA and 300:1 for trehalose/BSA) followed a similar pattern as the β values for all ratios under nitrogen conditions. For ratios of sugars to protein below the break point, the β values were significantly lower in the presence of oxygen as compared to nitrogen conditions (Figures III-7b and III-8b). Under oxygen conditions, the large decrease in β values at higher temperatures and low sugar to protein ratios was probably related to the oxygen molecules ability to penetrate certain parts of the matrix as it softens at higher temperatures. When oxygen is present, there is a broader distribution of lifetime values, as various sites will have different $k_Q[O_2]$ values due to different mobilities at high temperatures. These breakpoints in the lifetime values correlate strongly with the oxygen quenching or oxygen permeability data that will be discussed next.

Phosphorescence Decay Rate Constants

Analysis of the Ery B lifetimes in terms of the underlying photophysical rate constants allows us to calculate the molecular mobility (k_{TS0}) and oxygen quenching or oxygen permeability ($k_Q[O_2]$) of the matrix. These parameters provide additional insight as to what processes are taking place in the amorphous sucrose/BSA and trehalose/BSA matrices. Under nitrogen conditions, the nonradiative decay rates are k_{TS0}, the rate of intersystem crossing from the triplet state to the ground state without the release of a photon, and k_{TS1}, the rate reflecting reverse intersystem crossing from the excited triplet state to the singlet state. k_{RP}, or the radiative rate of phosphorescence for Ery B, is known to be $41s^{-1}$ (Duchowicz et al., 1998; Lettinga et al., 2000). k_{TS1} was easily calculated from the energy gap data between the excited triplet state and singlet state leaving us with the value for k_{TS0}. This calculation is an estimate of the lower limit k_{TS0} based on maximum values of k_{TS1} (see Materials and Methods for more details).

Molecular Mobility

k_{TS0} increased with temperature for all ratios of sucrose to protein (Figures III-9a and III-9b), which was expected since the matrices become more mobile as temperature increases. It was anticipated that as the ratio of sucrose to BSA increased, the k_{TS0} values would decrease due to the increased rigidity of the matrix. This was not the case, and we were unable to draw any correlations between the ratio of sucrose to protein and the matrix mobility, although it was interesting that there was a sharp decrease in k_{TS0} at the 30:1 ratio of sucrose to BSA (Figure III-9b). The error bars included in Figure III-9a were calculated from the proportional errors (as a percentage) in the lifetime data (Figure III-6a). These error bars do not take into account propagation of error in the estimation

for the minimum k_{TS0} values by altering the k^o_{TS1} values to maximize k_{TS1} (Equation 5). This factor acknowledges that the differences between the ratios of sugar to protein might actually be within experimental error, and too much emphasis should not be put on these data besides the fact that molecular mobility increases systematically with temperature for all ratios in the binary systems.

In the trehalose/BSA matrix k_{TS0} values also increased at all ratios as the temperature increased. Unexpectedly, the k_{TS0} values increased as the ratio of trehalose to BSA increased (Figure III-10a and III-10b). The 1000:1 ratio had significantly higher k_{TS0} values (and experimental errors) as compared to the other tested ratios, and this was most likely attributed to the observed phase separation and crystallization.

k_{TS0} was further analyzed by plotting the log of k_{TS0} versus the log molar ratio of sugar to BSA (Figures III-11a and III-11b). These plots provide a better comparison between sucrose and trehalose in regards to their effect on the molecular mobility of BSA films, since the x-axis (ratio of sugar to BSA) is on the same log scale.

Pure BSA (Nack and Ludescher, 2006) and pure sucrose (You and Ludescher, 2006) model systems displayed a biphasic curve for k_{TS0} with a dramatic increase at ~60°C, which was absent in both of the sugar/protein mixtures. The sugar/protein mixtures exhibited linear curves, which were significantly lower in value, as compared to the aforementioned model amorphous BSA (Nack and Ludescher, 2006) and sucrose (Pravinata et al., 2005) films. This suggested that the interactions between sugar and BSA lower the overall molecular mobility of the matrices.

Oxygen Permeability

When calculating the nonradiative rates for Ery B in the presence of oxygen we must account for k_{TS1}, k_{TS0}, and also $k_Q[O_2]$, which describes the collisional quenching of the triplet state by oxygen molecules. Permeability is equal to the rate of diffusion multiplied by the solubility of the gas (P=DS). $k_Q[O_2]$ is proportional to both the rate of oxygen diffusion (k_Q) and the thermodynamics of oxygen solubility ($[O_2]$) (Simon-Lukasik and Ludescher, 2004), hence it reflects the permeability of the sugar/protein matrix to oxygen.

Differences in oxygen quenching between ratios of sucrose to BSA were more apparent at higher temperatures suggesting that temperature was a key component for oxygen permeability through the sucrose/BSA matrix (Figure III-12a). Figure III-12b, however, showed that in the log plot of the rate $k_Q[O_2]$ increased systematically with temperature. The lower ratios of sucrose/BSA and pure BSA matrices, displayed active oxygen quenching. Figures III-12a and III-12b show a distinct decrease in oxygen quenching, or permeability, as the ratio of sucrose to BSA increased from 10:1 to 30:1. At sucrose to BSA ratios above 30:1, oxygen permeability was significantly lower than observed in the lower sucrose/BSA matrices.

In Figure III-13a we observe that the addition of trehalose to the BSA matrix greatly affected $k_Q[O_2]$ values, and also that $k_Q[O_2]$ increased greatly at higher temperatures. A log plot of $k_Q[O_2]$ versus molar ratio of trehalose to BSA displayed a gradual decrease in oxygen permeability as trehalose concentrations increased up until the 100:1 ratio (Figure III-13b). A sharp decline in oxygen permeability was observed between the 100:1 and 300:1 ratio, and oxygen permeability was barley detectable at

ratios above 300:1. Slightly negative values for $k_Q[O_2]$ were calculated at temperatures 20°C and below for the 1000:1 ratio, which are represented as 0 s^{-1}. The negative values are attributed to negligible oxygen quenching of the excited Ery B molecules in the triplet state.

$k_Q[O_2]$ was further analyzed by plotting the log of $k_Q[O_2]$ versus the log molar ratio of sugar to BSA (Figures III-14a and III-14b). This allows for a facile comparison between sucrose and trehalose in regards to their ability to lower oxygen permeability, since the x-axis is on the same log scale. These plots show that between the 10:1 and 30:1 ratio in the sucrose/BSA matrix there is a distinct decrease in oxygen permeability, and in the trehalose/BSA matrix, this trend was noticed between the 100:1 and 300:1 ratios. As explained previously, the 0 s^{-1} rate values in Figure III-14b for temperatures 0-20°C at the 1000:1 ratio were a result of slightly negative values for $k_Q[O_2]$.

Further analysis of the temperature effect on k_{TS0} and $k_Q[O_2]$ was carried out via Arrhenius plots for sucrose/BSA (Figures III-15a and III-15b). From these plots, Activation energies (E_A) were calculated (Figure III-16). E_A for k_{TS0} values increased as sucrose was added. Values ranged from 1.0 kJ mol^{-1} in pure BSA to 2.7 kJ mol^{-1} at the 1000:1 ratio. The E_A values for $k_Q[O_2]$ essentially decreased as the ratio of sucrose to BSA increased, ranging from 48.0 kJ mol^{-1} at 0.1:1 to 12.6 kJ mol^{-1} at 1000:1.

Arrhenius plots for k_{TS0} and $k_Q[O_2]$ in the trehalose/BSA matrices are shown in Figures III-17a and III-17b. E_A values were calculated and are shown in Figure III-18. Very similar to what we observed in the sucrose/BSA matrix, E_A values for k_{TS0} increased ranging from 1.1 kJ mol^{-1} in pure BSA to 2.5 kJ mol^{-1} at the 1000:1 ratio. The E_A values for $k_Q[O_2]$ were essentially constant (35-37 kJ mol^{-1}) from pure BSA through the molar

ratio of 100:1, and then a sharp decrease in activation energy was observed between 100:1 and 300:1. The trehalose to BSA ratios of 300:1, 600:1, and 1000:1 were relatively constant (~21 kJ mol^{-1}).

Oxygen Permeability and Molecular Mobility

Despite the dramatically different E_A values seen between k_{TS0} and $k_Q[O_2]$, there was a direct correlation between oxygen permeability and molecular mobility (except for the sugar dominated matrices) which varied from linear to biphasic (Figures III-19 and III-21). In all cases, however, both parameters increased with temperature. Comparing these plots to amorphous protein model systems, we observed a direct linear dependence of oxygen permeability on molecular mobility in the BSA matrix (Nack and Ludescher, 2006) and a biphasic curve in β-lactoglobulin (Sundaresan and Ludescher, 2007). When the ratios reached 1000:1 sucrose/BSA and 600:1 in trehalose/BSA, there was no longer a direct correlation, mainly because the oxygen permeability values were negligible.

For both the sucrose/BSA and the trehalose/BSA matrices, the slopes for $k_Q[O_2]$ versus k_{TS0} were calculated at high (70-100°C) and low temperatures (0-20°C). In both matrices, we noticed that the slopes for the high temperature range decreased as the ratio of sugar to BSA increased (Figures III-20 and III-22). Also, the high temperature slopes eventually intersected with the low temperature slopes at 100:1 in the sucrose/BSA and 300:1 in the trehalose/BSA matrices, meaning that the higher ratios of sugar to BSA no longer displayed a biphasic trend due to temperature.

Discussion and Conclusions

Previous studies in our lab have focused on the use of novel luminescent techniques utilizing the phosphorescent probe Ery B in model protein and sugar films. In

this study we have applied these luminescent techniques to a more complicated binary system made of sugars and protein. This study aimed to determine the stabilizing and preserving effects of the sugar on the previously studied amorphous BSA film, and also tested the validity of this probe in more complicated model food systems.

Ery B proved to be effective as an indicator of the extent of the dipolar relaxations (lowering frequency values) and collisions around the excited triplet state (lowering intensity and lifetime values), the change in matrix heterogeneity as a function of temperature, and also as a relative measure of the oxygen permeability in the sugar/protein matrix. Similar to the simple model protein matrices tested previously (BSA (Nack and Ludescher, 2006) and β-lactoglobulin (Sundaresan and Ludescher, 2007)), oxygen permeability seemed dependant on molecular mobility. We found specific ratios of sugar to protein where the oxygen permeability was significantly reduced, and eventually thwarted. These data are very useful for understanding oxygen barrier applications in edible films for both the food and pharmaceutical industries.

Gas permeability is an important characteristic for edible films and amorphous foods. Proteins and polysaccharides are thought to be excellent oxygen barriers due to their tightly packed and ordered hydrogen bonded network and low solubility (McHugh and Krochta, 1994). The ease of mass transfer essentially determines the film's barrier properties. The permeability of O_2 and CO_2 through packaging material is traditionally measured using the double chamber gas transmission cell. Such methods have been employed to assess the permeabilities of several types of edible films from polysaccharide, protein, and/or lipid sources (Gontard et al., 1996). Altering conditions to represent the food surface and external package environment allows for direct

measurements of diffusion through freestanding packaging films and other edible films. The gas transmission cell, conversely, can not be used as a direct measurement of diffusion through edible films applied on food surfaces (Simon-Lukasik and Ludescher, 2004) or between food layers. Our research introduces a novel and noninvasive spectroscopic technique to measure O_2 permeability in amorphous food products and also edible films applied to food surfaces. Comparing a probe's lifetime in oxygen and anoxic conditions provides a rapid and simple indicator of the extent of oxygen permeability through the desired matrix (Buettner, 1964). This study shows that as the ratio of sugar to protein increases the oxygen permeability of the matrix decreases. These results aid in the development of edible films designed to provide an oxygen barrier on food or pharmaceutical surfaces.

The sucrose/BSA data showed correlations between the emission energy, lifetimes, and beta values as related to oxygen permeability (in terms of significant trend variations between the 10:1 and 30:1 ratios of sucrose to BSA) over the temperature range of 0-100°C. At the 30:1 sucrose to BSA ratio we saw a distinct increase in emission energies of the Ery B probe, meaning that at this ratio the dipolar relaxations around the probe are less pronounced. The lifetimes, or amount of time that the probe stays in the excited state, also showed a sharp increase at the 30:1 ratio when oxygen was present. We hypothesize that from pure BSA through the 30:1 ratio, oxygen was able to lower the lifetime values due to additional quenching by the oxygen molecules, which indicates much higher oxygen permeabilities at the low sugar ratios. The beta values displayed a distinct increase at ratios 30:1 and above, meaning that the matrix was more heterogeneous at lower sucrose concentrations. These three measured values all correlate

to the break point of decreased oxygen permeability observed in the oxygen permeability data at the ratio of 30:1, but the question that remains unanswered is which measured parameter, if any, is most responsible for the decrease in oxygen permeability at the higher ratios of sucrose to BSA.

The trehalose/BSA matrix did not have such distinct trends as the sucrose/BSA matrix in regards to relationships between the emission energy and calculated oxygen permeability, but similar generalizations were observed between lifetimes and oxygen permeability.   First off, the lifetime data when oxygen was present displayed a drastic increase in values at ratios of 100:1 and 300:1 (the ratios where a noticeable decrease in oxygen permeability was observed). Similar to the sucrose/BSA results, the beta values showed that at 100:1 and below, the matrix was more heterogeneous. So again, the increase in oxygen permeability seems to be directly related to dynamic interactions with oxygen and the matrix at the lower trehalose to BSA ratios, indicated by the lower values for β and τ.

The apparent activation energies for k_{TS0} and $k_Q[O_2]$ as a function of the molar ratio of sucrose/BSA and trehalose/BSA helped us to understand the molecular processes within the matrices. Both matrices displayed significantly higher E_A values for $k_Q[O_2]$ as compared to $k_{TS0.}$ A three fold decrease in E_A values was observed from pure BSA to the 1000:1 ratio of sucrose/BSA (essentially a sucrose matrix). Similar observations were observed in the trehalose/BSA matrix, although the decrease in E_A was two fold, and a sharp decrease was observed between the 100:1 and 300:1 ratio (where we also noticed the drastic decrease in oxygen permeability). We hypothesize that at low sugar to protein ratios the higher E_A values were a direct result of the matrix being composed mostly of

BSA molecules, which are much larger than sugar molecules, requiring more energy to flex or move, allowing oxygen to permeate through the "channels." At the higher ratios of sugar to BSA, the sugar molecules are more tightly packed, hindering oxygen permeability, and requiring less energy (lower E_A) to participate in molecular motions due their smaller size.

Activation energy values for k_{TS0} increased 2-3 fold from pure BSA to the 1000:1 ratios in both of the sugar/BSA matrices. k_{TS0} is a physically different process as compared to $k_Q[O_2]$, and k_{TS0} monitors the various nonradiative relaxations from the triplet to ground state due to collisions between the matrix and the probe. When the matrix is dominated by sugar, the tightly packed nature of the matrix inhibits any large scale motions and also the number of different motions that can take place. The increasing E_A values with increasing ratios of sugar to BSA is most likely due to coupling of vibrational motions. Also, at the higher sugar to BSA ratios, there was less oxygen permeation, which could affect the activation energy values.

Oxygen permeability and molecular mobility were related in both of these matrices, as explained in the results section. These binary systems displayed both linear and biphasic correlations between k_{TS0} and $k_Q[O_2]$ depending on the ratio of sugar to protein, with no obvious explanation as to why this shift occurred. We are unable to draw any conclusions between ratios within each sugar/protein mixture for k_{TS0}, hinting that k_{TS0} might not directly correlate to molecular mobility in more complex binary systems, as compared to the previously studied model amorphous systems of amorphous BSA (Nack and Ludescher, 2006), sucrose (Pravinata et al., 2005), and β-lactoglobulin (Sundaresan and Ludescher, 2007). k_{TS0} values were highly dependent on the k^o_{TS1} value

for the given ratio of sugar to BSA. Remembering that we calculated the value of k^o_{TS1} to be the maximum value where k_{TS0} still increased with temperature (giving minimum values for k_{TS0}), we noticed that our final k_{TS0} values were very sensitive to the precision of this calculation (the gap between the two closest lifetime data points with increasing temperature controls the k^o_{TS1}, and if the lifetime values were very close between temperature increments, a low k^o_{TS1} and a high k_{TS0} was observed). The aforementioned relationship between k_{TS0} and k^o_{TS1} introduced large systematic errors in the calculation, and we thus need to find a method for the direct measurement of k^o_{TS1} when comparing ratios for binary systems. Interestingly, the values of k^o_{TS1} increased as the ratio of sugar to protein increased, leading us to believe that the addition of sugars favor reverse intersystem crossing from the excited triplet state back to the singlet state.

Trehalose is known to be the most effective carbohydrate in terms of protection of proteins during dehydration and storage (Leslie et al., 1995). Many studies have been conducted to investigate the properties that make trehalose superior to other carbohydrates in its stabilizing ability, and the mechanism is still not fully understood. Green and Angel (1989) and Kaushik and Bhat (2003) believe that the superiority is a direct consequence of trehalose having the highest T_g among tested sugars. This, however, can not be the sole reason, because recent studies have shown that compounds with much higher T_g values such as maltodextrin and poly-(vinyl)pyrrolidone, have less of a stabilizing effect on membranes and proteins (Crowe et al., 1994; Mazzobre et al., 1997). As stated earlier, it is proposed that both hydrogen bonding and the glassy state are responsible for stabilization (Sun and Davidson, 1998). Aldous et al. (1995) suggested that superior stabilizing ability of trehalose might be due to its ability to form

hydrate crystals at temperatures above T_g, thus reducing the initial moisture contents of the remaining amorphous phase and preventing the formation of a full crystalline matrix. This proposed mechanism is thermodynamically favorable, but kinetically slow due to the low molecular mobility in the amorphous state, and more studies need to be conducted to verify this hypothesis (Miller et al., 1997). Crowe et al. (1996) made a similar argument by showing that the formation of trehalose dihydrate crystals sequester water (in a mixture with liposomes), which might otherwise participate in lowering the T_g to below ambient temperatures, decreasing the stability of the system.

The T_g of trehalose (T_g ~106ºC; Roe and Labuza, (2005)) is 20-40ºC higher than that of sucrose. This alone corresponds to an increase of 2-3 orders of magnitude in the stability of biomaterials, and a decrease of 4-6 orders of magnitude in the rates of relaxations according to Williams-Landel-Ferry kinetics (as reviewed by Sun and Davidson (1998)). Below T_g, the free volume of an amorphous solid is reduced, which limits the diffusion of molecules (Miller et al., 1997), thus showing that the stability of protein/carbohydrate glasses depends largely on molecular mobility (Yoshioka et al., 1997). Trehalose glasses have also shown a greater ability to resist phase separation and crystallization when compared to other disaccharides, which is probably due to restricted molecular motions (Sun and Davidson, 1998).

As reviewed above, in many studies trehalose has proven to be the exceptional disaccharide stabilizer of dried proteins, although the exact mechanism is still up for debate among the authors. This study, on the contrary, displayed sucrose as the more effective stabilizer of sugar/BSA systems, at least in regards to thwarting oxygen permeability at lower ratios of sugar to protein. This specific study gives us additional

insight as to what processes might be responsible for lowering oxygen permeability in the sucrose/BSA system. Sun and Davidson (1998) reported trehalose to have the highest potential for hydrogen bonding of disaccharide sugars to biomaterials, however, there is no clear correlation between preservation of biomaterials and the type and number of hydrogen bonds.

Allison et al. (1999) found contrasting results using IR, where sucrose was more effective than trehalose in stabilizing native lysozyme through direct hydrogen bonding between the protein and sucrose. Another study provided evidence that even under evaporation drying methods, ~3% water was still "trapped" in the mixtures of trehalose and sucrose with β-lactoglobulin (López-Díez and Bone, 2000). This is important to note because another study by Lins et al. (2004) showed that when trehalose was introduced to lysozyme, the trehalose molecules moved toward the protein, but then clustered and did not preferentially exclude the water surrounding the protein, or more importantly, hydrogen bond to the protein, and instead, hydrogen bonded to each other leading to crystallization. Furthermore, sugars in the presence of water have a lower ability to form intermolecular sugar to sugar hydrogen bonds "quickly" (required for amorphous systems) since hydrogen bonding with water is more prevalent in crystalline forms thus leading to crystallization and phase separation (López-Díez and Bone, 2000), which we observed in the trehalose/BSA matrix at ratios over 600:1. Crystallization and phase separation, or cracking, (monitored via a Labophot-2 high magnification microscope equipped with a Martin Microscope Company MM99 adaptor and a Nikon Coolpix 5700 high resolution camera) was not observed in the sucrose/BSA matrix. Therefore, this might be a key indicator that the phase separation at the higher ratios of trehalose to BSA

may be responsible for the increased oxygen permeability as compared to the sucrose/BSA matrix, since there is no interaction between proteins and sugars when sugar crystals are present (López-Díez and Bone, 2000).

Phase separation and crystallization lead to dramatic changes in the composition of the remaining amorphous regions, resulting in higher local moisture contents (Sun and Davidson, 1998), which also may lead to increased oxygen transport in the trehalose/BSA films. More studies are needed which focus on phase separation, and the possible reason for the previous lack of studies might be due to the experimental limitations for detecting phase separation in amorphous globular proteins (Hill et al., 2005).

Differential scanning calorimetry (DSC) has been used as the main method to detect the formation of two distinct amorphous phases by means of the observation of two glass transitions. The glass transition thermal event in protein rich dispersions is usually very weak, and therefore, is not easily detected by DSC (Hill et al., 2005).

The chemical nature of the sugar may play a crucial role in phase separation. Hydrogen bonding in a model sucrose/polyvinylpyrrolidone mixture appeared to be greater than in other sugars such as trehalose, maltose, lactose, raffinose, and maltodextrin (Taylor and Zografi, 1998). The more effective hydrogen bonding between sucrose/polyvinylpyrrolidone resulted in better mixing and less of a tendency for these sugars to form two separate amorphous phases (sugar rich and protein rich) (Taylor and Zografi, 1998). If indeed, there are correlations between protein/sugar hydrogen bonding, the tendency for phase separation, and mixture stability, the overall stability of the mixtures would show the sucrose/polyvinylpyrrolidone mixture to be the most stable (Hill et al., 2005). Sucrose has also been shown to be a more effective stabilizer,

compared to trehalose, of the native structure of lysozyme during freeze drying (Allison et al., 1999). Indirect evidence of a strong tendency for sucrose to form a single amorphous protein/sugar phase has been obtained from studies of the crystallization of glycine, where freeze concentrated sugar/glycine systems showed almost complete crystallization when the sugar was trehalose or raffinose, whereas glycine remained mostly amorphous in the sucrose system (as reviewed by Hill et al. (2005)). Based on these observations, it is possible that there is a greater tendency for the trehalose/BSA mixtures to separate phases when compared to the sucrose/BSA systems.

The decrease in oxygen permeation with the addition of sugar to the amorphous BSA matrix may have been due to lower oxygen solubility or adsorption in sugar/BSA matrices. From our data we would conclude that the sucrose/BSA matrix was less soluble to oxygen. Sothorrvit and Krochta (2000) linked the excellent oxygen barrier properties of sucrose in β-lactoglobulin films to low hygroscopicity during drying and the bulky ring structure which slows migration and crystallization. The size and structure of sucrose prevents the disruption of the hydrogen bonding network between protein chains, thus lowering permeability. Sucrose molecules may also obstruct oxygen permeation due to their preferential intermolecular bonding with each other (Sothorrvit and Krochta, 2000). Sucrose was also the least effective plasticizer of the studied β-lactoglobulin films, having a more rigid and possibly less permeable matrix compared to the other sugars studied (Sothorrvit and Krochta, 2000).

Other arguments for sucrose as an effective stabilizer of proteins include that it has shown promise as a protectant by increasing the T_d (sucrose's preferential interactions with the native state are thermodynamically favored to that of the denatured state) and

increasing the overall viscosity (Baier and McClements, 2001; Baier and McClements, 2003, 2006). Baier and McClements (2006) showed that increasing the sucrose percentage in BSA solutions increased the thermal denaturation temperature and final gel strength. These findings were attributed to increasing the thermal stability and attraction between globular BSA molecules through the steric exclusion effect, due to the protein trying to minimize interaction with the solvent. Interestingly, the T_g and crystallization temperature of amorphous sucrose increased with the addition of BSA, which suggests that proteins may also aid in the stabilization of amorphous sucrose (Imamura et al., 1998).

From these studies we were able to characterize molecular mobility and oxygen permeation in the sucrose/BSA and trehalose/BSA matrices, and we were successful in relating oxygen permeability to molecular mobility as a function of the ratio of sugar to BSA. Adding sugars in ratios ranging from 0.1:1 sugar/BSA to 1000:1 sugar/BSA, we generated very promising results, showing that the oxygen permeability is inversely related to the amount of sugar in the sample. The amorphous sugar/BSA matrix, as compared to pure BSA, most likely experiences an increased viscosity and/or reduction in free volume, which may be responsible for the reduction in molecular mobility as compared to pure BSA, and thus the lack of oxygen permeability above the 30:1 and 300:1 ratios of sucrose/BSA and trehalose/BSA, respectively. The addition of sugar to the amorphous BSA matrix may also lower the oxygen solubility or adsorption of the matrix, thus increasing barrier properties in regards to oxygen. This information is useful in designing edible films aimed at reducing the permeability of oxygen, which in turn reduces many degradative processes in foods.

Chapter 3: Tables and Figures

Table III-1: The estimated maximum k^o_{TS1} values for Ery B in amorphous sucrose/BSA (a) and trehalose/BSA (b) based on calculations explained in Equation 5 (Materials and Methods).

a)

Ratio Sucrose/BSA	Estimated k^o_{TS1}
Pure BSA	$5.9 \times 10^7\ s^{-1}$
0.1:1	$6.4 \times 10^7\ s^{-1}$
1:1	$6.5 \times 10^7\ s^{-1}$
10:1	$5.6 \times 10^7\ s^{-1}$
30:1	$5.0 \times 10^7\ s^{-1}$
60:1	$4.6 \times 10^7\ s^{-1}$
100:1	$4.0 \times 10^7\ s^{-1}$
1000:1	$1.5 \times 10^7\ s^{-1}$

b)

RatioTrehalose/BSA	Estimated k^o_{TS1}
Pure BSA	$6.3 \times 10^7\ s^{-1}$
1:1	$6.5 \times 10^7\ s^{-1}$
10:1	$6.1 \times 10^7\ s^{-1}$
100:1	$5.7 \times 10^7\ s^{-1}$
300:1	$4.5 \times 10^7\ s^{-1}$
600:1	$4.7 \times 10^7\ s^{-1}$
1000:1	$4.8 \times 10^7\ s^{-1}$

Table III-2: Calculated ΔE_{TS} values, the energy gap between S_1 and T_1, and the standard deviations which were entered into the Student T-Test for erythrosin B embedded in the sucrose/BSA (a) and trehalose/BSA (b) matrices.

a)

Sucrose

Ratio of Sucrose : BSA	ΔE_{TS} (J)	STDEV
Pure BSA	33480	737
0.1:1	33734	444
1:1	34186	535
10:1	33759	609
30:1	33878	441
60:1	33301	472
100:1	33865	173
1000:1	33226	762
Overall Average	33679	322

b)

Trehalose

Ratio of Trehalose : BSA	ΔE_{TS} (J)	STDEV
Pure BSA	33480	737
1:1	34176	452
10:1	33597	235
100:1	33685	804
300:1	33536	127
600:1	33135	226
1000:1	33159	462
Overall Average	33538	351

Table III-3: Matrix composition for the studied molar ratios of sucrose to BSA (a) and trehalose to BSA (b).

a)

Molar Ratio of Sucrose:BSA	Weight % Sucrose
0.1:1	0.05
1:1	0.5
10:1	5.2
30:1	13.4
60:1	23.5
100:1	34.0
1000:1	83.7

b)

Molar Ratio of Trehalose:BSA	Weight % Trehalose
1:1	0.5
10:1	5.2
100:1	34.0
300:1	60.7
600:1	75.5
1000:1	83.7

Figure III-1: Delayed emission spectra of erythrosin B in amorphous Sucrose/BSA (a) and Trehalose/BSA (b) (ratios 100:1) films as a function of temperature (excitation at 525 nm). The spectra were collected at 10°C intervals from 0 to 100°C.

a)
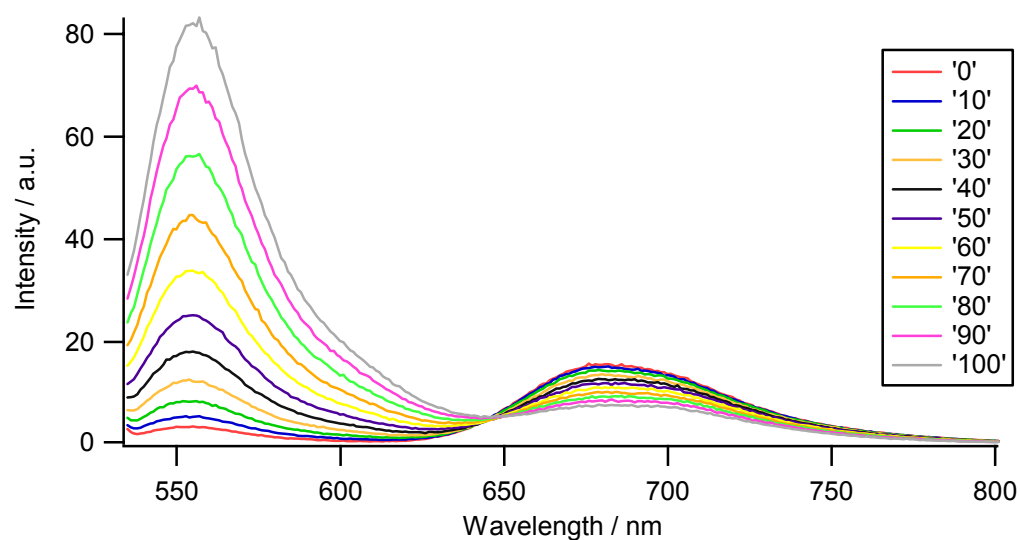
b)
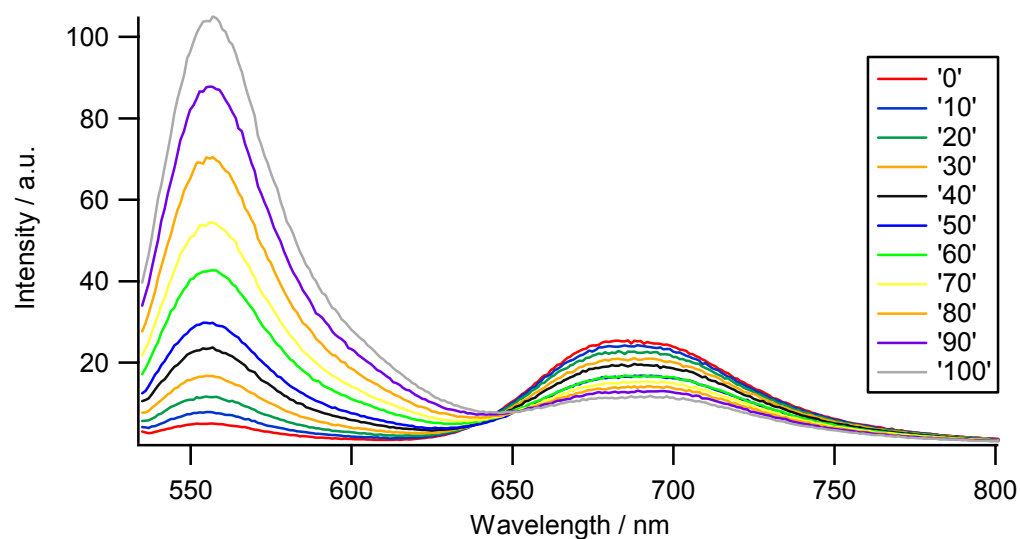
Figure III-2: Peak energy (v_P) for sucrose/BSA (a) and trehalose/BSA (b) ratios for phosphorescence emission from erythrosin B as a function of temperature.

a)
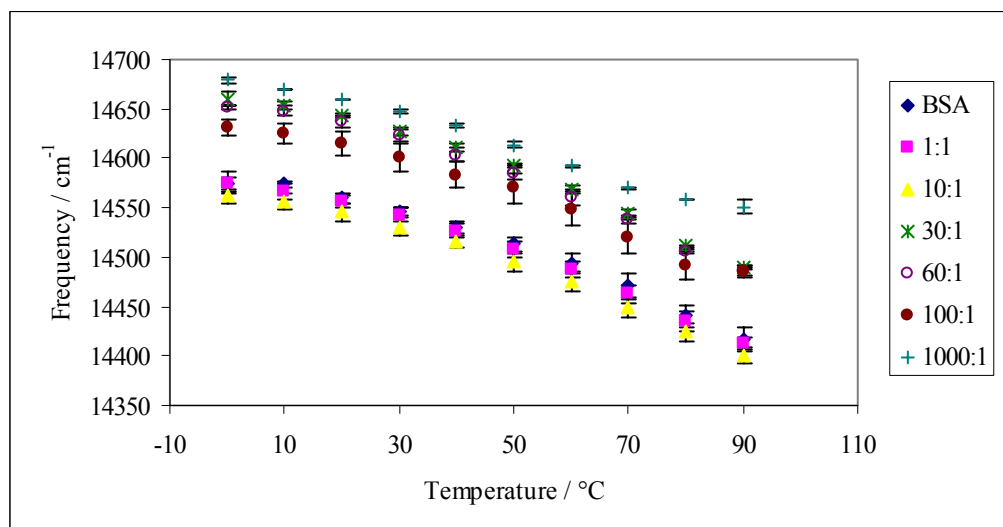
b)
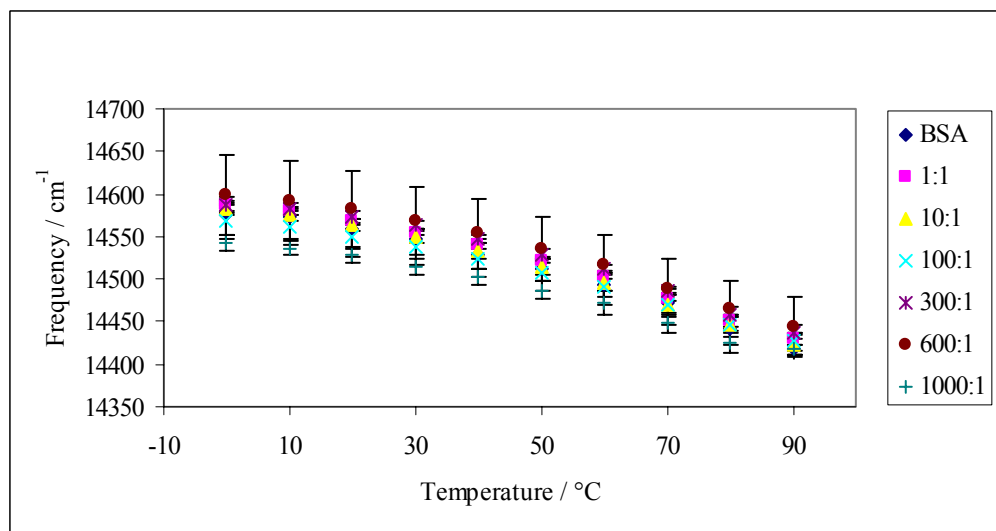
Figure III-3: Plots of ν_P versus ratio of sucrose to BSA (a) and trehalose to BSA (b).

a)
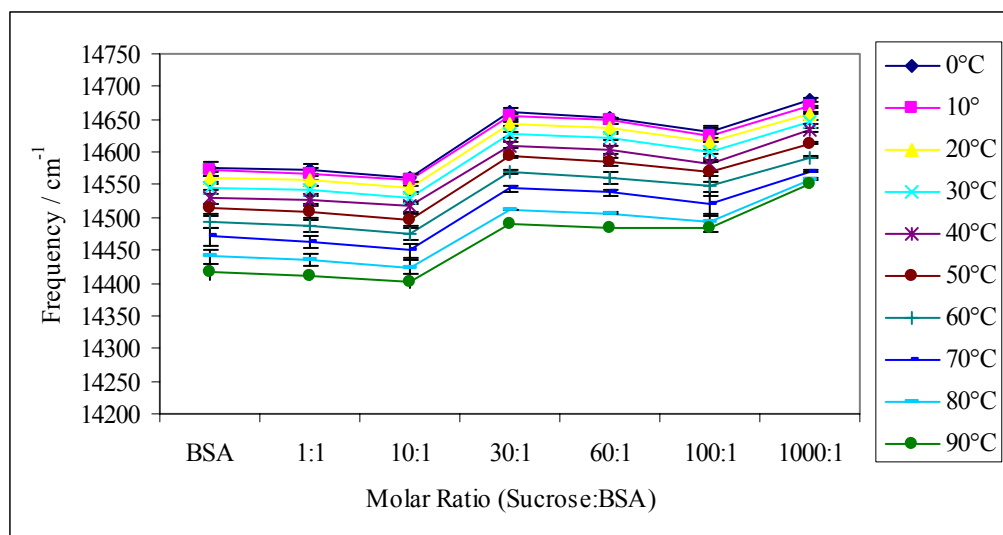
b)
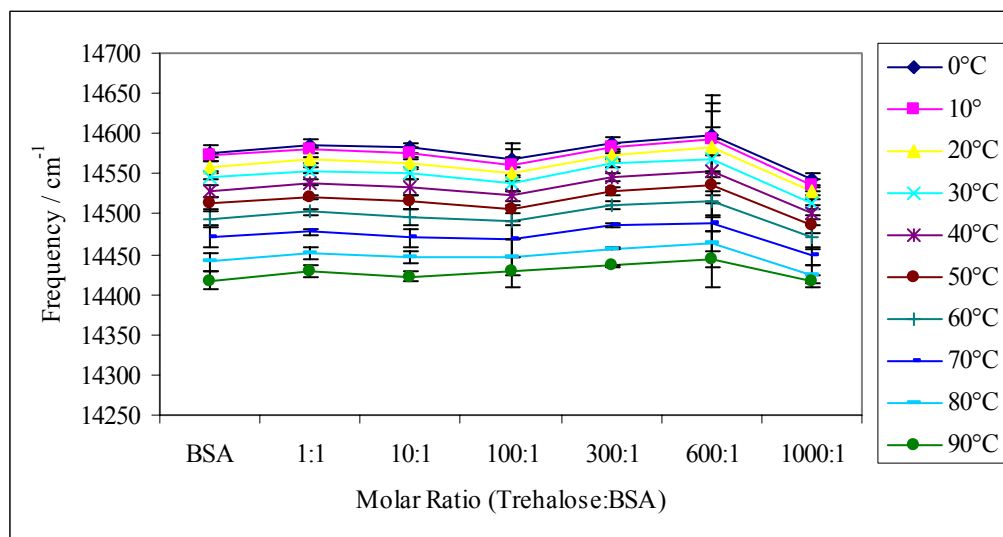
Figure III-4: Bandwidth or full width at half maximum for sucrose/BSA (a) and trehalose/BSA (b) ratios for phosphorescence emission from erythrosin B as a function of temperature.

a)
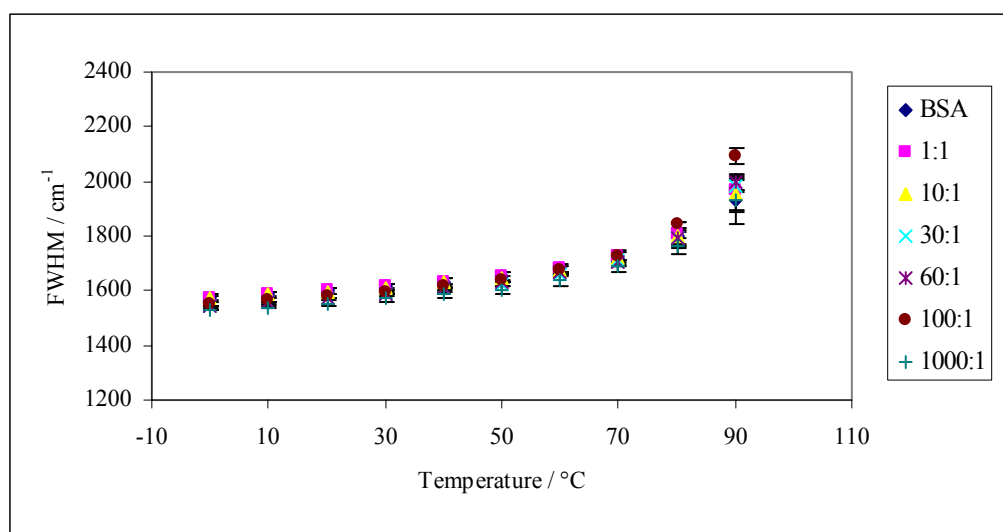
b)
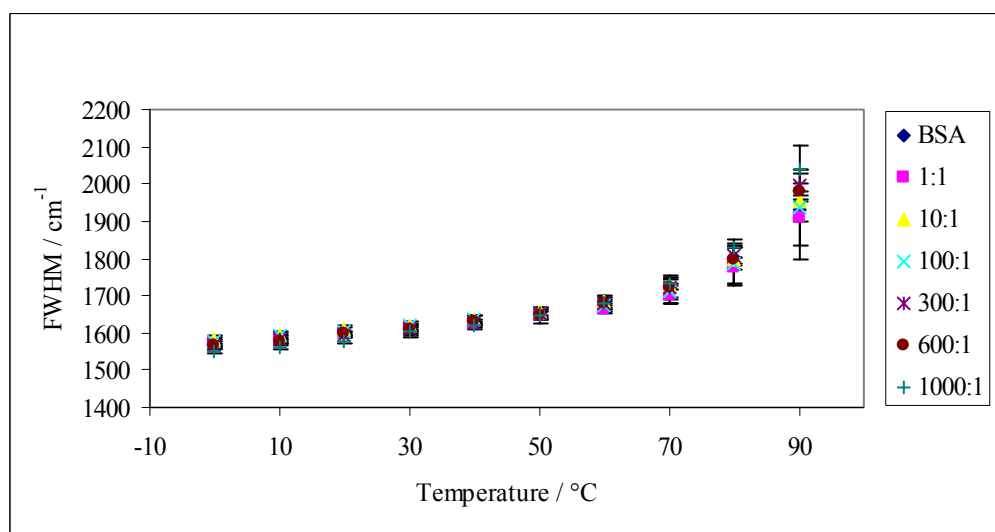
Figure III-5: Lifetimes equilibrated against nitrogen (a) and air (b) from a stretched exponential model fit to phosphorescence intensity decay data from Ery B in sucrose/BSA films.

a)
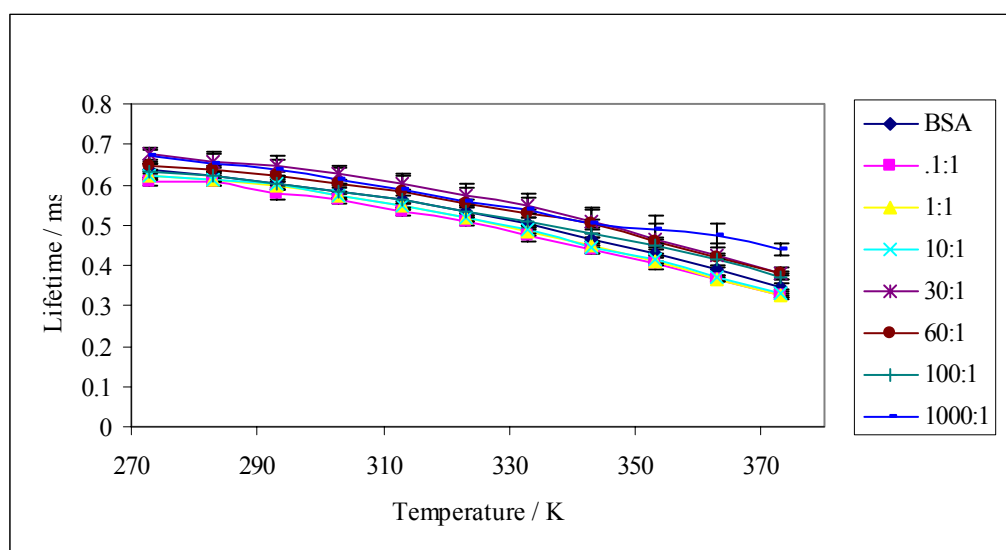
b)
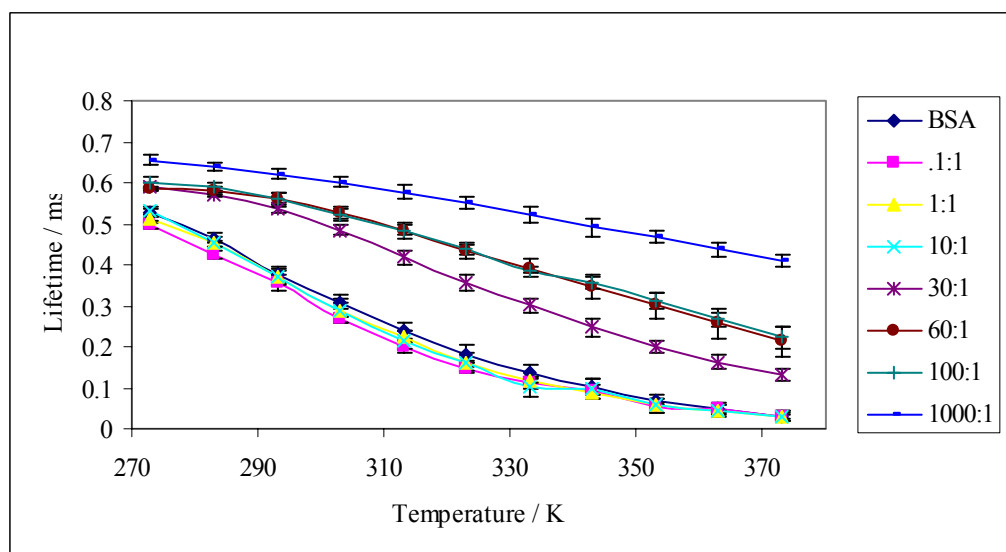
Figure III-6: Lifetimes equilibrated against nitrogen (a) and air (b) from a stretched exponential model fit to phosphorescence intensity decay data from Ery B in trehalose/BSA films.

a)
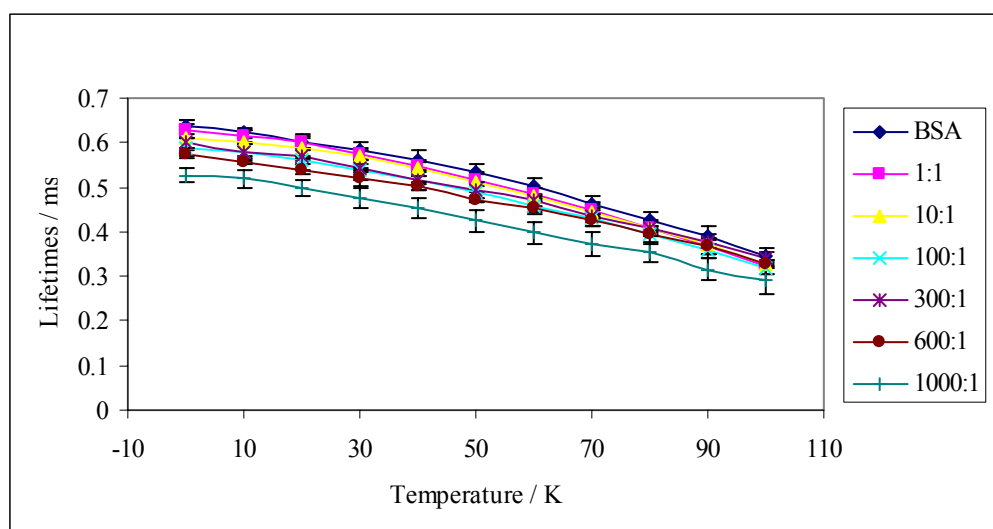
b)
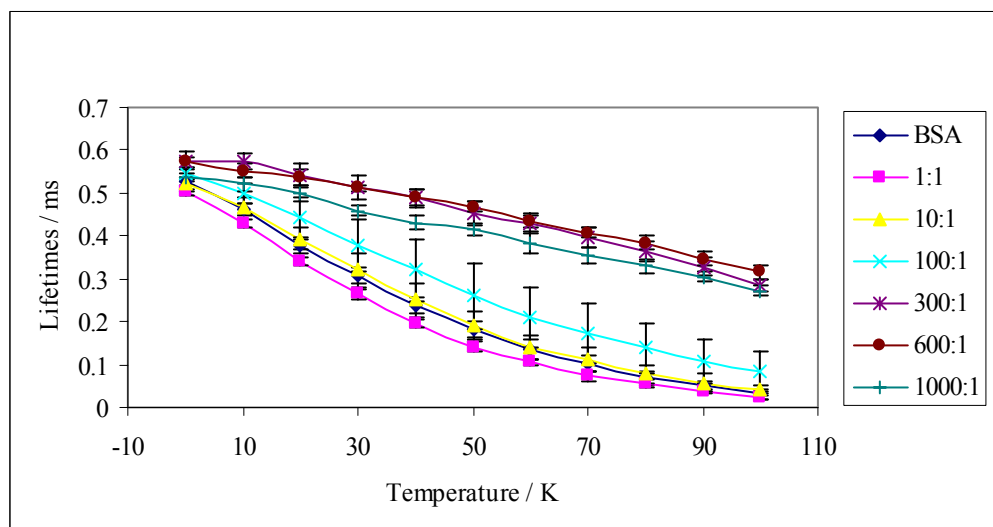
Figure III-7: Beta values (stretching factor) equilibrated against nitrogen (a) and air (b) from a stretched exponential model fit to phosphorescence intensity decay data from Ery B in sucrose/BSA films.

a)
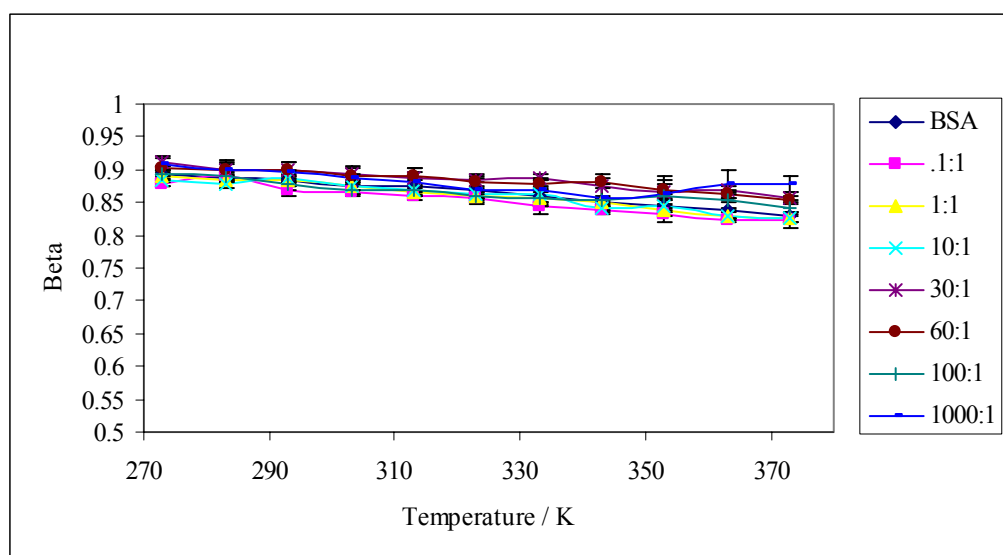
b)
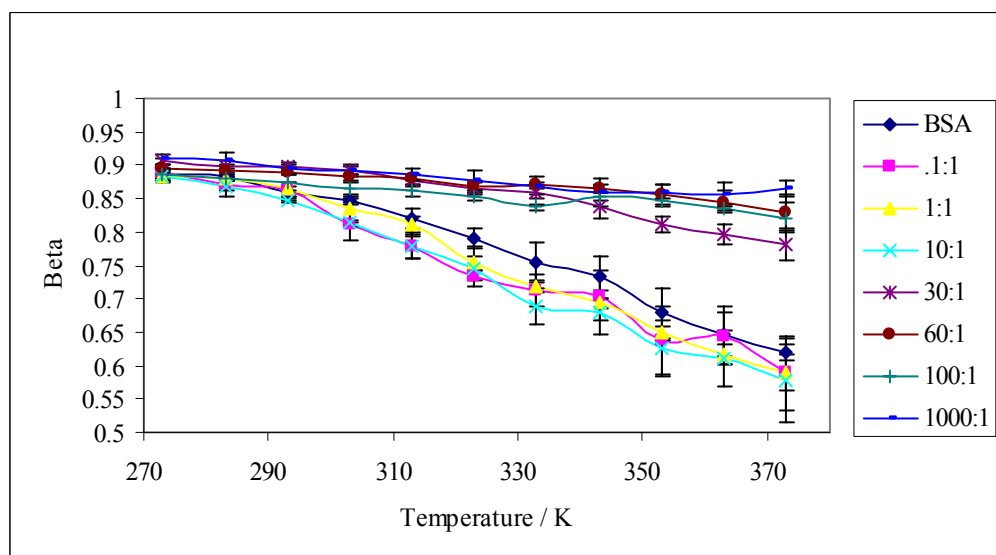
Figure III-8: Beta values (stretching factor) equilibrated against nitrogen (a) and air (b) from a stretched exponential model fit to phosphorescence intensity decay data from Ery B in trehalose/BSA films.

a)
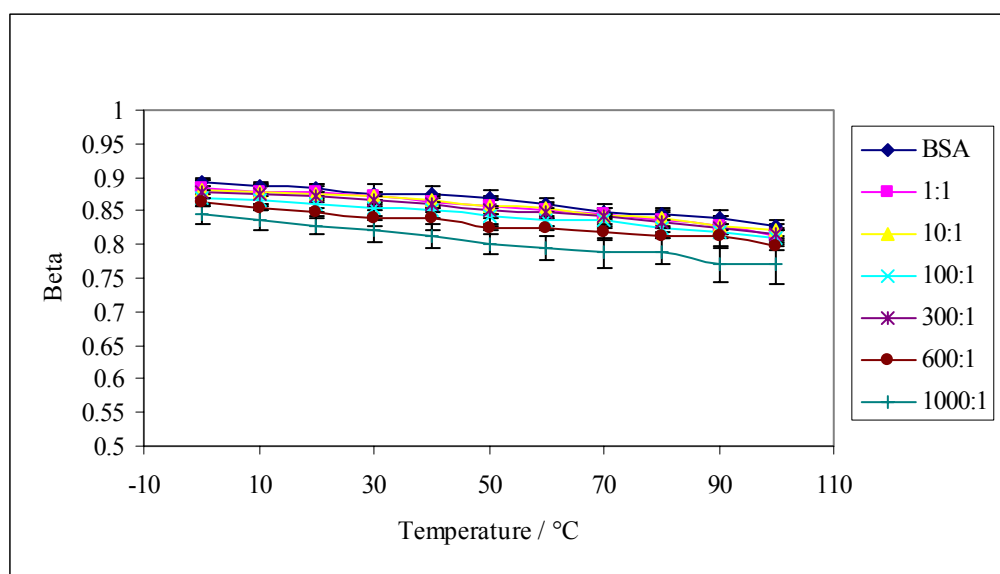
b)
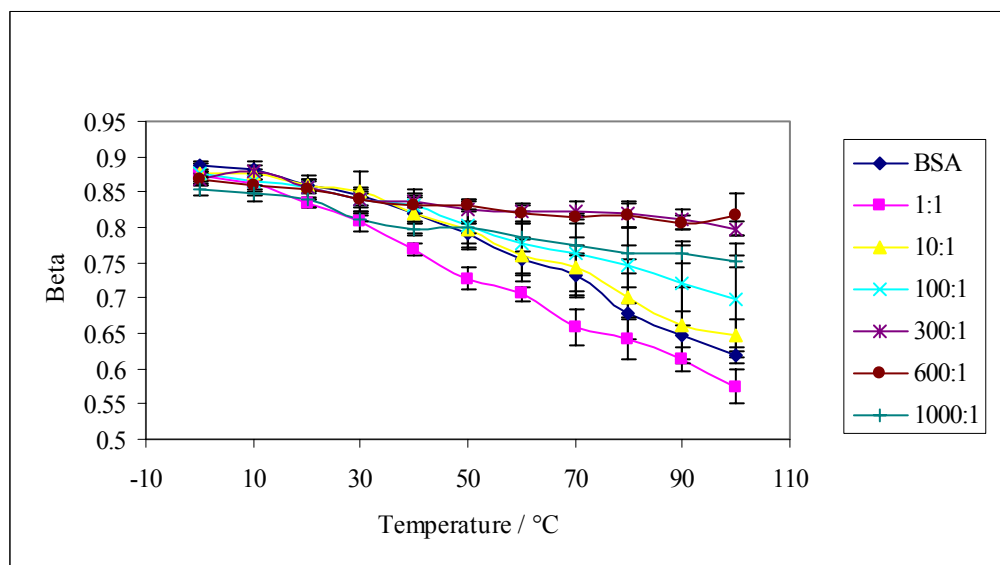
Figure III-9: Temperature dependence of the rates for non-radiative quenching k_{TS0} as a function of temperature (a) and log plots of k_{TS0} as a function of the molar ratio of sucrose to BSA (b).

a)
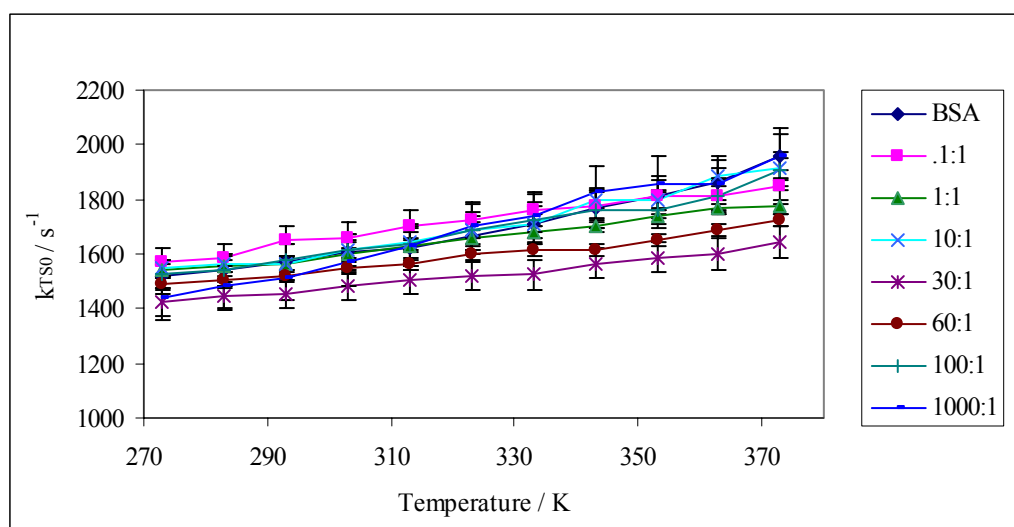
b)
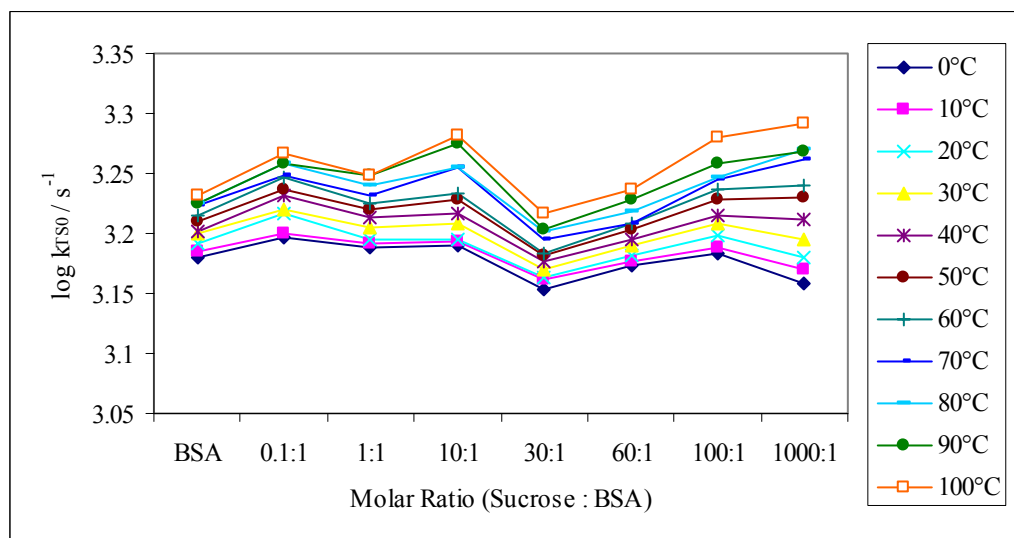
Figure III-10: Temperature dependence of the rates for non-radiative quenching k_{TS0} as a function of temperature (a) and log plots of k_{TS0} as a function of the molar ratio of trehalose to BSA (b).

a)
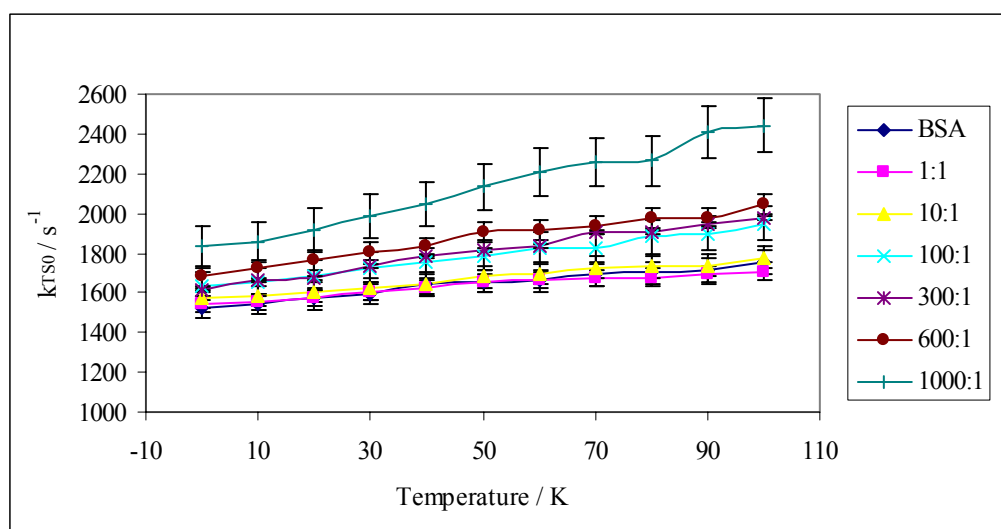
b)
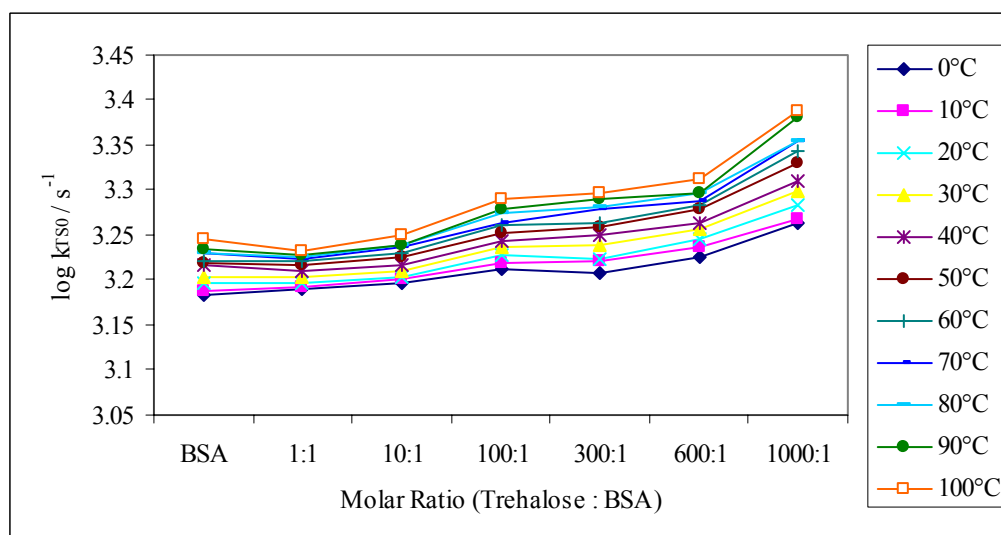
Figure III-11: Data from III-9b and III-10b plotted with the sugar to protein ratios (x-axis) for sucrose to BSA (a) and trehalose to BSA (b) on a log scale for comparison between the sugars.

a)
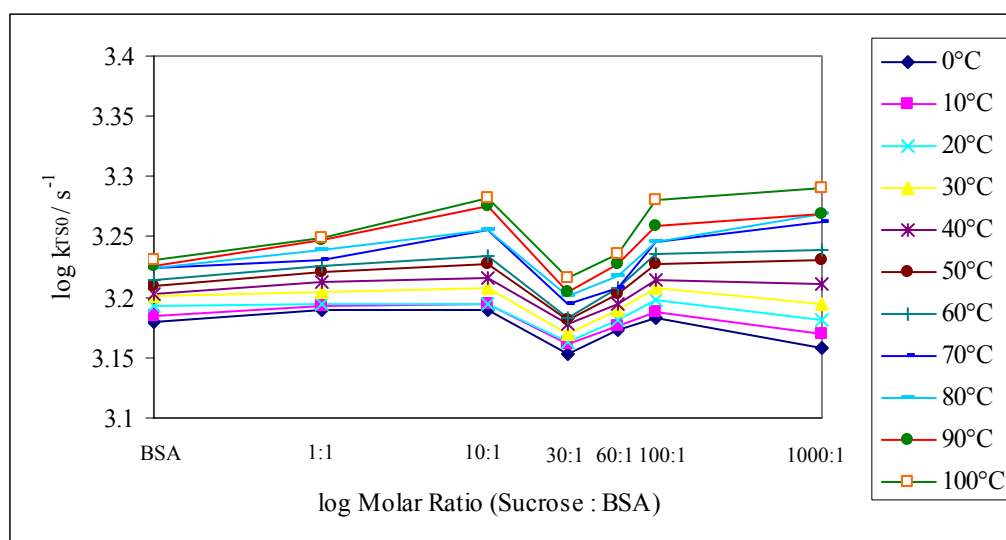
b)
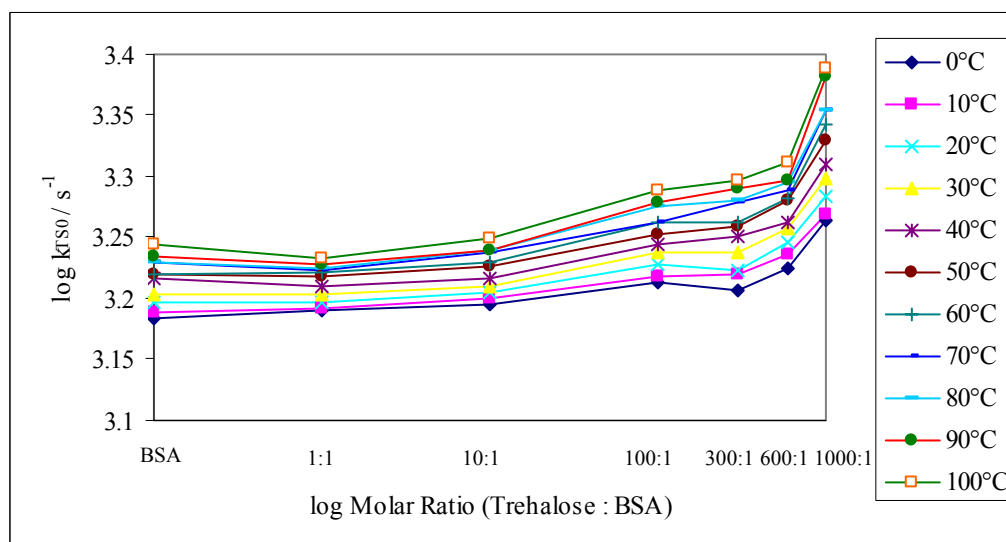
Figure III-12: Temperature dependence of the rates for oxygen quenching $k_Q[O_2]$ as a function of temperature (a) and log plots of $k_Q[O_2]$ as a function of the molar ratio of sucrose to BSA (b).

a)
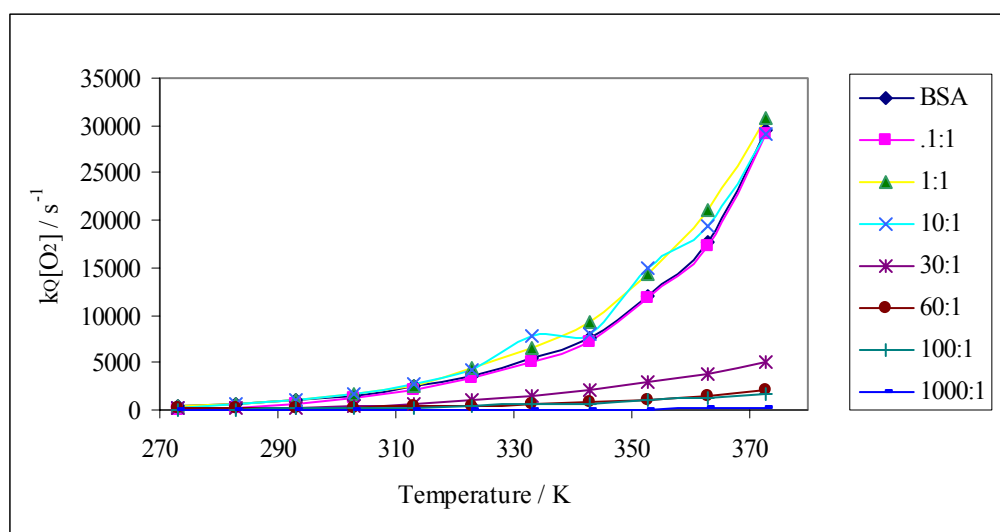
b)
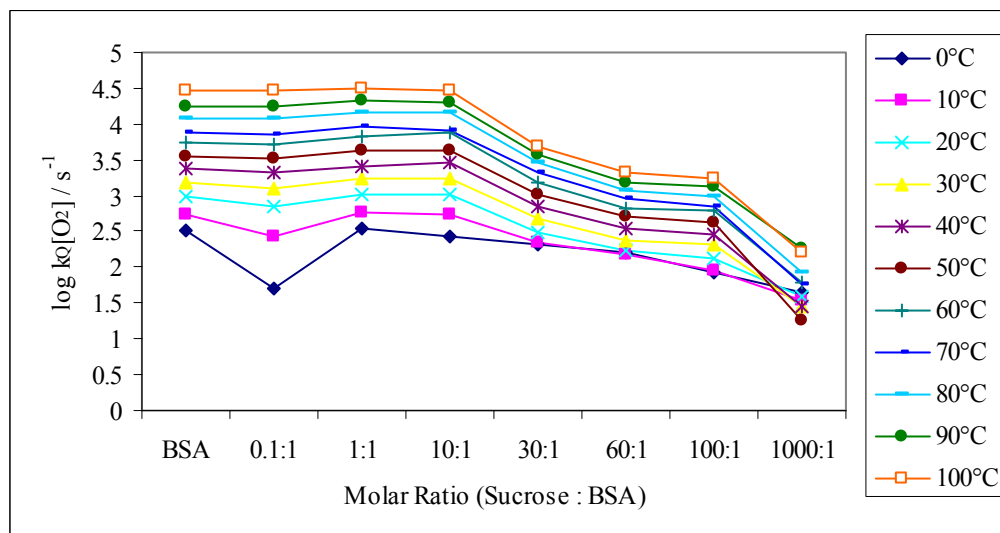
Figure III-13: Temperature dependence of the rates for oxygen quenching $k_Q[O_2]$ as a function of temperature (a) and log plots of $k_Q[O_2]$ as a function of the molar ratio of trehalose to BSA (b).

a)
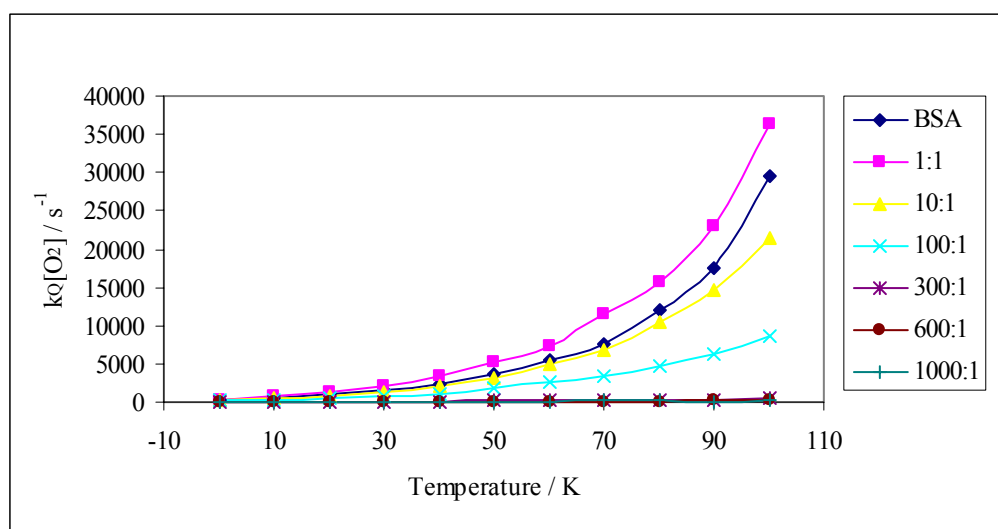
b)
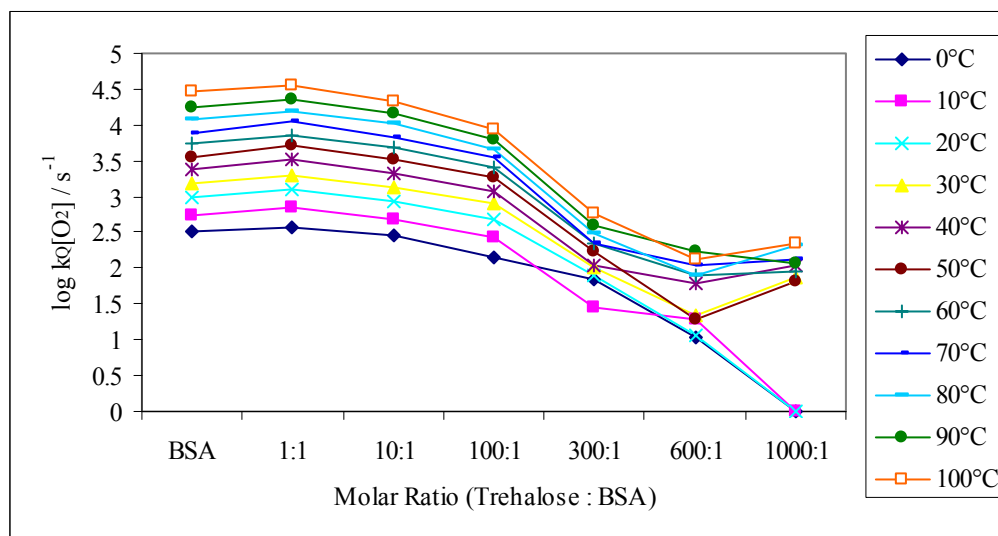
Figure III-14: Data from III-11b and III-12b plotted with the sugar to protein ratios (x-axis) for sucrose to BSA (a) and trehalose to BSA (b) on a log scale for comparison between the sugars.

a)
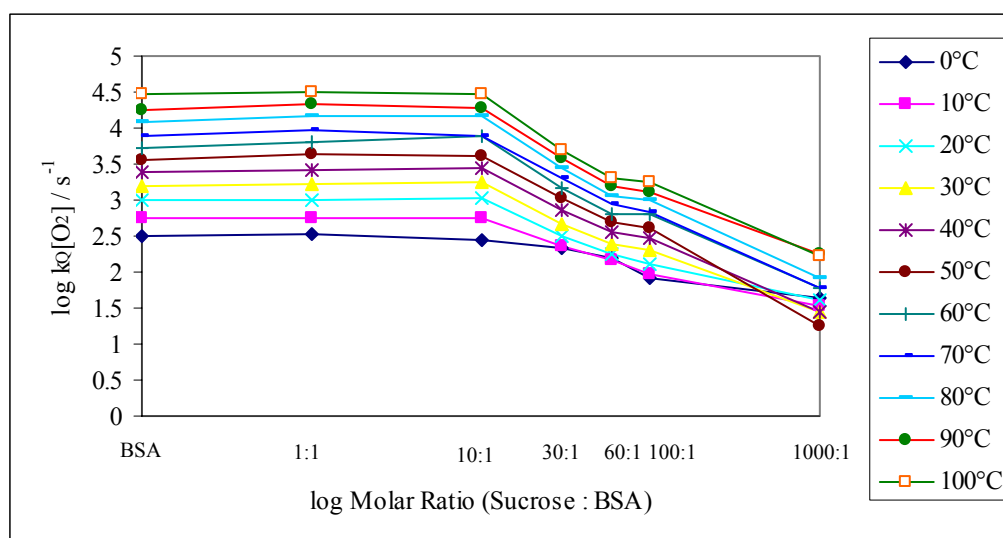
b)
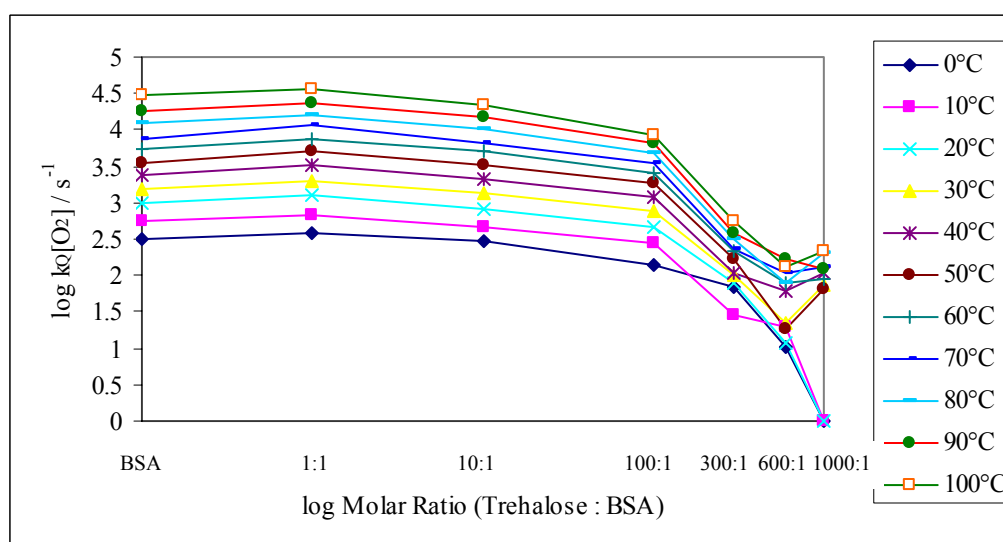
Figure III-15: Arrhenius plots of k_{TS0} (a) and $k_Q[O_2]$ (b) for the various molar ratios of sucrose to BSA.

a)
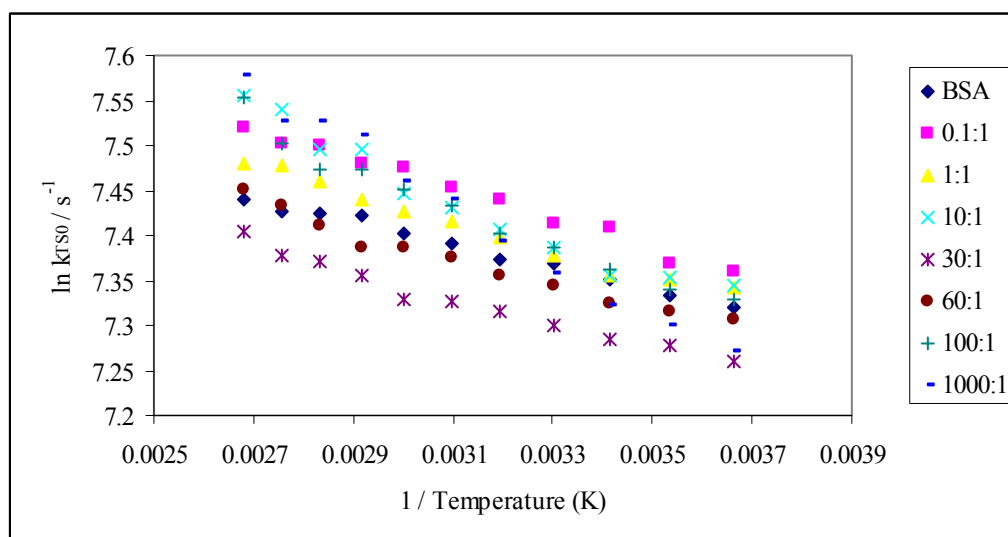
b)
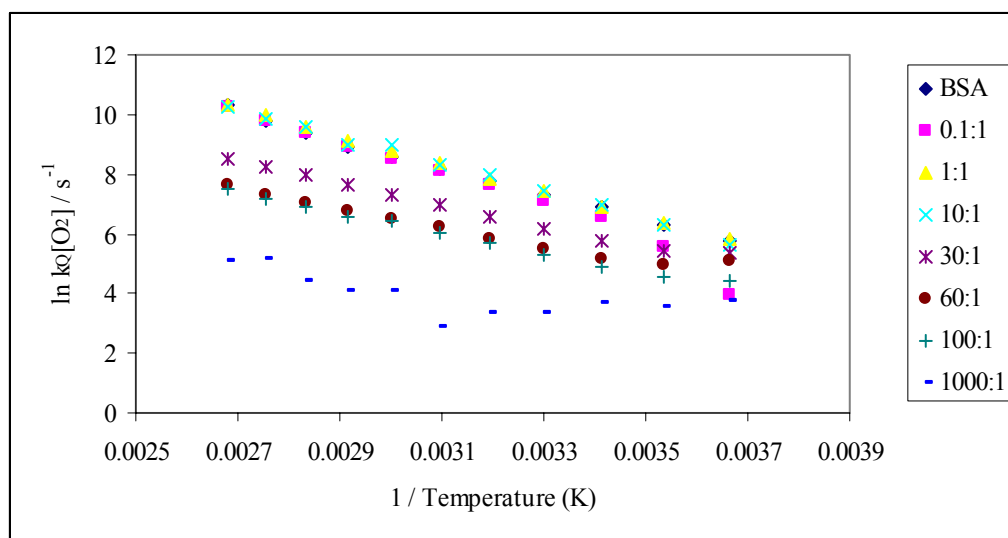
Figure III-16: Activation energies for k_{TS0} and $k_Q[O_2]$ over the temperature range of 0-100°C in the sucrose/BSA matrix.
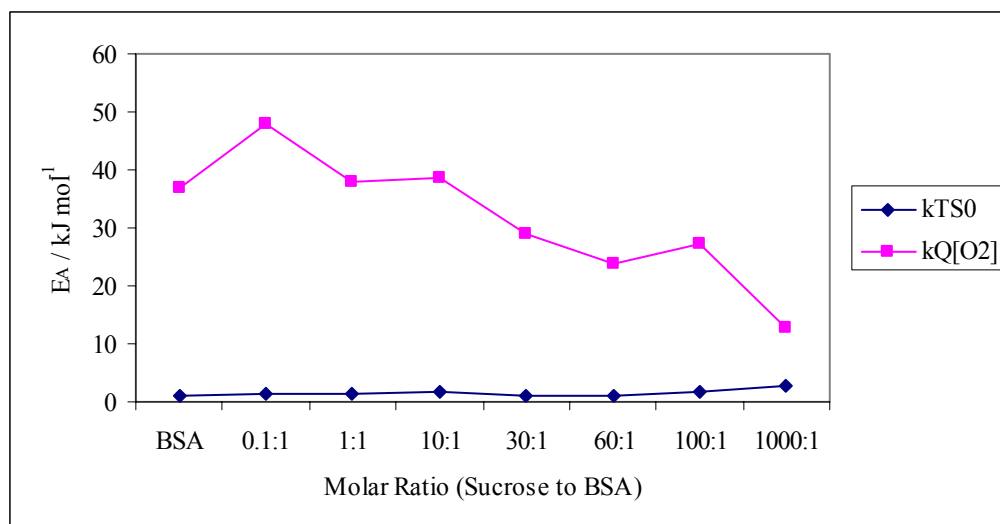
Figure III-17: Arrhenius plots of k_{TS0} (a) and $k_Q[O_2]$ (b) for the various molar ratios of trehalose to BSA.

a)
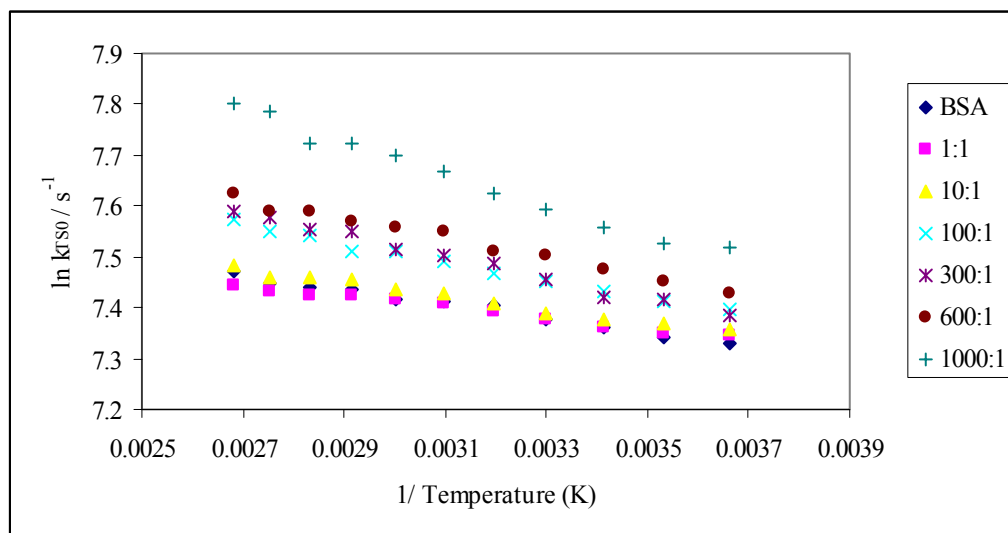
b)
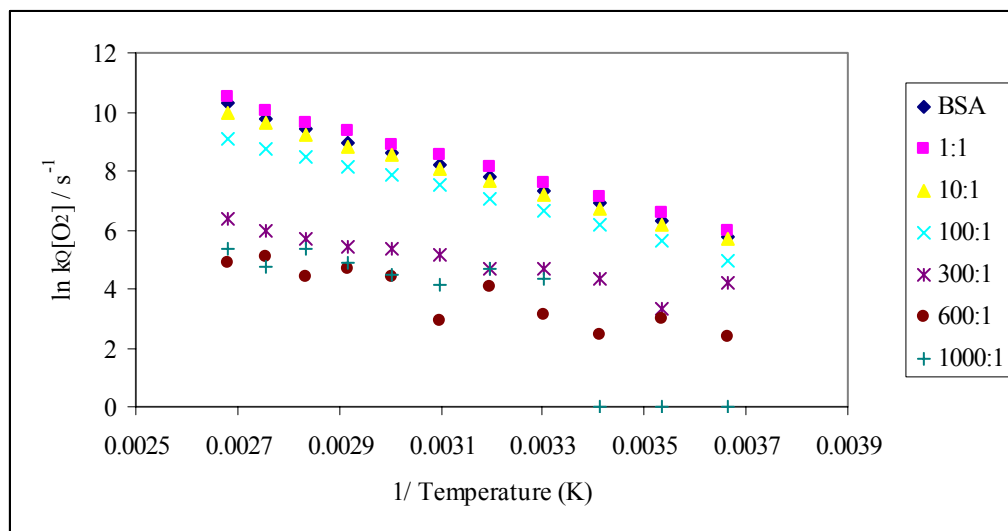
Figure III-18: Activation energies for k_{TS0} and $k_Q[O_2]$ over the temperature range of 0-100°C in the trehalose/BSA matrix.
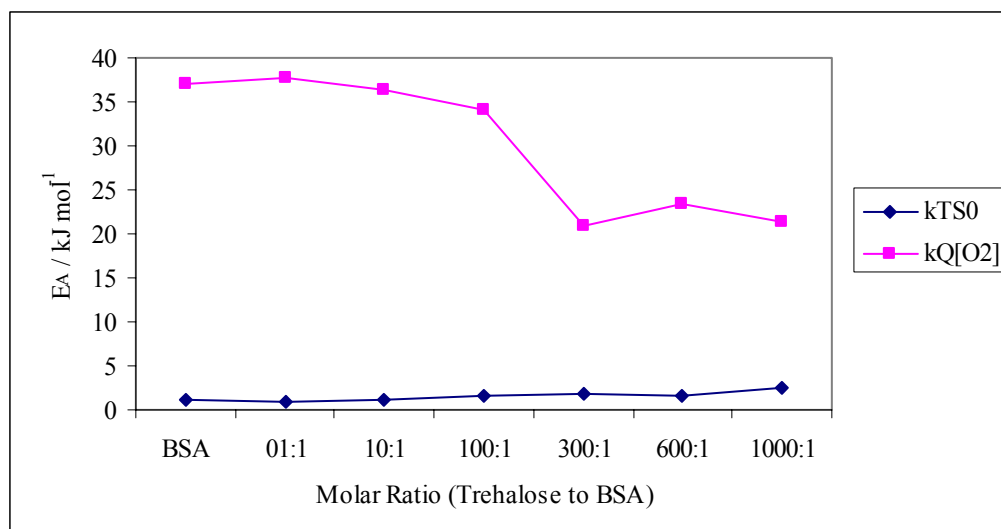
Figure III-19: Plot of $k_Q[O_2]$ versus k_{TS0} for sucrose/BSA; data from Figures III-9a and III-12a, respectively.
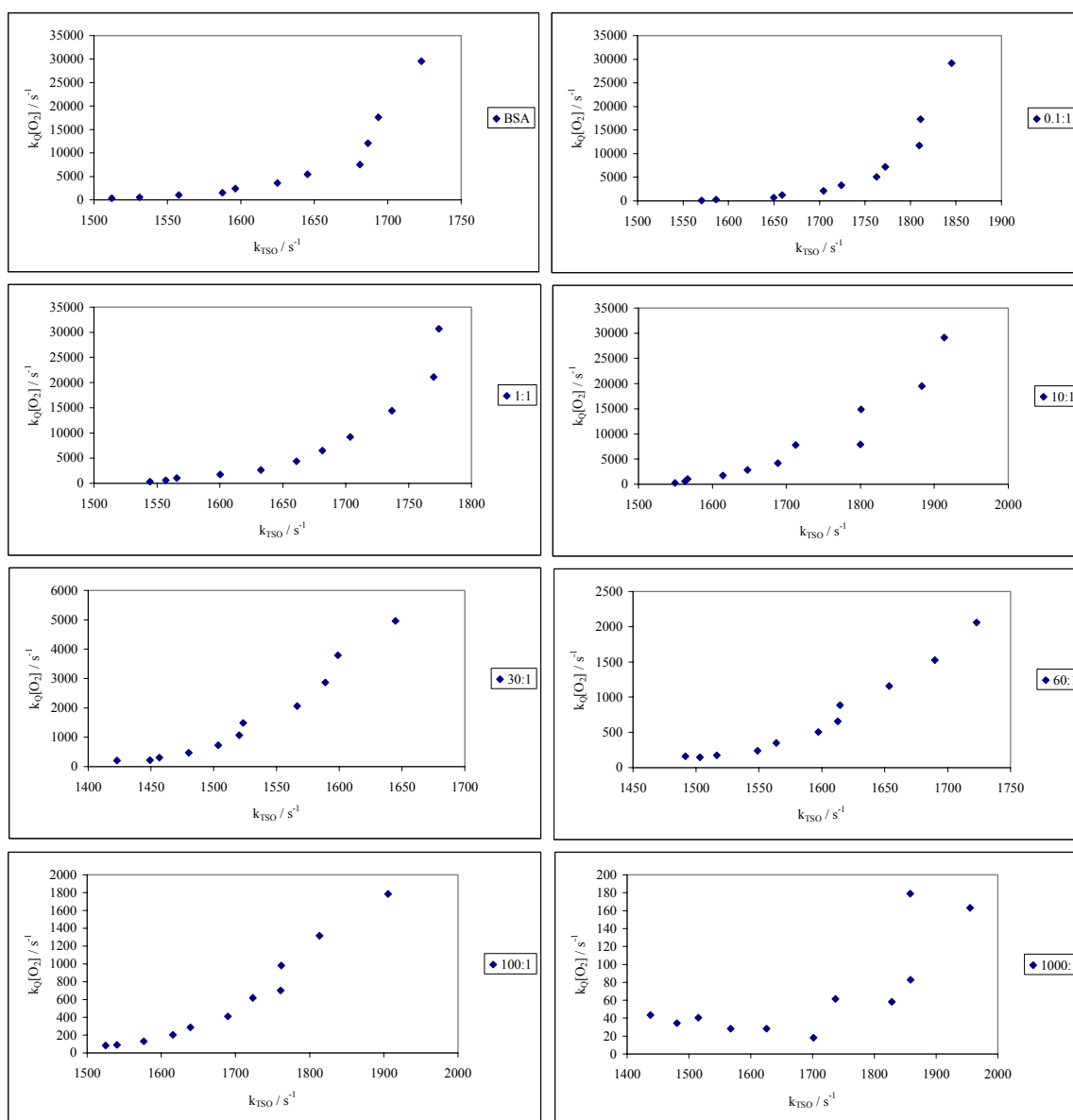
Figure III-20: A plot of the slopes for the $k_Q[O_2]$ vs k_{TS0} plot (Figure III-19) at high (70-100°C) and low (0-20°C) temperatures.
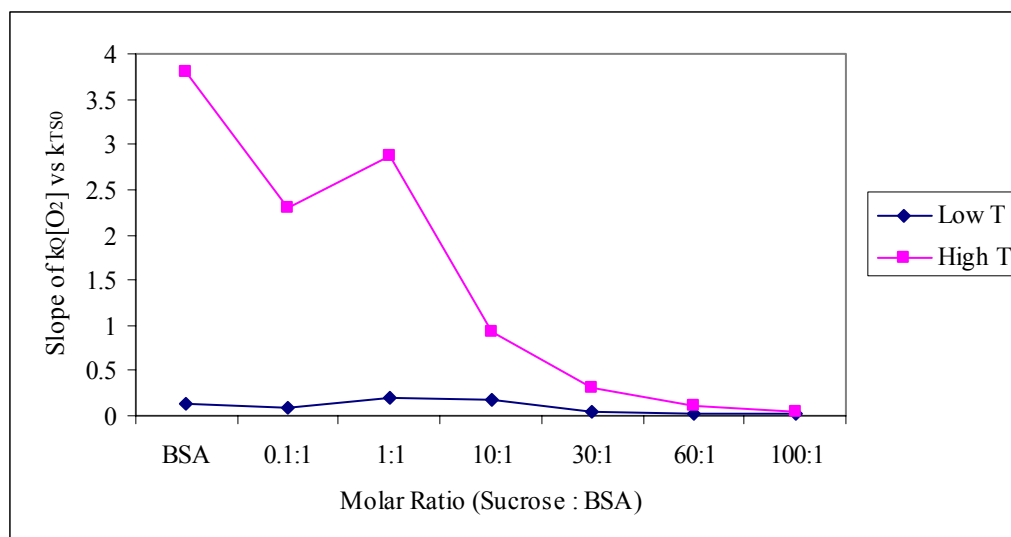
Figure III-21: Plot of $k_Q[O_2]$ versus k_{TS0} for trehalose/BSA (b); data from Figures III-10a and III-13a, respectively.
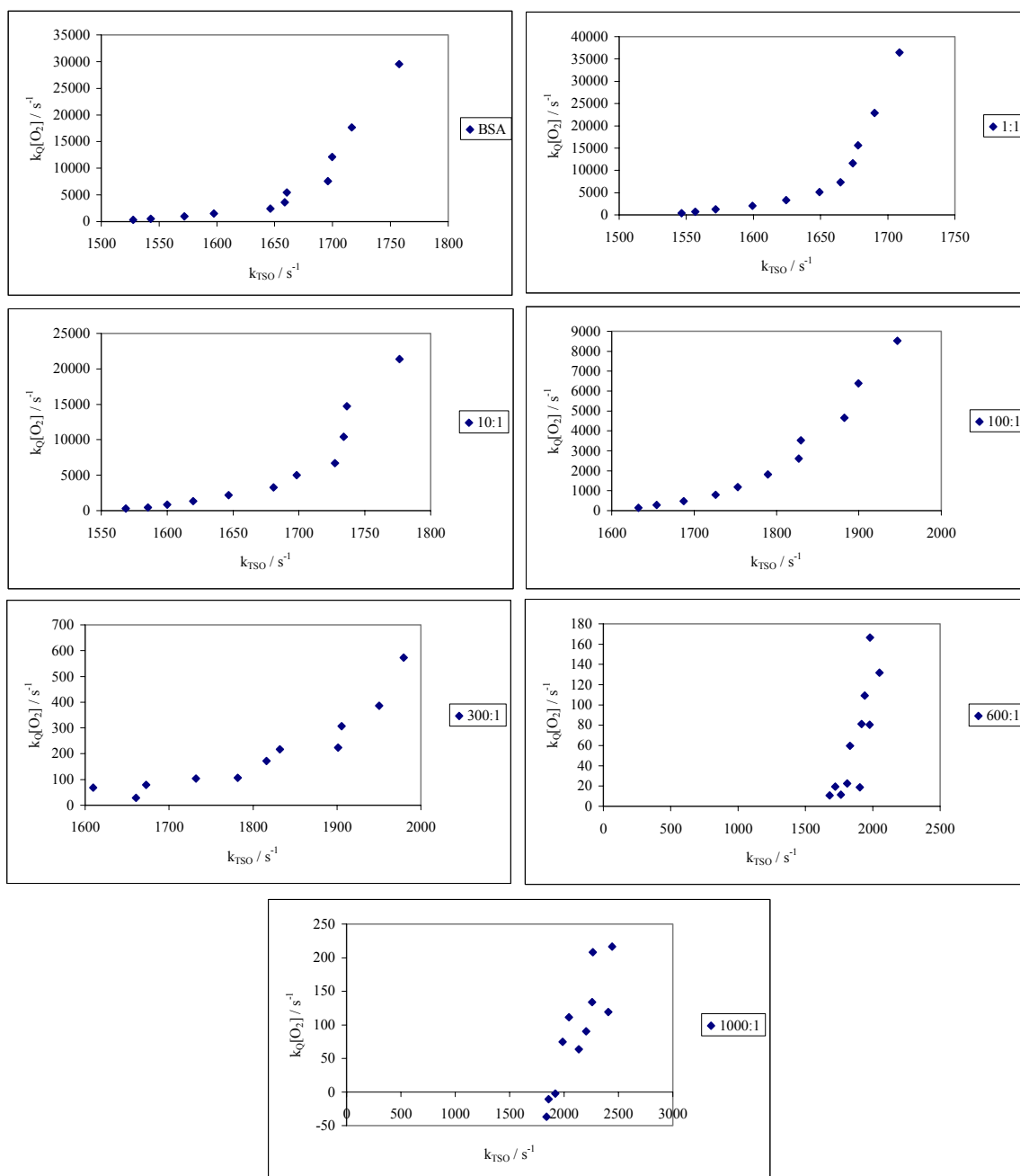
Figure III-22: A plot of the slopes for the $k_Q[O_2]$ vs k_{TS0} plot (Figure III-21) at high (70-100°C) and low (0-20°C) temperatures.
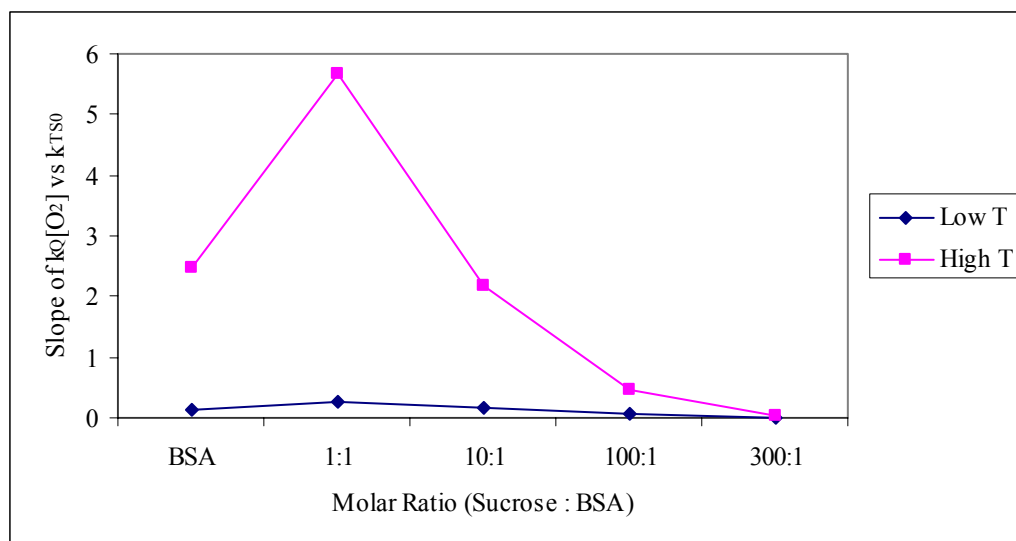
Chapter 4 References

Aldous, B. J., Auffret, A. D., and Franks, F. (1995). The crystallization of hydrates from amorphous carbohydrates. *Cryo-Letters* **16**, 181-186.

Allison, S. D., Chang, B., Randolph, T. W., and Carpenter, J. F. (1999). Hydrogen Bonding between Sugar and Protein Is Responsible for Inhibition of Dehydration-Induced Protein Unfolding. *Archives of Biochemistry and Biophysics* **365**, 289-298.

Anker, M., Stading, M., and Hermansson, A. M. (2001). Aging of whey protein films and the effect on mechanical and barrier properties. *Journal of Agricultural and Food Chemistry* **49**, 989-995.

Baier, S., and McClements, D. J. (2001). Impact of preferential interactions on thermal stability and gelation of bovine serum albumin in aqueous sucrose solutions. *J Agric Food Chem* **49**, 2600-8.

Baier, S. K., and McClements, D. J. (2003). Combined influence of NaCl and sucrose on heat-induced gelation of bovine serum albumin. *J Agric Food Chem* **51**, 8107-12.

Baier, S. K., and McClements, D. J. (2006). The effect of binary cosolvent systems (glycerol-sucrose mixtures) on the heat-induced gelation mechanism of bovine serum albumin. *International Journal of Food Science and Technology* **41**, 189-199.

Belton, P. S., and Gil, A. M. (1994). Ir and Raman-Spectroscopic Studies of the Interaction of Trehalose with Hen Egg-White Lysozyme. *Biopolymers* **34**, 957-961.

Buettner, A. V. (1964). Flash Photolysis in Thin Films of Gelatin and Other Polymers. *J. Phys. Chem.* **68**, 3253-3259.

Carpenter, J. F., and Crowe, J. H. (1988). Modes of stabilization of a protein by organic solutes during desiccation. *Cryobiology* **25**, 459-470.

Carpenter, J. F., and Crowe, J. H. (1989). An infrared spectroscopic study of the interactions of carbohydrates with dried proteins. *Biochemistry* **28**, 3916-22.

Carpenter, J. F., Martin, B., Loomis, S. H., and Crowe, J. H. (1988). Long-term preservation of dried phosphofructokinase by sugars and sugar/zinc mixtures. *Cryobiology* **25**, 372-6.

Champion, D., Le Meste, M., and Simatos, D. (2000). Towards an improved understanding of glass transition and relaxations in foods: molecular mobility in the glass transition range. *Trends in Food Science & Technology* **11**, 41-55.

Chen, R. (2003). Apparent stretched-exponential luminescence decay in crystalline solids. *Journal of Luminescence* **102-103**, 510-518.

Crowe, J. H., Carpenter, J. F., and Crowe, L. M. (1998). The Role of Vitrification in Anhydrobiosis. *Annual Review of Physiology* **60**, 73.

Crowe, J. H., Leslie, S. B., and Crowe, L. M. (1994). Is vitrification sufficient to preserve liposomes during freeze-drying? *Cryobiology* **31**, 355-66.

Crowe, L., Reid, D., and Crowe, J. (1996). Is trehalose special for preserving dry biomaterials? *Biophys. J.* **71**, 2087-2093.

Duchowicz, R., Ferrer, M. L., and Acuna, A. U. (1998). Kinetic Spectroscopy of Erythrosin Phosphorescence and Delayed Fluorescence in Aqueous Solution at Room Temperature. *Photochemistry and Photobiology* **68**, 494-501.

Fasman, G. D. (1989). "Practical Handbook of Biochemistry and Molecular Biology," CRC Press, Boca Ranton, FL.

Fennema, O. R. (1996). Food Chemistry. (O. R. Fennema, ed.), pp. 17-94. Marcel Dekker, Inc., New York.

Gontard, N., Thibault, R., Cuq, B., and Guilbert, S. (1996). Influence of relative humidity and film composition on oxygen and carbon dioxide permeabilities of edible films. *Journal of Agricultural and Food Chemistry* **44**, 1064-1069.

Green, J. L., and Angell, C. A. (1989). Phase relations and Vitrification in Saccharide-Water Solutions and the Trehalose Anomaly. *Journal of Physical Chemistry* **93**, 2880-2882.

Guillet, J. (1985). "Polymer photophysics and photochemistry : an introduction to the study of photoprocesses in macromolecules," Cambridge University Press, New York.

Hill, J. J., Shalaev, E. Y., and Zografi, G. (2005). Thermodynamic and dynamic factors involved in the stability of native protein structure in amorphous solids in relation to levels of hydration. *Journal of Pharmaceutical Sciences* **94**, 1636-1667.

Hurtubise, R. J. (1997). Solid-matrix luminescence analysis: photophysics, physicochemical interactions and applications. *Analytica Chimica Acta* **351**, 1-22.

Imamura, K., Suzuki, T., Kirii, S., Tatsumichi, T., and Okazaki, M. (1998). Influence of protein on phase transition of amorphous sugar. *Journal of Chemical Engineering of Japan* **31**, 325-329.

Kaushik, J. K., and Bhat, R. (2003). Why is Trehalose an Exceptional Protein Stabilizer? *The Journal of Biological Chemistry* **278**, 26458-26465.

Korolev, V. V., Bolotsky, V. V., Shokhirev, N. V., Krissinel, E. B., Bagryansky, V. A., and Bazhin, N. M. (1995). Diffusion of Molecular-Oxygen in Glassy Matrices, Studied by Luminescence Quenching. *Chemical Physics* **196**, 317-325.

Lakowicz, J. R. (1999). "Principles of fluorescence spectroscopy," Second/Ed. Kluwer Academic/Plenum Press, New York.

Lam, S. K., Chan, M. A., and Lo, D. (2001). Characterization of phosphorescence oxygen sensor based on erythrosin B in sol-gel silica in wide pressure and temperature ranges. *Sensors and Actuators B: Chemical* **73**, 135-141.

Lee, K. C. B., Siegel, J., Webb, S. E. D., Leveque-Fort, S., Cole, M. J., Jones, R., Dowling, K., Lever, M. J., and French, P. M. W. (2001). Application of the Stretched Exponential Function to Fluorescence Lifetime Imaging. *Biophys. J.* **81**, 1265-1274.

Lesch, H., Schlichter, J., Friedrich, J., and Vanderkooi, J. M. (2004). Molecular Probes: What Is the Range of Their Interaction with the Environment? *Biophys. J.* **86**, 467-472.

Leslie, S. B., Israeli, E., Lighthart, B., Crowe, J. H., and Crowe, L. M. (1995). Trehalose and sucrose protect both membranes and proteins in intact bacteria during drying. *Applied & Environmental Microbiology* **61**, 3592-7.

Lettinga, M. P., Zuilhof, H., and van Zandvoort, M. A. M. J. (2000). Phosphorescence and fluorescence characterization of fluorescein derivatives immobilized in various polymer matrices. *Physical Chemistry Chemical Physics* **2**, 3697-3707.

Lindsey, C. P., and Patterson, G. D. (1980). Detailed comparision of the Williams-Watts and Cole-Davidson functions. *J. Chem. Phys.* **73**, 3348-3357.

Lins, R. D., Pereira, C. S., and Hunenberger, P. H. (2004). Trehalose-protein interaction in aqueous solution. *Proteins-Structure Function and Bioinformatics* **55**, 177-186.

López-Díez, E. C., and Bone, S. (2000). An investigation of the water-binding properties of protein + sugar systems. *Physics in Medicine and Biology* **45**, 3577-3588.

Mazzobre, M. F., del Pilar Buera, M., and Chirife, J. (1997). Protective Role of Trehalose on Thermal Stability of Lactase in Relation to its Glass and Crystal Forming Properties and Effect of Delaying Crystallization. *Lebensmittel-Wissenschaft und-Technologie* **30**, 324-329.

McHugh, T. H., and Krochta, J. M. (1994). Sorbitol- vs Glycerol-Plasticized Whey Protein Edible Films: Integrated Oxygen Permeability and Tensile Property Evaluation. *Journal of Agricultural and Food Chemistry* **42**, 841-845.

Miller, D. P., dePablo, J. J., and Corti, H. (1997). Thermophysical properties of trehalose and its concentrated aqueous solutions. *Pharmaceutical Research* **14**, 578-590.

Nack, T. J., and Ludescher, R. D. (2006). Molecular mobility and oxygen permeability in amorphous bovine serum albumin films. *Food Biophysics* **1**, 151-162.

Nemkovich, N. A., Rubinov, A. N., and Tomlin, V. I. (1991). "Inhomogeneous broadening of electric spectra of dye molecules in solutions," Plenum Press, New York.

Parker, C. A. (1968). "Photoluminescence of Solutions," Elsevier Publishing Company, Amsterdam.

Pravinata, L. C., You, Y., and Ludescher, R. D. (2005). Erythrosin B Phosphorescence Monitors Molecular Mobility and Dynamic Site Heterogeneity in Amorphous Sucrose. *Biophys. J.* **88**, 3551-3561.

Richert, R. (1997). Evidence for dynamic heterogeneity near T-g from the time-resolved inhomogeneous broadening of optical line shapes. *Journal of Physical Chemistry B* **101**, 6323-6326.

Richert, R., and Heuer, A. (1997). Rate-memory and dynamic heterogeneity of first-order reactions in a polymer matrix. *Macromolecules* **30**, 4038-4041.

Roe, K. D., and Labuza, T. P. (2005). Glass Transition and Crystallization of Amorphous Trehalose-Sucrose Mixtures. *International Journal of Food Properties* **8**, 559-574.

Shah, N. K., and Ludescher, R. D. (1995). Phosphorescence Probes of the Glassy State in Amorphous Sucrose. *Biotechnology Progress* **11**, 540-544.

Simon-Lukasik, K. V., and Ludescher, R. D. (2004). Erythrosin B phosphorescence as a probe of oxygen diffusion in amorphous gelatin films. *Food Hydrocolloids* **18**, 621-630.

Slavic, J. (1994). "Fluorescent probes in cellular and molecular biology," CRC Press, Inc., Boca Raton.

Sothornvit, R., and Krochta, J. M. (2000). Plasticizer effect on oxygen permeability of beta-lactoglobulin films. *Journal of Agricultural and Food Chemistry* **48**, 6298-6302.

Strambini, G. B., and Gonnelli, M. (1985). The indole nucleus triplet-state lifetime and its dependence on solvent microviscosity. *Chemical Physics Letters* **115**, 196-200.

Sun, W. Q., and Davidson, P. (1998). Protein inactivation in amorphous sucrose and trehalose matrices: effects of phase separation and crystallization. *Biochimica et Biophysica Acta (BBA) - General Subjects* **1425**, 235-244.

Sundaresan, K. V., and Ludescher, R. D. (2007). Molecular mobility and oxygen permeability in amorphous Beta -lactoglobulin films. *Food Hydrocolloids* **In Press**.

Taylor, L. S., and Zografi, G. (1998). Sugar-polymer hydrogen bond interactions in lyophilized amorphous mixtures. *Journal of Pharmaceutical Sciences* **87**, 1615-1621.

Williams, G., and Watts, D. C. (1970). Nonsymmetrical dielectric relaxation behavior arising from a simple empirical decay function. *Trans. Faraday Soc.* **66**, 80-85.

Yoshioka, S., Aso, Y., and Kojima, S. (1997). Dependence of the molecular mobility and protein stability of freeze-dried gamma-globulin formulations on the molecular weight of dextran. *Pharmaceutical Research* **14**, 736-741.

Chapter 4: Analysis of the molecular mobility and oxygen permeability in gelatin films as a function of temperature.

Introduction

Gelatin is a multifunctional protein with an extended fibrous structure that has been used widely in the food, pharmaceutical, biomedical, and photographic industries (Bigi et al., 2001; Simon-Lukasik and Ludescher, 2004; Stainsby, 1987). These fibrous proteins are intermediate in complexity between homopolymers and globular proteins (Renou et al., 2004). Gelatin is the product of denatured and partly degraded animal collagen, usually derived from cattle bones, cattle hides, and pork skins (Bailey and Light, 1989; Hinterwaldner, 1977), and gelatin exhibits many functional properties that are either absent in collagen, or only shown to a slight extent (Kozlov and Burdygina, 1983). In the food industry, gelatin is used to form gels, modify texture and viscosity, bind water, control crystal growth, stabilize foams and emulsions, and to form edible films (Jones, 1977; Krochta and DeMulder-Johnston, 1997; Stainsby, 1987). The functional versatility reflects both the physical properties of the long flexible polymer and also the wide array of chemical interactions possible in a peptide containing 20 diverse amino acid side chains (Figure IV-1) (Stainsby, 1977), that conform to a wide range of functional and film-forming properties depending on the various preparation conditions. Gelatin forms high molecular weight compounds very similar to that of rigid chain synthetic polymers (Kozlov and Burdygina, 1983) due to the linear structure, limited monomer composition, and polydispersity (Simon-Lukasik and Ludescher, 2004). Much of gelatin's versatility stems from the fact that it is the only food protein which undergoes a thermally reversible helical coil transition (Guenet, 1992; Stainsby, 1977) which

depends greatly on the presence of cross-links, molecular weight, and concentration (as reviewed by Kozlov and Burdygina (1983)). For a more detailed description of the functional attributes of gelatin in the food industry, please refer to Figure IV-2.

Gelatin Production

The ultimate goal in the production of gelatin from collagen is to convert the insoluble collagen into the maximum quantity of purified soluble gelatin having desirable physiochemical properties such as high gel strength, viscosity, and clarity (Hinterwaldner, 1977). Gelatin is produced by the hydrolysis of water insoluble collagen through three major steps: the elimination of non-collagenous material from the raw material, followed by the controlled hydrolysis conversion of collagen to gelatin, and the subsequent recovery and drying of the final product (Hinterwaldner, 1977; Liu, 2002; Stainsby, 1987; Veis, 1964).

Both acid and lime processes, yielding gelatin type A and B, respectively, can be used for the removal of the non-collagenous material through various washing and extraction steps. We chose type A gelatin derived from porcine skin, because it is currently the most commonly used gelatin in North America for edible applications (Gelatin Manufactures Institute of America, 2001). Both of these processes use heating and pH extremes to denature the native collagen fold, and the conversion of chemical groups on amino acids may occur. The ease with which the gelatin can be extracted from the collagen fibers depends greatly on the age of the animal, with collagen from older animals requiring excessive heat or pH treatments (Hinterwaldner, 1977) due to the excessive cross-links that form over time. The breaking of covalent bonds destroys many of the linkages responsible for holding native collagen fibrils together without the

cleavage of any peptide bonds (Stainsby, 1987; Veis, 1964). The cross-links in collagen taken from young animals and porcine skin require only mild treatments of acid, and therefore, the resulting type A gelatin has isoelectric points between pH 6-9 and there is little or no deamidization of the side chains of asparagine and glutamine, yielding a positive charge in all food uses (Stainsby, 1987). The pH, acid, time, temperature, and number of extractions vary between processors depending on product needs, equipment, and capital expenditures (Gelatin Manufactures Institute of America, 2001). Extraction procedures are closely controlled in the manufacturer of gelatin since they influence both the quality and quantity of the final product. Earlier extractions have a higher molecular weight, are more viscous, form stronger gels, and are more optically clear. Gelatin removed from the later extractions has a yellowish color, lower gel strength, and lower molecular weight, as a result of the increasingly higher temperatures as the extraction process proceeds (Gelatin Manufactures Institute of America, 2001). After extensive filtration, deionization, and dehydration steps, water soluble gelatin is recovered. Please refer to Figure IV-3 for a more detailed process flow of the conversion of collagen to gelatin.

Gelatin Gels

Gelatin is probably best known as a gelling agent, and different types and grades of gelatin are used in a wide range of food products such as marshmallows, gelatin desserts, and gummy bears. When a hot aqueous solution of gelatin is cooled, the viscosity progressively increases with time, and the solution will eventually gel or set (Stainsby, 1977). The setting of a gelatin solution to a gel depends on the ability of the molecules to aggregate (Johns and Courts, 1977). When a dilute solution of gelatin is

cooled, renaturation involves association between components differing in their degree of cross-linking, chain length, chemical composition, and molecular weight (Stainsby, 1987). The molecular weight of gelatin increases with time, and it can be assessed through specific viscosity measurements or light scattering (Dickinson et al., 1985) due to the localized formation of collagen helices of various lengths. The preservation of the amino acid sequence rich in Glycine-Proline-Proline triplets during gelatin manufacture is vital to gel preservation because these triplets are believed to assemble into the stabilizing helices (Stainsby, 1987). This higher level of organization develops through self assembly of the collagen-like helical zones, eventually producing a fibrillar network with a much increased viscosity. For this to occur, suitable regions of polar and nonpolar regions must be present on adjacent helices, and the resulting gel network is held together entirely by noncovalent cooperative binding. This type of interaction is disrupted by heating, and therefore, the gel network is thermoreversible (Stainsby, 1987). Among the gel-forming agents of natural origin, gelatin is exceptionally versatile, yielding stable gels over a wide range of pH not requiring any other specific chemical or ion additions to induce gelation (Stainsby, 1977). Gelatin gels are not of concern in our studies, as we focus instead on dried amorphous films in the glassy region which are well below the sol/gel transition due to the lack of water in the system.

Gelatin Structure

As a gelatin gel ages, water is pushed out of the protein matrix, and the gel condenses to a rubbery film that forms a glass upon drying. Amorphous solid gelatin is an entangled polymer network with a variable number of physical cross-links which depend on the specific time and temperature of drying (Lukasik and Ludescher, 2006b).

The intermolecular binding involved in gel formation is entirely noncovalent cooperative binding which leads to the gel's complete thermoreversibility, thus explaining why gelatin gels melt easily with heat (for example in the mouth) (Bailey and Light, 1989). Initially, gelatin gels were thought of as partially crystalline glassy polymers. The "fringed" micelle model was developed by Abitz et al. (1930), where they proposed that the gelatin micelles were regions of extended parallel polypeptide chains almost crystalline in structure with relatively open ends generating the so called micelle. Slade et al. (1989) have suggested that although gelatin gels are often described as partially crystalline, the cross-links are actually not crystals, and rather they are local microcrystalline and amorphous regions covalently linked through individual polymer chains.

Gelatin Films and Oxygen Permeability

Edible protein films are studied in great detail within the food industry hoping to extend shelf life or to make other quality improvements. Current studies involve applications as a gas and moisture barrier, ingredient carrier, enhance color stability, retain flavor and aroma, and to improve mechanical strength and stability (Gennadios et al., 1997; Jongjareonrak et al., 2006; Krochta and DeMulder-Johnston, 1997; McHugh, 2000). More specifically, gelatin films have been used as an adhesive (Jones, 1977), oxygen barrier, ingredient carrier, and mold retardant (Krochta and DeMulder-Johnston, 1997). Meat products treated with a gelatin dip have shown superior oxidative stability and improved color retention (Cutter, 2006). It has also become the primary ingredient in many pharmaceutical capsule and tablet applications (Wood, 1977). Gelatin film research has focused on relating the effects of formulations and casting temperatures to

mechanical and barrier properties. Casting temperature, which modifies the helix content and number of cross-links, along with plasticizer concentrations and interactions with co-polymers have received the most attention (Lukasik, 2005). There has been very little research with the goal of connecting the macroscopic properties of gelatin films with molecular mobility and oxygen permeability, besides measurements of T_g (Marshall and Petrie, 1980; Pinhas et al., 1996; Sobral and Habitante, 2001).

One of the largest problems in the packaging of foods is oxygen permeability, and the development of edible films which provide an increased barrier to oxygen would be vital for the extension of shelf life. Edible films that are easily degradable and environmentally safe are desired (Chambi and Grosso, 2006; Emmambux et al., 2004), and of these "natural" edible films, gelatin displays excellent barrier properties to oxygen. Oxygen permeability is equal to the diffusion coefficient and the solubility of oxygen in the gelatin film ($P=DS$). The permeability depends not only on the size of the permeating gas molecules, but also how strongly the film's polymer chains are held together by intermolecular forces, which influence the morphology of the films (Scherzer, 1997). Furthermore, barrier efficiency is increased by high degrees of molecular orientation (lowering free volume of the polymer chains) and hydrogen bonding (Koros, 1990). Permeability is also greatly affected by external factors such as temperature and moisture which can disrupt the bonding network. Gelatin meets the above requirements and is thus an excellent candidate for use in edible films desiring high barrier properties against oxygen permeation. Gelatin has large amounts of amide and hydroxyl groups which have been found to be a key component in high barrier films due to there capacity to form hydrogen bonds (Salame, 1986). These bonds lead to

gelatin's highly ordered structure, similar to that of the helical coil in its native collagen (Ward and Courts, 1977).

Oxygen diffusion is typically measured directly through freestanding films via a gas transmission cell. This is relevant for packaging and edible film applications when conditions on both sides of the film are modified to that of the actual conditions surrounding the food product (the external and internal environment of the food package). Gas transmission cell experiments are not capable of direct measurements of edible films which are in direct contact with the food surface, and our phosphorescent techniques can potentially measure the relative oxygen permeability through a wide variety of foods and food surfaces (Simon-Lukasik and Ludescher, 2004).

Gelatin as a Model System and Aim

Gelatin has a wide array of uses in the food, pharmaceutical, and photographic industries. It's well documented history as a functional ingredient has continued to generate interest from all these areas of study, aiming to better understand what exactly gives gelatin the desired functional attributes. A correlation between the desired functional aspects with the underlying molecular structure and dynamic interactions is needed. Our focus will be on the continuation of studies aimed at providing a better understanding of dynamic site heterogeneity, molecular mobility, and oxygen permeability in cold cast gelatin matrices via Erythrosin B (Ery B) phosphorescence. Previous work by Simon-Lukasik and Ludescher (2004) and Lukasik and Ludescher (2006b) focused on these parameters as a function of relative humidity, casting conditions, and presence of plasticizers. The goal of our research is to look at the temperature effects on these physical processes in cold cast (films cast at room

temperature where gelatin macromolecules have many cross-links and collagen-like helical structures) gelatin films by monitoring matrix dipolar relaxation via emission energy (ν_P) and bandwidth (FWHM) as a function of temperature, phosphorescence intensity decays and the subsequent calculations of molecular collisional quenching (k_{TS0}) and quenching due to oxygen ($k_Q[O_2]$) from the lifetime data (τ), matrix dynamic site heterogeneity determined through time resolved emission energies (ν_P) and intensity decays (τ and β) with varying emission wavelengths, and the determination of the apparent activation energies (E_A) for deexcitation of the triplet state due to molecular collisions.

Materials and Methods

Gelatin Preparation

A solution of gelatin was prepared in distilled deionized water at an approximate concentration of 100 mg/mL. This concentration was selected to achieve maximum recovery of the protein after lyophilization (Lukasik, 2005). VEE GEE 300 Bloom type A Superclear porcine gelatin (Vyse Gelatin Company, Schiller Park, IL) was used for these experiments. The aqueous solution was dialyzed in a regenerated cellulose dialysis tube having a 1000 Da molecular weight cutoff (Spectrum, Houston, TX) against 0.1 M potassium chloride for 24 hrs with frequent changing of the buffer to define the presence of counter ions. The solution was then dialyzed against distilled deionized water for 72 hours with frequent changing of the water to minimize the presence of counter ions. Throughout the dialysis process the solution was kept above 65°C to ensure that the gelatin remained in the unfolded state, maximizing the effectiveness of the dialysis process. The gelatin solution was then rapidly frozen in a Labconco shell freezer (Kansas

City, MO) and then annealed in a standard freezer overnight. The frozen sample was placed in a freeze drier (Labconco Model 4.5, Kansas City, MO) for 36 hours to remove any residual moisture. The freeze dried protein was then sealed in a screw-cap plastic container and stored under refrigeration.

Probe Preparation

A 10-mg/ml stock solution of Ery B free acid (Molecular Probes, Inc., Eugene, OR, USA) was prepared in N,N-dimethlyformamide (DMF; Sigma- Aldrich, Milwaukee, WI, USA). DMF has negligible effects on the spectroscopic properties of the probe in amorphous sucrose at a variety of concentrations (Pravinata et al., 2005; You and Ludescher, 2006). This concentration was selected to simplify the addition of the probe to the gelatin solution, and the solvent was selected for probe stability during long-term storage. The 10-mg/ml stock solution of Ery B free acid was added to the gelatin solution in a ratio of 6 µL/ml (5.6×10^{-5} mol dye / mol amino acid residues). It was found that below 5µL/ml, an unacceptable signal to noise ratio was observed. At this concentration, it was determined that Ery B does not aggregate, existing only as individual molecules monitoring the molecular mobility of the protein (Pravinata et al., 2005; You and Ludescher, 2006). The Ery B gelatin films were made by heating the solution to 65°C and pipetting 40 µl of the solution onto quartz slides (13.0 x 30.0 x 0.6 mm; Wilmad Lab Glass, Buena, NJ) and spreading the solution over an area approximately 15X10 mm before the gelatin set. Before use, to improve the surface activity for spreading the gelatin solutions, the slides were soaked in Terg-A-Zyme, washed in Alconox soap, rinsed with double-distilled water, and rinsed with ethanol. After spreading, the slides were dried under constant flow of air for 30 minutes at room

temperature, allowed to set, and then transferred to a desiccator over phosphorus pentoxide for at least 1 week. A study by Yakimets et al. (2005) found that gelatin films contained 0.8% water at ambient temperature under phosphorous pentoxide conditions. The slides were stored at 23.0 +/- 1°C protected from light to prevent any photobleaching of the Ery B, and desiccant was refreshed as needed to maintain a relative humidity close to 0%.

Phosphorescence Measurements

To prevent oxygen quenching of the triplet state, a virtually oxygen free nitrogen stream was generated by passing high purity nitrogen through a Supelco carrier gas purifier (Bellfonte, PA). This gas line was routed into the sample compartment and directly into the quartz fluorescence cuvette that held the slide. The cuvette was capped with a lid having inlet and outlet ports for the gas line, thus all experiments were done at constant pressure. The cuvette was flushed for at least 30 minutes to ensure that oxygen was eliminated. The sample compartment was jacketed, and dry air was used to prevent condensation on the slide and cuvette faces when experimental conditions were below room temperature.

Measurements were made on a Cary Eclipse fluorescence spectrophotometer (Varian Instruments, Walnut Creek, CA) equipped with a temperature controller and multi-cell holder. This instrument, which collects in analog mode, uses a high intensity pulsed lamp and a time delay was used to avoid any fluorescence during the lamp pulse. Phosphorescence and delayed fluorescence emission scans were collected over the range from 535-800 nm with an excitation wavelength of 525 nm. The excitation and emission monochromators were both set at 10 nm band pass. Each data point (collected at 1 nm

intervals with a 0.1 s averaging time) was collected from a single flash with a 0.2 ms delay, 0.5 ms gate time, and 4.0 ms total decay time. Excitation scans were collected using the same electronic parameters over the range of 400-600 nm with a 688 nm emission wavelength and both monochromators set at 10 nm.

Lifetime measurements were collected under air or under the nitrogen purge, and the following experimental parameters were the same in both instances. Samples were excited at 540 nm and the emission was measured at 685 nm with a 20 nm bandpass for both excitation and emission monochromators. Each time-resolved decay was the average of 40 cycles, and for each cycle data was collected from a single flash with a delay of 0.1 ms, a 0.02 ms gate time, and 4.0 ms total decay time. All experiments were done in at least triplicate and the standard deviation of the averages was calculated to validate reproducibility. All lifetime experiments were conducted over a temperature range of 0-100°C, and temperature was increased at ten degree increments with a 15 minute delay between readings.

Data Analysis

The emission spectra were analyzed by fitting both the delayed fluorescence and the phosphorescence to a lognormal function.

$$I(\nu) = I_0 \exp\{-\ln(2)[\ln(1+2b(\nu-\nu_P)/\Delta)/b]^2\} \qquad (1)$$

In this equation I_0 is the maximum intensity value of the emission spectra, ν_P is the frequency in cm^{-1} of the emission maximum, Δ is the line width parameter, and b is the asymmetry parameter. The bandwidth of the emission, the full width at half maximum (Γ), is related to b and Δ.

$$\Gamma = \Delta \sinh(b)/b \qquad (2)$$

Emission spectra were fit using the program Igor (Wavemetrics, Inc., Lake Oswego, OR). We also analyzed some data by fitting with the program Nfit (Island Products, Galveston, TX), to make sure that the results agreed in both fitting programs.

Phosphorescence lifetimes were determined by nonlinear least-squares analysis with the statistical program Igor. Fits were judged satisfactory if the r^2 values were in the range of 0.995-1.0 and the modified residuals ((data – fit)/data$^{1/2}$) varied randomly about zero. Data was analyzed using a stretched exponential, or Kohlrausch-Williams-Watts (KWW), decay model which has been shown to be appropriate to describe the wide distribution of relaxation times (Champion et al., 2000) for the molecular processes that depopulate excited states in tissues (Lee et al., 2001), crystalline solids (Chen, 2003), super cooled liquids (Richert, 1997), and amorphous protein solids (Nack and Ludescher, 2006; Simon-Lukasik and Ludescher, 2004; Sundaresan and Ludescher, 2007):

$$I(t) = I(0) \exp[-(t/\tau)^\beta] + c \qquad\qquad (3)$$

Where I(t) is the intensity as a function of time following pulsed excitation, I(0) is the initial intensity at time zero, τ is the KWW lifetime, and β is the stretching exponent which characterizes the distribution of the decay times (Richert and Heuer, 1997). Further explanation of the parameters of the stretched exponential equation is provided in the results section.

The phosphorescence lifetime is the inverse sum of the rate constants associated with the various processes that depopulate the excited triplet state.

$$\tau^{-1} = k_P = k_{RP} + k_{TS1} + k_{TS0} + k_Q[O_2] \qquad\qquad (4)$$

This equation can be used to calculate k_{TS0}, the rate of collisional quenching to the ground state, if k_{RP}, k_{TS1}, and $k_Q[O_2]$ are known. Under anoxic conditions $k_Q[O_2]$, the rate

of oxygen quenching, is zero; k_{RP}, the radiative decay rate of the triplet state, is 41 s^{-1} for erythrosin B (Duchowicz et al., 1998; Lettinga et al., 2000); k_{TS1}, the rate of reverse intersystem crossing from the excited triplet state to the excited singlet state, depends on ΔE_{TS}, the energy gap between S_1 and T_1 (Simon-Lukasik and Ludescher, 2004):

$$k_{TS1}(T) = k^o_{TS1} \exp(-\Delta E_{TS}/RT) \qquad (5)$$

The slope of a Van't Hoff plot of the natural log of the ratio of delayed fluorescence (I_{DF}) to phosphorescence (I_P) intensity versus inverse temperature provides a measure of ΔE_{TS} (Duchowicz et al., 1998):

$$d[\ln(I_{DF}/I_P)]/d(1/T) = -\Delta E_{TS}/R \qquad (6)$$

(where R = 8.314 J K^{-1} mol^{-1}). Literature values of k^o_{TS1} for Ery B vary greatly depending on the matrix in which the probe was embedded. Calculated values range from 0.3 x 10^7 s^{-1} in ethanol and 6.5 x 10^7 s^{-1} in water (Duchowicz et al., 1998) to 111 x 10^7 s^{-1} in solid polyvinyl alcohol (Lettinga et al., 2000), demonstrating the large range of values. The estimated maximum k^o_{TS1} values for Ery B in amorphous BSA is 4.4 x 10^7 s^{-1} (Nack and Ludescher, 2006) and 6.5 x 10^7 s^{-1} for amorphous β-lactoglobulin (Sundaresan and Ludescher, 2007). Assuming that $k_{TS1}(T)$ (calculated using Equation 5 with ΔE_{TS} = 33.23 +/- 0.3 kJ mol^{-1} for gelatin) cannot result in values for $k_{TS0}(T)$ that decrease with temperature. This procedure thus estimated the minimum possible values for $k_{TS0}(T)$.

Results

The delayed emission spectra for Ery B in the amorphous cold cast gelatin films over the temperature range of 0-100°C can be seen in Figure IV-4. The long wavelength emission band represents phosphorescence from the excited triplet state (T_1) and the short

wavelength band is delayed fluorescence, occurring after reverse intersystem crossing from the T_1 state back to the excited singlet (S_1) state and the subsequent release of the photon to the ground state (S_0). Our studies focus on phosphorescence, due to the relative time scales of protein motions in the amorphous state. The phosphorescence intensity peak decreases as temperature increases, because at higher temperatures there is more energy available for the excited Ery B molecules to participate in reverse intersystem crossing from the T_1 back the S_1 state, and as a consequence of this process, we observe an increase in delayed fluorescence as temperature increases. The energy gap (ΔE_{TS}) between the singlet and triplet states is easily calculated from the slope of $\ln(I_{DF}/I_P)$ vs $1/T$ as explained in the Materials and Methods Section, Equation 6. The ΔE_{TS} for gelatin was calculated to be 33.23 +/- 0.3 kJ mol^{-1}, which is similar to amorphous globular proteins, BSA and β-lactoglobulin, which had values of 32.9 +/- 0.5 kJ mol^{-1} and 33.6 +/- 0.8 kJ mol^{-1}, respectively (Nack and Ludescher, 2006; Sundaresan and Ludescher, 2007). Other amorphous carbohydrate matrices also showed similar values, such as sucrose (31.6 +/- 0.4 kJ mol^{-1}) (Pravinata et al., 2005), maltose (32.7 +/- 1.1 kJ mol^{-1}) (Shirke and Ludescher, 2005b), lactose (34.1 +/- 0.3 kJ mol^{-1}) and lactitol (34.0 +/- 0.3 kJ mol^{-1}) (Shirke et al., 2006). Values found in the literature for Ery B in various aqueous solutions vary significantly from the aforementioned amorphous systems. Examples include water (36.9 +/- 0.6 kJ mol^{-1}), aqueous sucrose (36.9 +/- 1.0 kJ mol^{-1}) (Pravinata et al., 2005), ethanol (28.5 +/- 2.5 kJ mol^{-1}) (Duchowicz et al., 1998), and polyvinyl alcohol (41.2 +/- 0.4 kJ mol^{-1}) (Lettinga et al., 2000). This review of previous reported ΔE_{TS} values displays that the energy gap is modulated by specific interactions in each matrix,

and that the state of the matrix plays a significant role in the amount of energy needed to overcome the energy gap between the S_1 and T_1 state.

The temperature dependence of the phosphorescence peak energy (ν_P) and the bandwidth (Γ), or full width at half maximum, are shown in Figures IV-5a and IV-5b, respectively. Gelatin showed an almost linear decrease in emission energy (besides the slight break in data ~40°C), with the emission values being considerably higher over the entire temperature range, much more than in the amorphous globular proteins BSA and β-lactoglobulin (Nack and Ludescher, 2006; Sundaresan and Ludescher, 2007). The fibrous gelatin matrix does not have a break point temperature at which we observe a significant increase in dipolar relaxation (decrease in emission energy). When compared to amorphous globular proteins, we can conclude that this matrix as a whole participates in less dipolar relaxation around the excited triplet state due the higher emission energy values (Pravinata et al., 2005; Richert, 2000). The emission bandwidth Γ measures the extent of inhomogeneous broadening due to the probe emitting from distinctly different sites within the matrix. Γ increased linearly until 70°C and then a more drastic increase was observed. From the emission energy data we can conclude that at higher temperatures gelatin has greater dipolar relaxation rates and a larger distribution of energetically distinct local environments within the matrix.

The phosphorescence emission intensity decay at 20°C in gelatin under nitrogen and dry air conditions along with the fits from the stretched exponential function (represented by the solid line through the raw data) are shown in Figure IV-6a. The modified residuals for these fits, shown in Figure IV-6b, varied randomly about zero indicating the stretched exponential model provides a satisfactory fit for the data. The

Kohlrausch-Williams-Watts lifetime (τ) and stretching factor (β) are the physically meaningful parameters of the fit intensity decay. The stretched exponential decay model was initially chosen because previous studies have shown its applicability for fitting the luminescence decays of amorphous solids (Jaba et al., 2000; Nack and Ludescher, 2006; Pravinata et al., 2005; Shirke et al., 2005; Simon-Lukasik and Ludescher, 2004). As expected, the stretched exponential model provided a statistically reasonable fit to the gelatin data.

Under both nitrogen and oxygen conditions, lifetime values (τ) decreased slowly and linearly until reaching 50°C, where the values declined more dramatically (Figure IV-7a). This slight break in the data is most likely due to matrix softening as the temperature increases. As τ values decrease the matrix is becoming less rigid. A similar trend was observed in all the amorphous carbohydrate and protein matrices studied in our laboratory.

The stretching factor (β) provides a measure of the width of the lifetime distribution required to adequately fit the intensity decay. As β values decrease from 1 (1 meaning the matrix is homogenous having only one lifetime), the matrix is becoming more heterogeneous. In other studied matrices, β values also decreased with an increase in temperature, although to a greater extent. Other protein matrices (BSA (Nack and Ludescher, 2006) and β-lactoglobulin (Sundaresan and Ludescher, 2007)) had considerably lower β values when oxygen was present. This was attributed to the oxygen molecules being capable of penetrating the matrix and hence altering the dynamic environment surrounding the probe. The gelatin films had higher β values when oxygen was present compared to films which were under constant nitrogen purge. The higher β

values in the presence of oxygen is due to the values not being statistically significant, since the error bars for the oxygen and nitrogen data overlap. Gelatin films may be somewhat impermeable to oxygen molecules, and thus the presence of oxygen molecules would not lower β as in other studied matrices.

Photophysical Rate Constants

Further analysis of lifetime measurements provide additional insight regarding the effect of temperature on matrix mobility and oxygen permeability in amorphous gelatin films. The underlying photophysical rate constants for the de-excitation of Ery B in amorphous gelatin films are easily calculated. As seen in Equation 4, the total rate of decay ($k_P = \tau^{-1}$) is equal to the sum of the radiative and nonradiative rates. The radiative decay rate (k_{RP}) for Ery B is constant at 41 s^{-1}. The reverse intersystem crossing rate (k_{TS1}) is calculated as described in the Materials and Methods section, and it increased from 15 s^{-1} at 0°C to 760 s^{-1} at 100°C (Figure IV-8a). Under nitrogen conditions, adding k_{RP} and k_{TS1} and subtracting this value from the total decay rate k_P, we are left with $k_{TS0,}$ or the vibrational relaxation rate due to collisional quenching. Based on the required assumptions in this calculation, k_{TS1} may be overestimated at the expense of k_{TS0}. Oxygen quenching ($k_Q[O_2]$), or permeability, is calculated directly from the lifetime differences in the presence and absence of oxygen.

Figure IV-8b shows a slight increase in molecular mobility (k_{TS0}) for the gelatin matrix over the temperature range of 0-100°C. k_{TS0} increased linearly from 1375 s^{-1} at 0°C to 1470 s^{-1} 100°C. The low values and small range of k_{TS0} correlates to the high rigidity seen in the matrix (from the lifetime values), and the small extent of dipolar relaxation around the excited triplet state (from the peak frequency values), which both

hint toward a less mobile matrix. The k_{TS0} data differs greatly as compared to the other amorphous sugars and proteins studied in our lab. In these previously studied matrices (sucrose (Pravinata et al., 2005), maltose, glucose, maltotriose (Shirke and Ludescher, 2005b), BSA (Nack and Ludescher, 2006), β-lactoglobulin (Sundaresan and Ludescher, 2007)), we were under the assumption that 1600 s^{-1} represented the basal level of nonradiative decay (Nack and Ludescher, 2006; Pravinata et al., 2005; Shirke et al., 2005; Sundaresan and Ludescher, 2007) for amorphous systems at or below room temperature. In these systems, the k_{TS0} versus temperature curve was biphasic with a dramatic increase in k_{TS0} values, usually around 60°C, and for example, BSA k_{TS0} values were 1590-2520 s^{-1} over the over the same temperature range (Nack and Ludescher, 2006). Gelatin does not show any drastic increases in k_{TS0} over this temperature range, and never reaches the assumed basal level of vibrational collisions (1600 s^{-1}) in amorphous matrices at low temperatures (Nack and Ludescher, 2006; Pravinata et al., 2005). From this data, we conclude that gelatin is a rigid non-mobile matrix that is relatively stable to heat treatments up to 100°C.

The oxygen quenching rate ($k_Q[O_2]$), or oxygen permeability, increased gradually and linearly until ~40°C, where there was a more drastic increase with each 10°C temperature increase (Figure IV-8b). This break in the curve correlated to the observed breakpoint from the Arrhenius plot of $k_Q[O_2]$ in Figure IV-8c, which was around 30°C. On a comparative basis with the globular proteins BSA (Nack and Ludescher, 2006) and β-lactoglobulin (Sundaresan and Ludescher, 2007), the oxygen permeability values are almost 15 times lower in gelatin.

Activation energies were calculated over the temperature range of 0-100°C for both k_{TS0} and $k_Q[O_2]$. The apparent activation energy (ΔE_A) for k_{TS0} was 0.5 kJ mol^{-1} (with an r^2 value of 0.92 based on a linear fit to data in Figure IV-8c), which was significantly smaller as compared to amorphous globular proteins, having values of 3.1 kJ mol^{-1} for BSA over the temperature range of 0-100°C (Nack and Ludescher, 2006) and 2.4 and 21.4 kJ / mol^{-1} at low (-10-50°C) and high (90-120°C) temperatures for β-lactoglobulin (Sundaresan and Ludescher, 2007). The low activation energy for k_{TS0} in gelatin would lead us to believe that throughout the tested temperature range for gelatin, the small changes in k_{TS0} are due to vibrational and small scale rotational motions, where the increase in ΔE_A for k_{TS0} at higher temperature in the other matrices represented collective motions of larger regions in the protein matrix (Hill et al., 2005; Nack and Ludescher, 2006).

The rate of oxygen quenching in gelatin had a much higher ΔE_A value of 26.0 kJ mol^{-1} (with an r^2 value of 0.99 based on a linear fit to data in Figure IV-8c) as compared to k_{TS0}. There is a slight break in the data around 70°C. This does not correlate to the breaks in the k_{TS0} (~40°C) data, and we hypothesized that molecular mobility and oxygen permeability were caused by different underlying physical motions (different small scale anharmonic motions and vibrations). Figure IV-8d, however, shows that these nonradiative processes for collectively depopulating the excited triplet state are indeed related in a linear fashion, with a slight break in the data around room temperature, which was where we noticed a break in the molecular mobility. This would lead us to believe that molecular mobility and oxygen permeability are related in the gelatin films, maybe

due to the coupling of small scale vibrational motions with larger scale cooperative (global) motions (Yoshioka and Aso, 2007).

Dynamic Site Heterogeneity

The effect of delay time on the peak frequency and full width at half maximum of the phosphorescence emission spectra of Ery B in cold cast gelatin films can be seen in Figures IV-9a and IV-9b. The peak frequency exhibited a blue shift (to higher energy) as a function of increased delay time (0.1, 0.6, 1.1, 1.6, and 2.1 ms) following excitation. This trend was observed at 20ºC, 40ºC, 60ºC, and 80ºC (with trends being parallel in nature and exhibiting a ~40 cm^{-1} increase for each 0.5 ms increase in delay time). These data do not follow the homogeneous relaxation model, where emission energy is expected to decrease as the delay time after excitation increases, since some of the emission energy is lost with increased delay time (Demchenko, 2002; Lakowicz, 1999; Richert, 2000). We interpret this data in the following manner: at the short delay times, the emission energy is the average from all the chromophores, and spectra collected with the long delay time measure the emission energies only from local high energy sites, which have long-lived chromophores. This blue shift with increased delay time was also observed in amorphous BSA (Nack and Ludescher, 2006), sucrose (Pravinata et al., 2005), and β-lactoglobulin (Sundaresan and Ludescher, 2007), and this theory is also supported through the lifetime data as a function of emission wavelength.

Phosphorescence intensity decays were measured as a function of emission energy, and τ is plotted as a function of emission wavelength in Figures IV-10 over the temperature range of 0-100°C. At lower temperatures there was a significant linear decrease in lifetime as the emission wavelength moved from blue to red (660-720 nm)

with the lifetime values being 0.76 ms and 0.65 ms, respectively. Lifetime values

continued to decrease monotonically, though less drastic, until 80°C. At temperatures

above 80°C the lifetime values were essentially constant across the entire emission

wavelength range, with the 100°C data constant at ~41 ms. As expected, the lifetime

values for all emission wavelengths decreased as temperature increased.

The stretching factor (β) as a function of emission wavelength is plotted in Figure

IV-10b. The β values were relatively constant across the wavelength range of 660-720

nm for temperatures below 70°C, and over the temperature range of 70-100°C values

peaked around 685 nm. This peak of β values at higher temperatures was also observed

in BSA (Nack and Ludescher, 2006), and suggests that at higher temperatures the blue

and red-shifted sites of the emission scan showed increased dynamic heterogeneity. At

temperatures above 70°C, the red and blue emission edges are monitoring the individual

local environments, emitting at the respected wavelengths, and we notice that the red and

blue edges are more heterogeneous. Beta values peaked at ~685 nm (peak emission

wavelength), which represents the averaged heterogeneity of the matrix as a whole. β

decreased systematically over the temperature range, once again suggesting that at higher

temperatures the matrix becomes more heterogeneous.

In previous studies of amorphous sugars and globular proteins (Nack and

Ludescher, 2006; Pravinata et al., 2005; Shirke and Ludescher, 2005b), it was thought

that the variation of lifetimes as a function of emission wavelength must be a reflection of

the variation in k_{TS0}, with probes in high energy sites having smaller values of k_{TS0} and

probes in low energy sites having higher k_{TS0} values. Figure IV-8a shows that as k_P

increases under nitrogen conditions, k_{TS1} shows a large rate increase in nonradiative

quenching as the temperature increased, but k_{TS0} is significantly larger over the temperature range, therefore having a greater effect on the nonradiative quenching of the probe. In the gelatin matrix, k_{TS0} seemed to be essentially constant over the temperature range of 0-100°C, but the plots of ln $(1/k_{TS0})$ versus $1/T$ at various emission wavelengths (Figure IV-11) and the subsequent ΔE_A values (Figure IV-12) showed that there are different localized motions (dynamic site heterogeneity) responsible for the slight increases in molecular mobility. The blue-shifted sites (660-680 nm) showed two different types of motions present at high and low temperatures, with ΔE_A values being approximately 10 times higher at the higher temperature range (70-100°C). The molecular motions for the red-shifted sites were constant over the temperature range with ΔE_A values of 0.01-0.03 kJ mol^{-1}, meaning that the lower energy sites are most likely participating in small scale vibrational motions over the entire tested temperature range. This being said, the values are still very low as compared to other amorphous matrices, thus molecular mobility may play a less significant role in the non-radiative quenching of the excited probe in the triplet state for fibrous dried proteins as compared to the previously studied globular proteins and sugars. The large increase in k_P values seen in Figure IV-8a is most likely a function of the increase in k_{TS1} at higher temperatures where we would expect an increase in reverse intersystem crossing due to the additional thermal energy available to overcome the energy gap between the triplet and singlet states.

Discussion

Previously, we have demonstrated the usefulness of phosphorescence from the luminescent probe Ery B as a novel means for determining molecular processes such as matrix dipolar relaxations, molecular mobility, oxygen permeability, and dynamic site

heterogeneity in various amorphous carbohydrates (sucrose (Pravinata and Ludescher, 2003; Pravinata et al., 2005), maltose and maltitol (Shirke and Ludescher, 2005a; Shirke et al., 2005), lactose and lactitol, (Shirke et al., 2006)) and globular proteins (BSA (Nack and Ludescher, 2006) and β-lactoglobulin (Sundaresan and Ludescher, 2007)) as a function of temperature. Gelatin, has only been studied in depth via phosphorescence as a function of relative humidity and plasticizer content (Lukasik and Ludescher, 2004, 2006a, b; Simon-Lukasik and Ludescher, 2004). The focus of this study was to monitor how molecular processes in gelatin are affected by changes in temperature, and then compare these results to that of the previously studied amorphous matrices. Ery B phosphorescence from the gelatin matrix was sensitive to both dipolar relaxations around the excited triplet state monitored by peak frequency values and also to molecular collisions via lifetime measurements. We were also able to better understand the dynamic site heterogeneity within this matrix by changing the delay times from which the peak frequency was collected and lifetime measurements as a function of emission wavelength.

Dipolar Relaxations

The dipolar relaxations of Ery B were monitored by peak frequency as a function of temperature. Because dipolar relaxations stabilize the Ery B triplet state and lower the emission energy (Richert, 2000; Stratt and Maroncelli, 1996), the decrease in peak energy with temperature provides direct evidence for an increase in the extent of dipolar relaxation, presumably because of an increase in the dipolar relaxation rate. The peak frequency trend had a break around 40°C which could reflect the onset of increased mobility of the protein side chains. The amorphous sugars all displayed a break in the

trend with increasing dipolar relaxation around their respected T_g values, and the amorphous globular proteins also displayed a break in their trends due to matrix softening, or possible denaturation. We hypothesize that the lack of increased dipolar relaxations over this temperature range stems from the fact that a dynamic transition for amorphous gelatin has not been met, since T_g has been found to be between 180-220°C in dried gelatin films (Marshall and Petrie, 1980; Pinhas et al., 1996; Sobral and Habitante, 2001). The slight decrease in frequency (increased dipolar relaxations) may be due to small scale reorientations around the excited state, and not from cooperative motions from rotations or vibrations of segmental protein portions which would occur above T_g. Also, when comparing the peak frequency values to the globular proteins, gelatin had much higher ν_P values, further backing our hypothesis that physically different dipolar relaxation processes are taking place in this fibrous protein.

Molecular Mobility

The triplet state lifetime decreases with temperature due to thermal activation of the reverse intersystem crossing rate to the excited singlet state (k_{TS1}) and collisionally activated nonradiative decay to the ground singlet state (k_{TS0}). k_{TS0}, because of its sensitivity to collisions between matrix groups and the probe, provides an estimate of the overall matrix mobility. Gelatin films are an entangled polymer network made of a variable number of physical cross-links, depending on the temperature and time of drying (Slade et al., 1989). These cross-links most likely modulate the molecular mobility of the matrix (Lukasik and Ludescher, 2006b). Molecular mobility in the cold cast amorphous gelatin film changed very little over the tested temperature range. The $k_{TS0}(T)$ curve lacked the biphasic nature (increase in mobility) observed in other amorphous protein

matrices, and it may be that this was due to the physical cross-links formed since gelatin films were set below the melting temperature of the collagen-like triple helices. Physical cross-links have been known to increase the macroscopic strength and thermal stability of gelatin films (Bigi et al., 2001; Menegalli et al., 1999), and it would be logical to assume that these films would also have a very low molecular mobility (even lower that what was hypothesized as the basal level of molecular mobility in BSA (Nack and Ludescher, 2006), sucrose (Pravinata et al., 2005), maltose and maltitol (Shirke et al., 2005), and β-lactoglobulin (Sundaresan and Ludescher, 2007)). Cross-linking yields a more rigid and thermally stabile gelatin film, especially at low water contents (Bigi et al., 2001). Under wet conditions, Bigi et al. (2001) found that the denaturation temperature of gelatin films increased greatly as the number of cross-links increased, and that the denaturation enthalpy decreased drastically, due to a reduction of hydrogen bonds which break endothermically and also an increase in covalent cross-links which break exothermically. Dried gelatin films, on the otherhand, maintained a constant denaturation temperate (~90°C) as the number of cross-links increased, and the denaturation enthalpy decreased significantly. This is because the dried films are dominated by covalent cross-links breaking exothermically, with little effects from hydrogen bonding (Bigi et al., 2001). Similarly, increased thermal stability of collagen is attributed to an increase in cross-links as the matrix ages (Bailey and Paul, 1999), and cross-links form at the expense of the ability to bind water (Bigi et al., 2000; Fraga and Williams, 1985).

A direct comparison of cold and hot cast films (as an effect of relative humidity) showed the cold cast film to be more mobile and heterogeneous (Lukasik and Ludescher, 2006b). It was speculated that the cross-links in the gelatin solution before drying

introduced physical constraints inhibiting efficient packing and subsequent interactions, leading to a more mobile environment. Our sample preparation included heating above 65°C and then drying at room temperature, avoiding the before mentioned cross-linking in the solution, which may have been why we observed lower molecular mobility. Also, the studies performed by Lukasik and Ludescher (2006a, 2006b), used a derivative of Ery B (erythrosin isothiocyanate) which was covalently bound to lysines, and therefore, was limited in the mobilities it could express. Since it is not possible to determine the triple helix content of these gelatin films, is it unknown how many cross-links are required to modulate the molecular mobility of this complex matrix (Lukasik and Ludescher, 2006b), which is very sensitive to preparation and storage conditions.

The apparent activation energy for molecular mobility that modulates k_{TS0} in gelatin over the temperature range of 0-100°C was very low (0.5 kJ / mol^{-1}) as compared to previously tested globular proteins. This is most likely a function of the types of motions taking place within the gelatin matrix, which was tested well under the estimated T_g for dried amorphous gelatin which is ~180-220°C (Kozlov and Burdygina, 1983; Marshall and Petrie, 1980; Pinhas et al., 1996; Slade and Levine, 1987; Sobral and Habitante, 2001). Kozlov and Burdygina (1983) reported that at ~200°C the helical structure of gelatin starts to degrade with the subsequent breaking of three-stranded segments into separate chains, and this is when gelatin macromolecules become highly mobile. At temperatures up to ~220°C, glassy state gelatin behaves as a brittle solid with low deformability, and the heating of gelatin in the glassy state, due to the large number of functional groups, actually increased the molecular interactions and material rigidity (Kozlov and Burdygina, 1983), most likely outweighing any increases of local small

scale molecular mobility. We can conclude that the motions within the gelatin matrix are small scale molecular vibrations and local rotations of individual amino acids, and not that of global large scale motions of coupled protein segments, which would only take place at temperatures above T_g.

Oxygen Permeability

Oxygen has proven to be a powerful quencher of the triplet state of Ery B in various amorphous proteins. Buettner (1964) conducted the initial experiments which shed light on this novel application of luminescence technology. These experiments demonstrated that comparisons of phosphorescence lifetimes in oxy and anoxic conditions provided a simple and rapid indicator of oxygen quenching in the gelatin matrix. Since the oxygen quenching constant $k_Q[O_2]$ is the product of the kinetics of oxygen diffusion (k_Q) and the thermodynamics of oxygen solubility $[O_2]$, this rate constant is essentially proportional to oxygen permeability (Nack and Ludescher, 2006).

The oxygen permeability for the cold cast gelatin films in this study was very low over the temperature range 0-100°C, with the maximum value of oxygen quenching rate being 1300 s^{-1} at 100°C. The curve was biphasic with a gradual increase in $k_Q[O_2]$ up until ~40°C and a more dramatic increase at higher temperatures. An Arrhenius plot of the data showed a linear trend as a function of temperature, with a slight break in the data around 40°C. The trend observed for $k_Q[O_2]$ follows similar trends as seen in the lifetime data under oxygen conditions, where the decrease in rigidity was gradual without a distinct break where the matrix softened significantly. Other amorphous matrices showed much more drastic break points in the oxygen quenching rates, and it is thought that these breaks correlated to the onset of oxygen permeability (and also segmental motions in

globular proteins). The slight break in these data was not the onset of permeability, but more of a matrix softening effect due to the higher temperatures. We hypothesize that the temperature of the gelatin films would have to be above 180°C (the lowest observed T_g for dried gelatin (Kozlov and Burdygina, 1983; Marshall and Petrie, 1980; Pinhas et al., 1996; Slade and Levine, 1987; Sobral and Habitante, 2001) to see the sort of break in oxygen permeation that was observed in BSA (Nack and Ludescher, 2006) and β-lactoglobulin (Sundaresan and Ludescher, 2007) at ~70°C. Lukasik and Ludescher (2006b) showed that the rate of oxygen diffusion was not affected by casting methods at low moisture contents. Other studies have demonstrated that phosphorescence from Ery B doped cold cast gelatin films showed very little oxygen quenching (Buettner, 1964; Simon-Lukasik and Ludescher, 2004). Gelatin films applied to polymer substrates and adhesives used in food packaging and studied via direct measurements of permeability, showed significant decreases in oxygen permeability regardless of whether the gelatin films were cross-linked (Scherzer and Schubert, 1998) or not cross-linked (Scherzer, 1997).

The rate of $k_Q[O_2]$ had a much higher ΔE_A value (26.0 kJ / mol^{-1}) as compared to k_{TS0}. There is a slight break in the data around 70°C. This does not correlated to the break in the k_{TS0} data (~40°C). From these data, one might hypothesize that these processes are not directly related, but a direct comparison of these parameters (Figure IV-8d), displays that these nonradiative processes for collectively depopulating the excited triplet state are indeed related in a linear fashion, with a slight break in the data around room temperature, which was where we noticed a break in the molecular mobility. The correlation between $k_Q[O_2]$ and k_{TS0} suggests the onset conditions for oxygen

permeability, although minimal, may correspond to a certain level of mobility in the matrix, and not to a specific temperature. The gelatin matrix was well under its T_g throughout the experimental temperature range, and this is most likely why there were no drastic changes in the rigidity, dipolar relaxations, molecular mobility, and oxygen permeability.

Dynamic Site Heterogeneity

We propose that dipolar relaxations, which lower the energy of the excited triplet state, and molecular motions, which quench the excited triplet state, are responsible for the dynamic heterogeneities within the amorphous gelatin matrix. These dynamic properties are only observable on the sub-nanosecond level in low viscous liquids (Stratt and Maroncelli, 1996), and are usually averaged out over their decays, thus not giving rise to spectral heterogeneities (Shirke and Ludescher, 2005a). The extremely low rates of molecular mobility observed in the cold cast amorphous gelatin matrix occur on the microsecond time scale, and therefore, it is possible to monitor variations of molecular mobility throughout the matrix via emission scans as a function of time, and intensity decays as a function of emission energy. The heterogeneities observed provide insight to the local environments within the rigid amorphous matrix.

The decrease in lifetime values across the emission band observed for Ery B in the gelatin matrix below 70°C is not consistent with the standard homogeneous relaxation model, where longer lifetime probes would have red-shifted (lower energy) emission wavelengths due to more extensive dipolar relaxations around the longer lived excited states (Pravinata et al., 2005; Stratt and Maroncelli, 1996). This decrease in lifetime is, however, consistent with the dynamic site heterogeneity model, where probes behave

differently depending on the distribution of molecular mobility within local environments (Nack and Ludescher, 2006; Pravinata et al., 2005; Shirke and Ludescher, 2005a). In the dynamic site heterogeneity model, probes with higher energy triplet states (blue-shifted) are in matrix sites with lower dipolar relaxation rates, while probes with the red-shifted emission energies would be in lower energy states as a result of faster dipolar relaxation rates. In addition, the probes in the higher energy regions have longer lifetimes (greater rigidity), and consequently lower k_{TS0} values. The probes in lower energy regions, on the other hand, have shorter lifetimes and thus higher k_{TS0} values.

k_{TS0} reflects both the vibrational coupling of Ery B from the excited triplet state to the ground state, and also the manner in which the ground state vibrational energy of the probe can be quenched by the surrounding matrix (Fischer et al., 2002). This vibrational coupling is related to the overall viscosity of the matrix (Strambini and Gonnelli, 1985), and therefore the molecular mobility of the matrix. The local environments within the matrix (blue and red-shifted sites) behave differently, where the blue-shifted sites have lower molecular mobility, and the red-shifted sites have faster modes of molecular mobility.

The activation energies for molecular mobility varied greatly over the emission band. The blue-shifted sites displayed higher activation energies for molecular mobility, and also showed separate values for high and low temperatures, whereas ΔE_A values for emissions 690-720 nm (red-shifted sites) were negligible and were not affected by temperature. The magnitude of ΔE_A has been related to the size of the reorientating groups that control the relaxations (Shirke and Ludescher, 2005a), with higher activation energies at the blue sites (especially at higher temperatures) correlating to collisions due

to larger cooperative motions. The low activation energies observed in the red-shifted sites and at low temperatures in the blue-shifted sites correlate to smaller localized vibrational motions within the gelatin matrix. Other matrices studied in our laboratory showed much higher ΔE_A values, and this is most likely because the gelatin matrix is well below its T_g. Even the larger cooperative motions in gelatin are probably caused by smaller collective groups of molecules when compared to globular proteins (gelatin had lower ΔE_A values).

Because the β values varied significantly as a function of emission wavelength, it appears that the Ery B molecules are distributed throughout varying local environments within the gelatin matrix. The β values varied systematically over the range of emission wavelengths, with the red and blue edges having the lowest β values, indicating increased heterogeneity in the local blue and red-shifted sites. The local regions have broader distributions of lifetimes and molecular mobility within the dynamic environments. At the approximate peak for emission energy (~685 nm), the lifetimes are the most evenly distributed, since the β values peak at around this wavelength.

Emission energy as a function of delay time showed that as the delay time from the initial flash increased the peak frequency values increased. This behavior was interpreted in terms of a heterogeneous emission model in which Ery B probes reside in distinct sites within the matrix, such that sites with higher emission energy have longer lifetimes (Nack and Ludescher, 2006; Pravinata et al., 2005). The short delay times correspond to the average emission energy from all the chromophores distributed throughout the matrix, and the long delay times measure the emission energies released

from local high energy sites (blue-shifted), that have long lived chromophores, further supporting the explanation of data through dynamic site heterogeneity.

Conclusions

This study demonstrates the usefulness of Ery B as an indicator of the types of molecular motions affecting mobility, oxygen permeability, and dynamic site heterogeneity in cold cast gelatin films over the temperature range of 0-100°C.   Analysis of the Ery B lifetime in the presence and absence of oxygen gave rates of vibrational quenching, k_{TS0}, which is a quantitative measure of the matrix molecular mobility, and also oxygen quenching, $k_Q[O_2]$, which is proportional to oxygen permeability. Molecular mobility was most likely limited to small scale anharmonic vibrational motions and rotations of side groups (very low k_{TS0} values), and these non-cooperative motions were expected to be an underlying cause of the very low oxygen permeability in the gelatin matrix.   Analysis of the peak frequency as a function of delay time and lifetime values as a function of emission wavelength demonstrated that gelatin is organized into distinct local environments with varying molecular mobilities.   These findings aid in understanding the complex molecular interactions in dried gelatin films, assisting in developing methods to control oxygen permeability in gelatin based edible films in the food industry which would extend shelf life by limiting the degradative processes caused by oxygen.

Chapter 4 Figures

Figure IV-1: Composition of acid-processed porcine skin gelatin.

Amino Acid	Residue Molecular Weight (Da)[1]	% Abundance
Glycine	57.05	33.00
Proline	97.15	13.19
Alanine	71.09	11.17
Hydroxyproline	131.13	9.07
Glutamic Acid	129.12	7.21
Arginine	156.19	4.90
Aspartic Acid	115.09	4.58
Serine	87.08	3.47
Lysine	128.17	2.66
Valine	99.14	2.59
Leucine	113.16	2.40
Threonine	101.11	1.79
Phenylalanine	147.18	1.36
Isoleucine	113.16	0.95
Hydroxylysine	144.17	0.64
Histidine	137.14	0.40
Methionine	131.19	0.36
Tyrosine	163.18	0.26
Average	**118 Da**	
Weighted Average	**93 Da**	

Modified from Lukasik (2005).

Figure IV-2: Functional properties of gelatin in foods.

Function	Application
Gel Former	gelled desserts, lunch meats, confectionery, pate', consomme', aspics
Whipping Agent	marshmallows, nougats, mousses, souffles, chiffons, whipped cream
Protective Colloid	Confectionery, icings, ice creams, frozen desserts and confections
Binding Agent	meat rolls, canned meats, confectionery, cheeses, dairy products
Clarifying Agent	beer, wine, fruit juices, vinegar
Film Former	coating for fruits, meats, deli items
Thickener	powdered drink mixes, bouillon, gravies, sauces, soups, puddings, jellies, syrups, diary products
Process Aid	microencapsulation of colors, flavors, oils, vitamins
Emulsifier	cream soups, sauces, flavorings, meat pastes, whipped cream, confectionery, dairy products
Stabilizer	cream cheese, chocolate milk, yogurt, icings, cream fillings, frozen desserts
Adhesive Agent	to affix nonpareils, coconut and other items to confections, to bond layered confections together, to bind frostings to baked goods, to bind seasonings to meat products

(Gelatin Manufactures Institute of America, 2001)
http://www.gelatin-gmia.com/html/rawmaterials_app.html

Figure IV-3: Commercial production of gelatin.

(Gelatin Manufactures Institute of America, 2001)
http://www.gelatin-gmia.com/html/rawmaterials.html
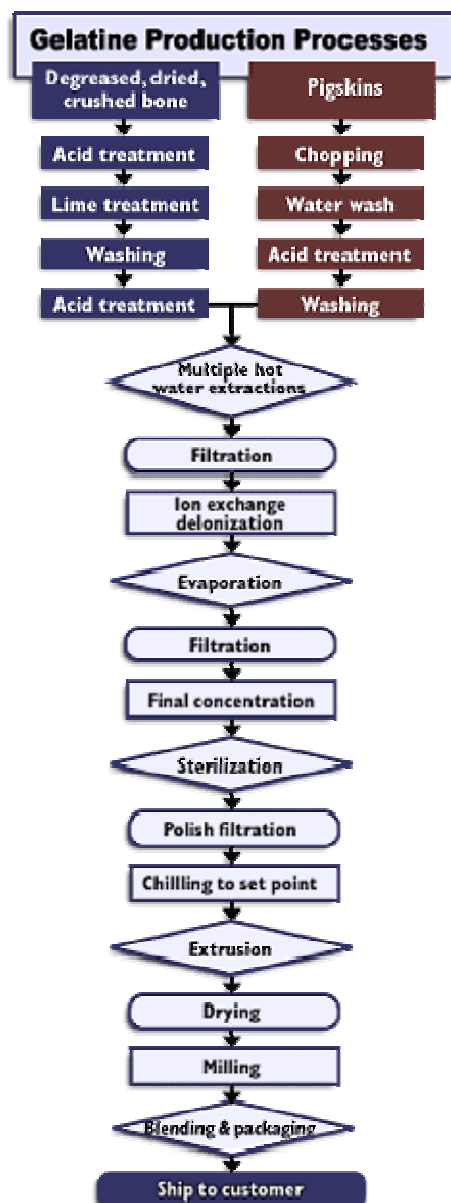
Figure IV-4: Delayed emission spectra of Ery B in amorphous gelatin film as a function of temperature (excitation at 525 nm). The spectra were collected at 10°C intervals from 0 to 100°C (curves plotted from high to low intensity at 685 nm).
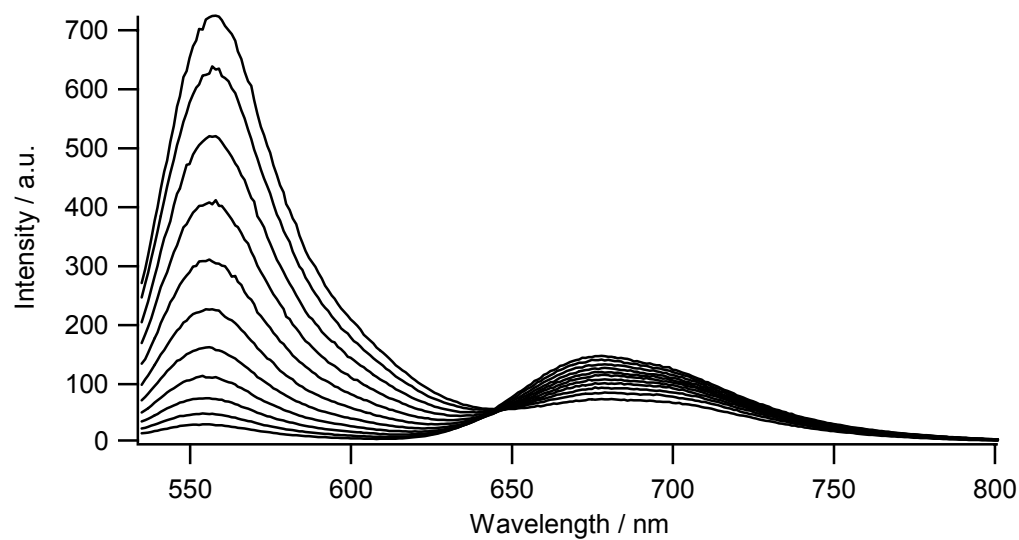
Figure IV-5: Peak energy ν_P (a) and bandwidth (full-width half maximum) (b) for phosphorescence emission from Ery B in amorphous gelatin film as a function of temperature. The delayed emission spectra were collected as a function of temperature (Figure IV-4) and were analyzed as described in Materials and Methods using equations 1 and 2.

a)
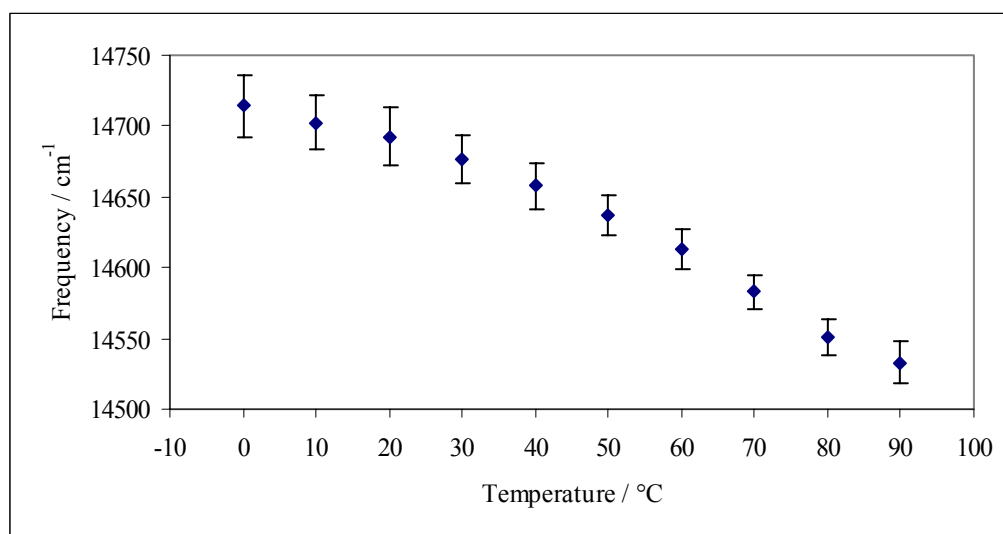
b)
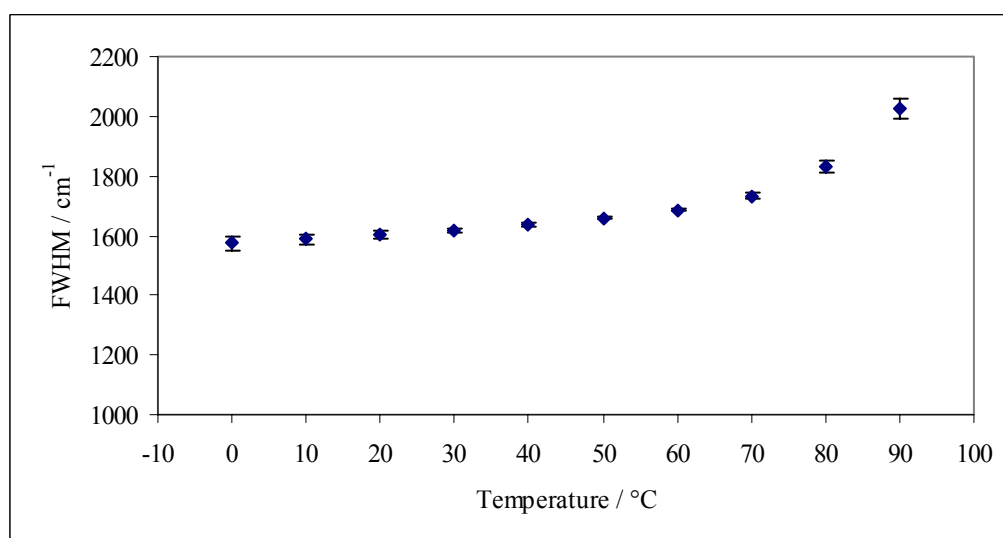
Figure IV-6: (a) Normalized phosphorescence intensity decays (I(t)/I(0)) of Ery B in amorphous gelatin film at 20°C equilibrated against nitrogen (blue) and against air (red). The solid lines through the data are fits using a stretched exponential model (equation 3, Materials and Methods) with the following parameters: $\tau = 0.69$ ms and $\beta = 0.92$ for data in nitrogen and $\tau = 0.63$ ms and $\beta = 0.91$ for data in air. (b) A plot of the modified residuals {(Data-Fit)/Data$^{1/2}$} for these fits for the data in nitrogen (blue line) and air (red line).

a)
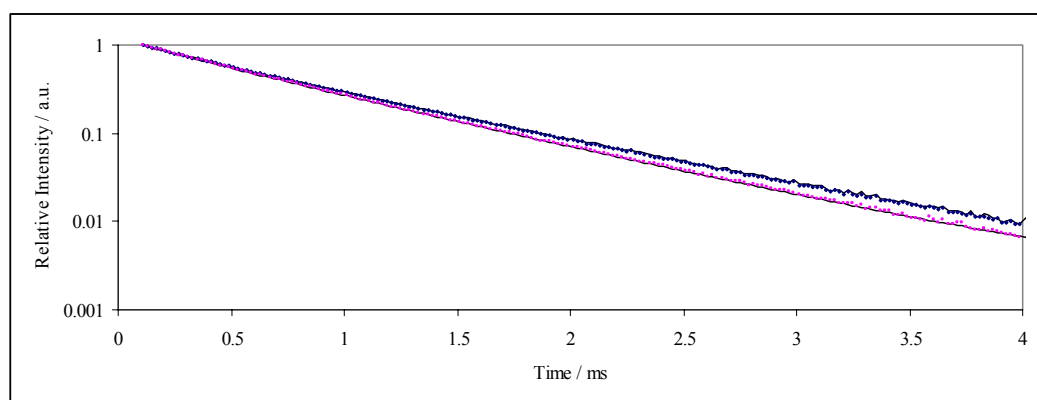
b)
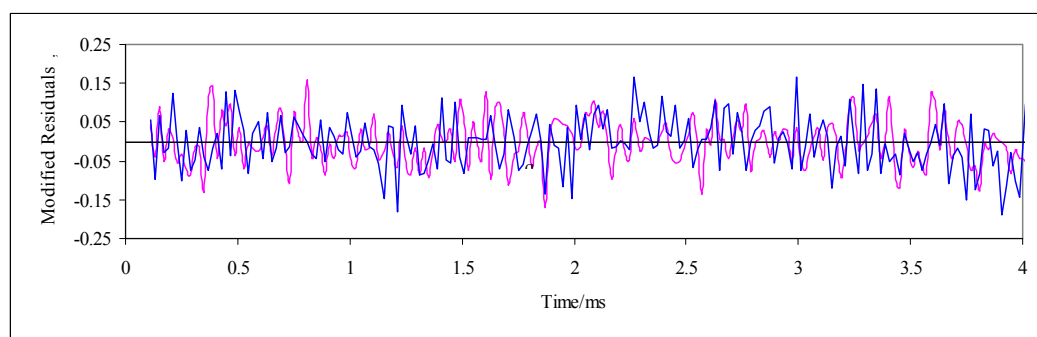
Figure IV-7: Lifetimes τ (a) and stretching exponents β (b) from a stretched exponential model fit (equation 3, Materials and Methods) for the phosphorescence intensity decay data from Ery B in gelatin films equilibrated against air.

a)
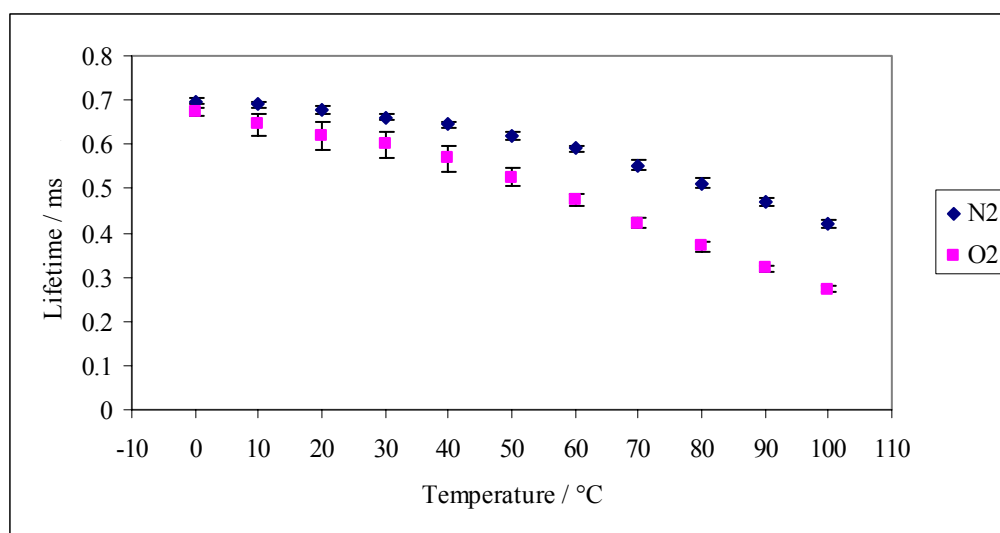
b)
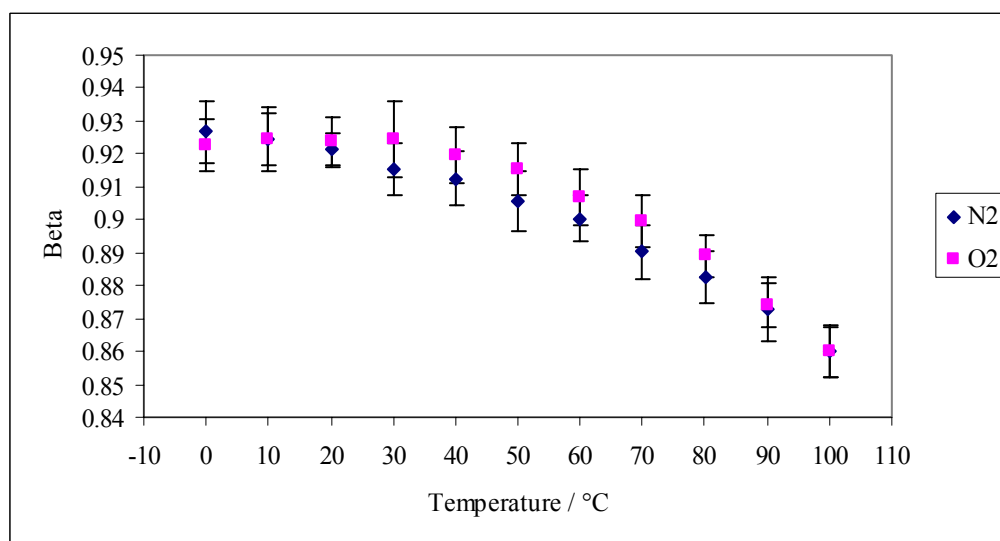
Figure IV-8: (a) Temperature dependence of the rates for non-radiative quenching (k_{TS1} and k_{TS0}) under nitrogen conditions calculated from the lifetime data in Figure IV-7a (see text for details of calculations). (b) k_{TS0} and $k_Q[O_2]$ in the presence of oxygen. (c) Arrhenius plot of k_{TS0} and $k_Q[O_2]$ (d) Plot of $k_Q[O_2]$ versus k_{TS0} over the temperature range of 0-100°C.

a)
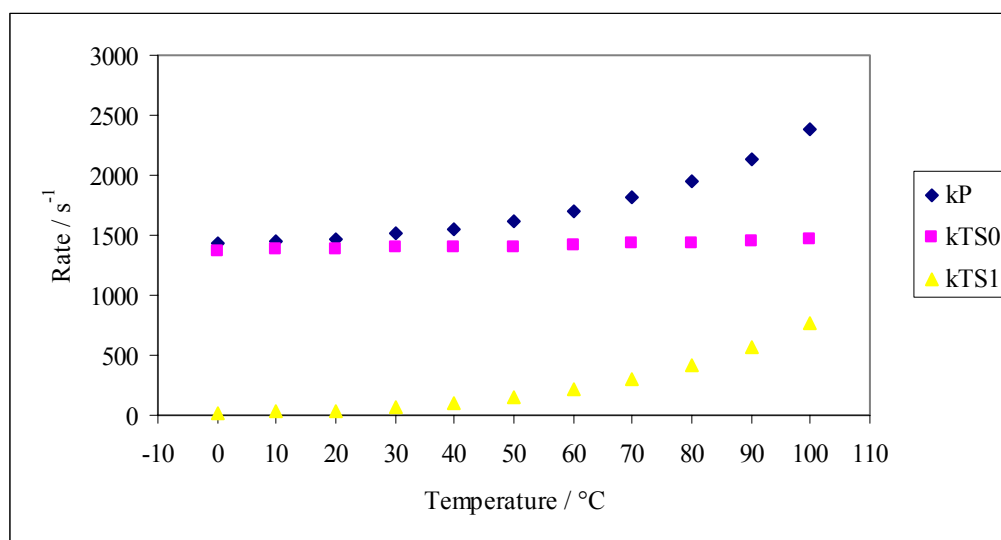
b)
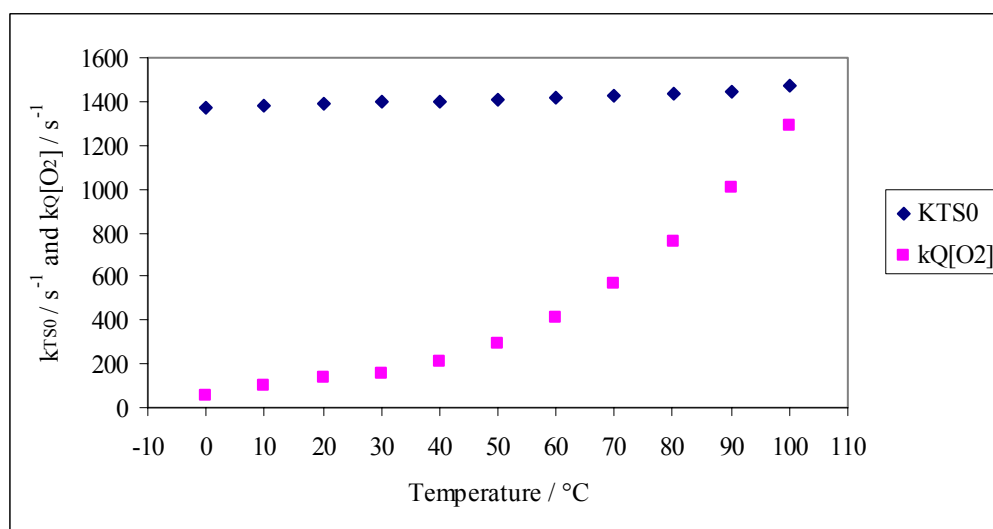
c)
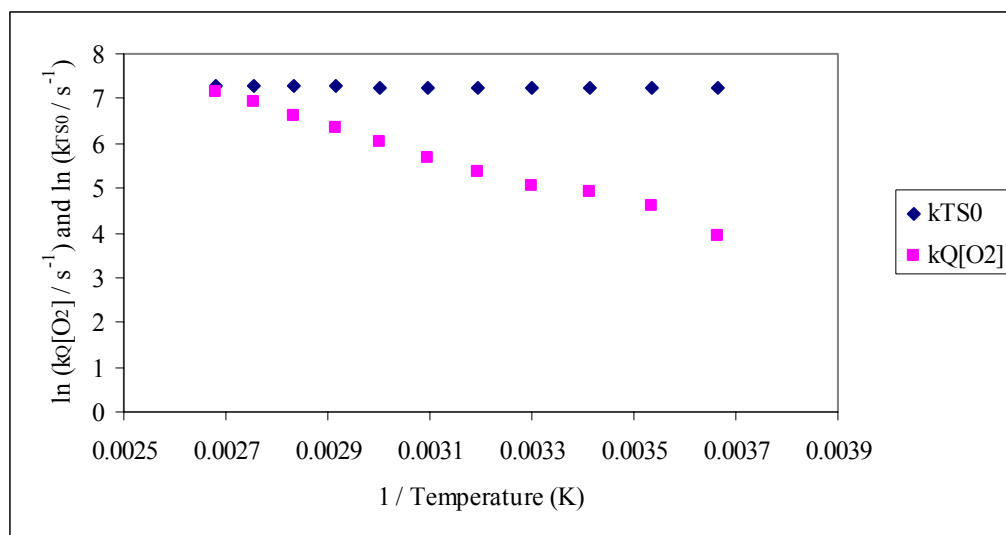
d)
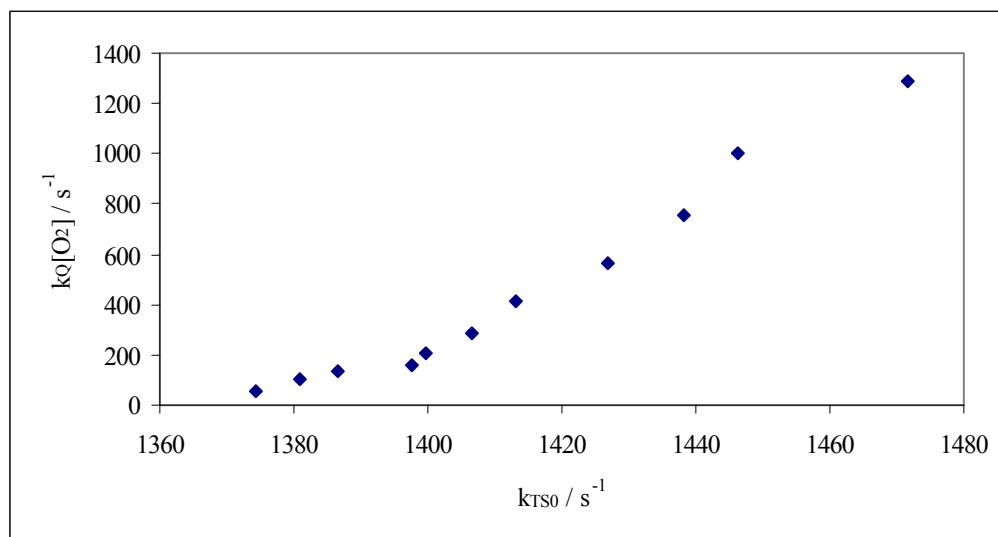
Figure IV-9: Effect of delay time on the peak frequency (a) and full width at half maximum (b) of the phosphorescence emission spectra of Ery B in gelatin films at 20ºC, 40ºC, 60ºC, and 80ºC determined from time-resolved emission spectra; peak frequency was calculated from analysis of emission spectra using a lognormal function (Equation 1, Materials and Methods).

a)
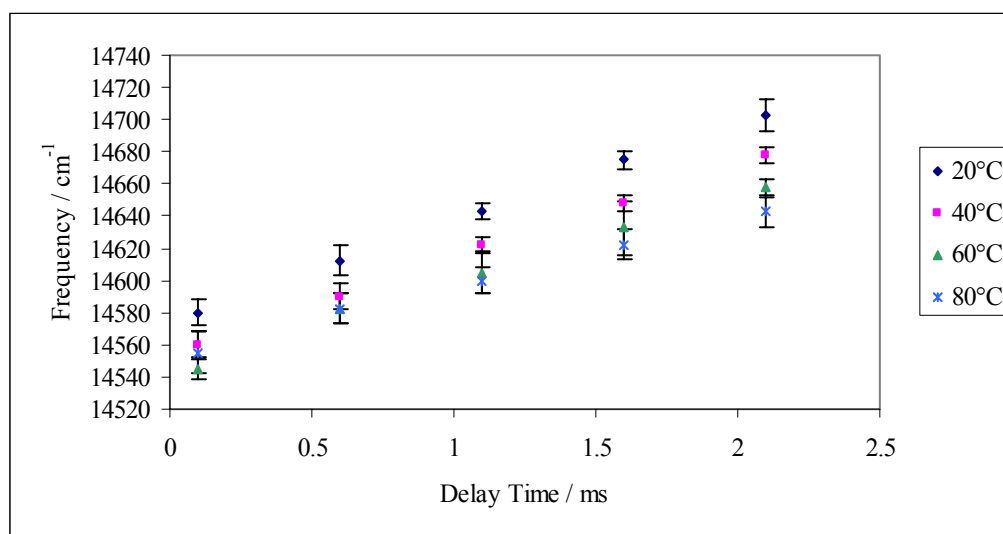
b)
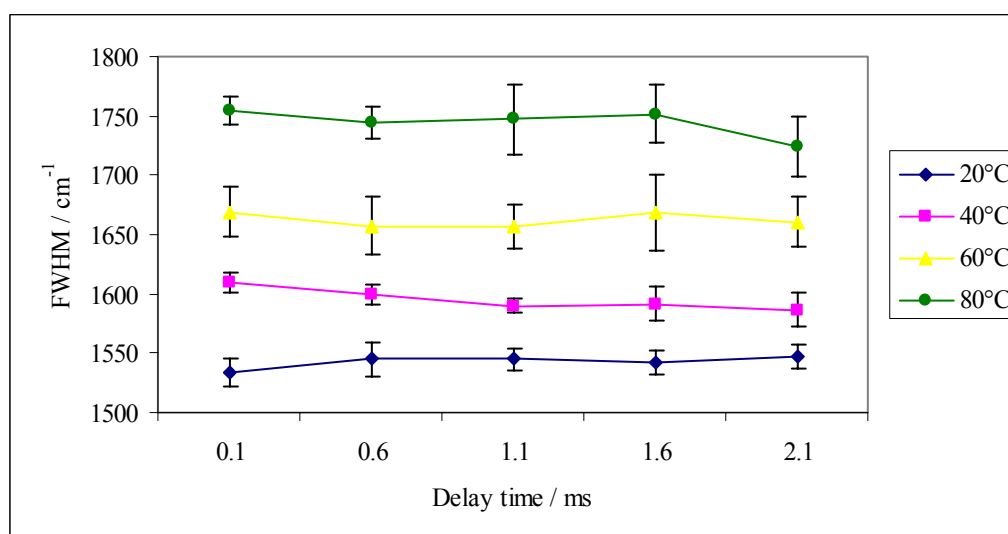
Figure IV-10: Lifetimes (a) and stretching exponents (b) from a stretched exponential model fit (Equation 3, Materials and Methods) to phosphorescence intensity decay data from Ery B in gelatin films under nitrogen conditions collected as a function of emission wavelength with excitation at 540 nm at temperatures from 0–100°C at 10°C intervals.

a)
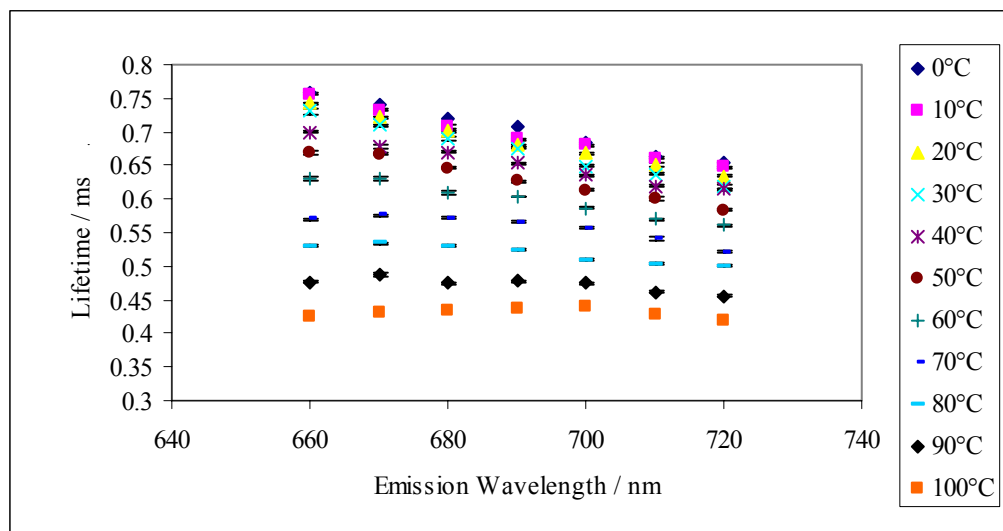
b)
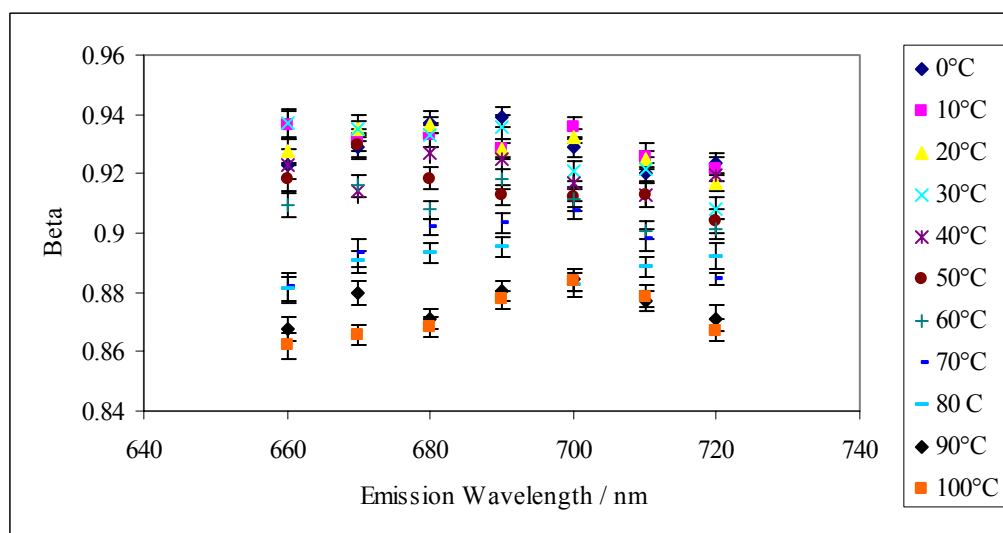
Figure IV-11: Arrhenius plots of k_{TS0} at various emission wavelengths as a function of temperature.
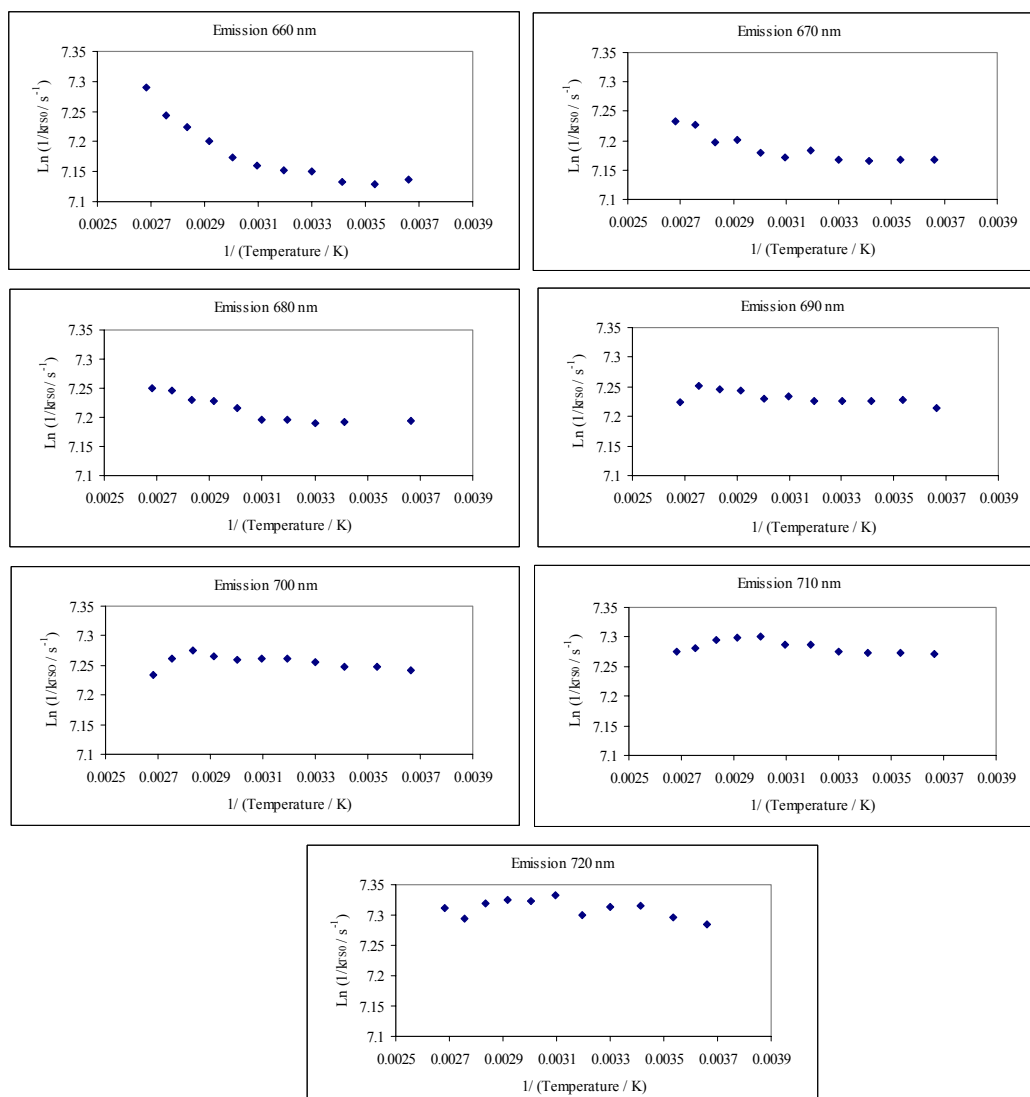
Figure IV-12: Activation energies for the non-radiative decay k_{TS0} of Ery B in amorphous gelatin at 0-30ºC (■), 70-100ºC (♦), and 0-100°C (▲); the activation energies were calculated from an Arrhenius analysis of k_{TS0} data calculated from the lifetimes in Figure IV-11.
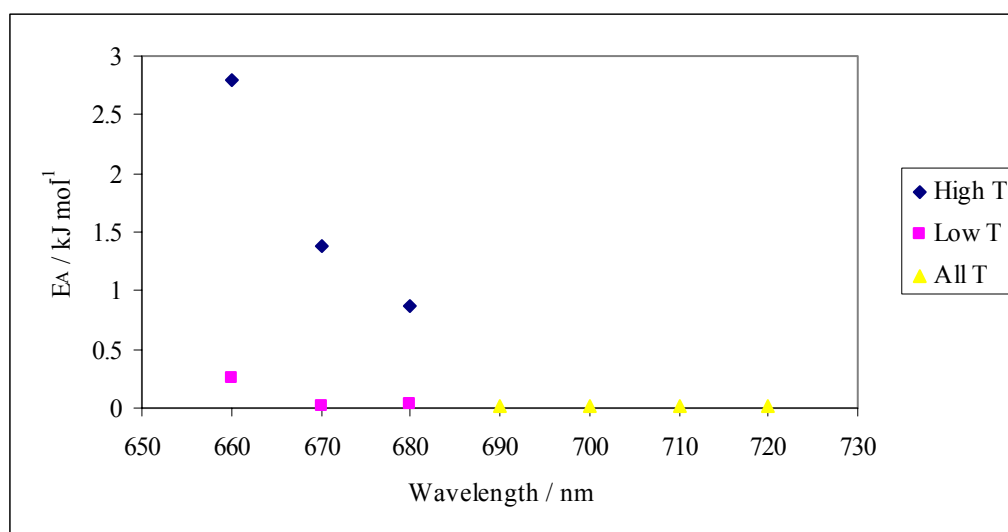
Chapter 4 References

Abitz, W., Gerngross, O., and Herrman, K. (1930). X-ray examination of gelatin micelles. *Naturwissenshaften* **18**, 754-755.

Bailey, A. J., and Light, N. D. (1989). "Connective tissue in meat and meat products," Elsevier Science Publishers, LTD, New York.

Bailey, A. J., and Paul, R. G. (1999). The mechanisms and consequences of the maturation and ageing of collagen. *Proceedings of the Indian Academy of Sciences-Chemical Sciences* **111**, 57-69.

Bigi, A., Borghi, M., Cojazzi, G., Fichera, A. M., Panzavolta, S., and Roveri, N. (2000). Structural and mechanical properties of crosslinked drawn gelatin films. *Journal of Thermal Analysis and Calorimetry* **61**, 451-459.

Bigi, A., Cojazzi, G., Panzavolta, S., Rubini, K., and Roveri, N. (2001). Mechanical and thermal properties of gelatin films at different degrees of glutaraldehyde crosslinking. *Biomaterials* **22**, 763-768.

Buettner, A. V. (1964). Flash Photolysis in Thin Films of Gelatin and Other Polymers. *J. Phys. Chem.* **68**, 3253-3259.

Chambi, H., and Grosso, C. (2006). Edible films produced with gelatin and casein cross-linked with transglutaminase. *Food Research International* **39**, 458-466.

Champion, D., Le Meste, M., and Simatos, D. (2000). Towards an improved understanding of glass transition and relaxations in foods: molecular mobility in the glass transition range. *Trends in Food Science & Technology* **11**, 41-55.

Chen, R. (2003). Apparent stretched-exponential luminescence decay in crystalline solids. *Journal of Luminescence* **102-103**, 510-518.

Cutter, C. N. (2006). Opportunities for bio-based packaging technologies to improve the quality and safety of fresh and further processed muscle foods. *Meat Science* **74**, 131-142.

Demchenko, A. P. (2002). The red-edge effects: 30 years of exploration. *Luminescence*, 19-42.

Dickinson, E., Stainsby, G., and Wilson, L. (1985). An adsorption effect on the gel strength of dilute gelatin-stabilized oil-in-water emulsions. *Colloid & Polymer Science* **263**.

Duchowicz, R., Ferrer, M. L., and Acuna, A. U. (1998). Kinetic Spectroscopy of Erythrosin Phosphorescence and Delayed Fluorescence in Aqueous Solution at Room Temperature. *Photochemistry and Photobiology* **68**, 494-501.

Emmambux, M. N., Stading, M., and Taylor, J. R. N. (2004). Sorghum kafirin film property modification with hydrolysable and condensed tannins. *Journal of Cereal Science* **40**, 127-135.

Fischer, C. J., Gafni, A., Steel, D. G., and Schauerte, J. A. (2002). The triplet-state lifetime of indole in aqueous and viscous environments: Significance to the interpretation of room temperature phosphorescence in proteins. *Journal of the American Chemical Society* **124**, 10359-10366.

Fraga, A. N., and Williams, R. J. J. (1985). Thermal properties of gelatin films *Polymer* **26**, 113-118.

Gelatin Manufactures Institute of America, I. (2001). How we make gelatin. New York. http://www.gelatin-gmia.com/html/rawmaterials.html.

Gennadios, A., Hanna, M. A., and Kurth, L. B. (1997). Application of edible coatings on meats, poultry and seafoods: A review. *Food Science and Technology-Lebensmittel-Wissenschaft & Technologie* **30**, 337-350.

Guenet, J. M. (1992). "Thermoreversible gelation of polymers and biopolymers," Academic Press, Inc., New York.

Hill, J. J., Shalaev, E. Y., and Zografi, G. (2005). Thermodynamic and dynamic factors involved in the stability of native protein structure in amorphous solids in relation to levels of hydration. *Journal of Pharmaceutical Sciences* **94**, 1636-1667.

Hinterwaldner, R. (1977). Technology of Gelatin Manufacture. *In* "The Science and Technology of Gelatin" (A. G. Ward and A. Courts, eds.), pp. 315-364. Academic Press, London.

Jaba, N., Kanoun, A., Mejri, H., Maaref, H., and Brenier, A. (2000). Time-resolved luminescence data on the 1060 nm transition in Nd3+-doped zinc tellurite glasses. *Journal of Physics-Condensed Matter* **12**, 7303-7309.

Johns, P., and Courts, A. (1977). Relationship between Collagen and Gelatin. *In* "The Science and Technology of Gelatin" (A. G. Ward and A. Courts, eds.), pp. 138-178. Academic Press, London.

Jones, N. R. (1977). Use of gelatin in edible products. *In* "The science and technology of gelatin" (A. G. Ward and A. Courts, eds.), pp. 366-394. Academic Press, New York.

Jongjareonrak, A., Benjakul, S., Visessanguan, W., Prodpran, T., and Tanaka, M. (2006). Characterization of edible films from skin gelatin of brownstripe red snapper and bigeye snapper. *Food Hydrocolloids* **20**, 492-501.

Koros, W. J. (1990). "ACS Symposium Series 423: Barrier Polymers and Structures.," American Chemical Society, Washington, DC.

Kozlov, P. V., and Burdygina, G. I. (1983). The structure and properties of solid gelatin and the principles of their modification. *Polymer* **24**, 651-666.

Krochta, J. M., and DeMulder-Johnston, C. (1997). Edible and biodegradable polymer films: Challenges and opportunities. *Food Technology* **51**, 61-74.

Lakowicz, J. R. (1999). "Principles of fluorescence spectroscopy," Second/Ed. Kluwer Academic/Plenum Press, New York.

Lee, K. C. B., Siegel, J., Webb, S. E. D., Leveque-Fort, S., Cole, M. J., Jones, R., Dowling, K., Lever, M. J., and French, P. M. W. (2001). Application of the Stretched Exponential Function to Fluorescence Lifetime Imaging. *Biophys. J.* **81**, 1265-1274.

Lettinga, M. P., Zuilhof, H., and van Zandvoort, M. A. M. J. (2000). Phosphorescence and fluorescence characterization of fluorescein derivatives immobilized in various polymer matrices. *Physical Chemistry Chemical Physics* **2**, 3697-3707.

Liu, D.-C. (2002). "Better Utilization of By-products from the Meat Industry." National Chung-Hsing University, Taichung, Taiwan.

Lukasik, K. V. (2005). Luminescent Probes of Structural and Dynamic Heterogeneity in Gelatin, Rutgers University, New Brunswick.

Lukasik, K. V., and Ludescher, R. D. (2004). Phosphorescence of erythrosin and fusin as a probe of dynamic heterogeneity in amorphous gelatin films. *Biophysical Journal* **86**, 159a-159a.

Lukasik, K. V., and Ludescher, R. D. (2006a). Effect of plasticizer on dynamic site heterogeneity in cold-cast gelatin films. *Food Hydrocolloids* **20**, 88-95.

Lukasik, K. V., and Ludescher, R. D. (2006b). Molecular mobility in water and glycerol plasticized cold- and hot-cast gelatin films. *Food Hydrocolloids* **20**, 96-105.

Marshall, A. S., and Petrie, S. E. B. (1980). Thermal transisitions in gelatin and aqueous gelatin solutions. *The Journal of Photographic Science* **28**, 128-134.

McHugh, T. H. (2000). Protein-lipid interactions in edible films and coatings. *Nahrung-Food* **44**, 148-151.

Menegalli, F. C., Sobral, P. J., Roques, M. A., and Laurent, S. (1999). Characteristics of gelatin biofilms in relation to drying process conditions near melting. *Drying Technology* **17**, 1697-1706.

Nack, T. J., and Ludescher, R. D. (2006). Molecular mobility and oxygen permeability in amorphous bovine serum albumin films. *Food Biophysics* **1**, 151-162.

Pinhas, M. F., Blanshard, J. M. V., Derbyshire, W., and Mitchell, J. R. (1996). The effect of water on the physicochemical and mechanical properties of gelatin. *Journal of Thermal Analysis* **47**, 1499-1511.

Pravinata, L. C., and Ludescher, R. D. (2003). Evidence for site-heterogeneity in amorphous sucrose from phosphorescence of erythrosin B. *Biophysical Journal* **84**, 287a-287a.

Pravinata, L. C., You, Y., and Ludescher, R. D. (2005). Erythrosin B Phosphorescence Monitors Molecular Mobility and Dynamic Site Heterogeneity in Amorphous Sucrose. *Biophys. J.* **88**, 3551-3561.

Renou, J.-P., Foucat, L., Corsaro, C., Ollivier, J., Zanotti, J.-M., and Middendorf, H. D. (2004). Dynamics of collagen from bovine connective tissues. *Physica B: Condensed Matter Proceedings of the Third European Conference on Neutron Scattering* **350**, E631-E633.

Richert, R. (1997). Evidence for dynamic heterogeneity near T-g from the time-resolved inhomogeneous broadening of optical line shapes. *Journal of Physical Chemistry B* **101**, 6323-6326.

Richert, R. (2000). Triplet state solvation dynamics: Basics and applications. *Journal of Chemical Physics* **113**, 8404-8429.

Richert, R., and Heuer, A. (1997). Rate-memory and dynamic heterogeneity of first-order reactions in a polymer matrix. *Macromolecules* **30**, 4038-4041.

Salame, M. (1986). Prediction of gas barrier properties of high polymers. *Polymer Engineering & Science* **26**, 1543-1546.

Scherzer, T. (1997). Barrier layers against oxygen transmission on the basis of electron cured methacrylated gelatin. *Nuclear Instruments and Methods in Physics Research B*, 382-391.

Scherzer, T., and Schubert, R. (1998). Oxygen permeability of electron beam cured gelatin methacrylate layers. *Polymers for Advanced Technologies* **9**, 777-785.

Shirke, S., Takhistov, P., and Ludescher, R. D. (2005). Molecular mobility in amorphous maltose and maltitol from phosphorescence of erythrosin B. *Journal of Physical Chemistry B* **109**, 16119-16126.

Shirke, S., and Ludescher, R. D. (2005a). Dynamic site heterogeneity in amorphous maltose and maltitol from spectral heterogeneity in erythrosin B phosphorescence. *Carbohydrate Research* **340**, 2661-2669.

Shirke, S., and Ludescher, R. D. (2005b). Molecular mobility and the glass transition in amorphous glucose, maltose, and maltotriose. *Carbohydrate Research* **340**, 2654-2660.

Shirke, S., You, Y. M., and Ludescher, R. D. (2006). Molecular mobility and dynamic site heterogeneity in amorphous lactose and lactitol from erythrosin B phosphorescence. *Biophysical Chemistry* **123**, 122-133.

Simon-Lukasik, K. V., and Ludescher, R. D. (2004). Erythrosin B phosphorescence as a probe of oxygen diffusion in amorphous gelatin films. *Food Hydrocolloids* **18**, 621-630.

Slade, L., and Levine, H. (1987). Polymer-chemical properties of gelatin in foods. *In* "Advances in Meat Research, Collagen as a food", Vol. 4, pp. 251-266. AVI, New York.

Slade, L., Levine, H., and Finley, J. W. (1989). Protein-water interaction: Water as a plasticizer of gluten and other protein polymers. *In* "Protein Quality and the Effects of Processing" (R. D. Phillips and J. W. Finley, eds.), pp. 9-124. Marcel Dekker, Inc, New York.

Sobral, P. J. A., and Habitante, A. M. Q. B. (2001). Phase transitions of pigskin gelatin. *Food Hydrocolloids* **15**, 377-382.

Stainsby, G. (1977). The physical chemistry of gelatin in solution. *In* "The science and technology of gelatin" (A. J. Ward and A. Courts, eds.), pp. 109-137. Academic press, London.

Stainsby, G. (1987). Gelatin Gels. *In* "Advances in Meat Research" (A. M. Pearson, T. R. Dutson and A. J. Bailey, eds.), Vol. 4. Van Nostrand Reinhold Company, New York.

Strambini, G. B., and Gonnelli, M. (1985). The indole nucleus triplet-state lifetime and its dependence on solvent microviscosity. *Chemical Physics Letters* **115**, 196-200.

Stratt, R. M., and Maroncelli, M. (1996). Nonreactive dynamics in solution: The emerging molecular view of solvation dynamics and vibrational relaxation. *Journal of Physical Chemistry* **100**, 12981-12996.

Sundaresan, K. V., and Ludescher, R. D. (2007). Molecular mobility and oxygen permeability in amorphous Beta -lactoglobulin films. *Food Hydrocolloids* **In Press**.

Veis, A. (1964). "The Macromolecular Chemistry of Gelatin," Academic Press, New York.

Ward, A. G., and Courts, A. (1977). "The Science and Technlogy of Gelatin," Academic Press Inc., London.

Wood, P. D. (1977). Technical and pharmaceutical uses of gelatin. *In* "The science and technology of gelatin" (A. G. Ward and A. Courts, eds.), pp. 414-437. Academic Press, New York.

Yakimets, I., Wellner, N., Smith, A. C., Wilson, R. H., Farhat, I., and Mitchell, J. (2005). Mechanical properties with respect to water content of gelatin films in glassy state. *Polymer* **46**, 12577-12585.

You, Y. M., and Ludescher, R. D. (2006). Phosphorescence of erythrosin B as a robust probe of molecular mobility in amorphous solid sucrose. *Applied Spectroscopy* **60**, 813-819.

Chapter 5: The molecular mobility and oxygen permeability in dried collagen sausage casings as a function of aging and temperature.

Introduction

The practice of consuming comminuted meats within an edible casing predates recorded history. Strong historical evidence states that the Chinese and Babylonians enjoyed such "sausage" type products as early as 3500 years ago, and Homer's Odyssey, written in 800 B.C. also documents the practice (Romans et al., 1985). Casings are used to form sausage products into specific shapes and to control portion size. Casings can be made from natural intestine sources, regenerated cellulose, and reconstituted or regenerated collagen (Wang, 1986). Collagen films extruded in the form of tubular casings are convenient and cheap edible packaging materials. The ground or chopped meat is stuffed into the casing, and the casing is eventually consumed as part of the product. As the manufacture of sausage type products became more automated, a uniform casing, as compared to natural gut casings, was desired. Collagen has numerous advantages over natural gut casings including a more uniform size, increased strength and flexibility to withstand various processing conditions, a cleaner more sanitary product, better consumer image, and greater consistency in the finished product (Bailey and Light, 1989; Hood, 1987; Osburn, 2002; Simelane and Ustunol, 2005). Collagen casings allow sausage manufactures to convert lower value meat portions into various sausages having higher consumer appeal and an increased retail price (Osburn, 2002).

Collagen casing technology originally stemmed from research on cotton bags or tubes which were dipped in a gelatin solution, serving as the first individual sausage casing (Hood, 1987). The gelatin films or "casings" had very little resistance to water transmission and required significant amounts of plasticizers to impart the desired

flexibility (Gennadios et al., 1997), and therefore, producing gelatin-based casings that were strong enough to withstand harsh stuffing conditions was very challenging. Other materials were tested, eventually leading to collagen.

Collagen casing manufacturing does not convert collagen to a solubilized product as done in the conversion of gelatin, but rather collagen casings result in a more fibrillar product retaining a relatively high proportion of the native collagen fiber. The extracted collagen is suspended in aqueous solvent and converted to an acid swollen gel or dough which is then extruded into the actual casings (Bailey and Light, 1989).

The collagen used in regenerated casings is derived from the corium layer of a bovine steer hide (type I collagen). The extracted collagen is chemically modified through an alkaline treatment procedure, enhancing acid swelling characteristics and disrupting the fiber structure. The chemical modification must be carefully regulated to avoid producing too much soluble collagen which would yield a casing with insufficient tensile strength (Hood, 1987).

Traditional dried casing slugs are made by two separate processes: the wet process and the dry process (See Figure V-1 for a detailed process flow). The North American wet process is an extension of the manufacture of cellulose and rubber tubing based upon extrusion, coagulation, and drying. First, cattle hides are dehaired, decalcified, ground into small pieces, and then mixed with acid to produce a viscous suspension (4-5% solids) through high shear homogenization. Cellulose or cellulose derivatives may be added to improve the mechanical properties of the casing. The slurry is then extruded into a woven fiber structure (realigning the collagen dough fibers) and passes through a coagulation bath of a highly concentrated salt solution (gaseous

anhydrous ammonia or ammonia hydroxide) and is subsequently formed into tubular casings. The high salt concentration and acid neutralization shrink the collagen fibers yielding a strong casing with a short but highly fibrillar structure. The casings are then washed and treated with plasticizers such as glycerol or sorbitol and cross-linkers such as gluteraldyhyde to improve casing pliability and strength (Osburn, 2002). Next, the casings are dried to about 10-15% moisture content (Bailey and Light, 1989; Hood, 1987) and shirred, where 50-60 feet of casing is collapsed (in a pleated fashion) down to a 7-9 inch rigid slug which fits easily over the sausage stuffing horn (Hood, 1987). In order to increase the shelf life of the casings, the slugs are usually vacuum sealed. The thickness and strength of the casing can be modified by the amount of plasticizers and cross-linking agents used (Bailey and Light, 1989). The wet process yields a more dispersed and fibrillar material (smaller units) as compared to the dry process (Bailey and Light, 1989), and the wet process can be operated at faster capacities, which typically correlates to greater profit margins.

The older European dry process, which was never adopted by American casing processors, involves the extrusion of a high solids acid-swollen collagen gel directly into a drier where neutralization and cross-linking are carried out, yielding relatively longer and larger fibers. The dry process has less waste water handling problems, but also involves more expensive equipment due to the need of high pressure plumbing (Hood, 1987).

Typical collagen casings have a collagen content of 50-65%, a moisture content of 10-15 %, a fat content of 3-6%, and the residual content is composed of additional additives such as cellulose and/or plasticizers and cross-linking agents (Bailey and Light,

1989; Hood, 1987). The thickness of collagen casings varies greatly depending on the desired application, but typical casing thicknesses are 1.1-1.4 mm (Bailey and Light, 1989).

Collagen casings are the most widely used edible sausage casings as alternatives to natural casings, and it is estimated that approximately 80% of all comminuted meat products requiring edible casings are stuffed into collagen casings (Simelane and Ustunol, 2005). The recent technology of continuous co-extrusion for making collagen encased sausages shows great promise with many of the large meat companies due to increased production volumes. Here, a collagen gel is co-extruded around the ground meat products in a very thin layer of orientated collagen fibers (Figure V-2), and is then passed through a salt brine solution to set the film and remove the water. Additionally, or alternatively, the film can be set by a cross-linking agent, usually glyceraldehyde or liquid smoke, to harden the casing (Joly et al., 2004). If the co-extruded sausages are smoked or cooked, the interactions between the meat proteins and collagen fibers are further enhanced yielding a stronger casing. These co-extruded sausages are more tender when compared to the reconstituted collagen casings, thus having better sensory attributes after cooking (Waldman, 1985). A process for producing linked co-extruded collagen casings was developed by Morgan et al. (1998) through chemically coagulating collagen with liquid smoke and a dehydrating agent, and this process has revolutionized large scale sausage production. The co-extrusion process is very fast and efficient, and currently collagen and collagen mixtures (such as with methylcellulose (Deacon and Kindleysides, 1973)) are the only materials suitable for this process.

Most of the studies carried out on collagen casings have focused on mechanical strength and permeability, as is the case with edible films composed of gelatin, and additional data on the microstructural aspects are needed. Initially, we planned on imbedding the erythrosin B (Ery B) probe in a collagen gel (a suspension of acid swollen fibers), similar to the way that casings are colored in industry to enhance external appeal in various sausage products (Morgan et al., 1998, 2001; Osburn, 2002), and subsequently making a thin film on a quartz slide as done in our lab for BSA (Nack and Ludescher, 2006), β-lactoglobulin (Sundaresan and Ludescher, 2007), and gelatin (Lukasik and Ludescher, 2004). Typical coloring agents used in casing production include annatto, Ery B, and caramel (Devro-Teepak, 1996), so this experimental method seemed ideal. A collagen gel pulled from production prior to the extrusion step was acquired from the Devro Corporation (Sandy Run, South Carolina). We were unable to embed Ery B (a water based probe) into the collagen slurry (insoluble in aqueous solutions), so an alternative and more applicable approach was devised by working backwards from a dried collagen casing obtained from Nitta Casings (Sommerville, NJ) and doping the casing with a solution of Ery B. This method was modified from a study on adhesion characteristics of collagen sausage casings (Barriga and Piette, 1996). The idea of preparing a film similar to that used in diffusion studies (Ho et al., 2001) was also contemplated, but it involved dissolving collagen in acetic acid, which would alter collagen properties, when compared to that of collagen casings.

Collagen casings must be able to withstand the rigors of high speed filling and linking operations, and casing strength can be modified by solids content, drying conditions, and the use of a cross-linking agent (Osburn, 2002). Treatment with

gluteraldhyde increased casing strength whether the casing was dry or re-wet (Rose, 1968). Miller and Marder (1998) found that exposing casings to ultraviolet radiation increased casing strength. Tanner and Wallace (1975) found that the addition of caramel to the collagen slurry resulted in decreased "fishmouthing" (the opening of casing ends when the sausage is cooked in a liquid) and also a more appealing finished color in smoked sausages (preventing the white spots that result from casing contact with smoke racks). Altering the setting salt solution by the addition of sucrose or polyethylene to the salt solution and drying to higher moisture contents also increased casing strength (Kidney, 1970). Miller (1983) injected a proteolytic enzyme into the collagen slurry before extrusion. The enzyme was not activated until the smoking or cooking step in sausage production, thus the casing remained strong during stuffing, and became more tender after cooking, greatly increasing consumer acceptance.

Atomic force microscopy has shown that oxygen affects surface interactions and adsorption in collagen films (De Cupere and Rouxhet, 2001) and that collagen films become more ordered in the presence of cross-linkers (Usha et al., 2004). The microstructural origins are not known, but molecular mobility is thought to be one of the contributing factors (De Cupere and Rouxhet, 2001). Ho et al. (2001) studied the diffusion of model drugs through collagen films, but did not look at the diffusion of oxygen. Differential scanning calorimetry has been used to study the denaturation processes in collagen fibrils, but the studies were conducted on collagen films (Usha et al., 2004) and solutions (Miles et al., 1995), and not collagen casings.

Phosphorescent techniques offer molecular data that may be the missing link in relating molecular mobility and oxygen presence to the physical and chemical properties

of the casing. This research will determine the molecular mobility and oxygen permeability in an actual collagen casings through the following experiments: matrix dipolar relaxation monitored by emission energy (ν_P) and bandwidth (FWHM) as a function of temperature, phosphorescence intensity decays and the subsequent calculations of molecular collisional quenching (k_{TS0}) and quenching due to oxygen ($k_Q[O_2]$) from the lifetime data (τ), matrix dynamic site heterogeneity determined through time resolved emission energies (ν_P) and intensity decays (τ and β) with varying emission wavelengths, and finally, the determination of the apparent activation energies (E_A) for deexcitation of the triplet state due to molecular collisions, calculated from the slope of the respective Arrhenius plot ($\ln(k_{TSO})$ or $\ln(k_Q[O_2])$) versus 1/T.

This will mark the first time our novel approaches for determining molecular mobility and oxygen permeability in model systems will be applied to an actual food product. To take these experiments one step further, we also decided to look at the casings as a function of time, similar to that of a shelf life study. Here we monitor the rigidity, heterogeneity, and oxygen permeability of the casings through phosphorescence intensity decays. This type is experiment is the first step towards making the phosphorescent techniques used in our lab applicable to actual food products.

Materials and Methods

Preparation of samples. A 10 mg/ml stock solution of erythrosin B free acid (Molecular Probes, Inc., Eugene, OR) was prepared in *N, N*-dimethlyformamide (DMF) (Sigma-Aldrich, Milwaukee, WI). DMF has negligible effects on the spectroscopic properties of the probe in amorphous sucrose at a variety of concentrations (Pravinata et al., 2005; You and Ludescher, 2006). This concentration was selected to simplify the

addition of the probe to the casing soaking solution, and the solvent was selected for probe stability during long term storage. The probe was added to distilled deionized water at a 0.01 mM concentration. At this concentration it was determined that Ery B does not aggregate, existing only as individual molecules which will disperse into the collagen casing.

Collagen casings were obtained from Nitta Casing, Inc (Somerville, NJ) and were kept under refrigeration in the original package until ready for use. 1.0 cm X 1.0 cm samples were cut and soaked in a 0.01 mM solution of Ery B for 24 hours. The soaked casings were then removed, blotted dry with paper towel, and dried under a constant air flow for one hour before being transferred to a desiccator over phosphorus pentoxide for at least one week. The slides were stored at 23.0 ± 1ºC protected from light to prevent any photobleaching of the Ery B and desiccant was refreshed as needed to maintain a relative humidity close to 0%. The dried collagen casings were placed on quartz slides (13 mm x 30 mm x 0.6 mm) (NSG Precision Cells, Farmingdale, NY) and slid into a fluorescence cuvette securing the casing into the desired testing position.

Phosphorescence Measurements

To prevent oxygen quenching of the triplet state, a virtually oxygen free nitrogen stream was generated by passing high purity nitrogen through a Supelco carrier gas purifier (Bellfonte, PA). This gas line was routed into the sample compartment and directly into the quartz fluorescence cuvette that held the sample. The cuvette was capped with a lid having inlet and outlet ports for the gas line, so all experiments were done at constant pressure. The cuvette was flushed for at least 30 minutes to ensure that oxygen was eliminated. The sample compartment was jacketed, and dry air was used to

prevent condensation on the cuvette faces when experimental conditions were below room temperature.

Measurements were made on a Cary Eclipse fluorescence spectrophotometer (Varian Instruments, Walnut Creek, CA) equipped with a temperature controller and multi-cell holder. This instrument, which collects in analog mode, uses a high intensity pulsed lamp and a time delay was utilized to avoid any fluorescence during the lamp pulse. Phosphorescence and delayed fluorescence emission scans were collected over the range 535-800 nm with an excitation wavelength of 525 nm. The excitation and emission monochromators were both set at a 10 nm bandpass. Each data point (collected at 1 nm intervals with a 0.1 s averaging time) was collected from a single flash with a 0.2 ms delay, 0.5 ms gate time, and 4.0 ms total decay time. Excitation scans were collected using the same electronic parameters over the range of 400-600 nm with a 688 nm emission wavelength and both monochromators set at 10 nm.

Lifetime measurements were collected under a dry air or nitrogen purge, and the following experimental parameters were the same in both instances. Samples were excited at 540 nm and the emission was measured at 685 nm with a 20 nm bandpass for both excitation and emission monochromators. Each time-resolved decay transient was the average of 40 cycles, and for each cycle data were collected from a single flash with a delay of 0.1 ms, a 0.02 ms gate time, and 4.0 ms total decay time. All experiments were done in at least triplicate and the standard deviation of the averages was calculated to validate reproducibility. For the lifetime experiments a temperature range of 0-100°C was used and temperature was increased at ten degree increments with a 13 minute delay between readings.

Intensity decays were collected as a function of emission wavelength over the emission range from 660-720 nm at 10 nm increments with an excitation wavelength of 540 nm. The temperature range was 0-100°C and the excitation and emission bandwidth were 20 nm and 10 nm, respectively, with a delay time of 0.1 ms, gate time of 0.01 ms, and a total decay time of 4.0 ms.

Data Analysis

The emission spectra were analyzed by fitting both the delayed fluorescence and the phosphorescence to a lognormal function.

$$I(\nu) = I_0 \exp\{-\ln(2)[\ln(1+2b(\nu-\nu_P)/\Delta)/b]^2\} \tag{1}$$

In this equation I_0, is the maximum intensity value of the emission spectra, ν_P is the frequency in cm^{-1} of the emission maximum, Δ is the line width parameter, and b is the asymmetry parameter. The bandwidth of the emission, the full width at half maximum (Γ), is related to b and Δ.

$$\Gamma = \Delta \sinh(b)/b \tag{2}$$

Emission spectra were fit using the program Igor (Wavemetrics, Inc., Lake Oswego, OR). We also analyzed some of the data by fitting with the program Nfit (Island Products, Galveston, TX), to validate that the results agreed in both fitting programs.

The phosphorescence time-resolved emission spectra collected as a function of delay time and temperature used an excitation wavelength of 540 nm and emission from 620-780 nm. Emission spectra were collected with delay times of 0.1, 0.6, 1.1, 1.6, and 2.1 ms after the lamp flash. The data were analyzed using equations 1 and 2.

Phosphorescence lifetimes were determined by nonlinear least-squares analysis with the statistical programs Igor and Nfit. Fits were judged satisfactory if the r^2 values

were in the range of 0.995-1.0 and the modified residuals ((data − fit)/data$^{1/2}$) varied randomly about zero. Data was analyzed using a stretched exponential, or Kohlrausch-Williams-Watts (KWW), decay model which has been shown to be appropriate to describe the wide distribution of relaxation times (Champion et al., 2000) for the molecular process that depopulate excited states in tissues (Lee et al., 2001), crystalline solids (Chen, 2003), super cooled liquids (Richert, 1997), and amorphous solids (Nack and Ludescher, 2006; Pravinata et al., 2005; Shirke et al., 2005; Shirke et al., 2006; Simon-Lukasik and Ludescher, 2004; Sundaresan and Ludescher, 2007):

$$I(t) = I(0) \exp[-(t/\tau)^\beta] + c \qquad (3)$$

Where I(t) is the intensity as a function of time following pulsed excitation, I(0) is the initial intensity at time zero, τ is the KWW lifetime, and β is the stretching exponent which characterizes the distribution of the decay times (Richert and Heuer, 1997). Further explanation of the parameters of the stretched exponential equation is provided in the results section.

The phosphorescence lifetime is the inverse sum of the rate constants associated with the various processes that depopulate the excited triplet state.

$$\tau^{-1} = k_P = k_{RP} + k_{TS1} + k_{TS0} + k_Q[O_2] \qquad (4)$$

This equation can be used to calculate k_{TS0}, the rate of collisional quenching to the ground state, if k_{RP}, k_{TS1}, and $k_Q[O_2]$ are known. Under anoxic conditions $k_Q[O_2]$, the rate of oxygen quenching, is zero; k_{RP}, the radiative decay rate of the triplet state, is 41 s^{-1} for Ery B (Duchowicz et al., 1998; Lettinga et al., 2000); k_{TS1}, the rate of reverse intersystem crossing from the excited triplet state to the excited singlet state, depends on ΔE_{TS}, the energy gap between S_1 and T_1 (Simon-Lukasik and Ludescher, 2004):

$$k_{TS1}(T) = k^o_{TS1} \exp(-\Delta E_{TS}/RT) \tag{5}$$

The slope of a Van't Hoff plot of the natural log of the ratio of delayed fluorescence (I_{DF}) to phosphorescence (I_P) intensity versus inverse temperature provides a measure of ΔE_{TS} (Duchowicz et al., 1998):

$$d[\ln(I_{DF}/I_P)]/d(1/T) = -\Delta E_{TS}/R \tag{6}$$

(where R = 8.314 J K^{-1} mol^{-1}). Literature values of k$^o_{TS1}$ for erythrosin B vary from 0.3 x 10^7 s^{-1} in ethanol and 6.5 x 10^7 s^{-1} in water (Duchowicz et al., 1998) to 111 x 10^7 s^{-1} in solid polyvinyl alcohol (Lettinga et al., 2000), and hence provides little guidance. We estimated the maximum possible value for k$^o_{TS1}$ in collagen casings to be 4.7 x 10^7 s^{-1} by assuming that $k_{TS1}(T)$ (calculate using Equation 5 with ΔE_{TS} = 33.69 kJ mol^{-1}; see results) cannot result in values for $k_{TS0}(T)$ that decrease with temperature. This procedure thus estimated the minimum possible values for $k_{TS0}(T)$.

Results

The delayed emission spectra from Ery B embedded in dried collagen casings are displayed in Figure V-3. The longer wavelength band corresponds to phosphorescence (the transition from the T_1 state to S_0) and the shorter wavelength band corresponds to the thermally activated delayed fluorescence (the transition from T_1 to S_1 to S_0). The ratio of delayed fluorescence intensity to phosphorescence intensity increases systematically with temperature, and a Van't Hoff analysis of this data was linear over the tested temperature range yielding a triplet to singlet activation energy ΔE_{TS} of 33.69 +/- 0.3 kJ mol^{-1} (see Equation 6 in the Materials and Methods for further details). The ΔE_{TS} for dried collagen casings was very close to that of the closely related amorphous gelatin matrix (33.23 +/- 0.3 kJ mol^{-1}) and was also similar to amorphous globular proteins, BSA and β-

lactoglobulin, which had values of 35.2 +/- 0.5 and 32.9 +/- 0.5 kJ mol^{-1}, respectively (Nack and Ludescher, 2006; Sundaresan and Ludescher, 2007). Other amorphous carbohydrate matrices also showed comparable values, such as sucrose (31.6 +/- 0.4 kJ mol^{-1}) (Pravinata et al., 2005), maltose (32.7 +/- 1.1 kJ mol^{-1}) (Shirke and Ludescher, 2005), lactose (34.1 +/- 0.3 kJ mol^{-1}) and lactitol (34.0 +/- 0.3 kJ mol^{-1}) (Shirke et al., 2006). Values found in the literature for Ery B in various aqueous solutions and solids vary significantly from the aforementioned amorphous systems. Examples include water (36.9 +/- 0.6 kJ mol^{-1}), 66% aqueous sucrose (36.9 +/- 1.0 kJ mol^{-1}) (Pravinata et al., 2005), ethanol (28.5 +/- 2.5 kJ mol^{-1}) (Duchowicz et al., 1998), and polyvinyl alcohol (41.2 +/- 0.4 kJ mol^{-1}) (Lettinga et al., 2000). This review of previous reported ΔE_{TS} values displays that the energy gap is modulated by specific interactions within each matrix, and that the state of the matrix plays a significant role in the energy gap between the S_1 and T_1 state.

The phosphorescence emission maximum decreased linearly with increasing temperature (Figure V-4a). At 0°C the peak frequency (ν_P) was 14700 cm^{-1} and values decreased ~25 cm^{-1} per 10°C increase in temperature until 90°C where values were essentially constant at 14545 cm^{-1} for 90°C and 100°C. The decrease in emission energy with increasing temperature was attributed to an increase in the rate of dipolar relaxation around the excited triplet state of Ery B (Pravinata et al., 2005; Richert, 2000). The emission bandwidth, or full width at half maximum (Γ), showed a gradual linear increase over the temperature range 0-70°C (Figure V-4b). The temperature range of 70-100°C displayed a more dramatic increase in Γ. Γ is a measure of the extent of inhomogeneous broadening due to the probes' ability to disperse itself into different sites varying in

emission energies; thus we conclude that at higher temperatures the matrix has a larger distribution of energetically distinct environments.

Time resolved phosphorescence intensity decays of Ery B in dried collagen casings were measured over the temperature range of 0-100°C. The phosphorescence intensity decay in the presence and absence of oxygen at 0°C along with the subsequent fits from the stretched exponential function (Equation 3 in the Materials and Methods section) are shown in Figure V-5a. The modified residuals for these fits (Figure V-5b) varied randomly about zero indicating that the stretched exponential model provides a satisfactory fit for the intensity decay.

The phosphorescence lifetime values decreased in an almost linear fashion whether or not oxygen was present, besides a very slight break in the data around 70°C where the decrease became slightly more pronounced. Lifetime values were ~0.62 ms at 0°C and decreased to ~0.33 ms at 100°C (Figure V-6a). This trend was similar to what we observed in structurally related fibrous amorphous gelatin (although the lifetimes were systematically shorter for the collagen casings), but differed greatly from the trends observed in amorphous BSA and β-lactoglobulin (Nack and Ludescher, 2006; Sundaresan and Ludescher, 2007). These globular proteins displayed a distinct break point in lifetime trends around 60-70°C, and also had much lower lifetime values when oxygen was present. The small differences between the lifetime values under nitrogen conditions and in the presence of oxygen hints that oxygen quenching may be negligible in dried collagen casings.

The stretching exponent (β) is a measure of the dynamic heterogeneity of the matrix. As β values decrease from 1 (meaning that the matrix is entirely homogeneous)

the matrix displays increased dynamic heterogeneity (Lindsey and Patterson, 1980). The lower the β value, the wider the distribution of lifetimes due to wider distributions of dynamically distinct environments in the matrix. β values decreased monotonically under nitrogen conditions and in the presence of oxygen (Figure V-6b), and the differences between oxic and anoxic conditions were negligible with β values of ~0.89 and ~0.81 at 0°C and 100°C, respectively. The β values were actually slightly higher when oxygen was present from temperatures 20-50°C, following to some extent, the trend observed in the amorphous gelatin films, but not as drastic. The β trends observed in amorphous gelatin and dried collagen casings were similar, but differed greatly from those seen in globular proteins (BSA (Nack and Ludescher, 2006) and β-lactoglobulin (Sundaresan and Ludescher, 2007)) where β values decreased significantly in the presence of oxygen above ambient temperature.

Photophysical Rate Constants

The decrease in lifetime values with temperature under nitrogen conditions reflects an increase in k_P (Equation 4, Materials and Methods), the rate of non-radiative decay of the excited T_1 state, due to increases in k_{TS1}, the rate of reverse intersystem crossing to the excited S_1 state, and k_{TS0}, the rate of intersystem crossing from the excited T_1 state to the ground S_0 state due to collisional quenching. The slightly lower lifetimes when oxygen is present are due to the additional collisional quenching by oxygen, $k_Q[O_2]$.

Figure V-7a displays the rates of nonradiative quenching under nitrogen conditions. Both k_{TS0} and k_{TS1} increase slowly until reaching temperatures of 70°C and 50°C, respectively. k_{TS1} is more sensitive to higher temperatures, and hence, a more

noticeable rate increase is observed. Figure V-7b shows plots of k_{TS0} and $k_Q[O_2]$ as a function of temperature. k_{TS0} increased linearly over the temperature range of 0°C to 70°C with values ranging from 1555 s^{-1} to 1738 s^{-1}. Above 70°C k_{TS0} values increased more dramatically (~250 s^{-1} for the four temperature increments) with the 100°C data point having a k_{TS0} value of 1989 s^{-1}.   This trend was similar to that seen for k_{TS0} values in amorphous BSA (Nack and Ludescher, 2006) and β-lactoglobulin (Sundaresan and Ludescher, 2007), but the k_{TS0} values were significantly higher than those observed in amorphous gelatin (Chapter 4).

$k_Q[O_2]$, or the oxygen quenching rates, were very low in the dried collagen casing matrix (Figure V-7b). The values ranged from 51 s^{-1} at 0°C to 188 s^{-1} at 100°C. The other amorphous proteins studied in our lab had much higher values of 80-1300 s^{-1} for gelatin, 200-10000 s^{-1} for β-lactoglobulin (Sundaresan and Ludescher, 2007), and 440-15000 s^{-1} for BSA (Nack and Ludescher, 2006) over the same temperature range.

The apparent activation energy (E_A) for k_{TS0} and $k_Q[O_2]$ were obtained from the slopes of the Arrhenius plots seen in Figure V-7c. The E_A value for k_{TS0} was 1.77 kJ mol^{-1} for the temperature range of 0-100°C (r^2 = 0.91) and 1.3 kJ mol^{-1} at low temperatures (0-50°C, r^2 = 0.98) and 5.1 kJ mol^{-1} at high temperatures (80-100°C, r^2 = 0.96). These values were significantly smaller than those seen in amorphous globular proteins, which had values of 3.1 kJ mol^{-1} for BSA over the temperature range of 0-100°C (Nack and Ludescher, 2006) and 2.4 and 21.4 kJ mol^{-1} at low (-10-50°C) and high (90-120°C) temperatures for β-lactoglobulin (Sundaresan and Ludescher, 2007), but higher than that in amorphous gelatin (0.5 kJ mol^{-1} (0-100°C)).

The $k_Q[O_2]$ E_A values for dried collagen casings was 10.23 kJ mol^{-1}. This is about three-fold lower than values for BSA (Nack and Ludescher, 2006) and gelatin, which were 29.9 kJ mol^{-1} and 26.0 kJ mol^{-1}, respectively. Despite the significantly different E_A values for k_{TS0} and $k_Q[O_2]$, these physically different processes seem to be related over the full range of temperature (Figure V-7d). The data follows a biphasic trend, with the 60-70°C temperature range serving as the break point in the trends, and this break point is mostly due to the fact that the $k_Q[O_2]$ values level off at 60°C.

The peak phosphorescence emission energy of Ery B in dried collagen casings exhibited a blue shift as the delay time after excitation increased, as seen in Figure V-8. This behavior follows the heterogeneous emission model, which was also observed in other amorphous sugars (Pravinata et al., 2005; Shirke et al., 2006) and proteins (Lukasik, 2005; Nack and Ludescher, 2006; Sundaresan and Ludescher, 2007). In this model, the Ery B molecules reside in distinct sites within the matrix, where the sites having higher emission energy have longer lifetimes (Pravinata et al., 2005). As the delay time increased from 0.1 ms to 2.1 ms, the peak frequency values increased 80-100 cm^{-1}. As expected, the peak frequencies decreased with increased temperature due to greater dipolar relaxation around the excited probe molecules.

Ery B intensity decays were collected as a function of emission wavelength (660-720 nm) over the temperature range of 0-100°C. The variations in lifetime values are shown in Figure V-9a. For the temperature range of 0-60°C lifetime values decreased as the emission wavelength shifted to the red, and this effect was more extreme at lower temperatures. At temperatures above 60°C, the lifetime values were relatively constant with emission wavelength. The lifetime values decreased at all emission wavelengths as

temperature increased, and ranged from 0.66-0.34 ms at 660 nm to 0.58-0.34 ms at 720 nm (for temperatures 0-100°C). Comparable variations in Ery B lifetimes as a function of emission wavelength were found in amorphous BSA (Nack and Ludescher, 2006), sucrose (Pravinata et al., 2005), maltose and maltitol (Shirke et al., 2005), and gelatin (Simon-Lukasik and Ludescher, 2004).

β values also varied systematically with emission wavelength and temperature (Figure V-9b). The β values for all temperatures tested peaked at the approximate emission peak frequency of ~685 nm (Figure V-3). The lower β values at the red and blue edges of the emission indicated that there is greater heterogeneity at the edges of the emission energy.

Arrhenius plots for k_{TS0} at various emission wavelengths are shown in Figure V-10. From these plots, E_A values were calculated (Figure V-11). E_A was essentially constant for the tested emission wavelength bands (~1.1 kJ mol^{-1}) for the temperature range of 0-30°C. At high temperature (70-100°C), E_A decreased as the emission wavelength increased, similar to what was observed in BSA (Nack and Ludescher, 2006) and sucrose (Pravinata et al., 2005).

Oxygen Permeability as Collagen Casings Age

Intensity decays were collected on the dried collagen casings as a function of time from when the casing packaging was opened. The collagen casings used in this study arrived in vacuum sealed polyethylene bags. Once the bag was opened for the initial casing experiments (labeled fresh casing in this study), the bag was left open in the refrigerator, and samples were pulled at one month intervals. The casing squares were then doped in the Ery B solution and dried as explained in the Materials and Methods

section. The aim of this experiment was to monitor the rigidity, heterogeneity, and oxygen permeability as a function of aging.

Lifetime plots are shown for Ery B doped dried collagen casings under nitrogen conditions and in the presence of oxygen as a function of time from when the original package was opened (Figure V-12). At 0°C the lifetime values under nitrogen conditions were essentially constant over the 4 month period with a range of 0.62-0.66 ms, while the samples in the presence of oxygen decreased (except for the one month sample) over time. More importantly, the gap between the nitrogen and oxygen data sets increased with time, which is related to oxygen permeability.

The stretching exponent (β) showed similar trends as observed for the lifetime data over time (Figure V-13). In the fresh casing experiment, oxygen did not affect the heterogeneity of the matrix. For the one month and two month samples, the β values decreased in the presence of oxygen above 30°C. β values for the 3 month sample were higher in the presence of oxygen until reaching 50°C, where the nitrogen purged samples had higher β values. The four month sample showed a drastic decrease in β over the full temperature range. It seemed that after four months the casing starts to break down (became more heterogeneous). This also corresponds to the end of the casing shelf life if the casing is not vacuum sealed after use (Doman, 2007).

Figure V-14 shows how $k_Q[O_2]$, or the oxygen permeability, of the collagen casings was affected by increased time from when the initial packaging was opened. As the dried collagen casing aged, it became more permeable to oxygen. The 4 month sample was ~3-4 time more permeable to oxygen as compared to the fresh casing.

Discussion

Ery B has proven to be an effective indicator of molecular mobility, oxygen permeability, and dynamic site heterogeneity in various model amorphous matrices in our laboratory, and here we have demonstrated its usefulness when embedded in collagen casings, an actual food component. This study also provided molecular information on how collagen casings "age" when stored under refrigeration conditions.

Molecular Mobility

We were able to monitor molecular mobility in dried collagen casings using Ery B as our phosphorescent indicator by monitoring dipolar relaxation and molecular collisions around the excited triplet state. Similar trends were observed in other amorphous matrices studied in our laboratory (Lukasik and Ludescher, 2006; Nack and Ludescher, 2006; Pravinata et al., 2005; Shirke and Ludescher, 2005; Shirke et al., 2005). The peak frequency values for the dried collagen casings were the same (within error) as the values found for gelatin (Chapter 4) and much higher than the values we observed in the amorphous globular proteins BSA (Nack and Ludescher, 2006) and β-lactoglobulin (Sundaresan and Ludescher, 2007). Therefore, we can conclude that collagen and gelatin (both fibrous proteins) have less dipolar relaxation stabilizing the excited Ery B molecules, most likely due to restricted motions in this rigid matrix.

k_{TS0} essentially monitors molecular collisions between the probe and the surrounding matrix. When the excited probe collides with the matrix, vibrational energy from the probe is lost to the matrix, lowering the emission intensity and lifetime. k_{TS0} serves as an direct indicator of the molecular mobility of the matrix. Collagen casings displayed increased softening around 70°C, due to the increased rate of molecular

mobility. This correlates to the denaturation temperature found in pure collagen films (extracted from rat tail tendon) of 67°C (Usha et al., 2004), which is thought to represent a phase transition involving changes in the protein network and long-range molecular order. Cross-linked collagen films had denaturation temperatures of 74°C (cross-linked with formaldehyde) and 107°C (cross-linked with chromium sulfate) (Usha et al., 2004). Since the collagen casings used in this study were cross-linked and dried (both increasing the denaturation temperature), we believe that the slight increase in molecular mobility around 70°C is due to a softening transition rather than denaturation. Similar softening transitions were observed in all carbohydrate and protein matrices studied in our lab, except the gelatin matrix described in the previous chapter (which had drastically lower molecular mobility and no observed softening transition).

The E_A values for molecular motions in the dried collagen casing demonstrate that the casing participates in at least two different modes of motion. At high temperatures, the greater E_A value (5.1 kJ mol^{-1}) was most likely due to larger segmental motions which are cooperative in nature. At low temperatures, the much lower E_A value of 1.3 kJ mol^{-1} was possibly due to small amplitude, localized vibrational motions. We assume that the slight increase in the k_{TS0} data at 70°C might relate to the softening transition in the collagen casing, thus allowing larger cooperative motions which would require more energy to activate. A study by Miles et al. (1995) showed that collagen can form various sized cooperative units of amino acid residues depending on the stabilizing interactions of molecules surrounding the cooperative unit within the fiber, further backing our explanation of the various E_A values for molecular mobility in the collagen casing.

Oxygen permeability

Oxygen is an efficient quencher of phosphorescence, and monitoring oxygen quenching via phosphorescent techniques has proven to be an effective method for monitoring the presence of molecular oxygen in a variety of polymeric matrices (Buettner, 1964; Masoumi et al., 1996; Simon-Lukasik and Ludescher, 2004). Lukasik and Ludescher (2006) and Simon-Lukasik and Ludescher (2004) have been able to successfully correlate oxygen quenching values $k_Q[O_2]$ with the oxygen diffusion rate in gelatin. Because the oxygen quenching constant, $k_Q[O_2]$, is proportional to both the kinetics of oxygen (k_Q) permeability and the thermodynamics of oxygen solubility ($[O_2]$) (Simon-Lukasik and Ludescher, 2004), it reflects the oxygen permeability in collagen casings.

The oxygen permeability values for collagen casings were the lowest calculated for any of the protein matrices tested in our lab. At 0°C the $k_Q[O_2]$ value was 50 s^{-1}, and the values increased slowly until 60°C where oxygen permeability plateaued at ~180 s^{-1}. Before testing the collagen casings, we had considered gelatin to be somewhat impermeable to oxygen (as compared to the globular proteins studied), but gelatin was 10 times as permeable when compared to collagen casings. We do not have a lower limit of detection, and were unsure how meaningful this data was since were not able to carry the associated lifetime errors through the calculation of $k_Q[O_2]$.

The E_A for oxygen permeability was 10.23 kJ mol^{-1}, which was 6-fold higher than the E_A for molecular mobility (1.77 kJ mol^{-1}) over the temperature range of 0-100°C. The greater E_A value for oxygen permeability appears to imply more delocalized collective motions of the collagen matrix are required for oxygen to have an effect on

dried collagen casings. As mentioned earlier, these processes are qualitatively different, where k_{TS0} monitors the vibrational coupling between the excited probe molecules and matrix due to collisions. $k_Q[O_2]$ measures the coupling between the translational motion of an oxygen molecule through the matrix and the movement of the matrix, monitored by the collisions between oxygen and the probe (Nack and Ludescher, 2006). The approximately linear correlation between the processes (except temperatures 60-70°C) demonstrates that the collective motions controlling oxygen permeation are somehow directly related to the small scale local vibrational motions monitored by k_{TS0}.

Oxygen Permeability as the Collagen Casings Age

As the collagen casing aged under refrigeration conditions, it became less rigid and more heterogeneous in the presence of oxygen and also more permeable to oxygen. We believe that these three outcomes are related, with the increased oxygen permeability being a consequence of the lower rigidity and the more heterogeneous environment as the casing ages in the presence of oxygen. The 4 month sample was 3-4 times (depending on the temperature) more permeable to oxygen than the fresh casing. We propose that as the casing aged, the microstructure of the casing started to break down and become less organized (the collagen fibers would no longer be woven into a network) allowing for oxygen to penetrate the matrix. Transmission electron micrographs of collagen casings reveal a considerable amount of banded structure similar to native collagen fibrils, providing evidence that the casing are formed by weaving countless fiber structures together (Borysko, 1985). The fact that the presence of oxygen lowered lifetime values with time means that as collagen casings age the oxygen quenching increased (and not due to aging itself, since the N_2 values did not decrease systematically with time). This

was most likely related to the more disorganized microstructure allowing for oxygen to penetrate the matrix and collide with the excited Ery B molecules. The increased heterogeneity in the presence of oxygen is presumed to be related to variations in oxygen quenching, or oxygen permeability, in the different local environments of the matrix (Sundaresan and Ludescher, 2007). The increased heterogeneity could also be a reflection of a greater distribution of molecular mobility during the reorganization of collagen fibers (matrix having additional sites with different mobilities). These molecular interactions could cooperatively loosen or tighter the collagen fibrils or fiber networks, consequently increasing heterogeneity.

Dynamic Site Heterogeneity

The emission peak frequency increased as the delay time after excitation increased, and lifetimes decreased systematically at higher temperatures (>60°C) as the emission wavelengths were shifted to the red. These data clearly show Ery B molecules with longer lifetimes have blue-shifted (higher energy) emission spectra, and probes with shorter lifetimes have red-shifted (lower energy) emission spectra, following the dynamic site heterogeneity model (Nack and Ludescher, 2006; Pravinata et al., 2005; Shirke et al., 2005; Stratt and Maroncelli, 1996) where blue-shifted probes are in more rigid local environments and have slower rates of both dipolar relaxations and molecular collisions, and red-shifted probes are in more mobile local environments having higher lifetimes and rates of dipolar relaxations. Heterogeneity variations within collagen sausage casing is very undesirable since it leads to casing breakage during the sausage stuffing process, and this parameter needs to be studied further.
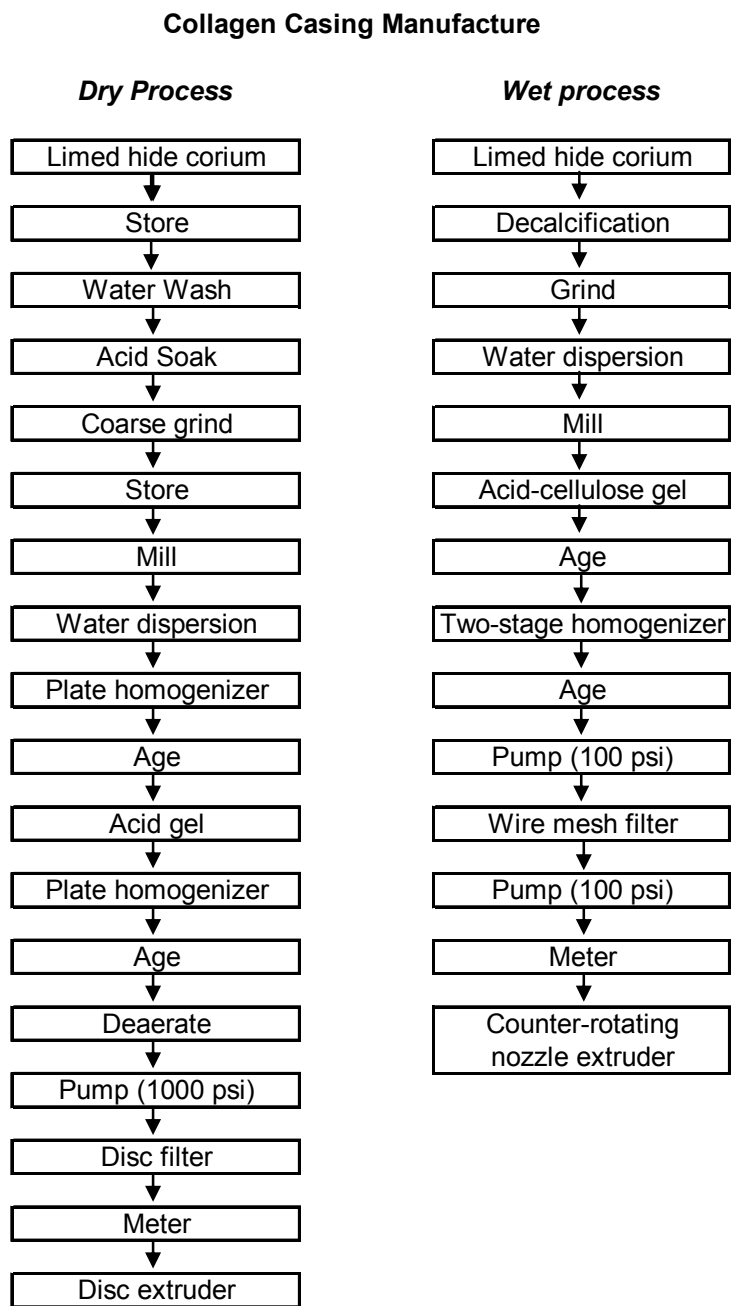
The E_A values for k_{TS0} at various emission wavelengths provided information pertaining to how matrix mobility varies throughout the collagen casing. At high temperatures, where the casings are slightly more mobile, E_A values were higher for probe molecules with blue-shifted emission wavelengths, and at lower temperatures and red-shifted emission wavelengths, E_A values were essentially constant and considerably lower. The higher E_A values for blue-shifted probes were attributed to lower molecular mobility at these rigid sites which could be a reflection of collective motions of larger regions within the casing (which would require more energy) as compared to the low E_A values for the red-shifted and low temperature probes, which are most likely due to harmonic small scale vibrational motions.

Conclusion

This study demonstrates that Ery B can be used as an indicator of molecular mobility, oxygen permeability, and dynamic site heterogeneity in dried collagen casings. To our knowledge this is the first time that a phosphorescent technique has been employed on a food product to determine these attributes. We have shown that fresh dried collagen casings are good barriers to oxygen permeation, but as the casings age, they become less rigid and more heterogeneous. Eventually, oxygen starts to penetrate the casing, which would lead to decreased shelf life of the stuffed sausages from various degradative oxidation reactions. This study will be useful in the development of other phosphorescent techniques to better understand how molecular process affect or control macroscopic events in food products, and eventually we hope this technique can be employed for in-line testing of food products to monitor oxygen content or various processes detrimental to the shelf life of a food product.

205

Chapter 5 Tables and Figures

Figure V-1: Process flow diagrams for the dry and wet technologies in the production of

collagen sausage casings.

Collagen Casing Manufacture

| *Dry Process*	*Wet process*
Limed hide corium	Limed hide corium
Store	Decalcification
Water Wash	Grind
Acid Soak	Water dispersion
Coarse grind	Mill
Store	Acid-cellulose gel
Mill	Age
Water dispersion	Two-stage homogenizer
Plate homogenizer	Age
Age	Pump (100 psi)
Acid gel	Wire mesh filter
Plate homogenizer	Pump (100 psi)
Age	Meter
Deaerate	Counter-rotating nozzle extruder
Pump (1000 psi)	
Disc filter	
Meter	
Disc extruder	

Reproduced from Hood (1987)

Figure V-2: Diagram of the nozzle end used for the co-extrusion of a collagen slurry onto a sausage batter.
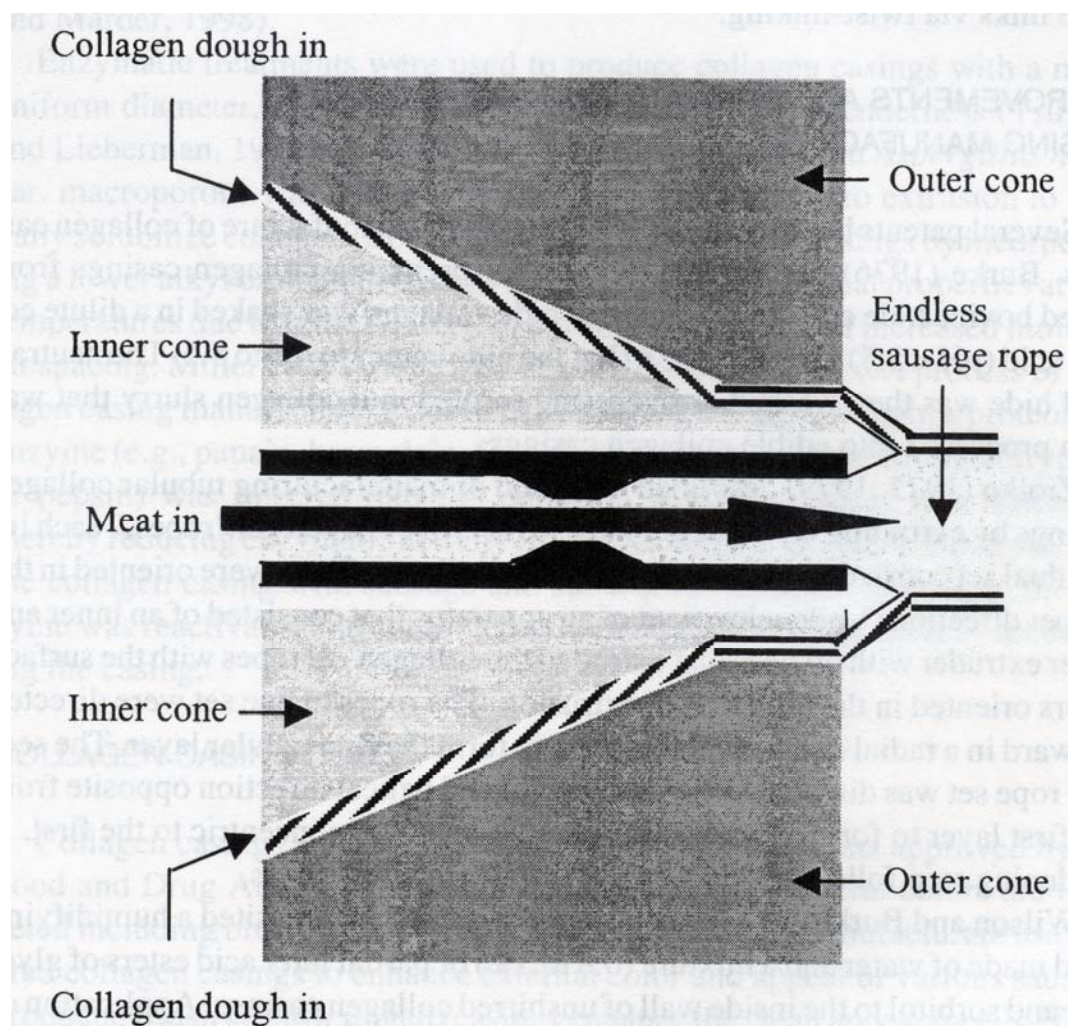
Modified from Smits (1985)

Figure V-3: Delayed emission spectra of Ery B in dried collagen casings as a function of temperature (excitation at 525 nm). The spectra were collected at 10°C intervals from 0 to 100°C (curves plotted from high to low intensity at 685 nm).

Figure V-4: Peak energy ν_P (a) and bandwidth (full-width half maximum) (b) for phosphorescence emission from Ery B in dried collagen casings as a function of temperature. The delayed emission spectra were collected as a function of temperature (Figure V-3) and were analyzed as described in Materials and Methods using Equations 1 and 2.
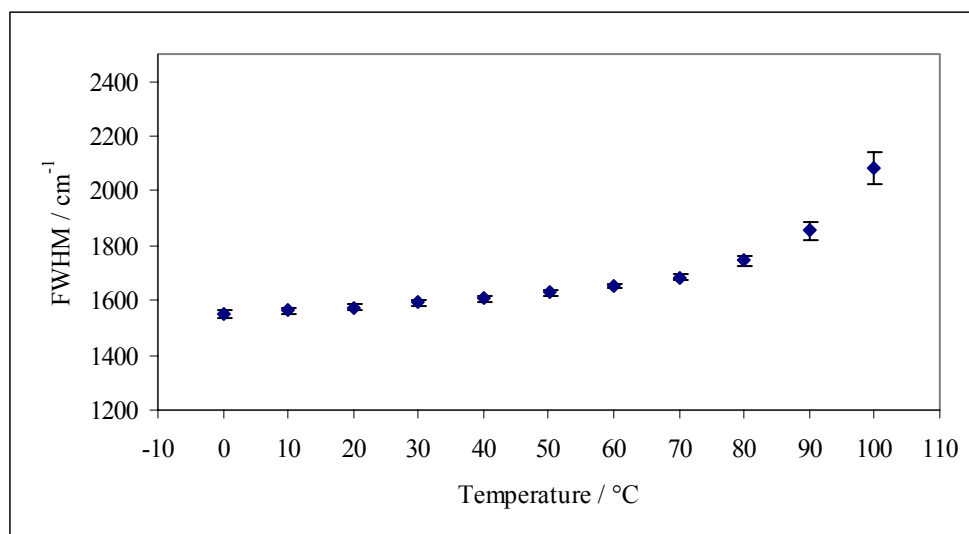
a)
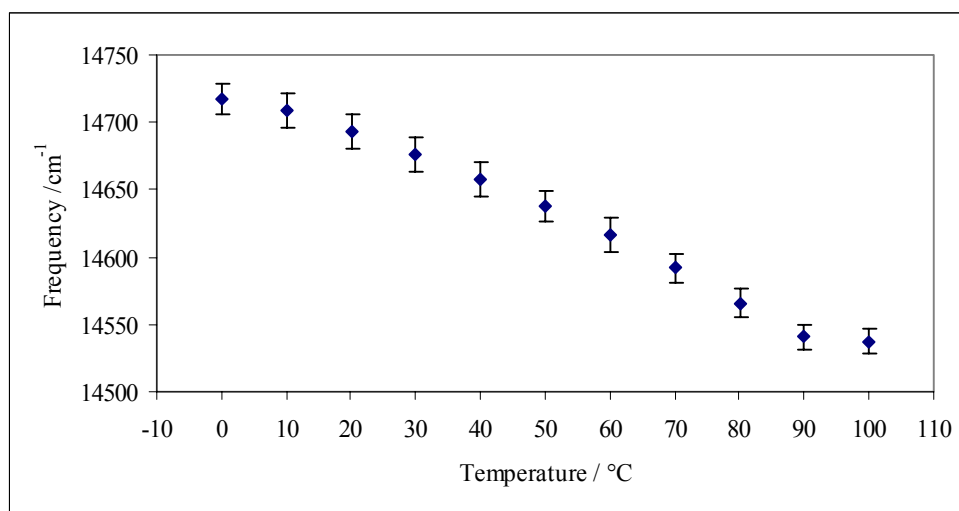
b)

Figure V-5: (a) Normalized phosphorescence intensity decays (I(t)/I(0)) of Ery B in dried collagen casings at 20ºC equilibrated against nitrogen (red) and against air (blue). The solid lines through the data are fits using a stretched exponential model (Equation 3, Materials and Methods) with the following parameters: $\tau = 0.59$ ms and $\beta = 0.88$ for data in nitrogen and $\tau = 0.55$ ms and $\beta = 0.89$ for data in air. (b) A plot of the modified residuals {(Data-Fit)/Data$^{1/2}$} for these fits for the data in nitrogen (red) and air (blue).
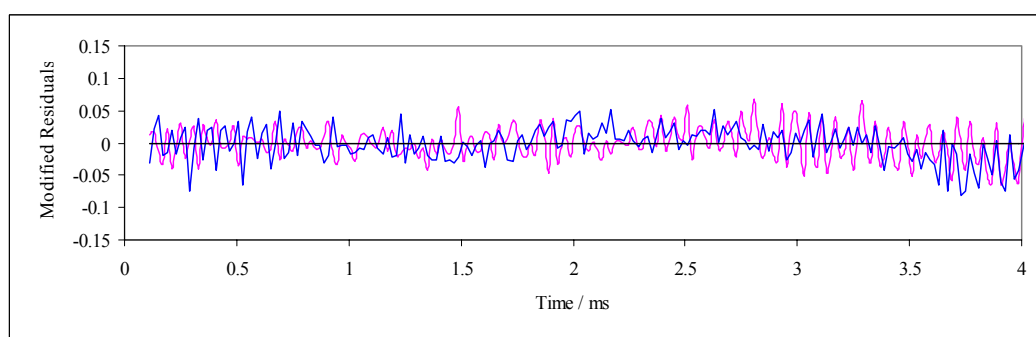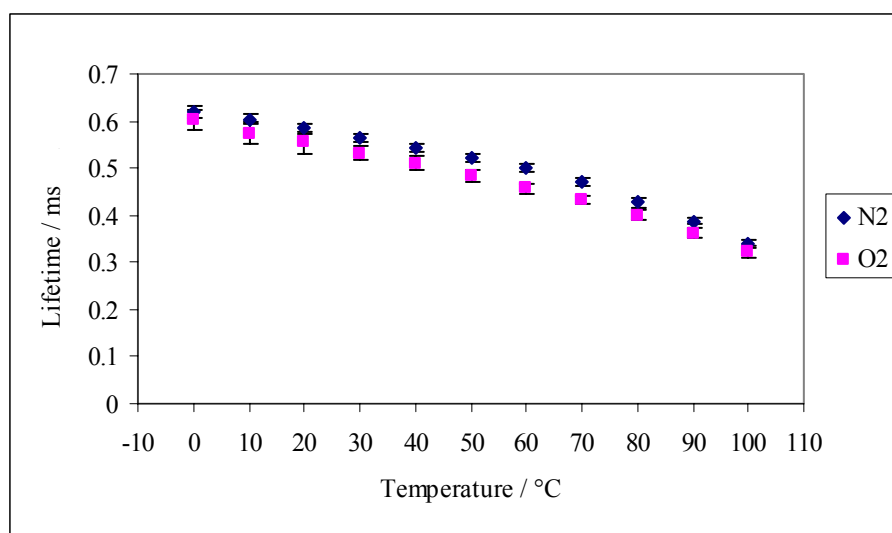
a)
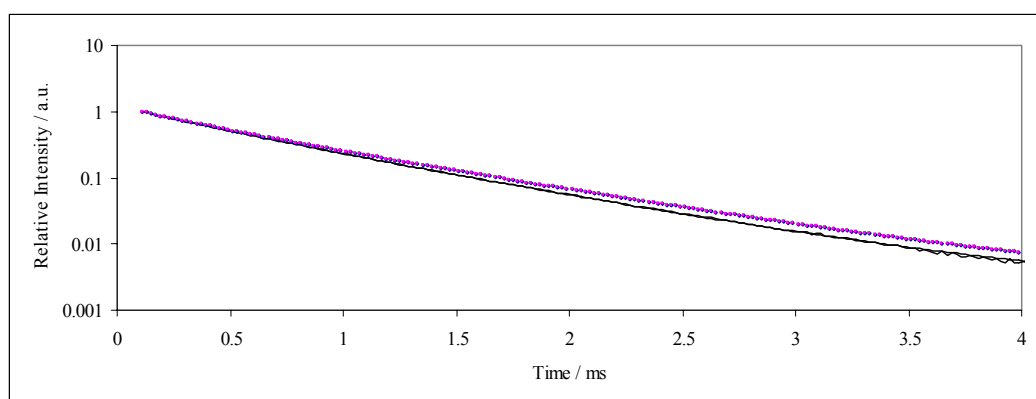
b)

Figure V-6: Lifetimes τ (a) and stretching exponents β (b) from a stretched exponential model fit (Equation 3, Materials and Methods) for the phosphorescence intensity decay data from Ery B in collagen casings equilibrated against nitrogen and air.
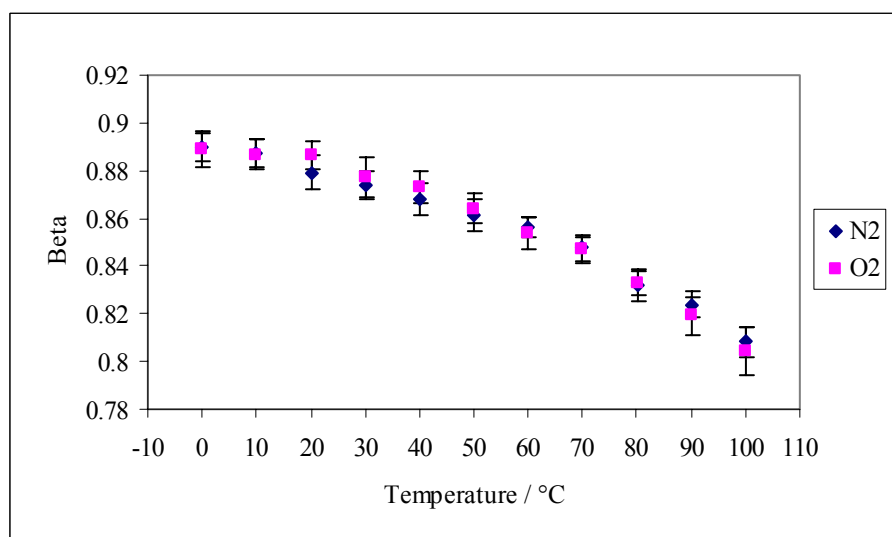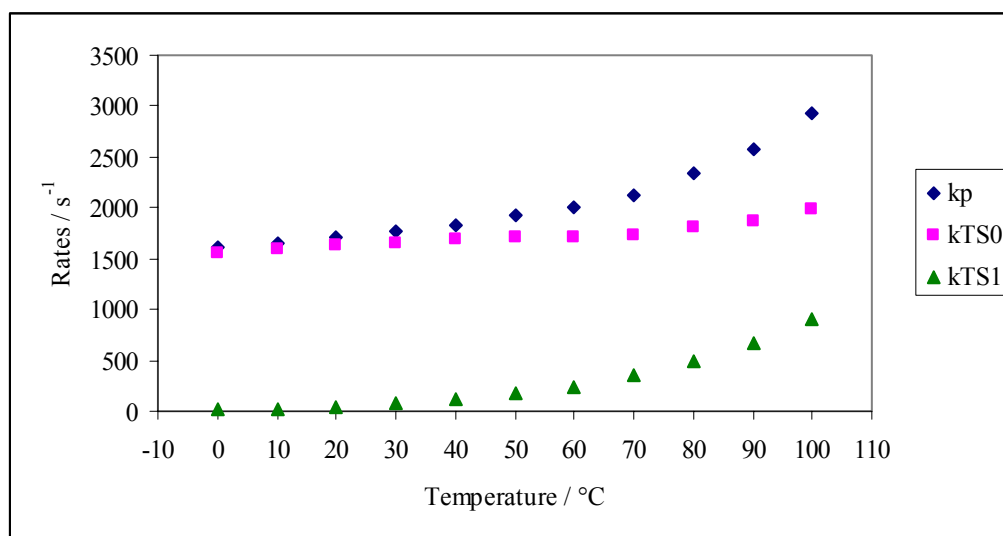
a)

b)

Figure V-7: (a) Temperature dependence of the rates for non-radiative quenching (k_{TS1} and k_{TS0}) under nitrogen conditions calculated from the lifetime data in Figure V-6a (see text for details of calculations).   (b) The rates of k_{TS0} and $k_Q[O_2]$ in the presence of oxygen. (c) Arrhenius plot of k_{TS0} and $k_Q[O_2]$. (d) Plot of $k_Q[O_2]$ versus k_{TS0} over the temperature range 0-100°C.

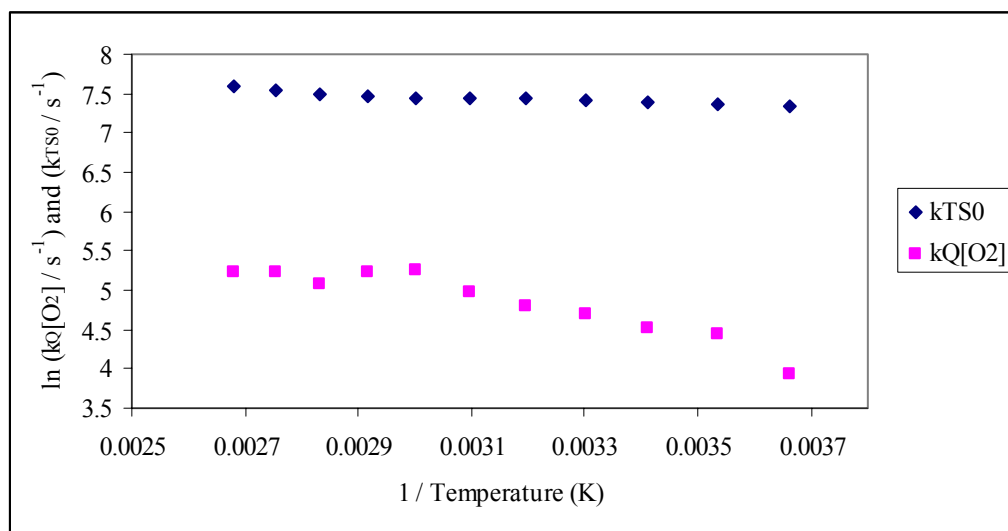a)

b)
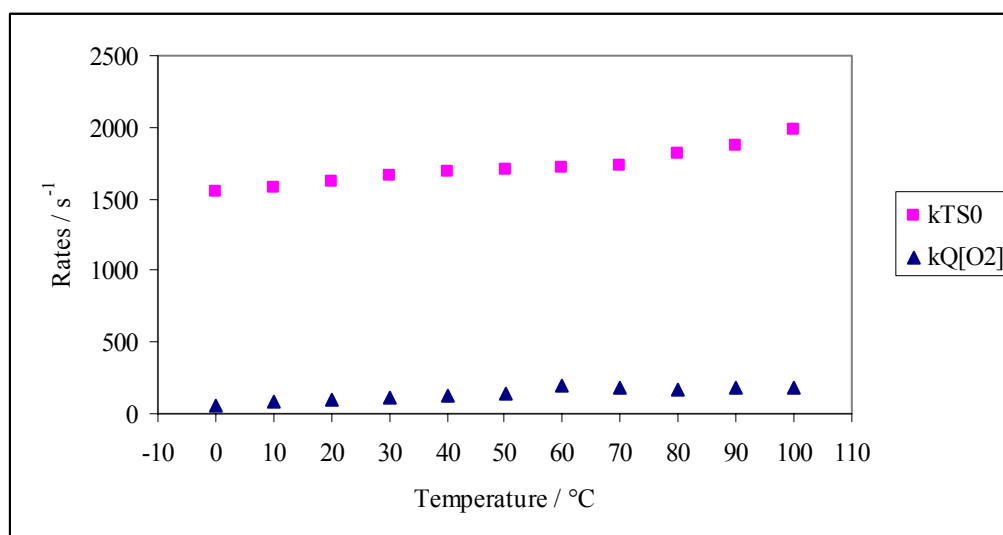
c)

d)
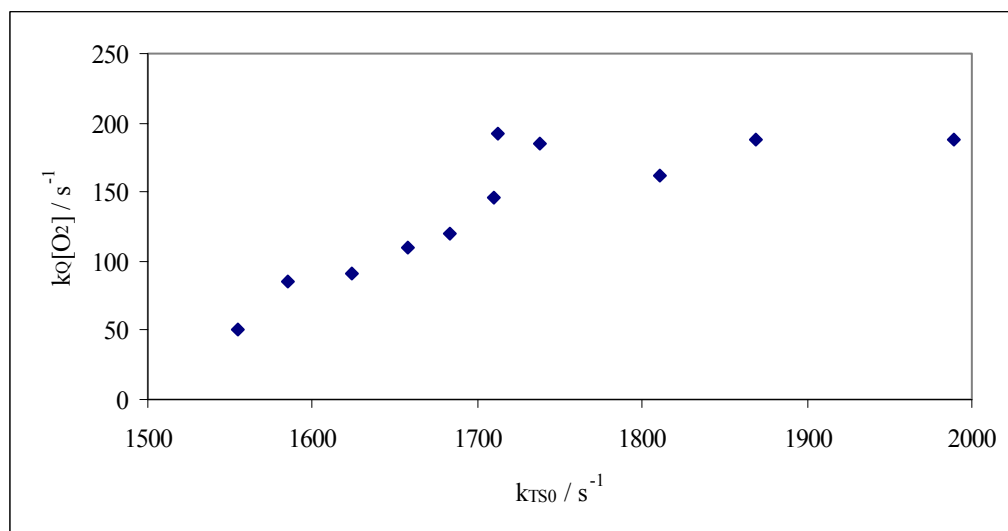
Figure V-8: Effect of delay time on the peak frequency (a) and full width at half maximum (b) of the phosphorescence emission spectra of Ery B in collagen casings at 20ºC, 40ºC, 60ºC, and 80ºC determined from time-resolved emission spectra; peak frequency was calculated from analysis of emission spectra using a lognormal function (Equation 1, Materials and Methods).

a)
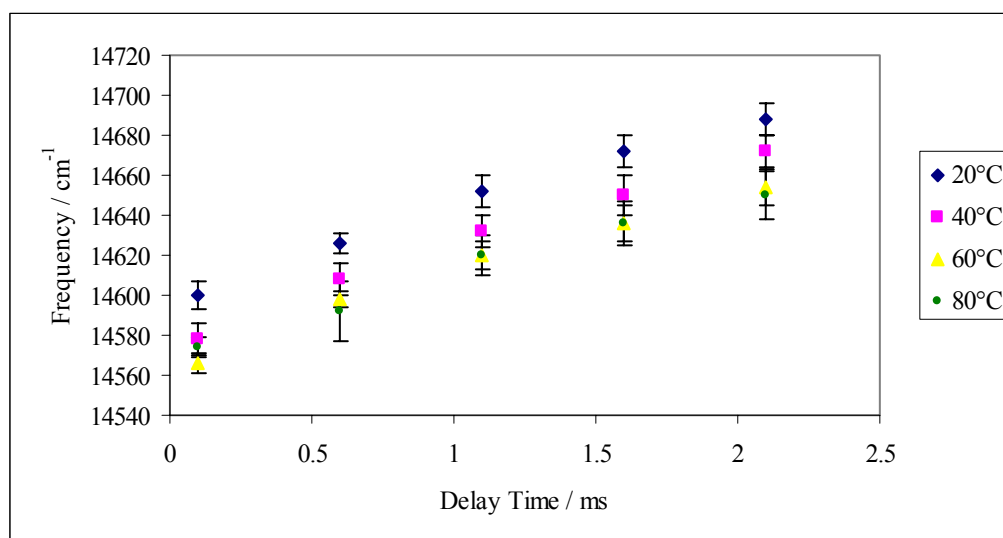
b)
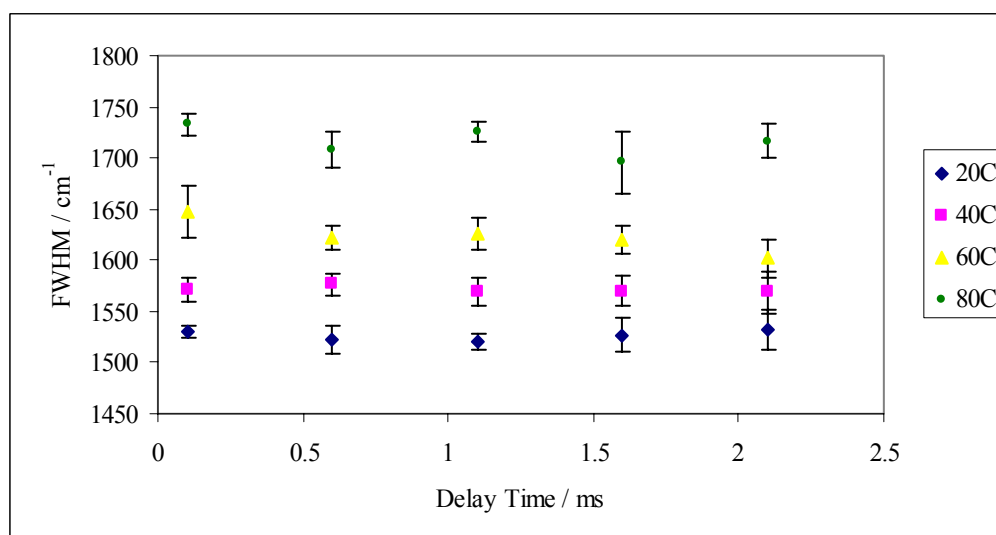
Figure V-9: Lifetimes (a) and stretching exponents (b) from a stretched exponential model fit (Equation 3 in the Materials and Methods section) to phosphorescence intensity decay data from Ery B in collagen casings under nitrogen conditions collected as a function of emission wavelength with excitation at 540 nm at temperatures from 0–100°C at 10°C intervals.

a)
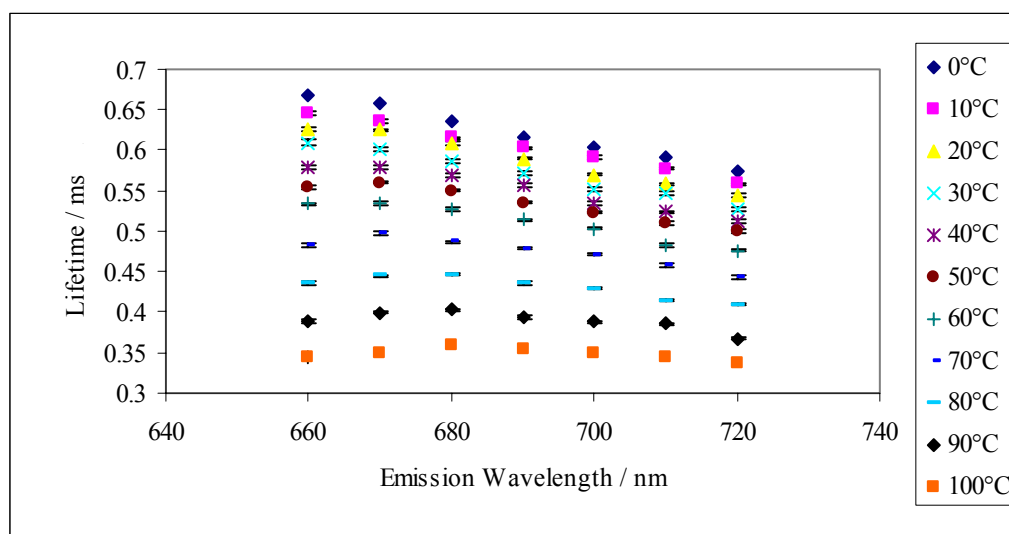
b)
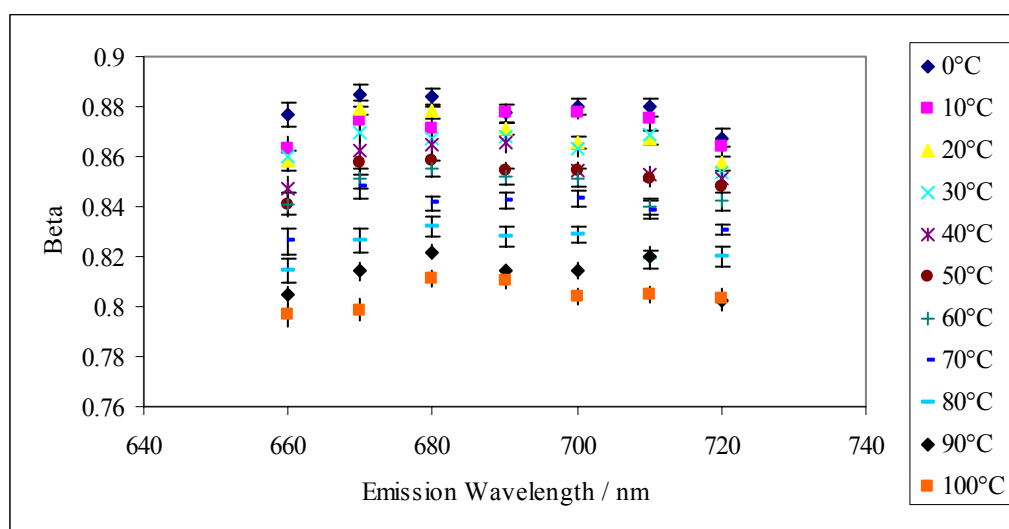
Figure V-10: Arrhenius plots of k_{TS0} at various emission wavelengths.
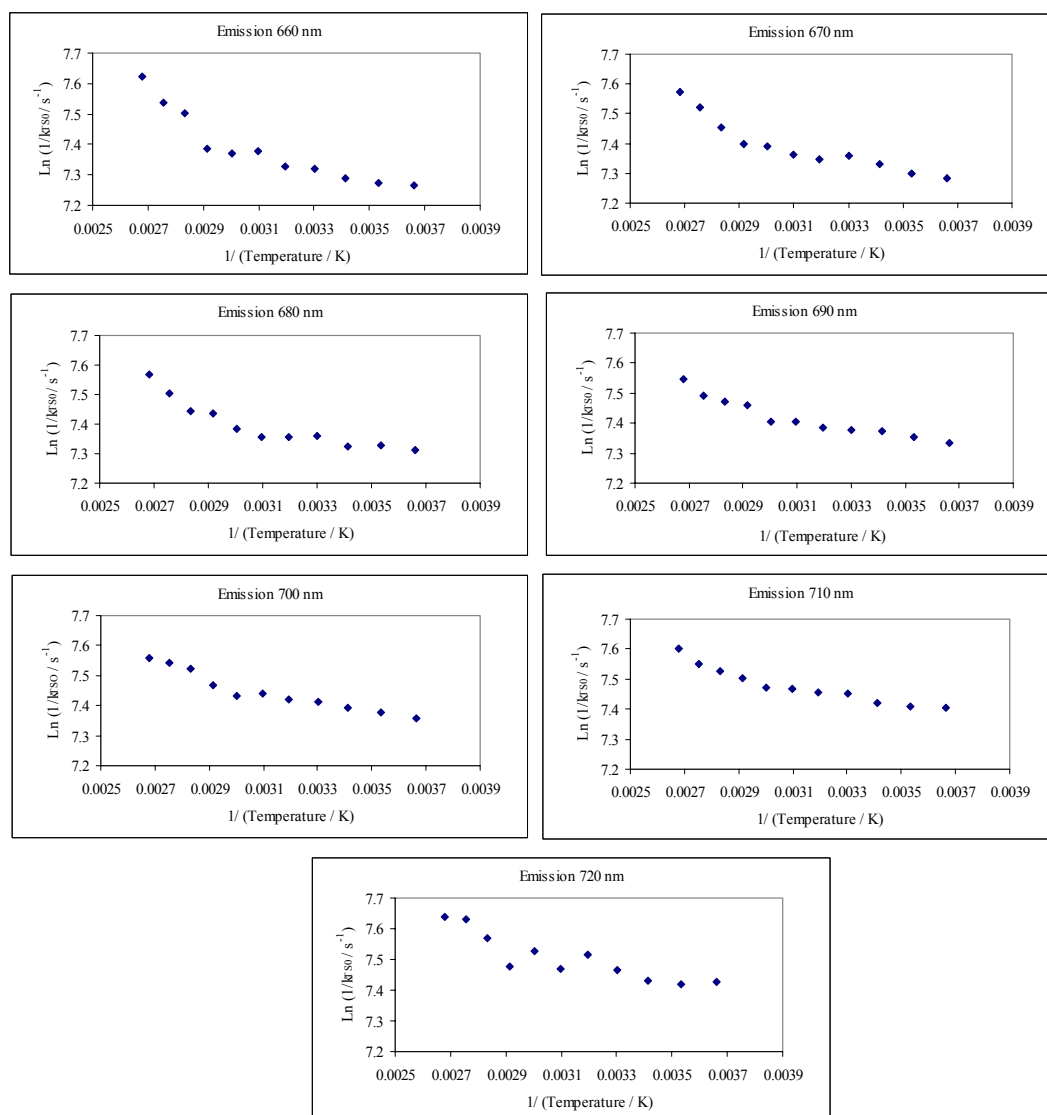
Figure V-11: Activation energies for the non-radiative decay k_{TS0} of Ery B in dried collagen casings at 0-30ºC (■), 70-100ºC (♦); the activation energies were calculated from an Arrhenius analysis of k_{TS0} data calculated from the lifetimes in Figure V-8.
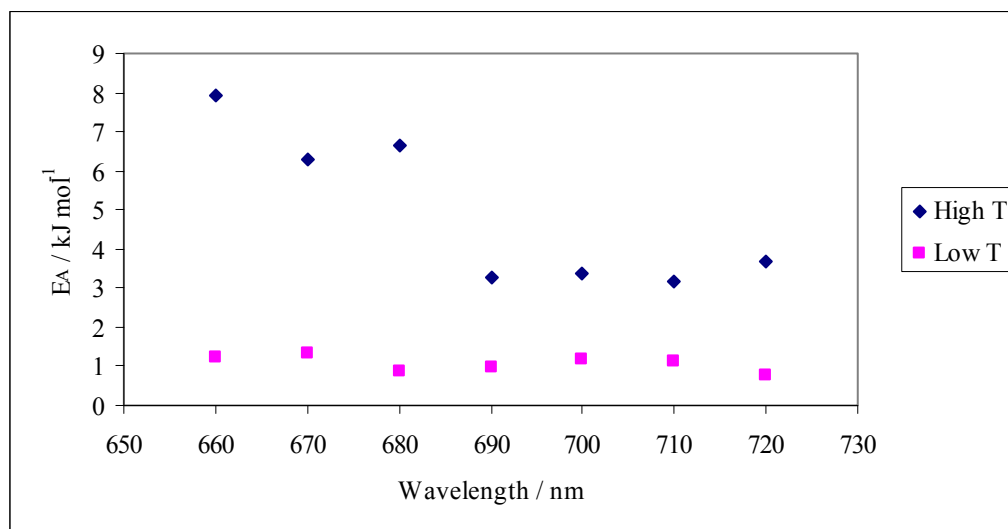
Figure V-12: Lifetimes determined from a stretched exponential model fit (Equation 3, Materials and Methods) for the phosphorescence intensity decay data from Ery B in collagen casings equilibrated against nitrogen and dry air as a function of time from when the collagen casing was removed from the bag.
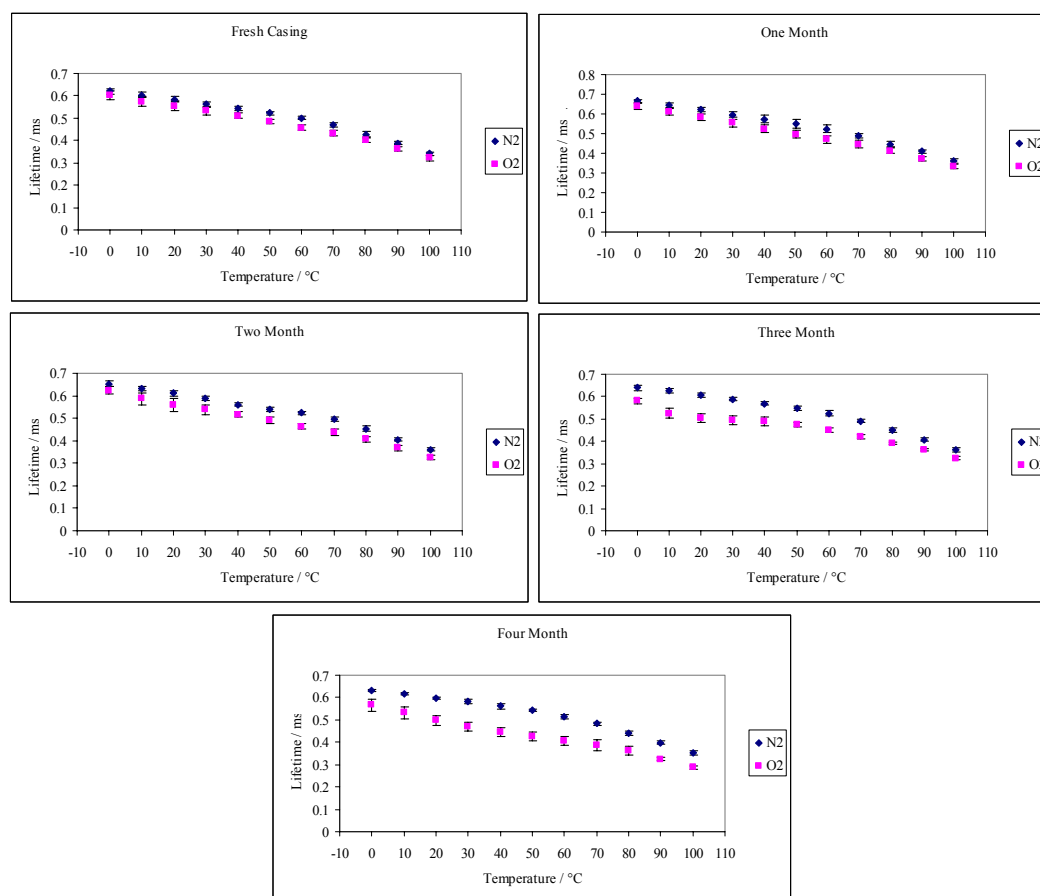
Figure V-13: Stretching exponents β from a stretched exponential model fit (Equation 3, Materials and Methods) for the phosphorescence intensity decay data from Ery B in collagen casings equilibrated against nitrogen and dry air as a function of the time from when the collagen casing was removed from the bag.
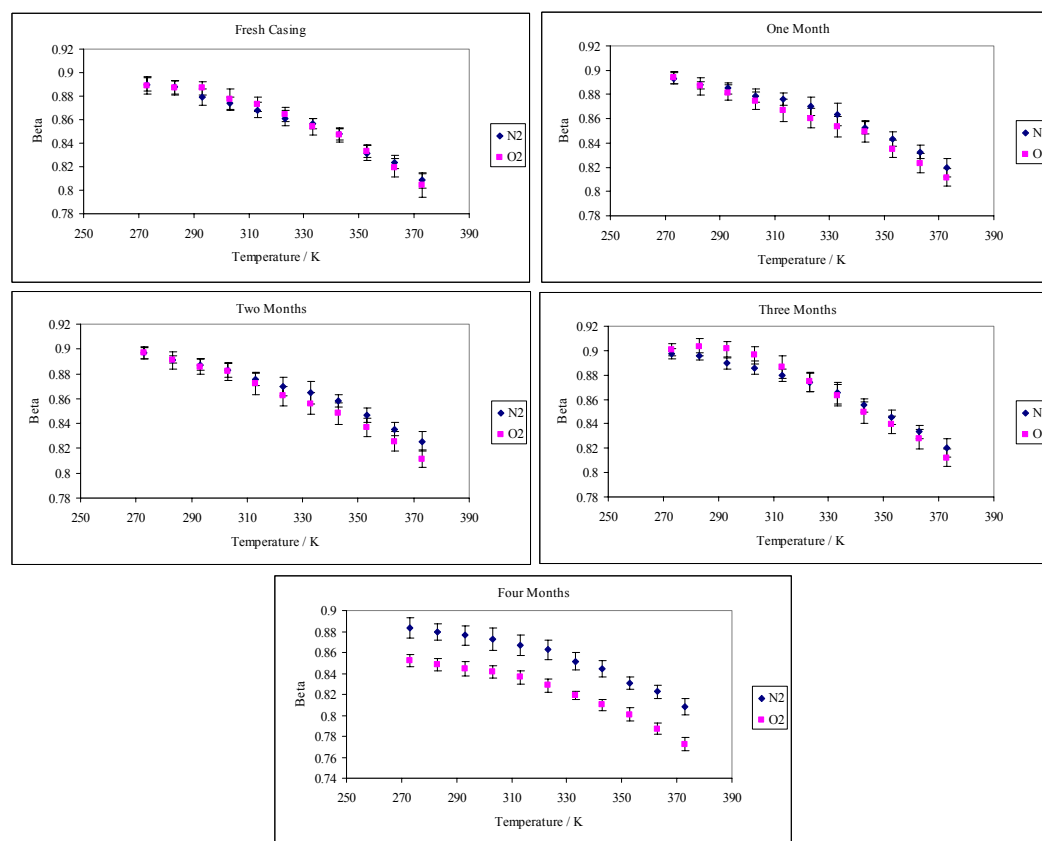
Figure V-14: $k_Q[O_2]$ as a function of temperature and time from when the collagen casing packages were opened.

Chapter 5 References

Bailey, A. J., and Light, N. D. (1989). "Connective tissue in meat and meat products," Elsevier Science Publishers, LTD, New York.

Barriga, M. I., and Piette, J. P. G. (1996). Reduction of adhesion of a Lactobacillus sp to collagen sausage casing by proteins. *Food Research International* **29**, 249-257.

Borysko, E. (1985). Characterization of regenerated collagen sausage casings by transmission of electron microscopy. (E. Inc., ed.), Sommerville, NJ.
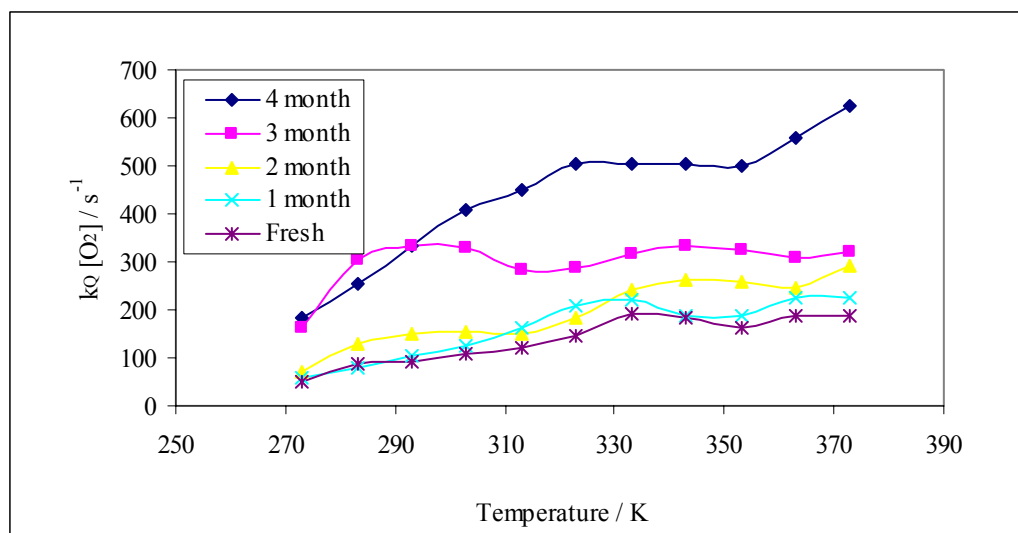
Buettner, A. V. (1964). Flash Photolysis in Thin Films of Gelatin and Other Polymers. *J. Phys. Chem.* **68**, 3253-3259.

Champion, D., Le Meste, M., and Simatos, D. (2000). Towards an improved understanding of glass transition and relaxations in foods: molecular mobility in the glass transition range. *Trends in Food Science & Technology* **11**, 41-55.

Chen, R. (2003). Apparent stretched-exponential luminescence decay in crystalline solids. *Journal of Luminescence* **102-103**, 510-518.

De Cupere, V. M., and Rouxhet, P. G. (2001). Collagen films adsorbed on native and oxidized poly(ethylene terephtalate): morphology after drying. *Surface Science* **491**, 395-404.

Deacon, M. J., and Kindleysides, L. (1973). Sausage Casing Technology, Food Technology. (N. D. Corporation, ed.), Vol. 3,767,821, pp. 88-89, US.

Devro-Teepak, I. (1996). "Product information-Collagen," Lisle, IL.

Doman, P. (2007). Personal Communication. (Nitta Casings, Inc.), Sommerville, NJ.

Duchowicz, R., Ferrer, M. L., and Acuna, A. U. (1998). Kinetic Spectroscopy of Erythrosin Phosphorescence and Delayed Fluorescence in Aqueous Solution at Room Temperature. *Photochemistry and Photobiology* **68**, 494-501.

Gennadios, A., Hanna, M. A., and Kurth, L. B. (1997). Application of edible coatings on meats, poultry and seafoods: A review. *Food Science and Technology-Lebensmittel-Wissenschaft & Technologie* **30**, 337-350.

Ho, H.-O., Lin, C.-W., and Sheu, M.-T. (2001). Diffusion characteristics of collagen film. *Journal of Controlled Release* **77**, 97-105.

Hood, L. L. (1987). Collagen in sausage casings. *In* "Advances in Meat Research: Volume 4 - Collagen as food" (A. M. Pearson, T. R. Dutson and A. J. Bailey, eds.), Vol. 4, pp. 109-126. AVI-Van Nostrand Reinhold, New York.

Joly, G., Kasica, J. J., O'Mara, R., and Shariff, R. (2004). Starch/Collagen casings for co-extruded food products. USA.

Kidney, A. J. (1970). Sausage Casing Technology. *In* "Food Technology Review" (E. Karmas, ed.), Vol. 14, pp. 122-123. Noyes Data Corporation, Park Ridge, NJ.

Lee, K. C. B., Siegel, J., Webb, S. E. D., Leveque-Fort, S., Cole, M. J., Jones, R., Dowling, K., Lever, M. J., and French, P. M. W. (2001). Application of the Stretched Exponential Function to Fluorescence Lifetime Imaging. *Biophys. J.* **81**, 1265-1274.

Lettinga, M. P., Zuilhof, H., and van Zandvoort, M. A. M. J. (2000). Phosphorescence and fluorescence characterization of fluorescein derivatives immobilized in various polymer matrices. *Physical Chemistry Chemical Physics* **2**, 3697-3707.

Lindsey, C. P., and Patterson, G. D. (1980). Detailed comparision of the Williams-Watts and Cole-Davidson functions. *J. Chem. Phys.* **73**, 3348-3357.

Lukasik, K. V. (2005). Luminescent Probes of Structural and Dynamic Heterogeneity in Gelatin, Rutgers University, New Brunswick.

Lukasik, K. V., and Ludescher, R. D. (2004). Phosphorescence of erythrosin and fusin as a probe of dynamic heterogeneity in amorphous gelatin films. *Biophysical Journal* **86**, 159a-159a.

Lukasik, K. V., and Ludescher, R. D. (2006). Molecular mobility in water and glycerol plasticized cold- and hot-cast gelatin films. *Food Hydrocolloids* **20**, 96-105.

Masoumi, Z., Stoeva, V., Yekta, A., Pang, Z., Manners, I., and Winnik, M. A. (1996). Luminescence quenching method for probing the diffusivity of molecular oxygen in highly permeable media. *Chemical Physics Letters* **261**, 551-557.

Miles, C. A., Burjanadze, T. V., and Bailey, A. J. (1995). The kinetics of the thermal denaturation of collagen in unrestrained rat tail tendon determined by differential scanning calorimetry. *J Mol Biol* **245**, 437-46.

Miller, A. T. (1983). Collagen Sausage Casing. Devro, Inc., United States.

Miller, A. T., and Marder, R. B. (1998). Process for strengthening collagen casings using ultraviolet irradiation Nitta Castings, Inc.

Morgan, T. F., Frame, G., and Kobussen, P. J. (1998). Process for producing a linked, co-extruded edible product. pp. 7. Devro PLC, Great Britain.

Morgan, T. F., Frame, G., and Kobussen, P. J. (2001). Process for producing a linked, co-extruded edible product. pp. 11. Devro PLC, Great Britain.

Nack, T. J., and Ludescher, R. D. (2006). Molecular mobility and oxygen permeability in amorphous bovine serum albumin films. *Food Biophysics* **1**, 151-162.

Osburn, W. N. (2002). Collagen Casings. *In* "Protein-Based Films and Coatings" (A. Gennadios, ed.), pp. 445-466. CRC Press, Boca Raton.

Pravinata, L. C., You, Y., and Ludescher, R. D. (2005). Erythrosin B Phosphorescence Monitors Molecular Mobility and Dynamic Site Heterogeneity in Amorphous Sucrose. *Biophys. J.* **88**, 3551-3561.

Richert, R. (1997). Evidence for dynamic heterogeneity near T-g from the time-resolved inhomogeneous broadening of optical line shapes. *Journal of Physical Chemistry B* **101**, 6323-6326.

Richert, R. (2000). Triplet state solvation dynamics: Basics and applications. *Journal of Chemical Physics* **113**, 8404-8429.

Richert, R., and Heuer, A. (1997). Rate-memory and dynamic heterogeneity of first-order reactions in a polymer matrix. *Macromolecules* **30**, 4038-4041.

Romans, J. R., Jones, K. W., Costello, W. J., Carlson, C. W., and Ziegler, P. T. (1985). "The Meat We Eat," Twelfth/Ed. The Interstate Printers and Publishers, Inc., Danville.

Rose, H. J. (1968). Method of Preparing an Edible Tubular Collagen Casing.

Shirke, S., and Ludescher, R. D. (2005). Molecular mobility and the glass transition in amorphous glucose, maltose, and maltotriose. *Carbohydrate Research* **340**, 2654-2660.

Shirke, S., Takhistov, P., and Ludescher, R. D. (2005). Molecular mobility in amorphous maltose and maltitol from phosphorescence of erythrosin B. *Journal of Physical Chemistry B* **109**, 16119-16126.

Shirke, S., You, Y. M., and Ludescher, R. D. (2006). Molecular mobility and dynamic site heterogeneity in amorphous lactose and lactitol from erythrosin B phosphorescence. *Biophysical Chemistry* **123**, 122-133.

Simelane, S., and Ustunol, Z. (2005). Mechanical Properties of Heat-cured Whey Protein–based Edible Films Compared with Collagen Casings under Sausage Manufacturing Conditions. *Journal of Food Science* **70**, E131-134.

Simon-Lukasik, K. V., and Ludescher, R. D. (2004). Erythrosin B phosphorescence as a probe of oxygen diffusion in amorphous gelatin films. *Food Hydrocolloids* **18**, 621-630.

Smits, J. W. (1985). The Sausage Coextrusion Process. *In* "Trends in Modern Meat Technology" (B. Krol, P. S. van Roon and J. H. Houben, eds.), pp. 60-62. The Netherlands: Center for Agricultural Publishing and Documentation, Wageningen, Netherlands.

Stratt, R. M., and Maroncelli, M. (1996). Nonreactive dynamics in solution: The emerging molecular view of solvation dynamics and vibrational relaxation. *Journal of Physical Chemistry* **100**, 12981-12996.

Sundaresan, K. V., and Ludescher, R. D. (2007). Molecular mobility and oxygen permeability in amorphous Beta-lactoglobulin films. *Food Hydrocolloids*. **In Press**.

Tanner, A. G., and Wallace, J. T. (1975). Caramel-Containing Collagen Sausage Casing and Smoked Sausage. (U. States, ed.). Devro, Inc.

Usha, R., Dhathathreyan, A., Mandal, A. B., and Ramasami, T. (2004). Behavior of collagen films in presence of structure modifiers at solid-liquid interface. *Journal of Polymer Science Part B-Polymer Physics* **42**, 3859-3865.

Waldman, R. C. (1985). Co-Extrusion-High Tech Innovation. *The National Provisioner*, 13-16.

Wang, P. Y. (1986). Meat Processing 1. *In* "Encyclopedia of Food Engineering" (C. W. Hall, A. W. Frall and A. L. Rippen, eds.), pp. 545-550. AVI, Westport, CT.

You, Y. M., and Ludescher, R. D. (2006). Phosphorescence of erythrosin B as a robust probe of molecular mobility in amorphous solid sucrose. *Applied Spectroscopy* **60**, 813-819.

Chapter 6: Conclusions from the model systems.

<u>*Introduction*</u>

The goal of this chapter is to analyze the differences between the model systems previously discussed. Significant variations between globular and fibrous proteins were observed and as sucrose and trehalose were added to BSA.

<u>*Results*</u>

The temperature dependence of the phosphorescence peak energy (ν_P) for BSA, gelatin, and collagen casings is shown in Figure VI-1. Gelatin, collagen casings, and BSA displayed biphasic decreases in emission energy with a break point at ~60°C, and emission values for gelatin and collagen casings were considerably higher than those in the amorphous globular protein BSA. When compared to amorphous globular proteins, we can conclude that collagen casings and gelatin participate in fewer dipolar relaxations around the excited triplet state due to higher emission energy values (Pravinata et al., 2005; Richert, 2000). The break point for BSA was more pronounced (greater decrease in peak frequency) than in gelatin and collagen casings. We hypothesize that the lack of increased dipolar relaxations over this temperature range for gelatin and collagen casings stems from the fact that a dynamic transition (T_g) for amorphous gelatin and collagen casings has not been reached, since T_g has been found to be between 180-220°C in dried gelatin films (Marshall and Petrie, 1980; Pinhas et al., 1996; Sobral and Habitante, 2001) and ~210°C in dried collagen films (Aisina et al., 1976). The slight peak frequency decrease in the fibrous proteins (increased dipolar relaxations) was most likely due to small scale reorientations around the excited state, and not from cooperative motions (rotations or vibrations of segmental protein portions), which would occur above T_g. At

higher temperatures all three matrices had greater dipolar relaxation rates, and there was an increase in the distribution of energetically distinct local environments (FWHM measurements) within the matrix.

Lifetime values are displayed in Figures VI-2a (under a nitrogen purge) and VI-2b (in the presence of oxygen) for BSA, gelatin, and collagen casings over the temperature range of 0-100°C. Under nitrogen conditions, lifetime values decreased due to collisions between the excited Ery B molecules and the matrix, and therefore, the lifetime values are thought of as an indicator of the matrix rigidity.   It was apparent that gelatin was significantly more rigid than the collagen casings and BSA. Initially, we hypothesized that gelatin and collagen casings would have similar lifetimes due to structure similarities, but this was not the case, with the collagen casings having significantly lower lifetime values. Possible explanations for the observed differences could have been because the collagen casings were not bound to the quartz slide, providing a more mobile environment, or that gelatin actually forms more cross-links and stronger non-covalent bonds, yielding a more rigid environment. The notion of the collagen casings not being bound to the quartz slide causing the lower lifetimes would mean that the "edge effect" was propagating throughout the entire film, which is not likely since the edges of the casing would make up less than 2% of the film thickness assuming an even distribution of the probe. It is more likely that the collagen casings had lower lifetimes due the nature of the large cable-like bundles of fibrils in collagen compared to the entangled networks in gelatin. The entangled network in gelatin forms strong, rigid, and tightly packed films with the probe dispersed through out the matrix, whereas the collagen casings have an open structure due to the massive fibrils of triple helices (~10

times the length of gelatin polypeptide chains). Not only are the collagen fibrils much larger than gelatin polypeptides, the fibrils are also very linear. Gelatin, on the other hand, has disordered or unraveled polypeptide chains which are more efficient in forming a network and space filling. Consequently, collagen has a less rigid matrix due to the open spaces available for molecular motions. We must also think about how Ery B interacts with each of these matrices. The probe distributes itself randomly throughout the entangled network in gelatin, while in the collagen casing matrix the probe bound primarily to the surface of the large triple helix fibrils. We assume that when the probe is bound to surfaces, lifetimes would be lower due to increased molecular collisions. Lower lifetimes for globular BSA were most likely an effect of globular proteins being unable to form intermingled structures as in fibrous proteins yielding a more "open" structure.

Under oxygen conditions, significant differences between the protein matrices are apparent due to differences in the efficiency of oxygen quenching (Figure VI-2b). Collagen and gelatin are known to be excellent barriers to oxygen, while BSA is not known for its ability to prevent oxygen migration. This is consistent with the lower lifetime values for BSA under oxygen conditions (oxygen is able to penetrate the matrix and quench the excited Ery B molecules lowering the lifetimes). All three matrices showed a break point around 55-60°C, although the trends are very different. BSA had a linear and dramatic decrease in lifetime values from 0°C to the break point, where the values leveled off; meaning oxygen was an efficient quencher of Ery B at low temperatures. The gelatin and collagen casing matrices followed similar trends until the break point, where gelatin had a more drastic decrease. This has been attributed to the fact that gelatin has a gel/sol phase transition around this temperature, and the softening

of the matrix would allow additional quenching. The collagen casings did not break down over the experimental temperature range, hence minimal changes in lifetime values, also demonstrating that the presence of oxygen has little effect on this matrix.

The molecular mobility of the protein matrices is shown in Figure VI-3a. BSA and collagen casings showed a gradual increase in k_{TS0} until ~60°C, where the increase became more drastic. Above the breakpoint, BSA was more mobile than the collagen casings. Gelatin, on the other hand, did not display an obvious breakpoint in k_{TS0} and had noticeably lower k_{TS0} values over the tested temperature range of 0-100°C. From this, we concluded that gelatin was considerably less mobile, and that the structure may only be participating in small scale harmonic vibrational motions. BSA and collagen casings seemed to participate in both vibrational and rotational motions, and possibly even translational motions above the breakpoint. The higher molecular mobility seen in the collagen casings, as compared to gelatin, is most likely related to the differences in molecular structure within the matrix. The entangled and tightly bound network in gelatin allows for less matrix mobility, while the more open fibrillar network in collagen allows for additional molecular movements, as discussed in the lifetime data discussion. In addition, Tseng et al. (2000) found that near free surfaces in collagen films the molecular mobility can be 10-100 times more mobile than in the bulk phase. Since the collagen films were not bound to the slide (having two free surfaces) this may have had a great effect on the overall mobility.

A log plot of oxygen permeability, $k_Q[O_2]$, versus temperature is shown in Figure VI-3b. At 0°C, BSA was ~10 times more permeable to oxygen than gelatin and collagen casings, and at 100°C, ~10 times greater than gelatin and ~100 times greater than

collagen casings. BSA and gelatin displayed similar increases in the rates of oxygen permeability, while the collagen casings had significantly slower rates of oxygen permeability over the temperature range of 0-100°C. The lower oxygen permeability in the collagen casings was most likely due to a lower oxygen solubility or adsorption in the collagen casings, the casings being much thicker than the gelatin films, or the highly cross-linked fibrillar casing having a smaller pore size. BSA remained at least ~10 times more permeable than the gelatin and collagen casings over the tested temperature range, most likely related to its globular structure. This data is very useful for food technologists looking at possible matrices for edible films in relation to oxygen barrier attributes.

The activation energies for $k_Q[O_2]$ were significantly larger for the proteins studied (29.9 kJ mol^{-1} for BSA, 26.0 kJ mol^{-1} for gelatin, and 10.2 kJ mol^{-1} for collagen) than that observed for k_{TS0} (3.1 kJ mol^{-1} for BSA, 0.5 kJ mol^{-1} for gelatin, and 1.8 kJ mol^{-1} for collagen) over the temperature range of 0-100°C. Thus, the molecular motions underlying oxygen permeability appear to involve more delocalized collective motions of the protein matrix. In part, this difference must reflect the qualitatively different processes that are being monitored: k_{TS0} measures the coupling of vibrational motions in the probe with local vibrational motions in the protein matrix, while $k_Q[O_2]$ measures the coupling of translational motion of an oxygen molecule with collective motions of the protein matrix. The linear dependence of the three matrices seen between k_{TS0} and $k_Q[O_2]$ in Figure VI-4, however, provides evidence that the collective motions which facilitate oxygen permeability are modulated in some direct fashion by the modes of local molecular mobility measured by $k_{TS0.}$ This plot also exemplifies the differences in

molecular mobility and oxygen permeability between the protein matrices. Gelatin displays the lowest molecular mobility, while collagen has the lowest oxygen permeability. The explanations for this were given before.

Differences in the oxygen quenching rate, between samples with different ratios of sucrose to BSA seemed more apparent at higher temperatures, suggesting that temperature was the key component for oxygen permeability through the sucrose/BSA matrix. Figure VI-5a, however, indicates that $k_Q[O_2]$ increased systematically with temperature at all sucrose/BSA ratios. The pure BSA and lower ratios of sucrose/BSA matrices, displayed active oxygen quenching. A distinct decrease in oxygen permeability was observed as the ratio of sucrose to BSA was increased from 10:1 to 30:1. At sucrose to BSA ratios above 30:1, oxygen permeability was significantly lower than observed in the lower sucrose/BSA matrices.

The addition of trehalose to the BSA matrix greatly affected $k_Q[O_2]$ values, and $k_Q[O_2]$ increased greatly at higher temperatures (Figure VI-5b). A log plot of $k_Q[O_2]$ versus molar ratio of trehalose to BSA showed a gradual decrease in oxygen permeability as trehalose concentrations increased up until the 100:1 ratio (Figure VI-5b). A sharp decline in oxygen permeability was observed at the 300:1 ratio, and oxygen permeability values were barley detectable at the ratios above 300:1. As explained in Chapter 3, the 0 s^{-1} rate values in Figure VI-5b for temperatures 0-20°C were a result of slightly negative values for $k_Q[O_2]$.

$k_Q[O_2]$ was further analyzed by plotting the log of $k_Q[O_2]$ versus the log molar ratio of sugar to BSA (Figures VI-5c and VI-5d) with the x-axis on the same log scale. This allows for a facile comparison between sucrose and trehalose in regards to its ability

to reduce oxygen permeability. These plots show that between the 10:1 and 30:1 ratio in the sucrose/BSA matrix there is a distinct decrease in oxygen permeability, and in the trehalose/BSA matrix, this trend was noticed between the 100:1 and 300:1 ratios.

Possible explanations why sucrose was more effective as compared to trehalose in lowering the oxygen permeability of BSA films were that sucrose was able to pack more efficiently thus lowering free volume, sucrose is less hygroscopic (residual water aids in oxygen transport), sucrose was more efficient in hydrogen bonding to BSA which also relates to the formation of a single phase (where the trehalose/BSA matrix displayed phase separation), or simply due to the fact that the sucrose/BSA matrix was more rigid and less mobile.

Conclusions

Ery B phosphorescence can be used for the monitoring of the modes, rates, and distribution of molecular mobility and oxygen permeability in model amorphous protein systems and in simple food systems. This technique provides the molecular detail necessary to connect food quality and stability to molecular structure, molecular mobility, and oxygen permeability. We have successfully tested many food ingredient model systems in our laboratory via this phosphorescent technique, and it is time to move forward and apply this technique to actual food products.

Chapter 6 Figures

Figure VI-1: Peak frequency values (ν_P) for BSA, gelatin, and collagen casings as a function of temperature.
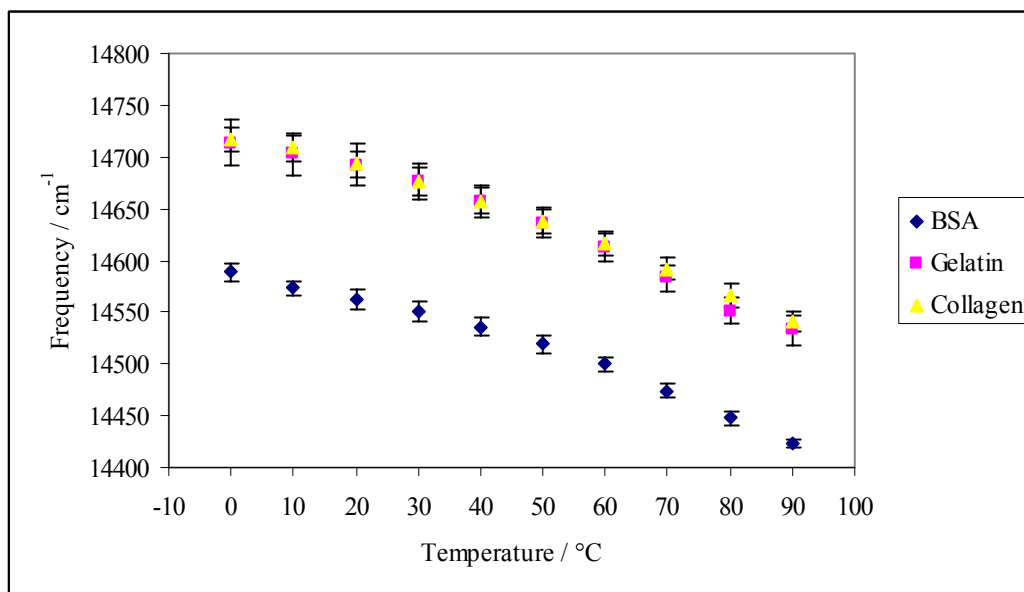
Figure VI-2: Lifetime values (τ) for BSA, gelatin, and collagen casings under nitrogen conditions (a) and in the presence of oxygen (b) as a function of temperature.

a)
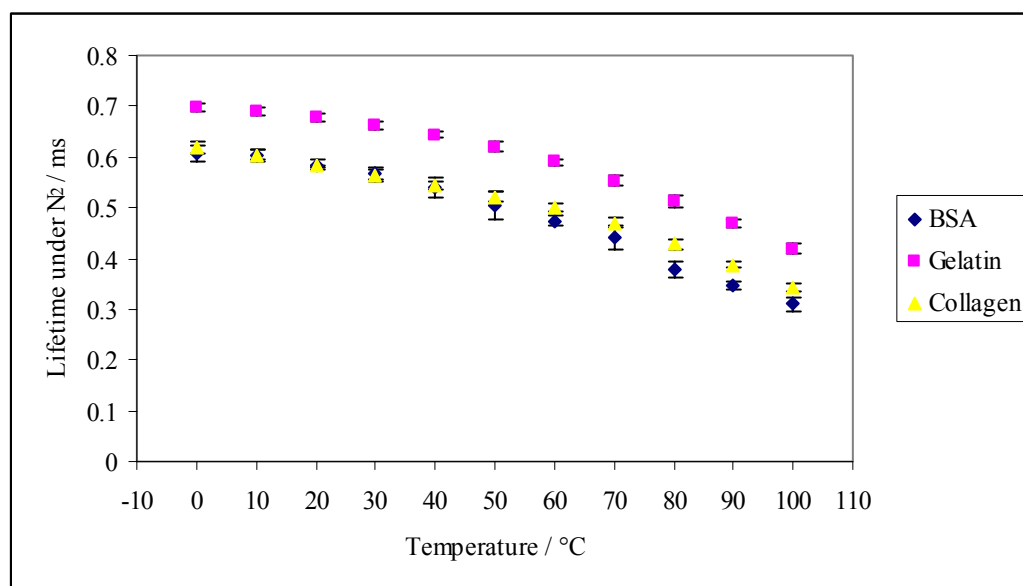
b)
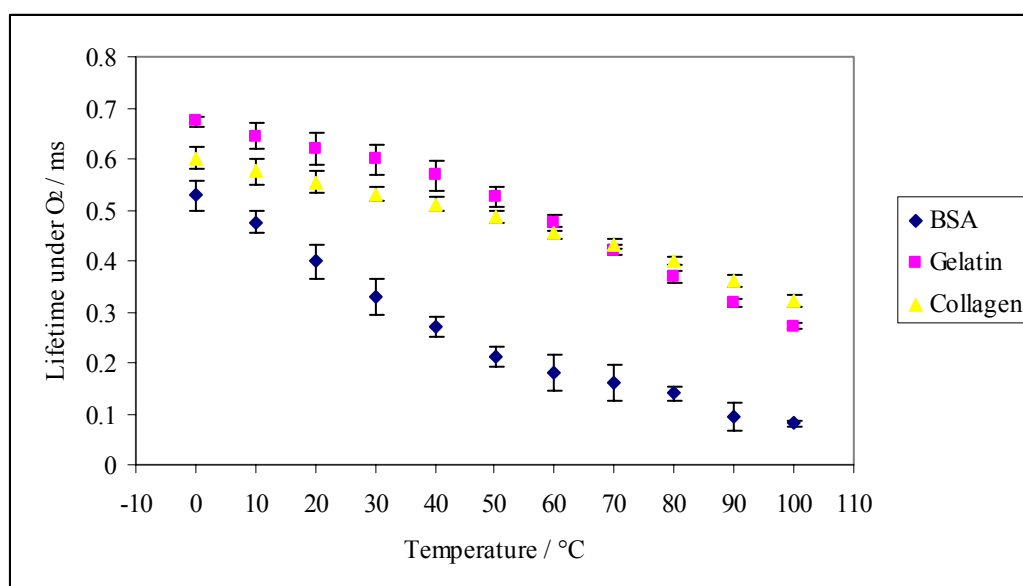
Figure VI-3: The molecular mobility (k_{TS0}) (a) and oxygen permeability ($k_Q[O_2]$) (b) of BSA, gelatin, and collagen casings as a function of temperature.

a)
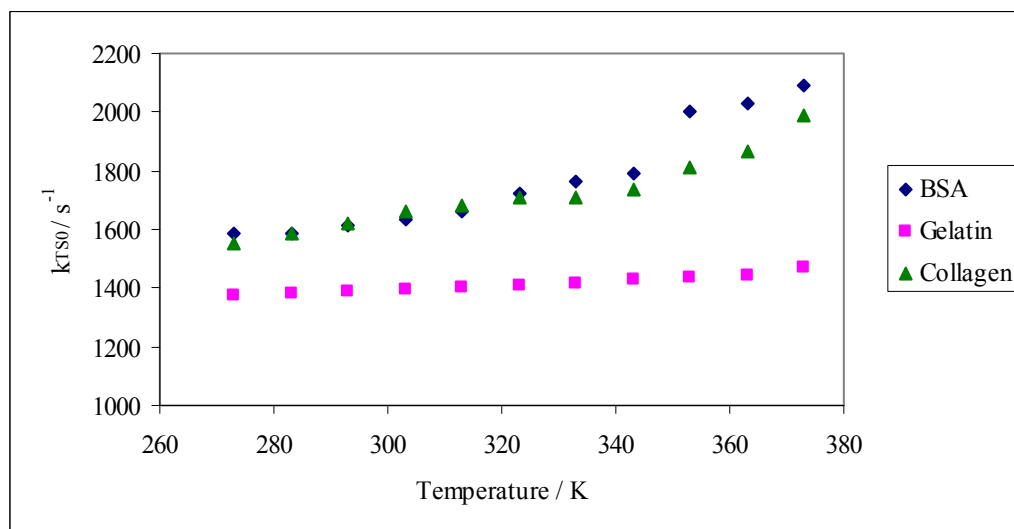
b)
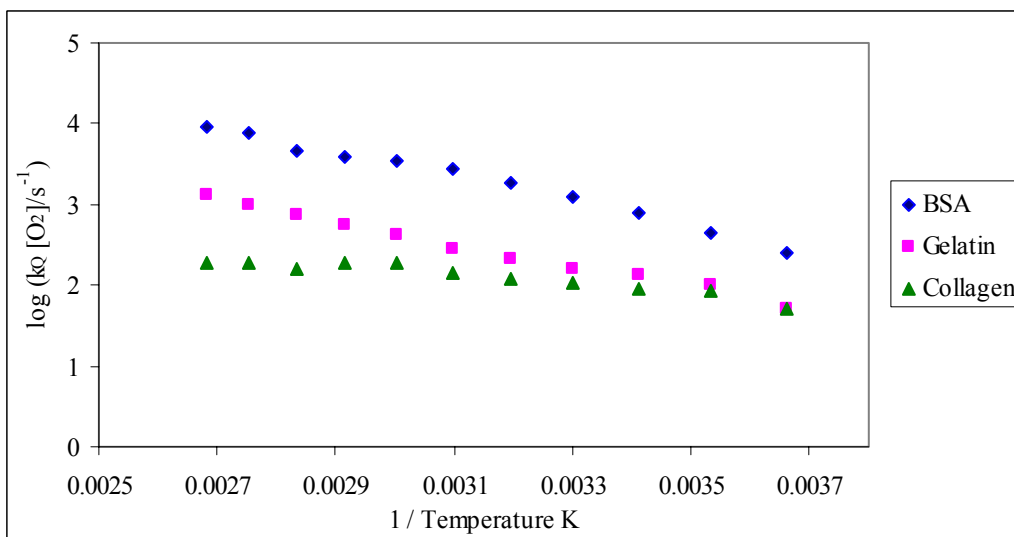
Figure VI-4: Plot of $k_Q[O_2]$ versus k_{TS0} for BSA, gelatin, and collagen casings.

Figure VI-5: Rates for oxygen quenching $k_Q[O_2]$ as a function of the molar ratio of sucrose to BSA (a) and trehalose to BSA (b). Figures VI-5c and VI-5d show data from VI-5a and VI-5b plotted with the sugar to protein ratios (x-axis) on a log scale for comparison between the sugars.

a)

b)

c)
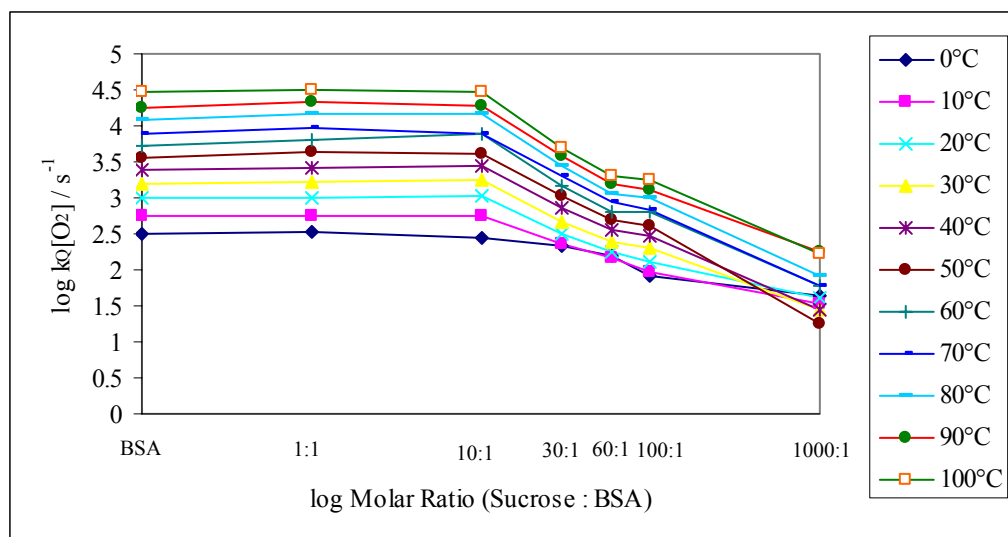
d)
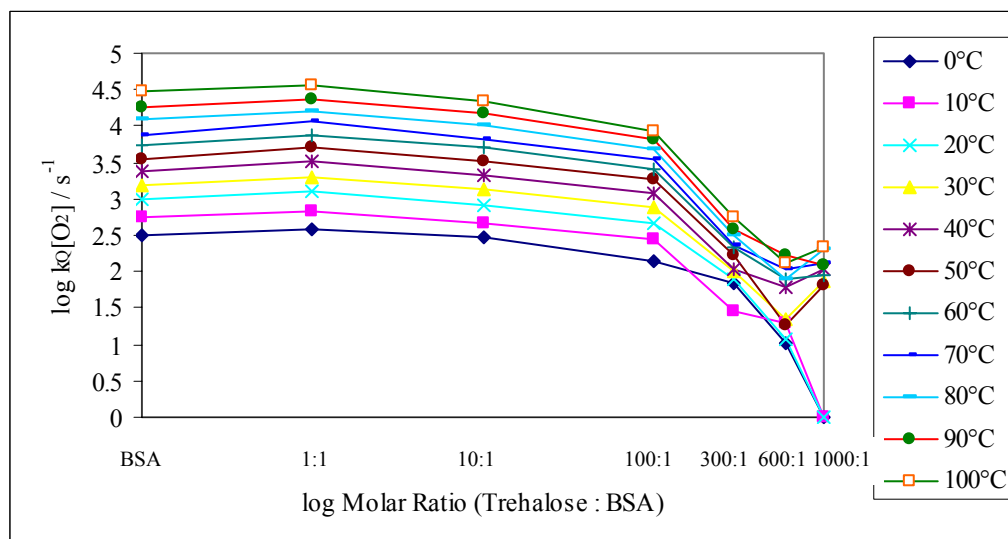
Chapter 6 References

Aisina, A. Y., Golubyatnikova, A. T., and Kutyanin, G. I. (1976). Similarities in the behavior of collagen and gelatin during heat drying. *Kozhevenno-Obuvnaya Promyshlennost* **12**. (Abstract)
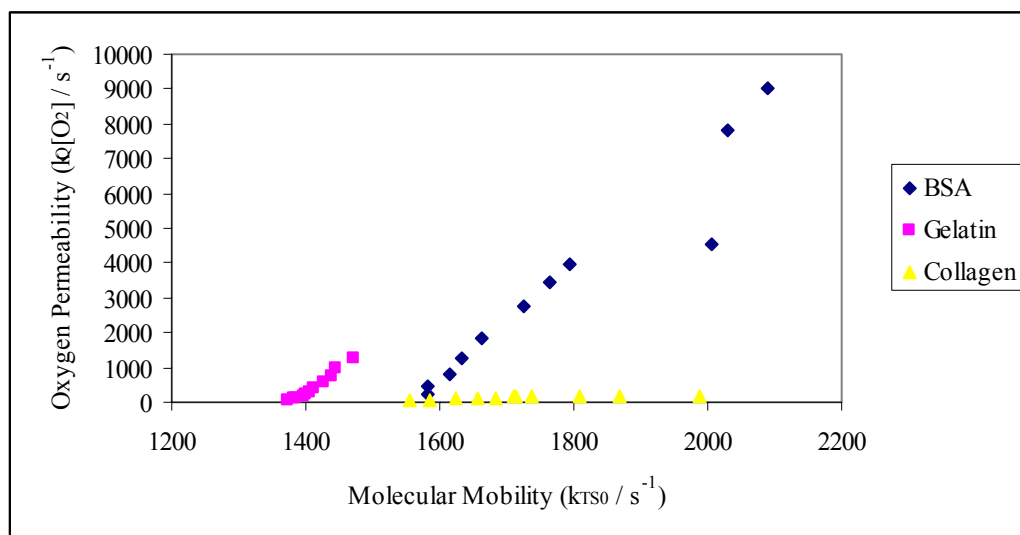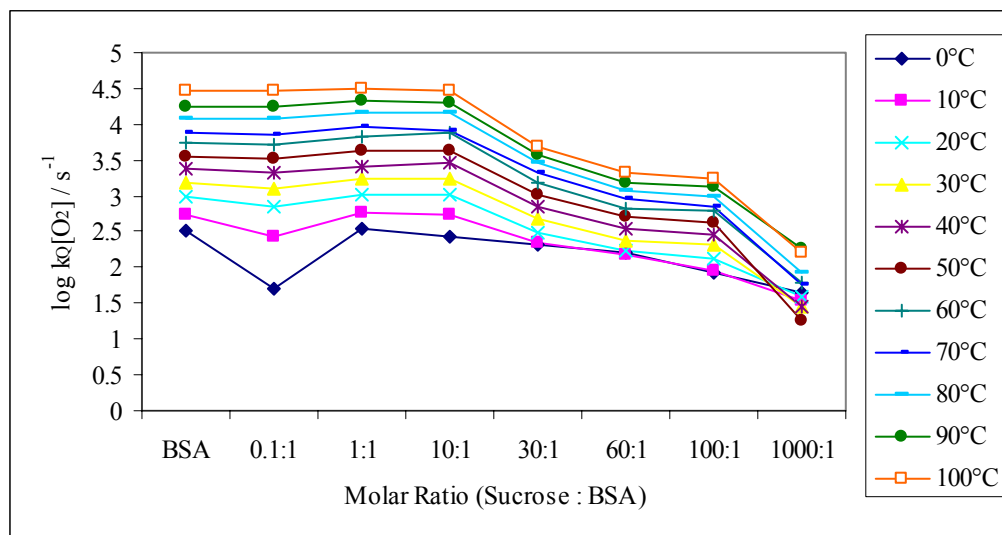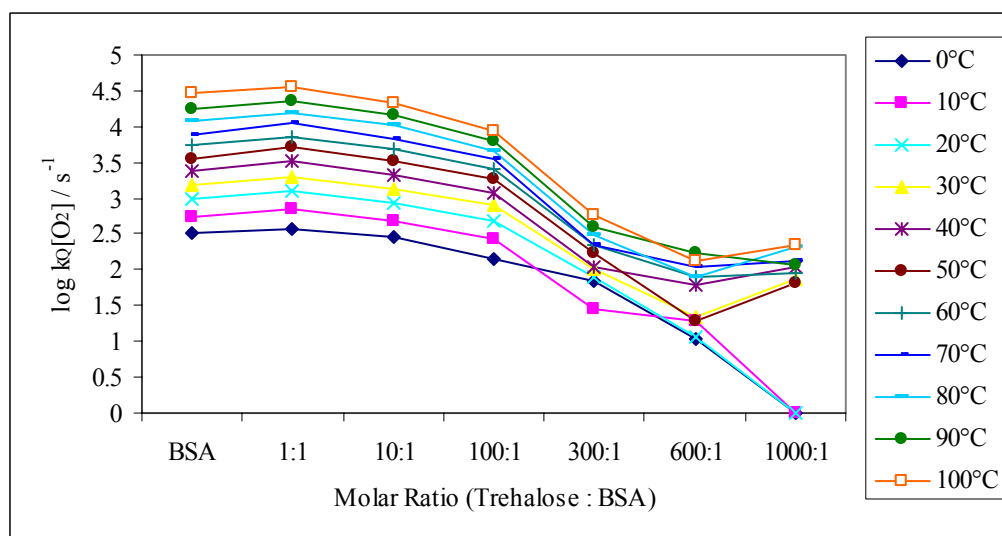
Marshall, A. S., and Petrie, S. E. B. (1980). Thermal transisitions in gelatin and aqueous gelatin solutions. *The Journal of Photographic Science* **28**, 128-134.

Pinhas, M. F., Blanshard, J. M. V., Derbyshire, W., and Mitchell, J. R. (1996). The effect of water on the physicochemical and mechanical properties of gelatin. *Journal of Thermal Analysis* **47**, 1499-1511.

Pravinata, L. C., You, Y., and Ludescher, R. D. (2005). Erythrosin B Phosphorescence Monitors Molecular Mobility and Dynamic Site Heterogeneity in Amorphous Sucrose. *Biophys. J.* **88**, 3551-3561.

Richert, R. (2000). Triplet state solvation dynamics: Basics and applications. *Journal of Chemical Physics* **113**, 8404-8429.

Sobral, P. J. A., and Habitante, A. M. Q. B. (2001). Phase transitions of pigskin gelatin. *Food Hydrocolloids* **15**, 377-382.

Tseng, K. C., Turro, N. J., and Durning, C. J. (2000). Molecular mobility in polymer thin films. *Phys Rev E Stat Phys Plasmas Fluids Relat Interdiscip Topics* **61**, 1800-11.

Chapter 7: The development of a phosphorescent technique to study sausages stuffed into erythrosin B doped collagen casings.

Introduction

Luminescence spectroscopy provides a powerful tool to understand the molecular motions and processes that control macroscopic properties in amorphous matrices. Optical techniques, such as phosphorescence, are rapid, sensitive, versatile, and offer a non-invasive means for studying food products through the introduction of a luminescent probe to the food matrix (You and Ludescher, 2006). Luminescent probes are sensitive to the surrounding matrix structure, the presence of quenching molecules (especially oxygen), specific functional groups, polarity, pH, and matrix mobility. This provides highly specific and detailed information about the local environment surrounding the probe (Sundaresan and Ludescher, 2007).

Many foods are packaged under vacuum or modified atmosphere packaging (MAP) with hopes of extending product shelf life, improving appearance, reducing degradation due to lipid oxidation, and slowing food deterioration as a result of microbial growth (O'Riordan et al., 2005). The concentration of residual oxygen in the package is critical for controlling the aforementioned processes (Cutter, 2002) along with monitoring the efficiency of the packaging lines and the integrity of the package (Fitzgerald et al., 2001). Current methods for measuring oxygen content are destructive to at least the package, and many times to the actual food product itself (as reviewed by O'Riordan et al. (2005)). The most common method used today for oxygen determination in a food package involves a headspace analyzer which aspirates a small amount of headspace gas and analyses for oxygen via electrochemical detection

(O'Mahony et al., 2006). Other methods used to monitor package integrity, which are also destructive to the product packaging, include the biotest, the electrolyte test, and the dye penetration or bubble test. These tests are laborious and time consuming and can not identify all packing leaks since they are not applicable for in-line product testing as a quality control measure and have to be used randomly off-line (as reviewed by Smiddy et al. (2002b)).

Extensive research has been applied to develop a non-destructive method for oxygen sensing within food packaging that is both cost effective and could be used at various points in production, distribution, and retail, assuring high standards for safety by achieving 100% quality control (Fitzgerald et al., 2001). Phosphorescence-based sensors have met these criteria. The technique involves placing the sensor component inside the package and interpreting the optical signal through the packaging material using a phosphorescence detector outside the package (Smiddy et al., 2002a). This phosphorescent technology for oxygen determination within the package can be done in real-time and package leaks (allowing oxygen into the package) can be determined in a timely manner before degradative processes take place (directly after packaging) (Smiddy et al., 2002a).

Oxygen sensors are typically luminescent long decaying dyes that are embedded in a polymer encapsulation medium and prepared as a film coating (Smiddy et al., 2002a). The most common dyes are complexes of ruthenium (II) and phosphorescent platinum (II)-porphyrins, which are embedded in polymers of polystyrene, polysulfone, and/or silicone (O'Riordan et al., 2005). Oxygen penetrates the polymer coating around the dye molecule via simple diffusion and quenches the phosphorescence of the dye

through molecular collisions. These sensors are then incorporated into the food packages, and satisfactory analytical results are achieved using lifetime based phosphorescent measurements performed with a simple LED-photodiode equipped with a fiber optic extension (Fitzgerald et al., 2001; Papkovsky et al., 1995). Successful systems using platinum octaethylporphin-ketone and polystyrene as the sensor and matrix, respectively, have been used to determine residual oxygen in modified atmosphere packed hams (Papkovsky et al., 2002), *sous vide* processed beef lasagna (O'Mahony et al., 2004), smoked fish (Fitzgerald et al., 2001), and cheese (O'Mahony et al., 2006). For a more detailed description of the experimental method, see Papkovsky et al. (1995). The sensors were convenient, affordable, and demonstrated high practical utility and potential for use on a large scale. The different sensor applications for food packaging include inserts, stickers attached to the inside of the package, and sensor spots printed directly on the packaging material (O'Riordan et al., 2005). The oxygen profiles during storage indicate quality changes within the food product and the efficiency of the packaging material (Fitzgerald et al., 2001). The downside of these phosphorescent dye complexes is that they are not FDA approved and food safety concerns, stemming from the dye complexes leaching into food products, require further evaluation.

Phosphorescence has also been used in the food industry for detecting certain food constituents. A phosphorescent method for the detection of tryptophan, an amino acid essential for human nutrition, in yogurt, was developed using heavy atom salt perturbers (Canabate-Diaz et al., 2003). Phosphorescence techniques have also been used successfully to detect the presence of the undesirable, naturally occurring biogenic amine, tryptamine, in beer. Tryptamine detection is important as it is linked with hypertension,

modification of blood pressure, and headaches (Canabate-Diaz et al., 2003). It is apparent that the concentrations of tryptophan and tryptamine deserve careful consideration. High performance liquid chromatography and gas chromatography coupled with mass spectrometry methods require a pretreatment and are very cumbersome (Canabate-Diaz et al., 2003), so rapid detection via phosphorescence was greatly desired.

Our laboratory has demonstrated the usefulness of erythrosin B (Ery B) as a phosphorescent indicator for the molecular mobility, oxygen permeability, and dynamic site heterogeneity in various amorphous model systems composed of amorphous sugars and proteins. These model systems were made up of pure components or mixtures of pure components with the goal of applying these luminescent techniques to an actual food product by embedding Ery B into an actual food system. Since Ery B is extremely sensitive to oxygen quenching, it is an excellent candidate for use as an oxygen sensor (typical vacuum and MAP food packages contain 0.07-0.55% and 1.15-1.26% oxygen, respectively (Smiddy et al., 2002a)) within various packaging conditions. Ery B, unlike the previously mentioned synthetic oxygen sensors, would also be able to determine the molecular mobility, oxygen permeability, and dynamic site heterogeneity of the packaged food product. Furthermore, Ery B is FDA approved and safety issues, such as leaching into the food product (O'Riordan et al., 2005), are not a concern as in many of the other oxygen sensors currently in the development stage.

For our model system, we chose to continue working with the collagen casing matrix. Here we embed Ery B into collagen casings (Ery B is currently one of the colorants used to dye sausage casings), stuff the casing with a sausage mixture, and then

package the sausages under variable conditions. The goal of this research is to establish a method to determine the effect of residual oxygen on the rigidity and heterogeneity of the packaged sausages. Future improvements of this method will allow us to correlate our measurements with oxygen concentrations within food packages and the chemical and biological processes responsible for reducing shelf-life.

Materials and Methods

Preparation of Samples

A 10 mg/ml stock solution of erythrosin B free acid (Molecular Probes, Inc., Eugene, OR) was prepared in *N, N*-dimethlyformamide (DMF) (Sigma-Aldrich, Milwaukee, WI). DMF has negligible effects on the spectroscopic properties of the probe in amorphous sucrose at a variety of concentrations (Pravinata et al., 2005; You and Ludescher, 2006). This concentration was selected to simplify the addition of the probe to the casing soaking solution, and the solvent was selected for probe stability during long term storage. The probe was added to distilled deionized water (0.01 mM concentration). At this concentration it was determined that the Ery B does not aggregate, existing only as individual molecules which will disperse into the collagen casing, with spectroscopic results having a high signal to noise ratio.

Casing Preparation

Collagen casings were obtained from Nitta Casing, Inc. (Somerville, NJ) and were kept under refrigeration until ready for use. Casings were soaked in a 0.01 mM solution of Ery B for 24 hours. Ery B is FDA approved for use in coloration of sausage casings in amounts consistent with good manufacturing procedure (FDA, 2002). The soaked casings were then removed, blotted with paper towel to remove excess dye solution, and

dried under a constant air flow for one hour. The casings were then stuffed with the sausage mixture.

Preparation of the Sausage

Fresh pork shoulder (80% lean) was obtained from the Nitta Casing Inc. pilot plant (Sommerville, NJ). The pork was then ground twice through a 1200 Watt meat grinder (Small Timer Super Grinder #SM-G50) using the medium cutting plate (3/8 inch). The meat was then held under refrigeration for 30 minutes to cool it back below 4°C. A standard spice mix for fresh bratwurst was obtained from Haen Meat Packing Inc. (Kaukauna, WI). This was scaled down from a 100 lb batch to a 10 lb batch due to processing constraints. Soy blend (soy flour, hydrolyzed protein from soy (2.8%), salt, and flavoring) was added to the spice mix yielding a final ratio of 3.0% in the finished product, and served as a binder and texture enhancer in the product. The spice mix and soy blend were added slowly to the 10 lb ground pork meat block, and water (less that 3.0% of the final product weight) was also added to ease the addition of the spices and soy binder. The spiced meat block, now considered fresh sausage, was put in a freezer for 30 minutes to ease the stuffing procedure (a colder meat block is less prone to sticking to the stuffer, and required less pressure for the stuffing process).

Probe Information

It is desirable for luminescent probes to have a high absorption coefficient, high quantum yields (Slavic, 1994), and they should be site specific and sensitive to the molecular environment. Phosphorescent probes can directly monitor the rigidity of the local environment (Strambini and Gonnelli, 1985), and this environment can be the interior or surface of a protein (Shah and Ludescher, 1995). Dye molecules are the most

sensitive reporters because of their extended π-electron system, strong dispersion interaction with the surrounding environment, very high quantum yields, and their range of long wavelength absorption bands often lies within the range easily accessible to laser spectroscopy (Lesch et al., 2004). Our studies are best suited with a phosphorescent probe. Ery B satisfies all of the previously mentioned requirements and also yields a phosphorescence emission time scale of 10^{-5} to 10^{-3} s corresponding to molecular motions in glassy environments, and has been shown to be a very sensitive oxygen sensor (Lam et al., 2001; Nack and Ludescher, 2006; Sundaresan and Ludescher, 2007). Ery B (tetra-iodofluorescein, FD & C red 3, or cherry red) is perhaps the most widely used phosphorescent probe to assess the molecular mobility of water soluble and membrane bound proteins, due to its large extinction coefficient and high phosphorescence quantum yield (Pravinata et al., 2005). The phosphorescent nature of Ery B is attributed to the xanthene ring with four iodine molecules. Phosphorescence from the triplet state of the luminescent probe Ery B can provide information about the subsequent relaxations, oxygen permeability, and dynamic site heterogeneity in the collagen casing due to its site specificity and high sensitivity.

Stuffing of the Ery B Doped Collagen Casings

The sausage was added to a 5 lb capacity stainless steel sausage stuffer (The Sausage Maker, Buffalo, NY). The Ery B doped collagen sausage casings were placed on the stuffing horn, and the sausage was hand-stuffed into the casings maintaining a uniform stuff by monitoring the speed and pressure of the stuffing process. Individual sausages were portioned into 5 inch sausages via twisting of the casings. The individual sausages were then either wrapped in saran wrap for the fresh samples (n=3), vacuum

sealed in a Model #225 Ultravac Single Chamber Packaging Machine (Koch Equipment, Kansas City, MO) and refrigerated at 2°C (n=3), or frozen and vacuum sealed and stored at -14°C (n=3). Two different bags were used for the vacuum sealed samples. Trials 1 and 2 used nylon/polyethylene high barrier 3 mil Safe Handling bags (Koch Equipment, Kansas City, MO), and trial 3 used the standard Food Saver channeled bags.

Phosphorescence Measurements

Measurements were made on a Cary Eclipse fluorescence spectrophotometer equipped with an external fiber optic coupler (Varian Instruments, Walnut Creek, CA). This instrument, which collects in analog mode, uses a high intensity pulsed lamp. A time delay was used to avoid any fluorescence during the lamp pulse. Before the fiber optic coupler could be used, it was aligned to optimize efficiency with which light passes through the coupling device. Alignment was carried out using the burner cleaning and alignment card provided by Varian Instruments (Walnut Creek, CA). The vertical and horizontal excitation adjustors were altered to optimize the light entering the excitation fibers. The same procedure was carried out for the emission vertical and horizontal adjustors. Lifetime measurements were collected under ambient air and light conditions. Samples were excited at 540 nm and the emission was measured at 685 nm with a 20 nm bandpass for both excitation and emission monochromators. Each time-resolved decay transient was the average of 100 cycles. Each cycle data was collected from a single flash with a delay of 0.1 ms, a 0.02 ms gate time, and 4.0 ms total decay time. All experiments were done in at least triplicate and the standard deviation of the averages was calculated to validate reproducibility.

Data Analysis

Phosphorescence lifetimes were determined by nonlinear least-squares analysis with the statistical programs Igor and Nfit. Fits were judged satisfactory if the r^2 values were in the range of 0.995-1.0 and the modified residuals ((data − fit)/data$^{1/2}$) varied randomly about zero. Data was analyzed using a stretched exponential, or Kohlrausch-Williams-Watts (KWW), decay model which has been shown to be appropriate to describe the wide distribution of relaxation times (Champion et al., 2000) for the molecular process that depopulate excited states in tissues (Lee et al., 2001), crystalline solids (Chen, 2003), super cooled liquids (Richert, 1997), and amorphous solids (Pravinata et al., 2005):

$$I(t) = I(0) \exp[-(t/\tau)^{\beta}] + c \qquad (1)$$

Where I(t) is the intensity as a function of time following pulsed excitation, I(0) is the initial intensity at time zero, τ is the KWW lifetime, and β is the stretching exponent which characterizes the distribution of the decay times (Richert and Heuer, 1997). Further explanation of the parameters of the stretched exponential equation is provided in the results section.

Results

Before testing the Ery B casings stuffed with sausage, we needed to validate that the fiber optic coupler provided comparable results to samples tested in the standard cuvette holder. One centimeter by one centimeter cross-sections of collagen casings were doped with Ery B and dried as explained in Chapter 5. These casings were then tested in both the internal sample holder within a quartz cuvette and also with the external fiber optic coupler. Next, the same casings were tested inside four different food grade

vacuum sealable bags via the external fiber optic coupler. These bags varied in gloss, thicknesses, and brand, but were all considered high oxygen barriers. As seen in Figures VII-1a and VII-1b, the lifetime and beta values were identical within error for all experimental trials. Bags 2 and 4 were chosen as the vacuum bags for the fiber optic experiments. Bag 2, the 3 mil Safe Handling pouch (Koch Equipment, Kansas City, MO), is widely used in the meat industry, and bag 4 (standard Food Saver Bag) has air release channels allowing for a tighter seal, hence less residual oxygen, on the particular vacuum sealer model used. For the vacuum sealed sausage samples, trials 1 and 2 used the Safe Handling bags and trial 3 used the Food Saver bags.

Figures VII-2a, VII-2b, and VII-2c show the lifetime values (as individual trials) over time. All data were collected at ambient conditions. Figure VII-2a mimics a sausage that would be sold in a retail case with no further barrier to the environment. The average shelf life for fresh sausages in this class is 3-5 days. A sharp increase in lifetime values at day 11 was observed. This was also when the sausage casings became noticeably dried out and off odors (presumably from microbial spoilage by *pseudomonas* spp.) were evident. There was no significant difference between the three trials, and the experiment was stopped after 15 days due to microbial concerns. The lifetimes for a sausage vacuum sealed and stored under refrigeration as a function of time are shown in Figure VII-2b. Days 1 and 3 were considerably lower than the next 47 days for all three trials, which remained constant (within error) at 0.27-0.30 ms. The lower lifetimes at days 1 and 3 were attributed to residual oxygen in the package. Oxygen levels were most likely reduced after day 3 through reactions with the meat mixture such as lipid oxidation

or binding to myoglobin (Gill and Jones, 1994), or oxygen being consumed by aerobic microorganisms (Gill and Mcginnis, 1995).

The data for the vacuum sealed frozen sausages varied considerably between trials, most likely due to the significant condensation on the frozen sausage/bag and the subsequent build-up of ice crystals between the sausage and packaging film while testing at room temperature. The lifetime values increased in a somewhat linear fashion from days 1-25 for trials 1 and 3, and then trial 1 plateaued at ~0.35 ms, while trial 3 displayed a sharp decrease, and then leveled off at ~0.31 ms. Trial 3 then increased in a step-like manor leveling off at days 11-21 and 25-40. The initial higher lifetime values for trial 3 was an effect of the food saver bag having air channels allowing for a tighter seal (less oxygen in the package and thus less quenching of the excited triplet state due to oxygen). It is assumed that if the testing conditions were under controlled temperature and humidity, these trials would have been much more consistent. Another possible explanation for the decreases in lifetime values could be that the package was structurally damaged allowing additional oxygen to enter and quench the excited triplet state. Since the lifetime values increased again after the plateaus, it is unlikely that this is the case, because lipid oxidation and microbial growth, which compete for the oxygen (increasing the lifetime), are not overly active at 0°C. Figure VII-3 shows the averaged lifetimes for the three trials as a function of time. It is evident that Ery B is very sensitive to packaging and storage conditions, and the significantly larger error bars for the frozen samples show that this experimental procedure needs to be improved.

Beta values for the fresh sausage are shown in Figure VII-4a. The three trials are the same within error. The values are relatively constant until day 9 when an increase is

observed. Day 9 was also when we saw the lifetime values increase, and this may be a reflection of microbial growth and the drying of the casing. β values for the vacuum sealed sausages stored under refrigeration were essentially indistinguishable from days 3-50, displaying the reproducibility of the method (Figure VII-4b). Similar to the lifetime data, day 1 was considerably lower than the rest of the data, and this is probably related to residual oxygen within the package. The β values for the frozen sausage samples followed a very similar trend as observed in the lifetimes for each trial. We can conclude that these transitions within this data set are also an effect of condensation on the outer package and the formation of ice crystals between the sausage and the package. The overall trend observed was an increase in β initially, indicating that the casings are becoming less heterogeneous, and then a leveling off of β. Previous matrices showed lower β values as casings aged, and this increase may be attributed to a reduction in available oxygen that interacts with the casing matrix. Figure VII-5 displays the averaged beta values for the three storage conditions. After 10 days, the frozen samples had the highest beta values which leveled off at ~0.73. The fresh vacuum sealed sausage casings were relatively unchanged from days 3-50 at ~0.69. The fresh unsealed sausages had considerably lower beta values (~0.50-0.58 for days 1-15) correlating to a more heterogeneous casing. Additionally, as the casing aged (or dried in this case) the β values increased.

Discussion, Conclusions, and Future Works

The ability to directly test food products in a noninvasive manner through packaging material would be a huge breakthrough in the food industry. We have successfully developed a safe, nontoxic, and affordable method for the determination of

rigidity, heterogeneity, and oxygen quenching (within the package) in actual sausage products via the Ery B doped collagen casings under ambient light conditions. The method could be used to monitor oxygen content within food packaging (with Ery B serving as the oxygen sensor) by setting up a standard curve with known oxygen contents and correlating lifetime values similar to the methods proposed by O'Mahony et al. (2006), O'Mahony et al. (2004), O'Riordan et al. (2005), Smiddy et al. (2002a), and Smiddy et al. (2002b).

Fresh sausages stuffed into Ery B doped casings showed drastic differences in lifetime and beta values between the packaging and storage conditions. Different oxygen concentrations within each of the different trials, and also oxygen's interactions with the casing in various packaging systems could account for the differences. The residual oxygen in these packages may be due to a number of factors such as the oxygen permeability of the packaging material, the ability of the food product to trap air, a poor seal, or the incomplete evacuation of the air when sealing under vacuum (as reviewed by Papkovsky et al. (2002)). The fresh unsealed sausages had considerably lower lifetimes when compared to the vacuum sealed trials. This was due to quenching of the excited triplet state by oxygen in the ambient air. The sudden increase in lifetime values at day 9 was probably an effect of the significant drying of the casing, yielding a more rigid environment. On day 9 we also observed increased microbial growth (as indicated by odors and a slimy surface). Microbial growth would lower oxygen concentrations (O'Mahony et al., 2006; O'Mahony et al., 2004), and therefore, increase lifetimes in sealed packages. Since this sample was open to ambient conditions, it is assumed that the casing drying was responsible for the increased lifetime. The vacuum sealed sausages

stored under refrigeration had constant lifetimes and beta values after day 3. This leveling off is most likely a result of equilibrium being reached between oxygen in the package and the available oxygen consumed by microorganisms (O'Mahony et al., 2006; O'Mahony et al., 2004) or bound to proteins in the casing/sausage (Gill and Jones, 1994). Gill (1996) found that in packages where oxygen is permeating slowly, muscle tissue can act as an oxygen scavenger to maintain a very low oxygen tension at the meat surface. Lifetimes and beta values also leveled off at day 26 in the frozen samples, although with noticeably larger errors. The most likely explanation for the longer time required to reach equilibrium was that under frozen conditions the rates of microbial growth and lipid oxidation (processes scavenging available oxygen) are greatly reduced. This information is very important to the food industry, because any drastic changes in product rigidity or heterogeneity would most likely correlate with product deterioration. These parameters will be studied in great detail in the years to come, hoping to make a definite correlation between these analytical measurements and the chemical and biological processes responsible for reducing the shelf-life of food products.

Future applications will focus on the development of an experimental testing chamber where the relative humidity and temperature can be controlled. We will also control oxygen concentration, thus allowing us to monitor oxygen permeability through the casing in the non-packaged sausages. The biggest hurdle in the initial experiments resulted from condensation and ice crystal formation on the frozen samples when tested at room temperature. This would be eliminated through the development of a controlled testing chamber. The sensitivity of lifetime measurements to temperature has been

demonstrated in many protein-based matrices in our lab, and it is essential to control the experimental conditions with more precision.

We would also like to work with Ocean Optics (Dunedin, FL) to test this procedure with their hand-held spectrophotometers making this technique applicable to in-line testing in the food industry. Ocean Optics currently sells oxygen patches, which are integrated into food and beverage packaging. When used with a blue LED fluorometer, the oxygen amount can be quantativly reported. Ery B could easily be developed as a non-invasive oxygen sensor for use within food packaging by calibrating the Ery B emission shift or lifetimes with known oxygen concentrations (measured via a commercial headspace analyzer). This phosphorescent technique, taking mere seconds, would allow instant quality control measures indicating if a package was leaking due to a faulty seal or damage during distribution. We also hope to correlate our phosphorescence data to actual degradative reactions (lipid oxidation, color changes, off odors) and deterioration due to microbial growth, which limit the shelf life of food products. Lipid oxidation (O'Mahony et al., 2004; Smiddy et al., 2002a; Smiddy et al., 2002b) and microbial growth (O'Mahony et al., 2006; O'Mahony et al., 2004) have already been correlated to oxygen concentrations within food packaging using platinum (II) complexes of octaethylporphine-ketone oxygen sensors. Ery B embedded into the food product could provide oxygen concentration data within the package along with information about the conditions of the actual food product (rigidity and heterogeneity). This technique has already hinted towards the effectiveness of Ery B as an oxygen sensor in food packaging, and further tests could validate this technique by testing packages with known oxygen concentrations and correlating this to lifetime values. This continuous

non-destructive assessment of the internal environment of a food package and the food itself will provide a more realistic approach to shelf life stabilities of oxygen sensitive foods.

Chapter 7 Figures

Figure VII-1: Standardization of the fiber optic coupler. A dried casing sample was tested in the following ways: standard fluorescence cuvette inside the sample holder, external fiber optic, and with the fiber optic while in 4 different polyethylene vacuum bags. See text for bag details. Lifetime values are shown in Figure VII-1a and beta values in VII-1b.
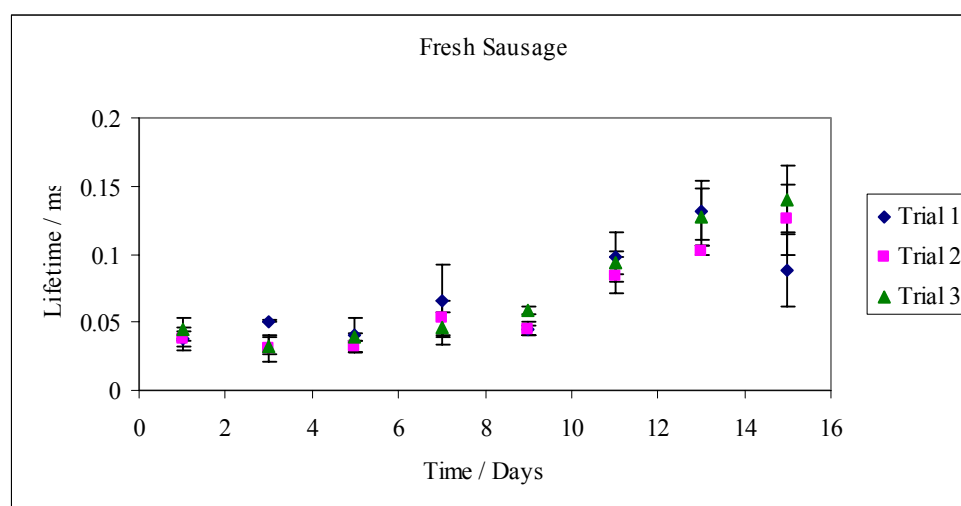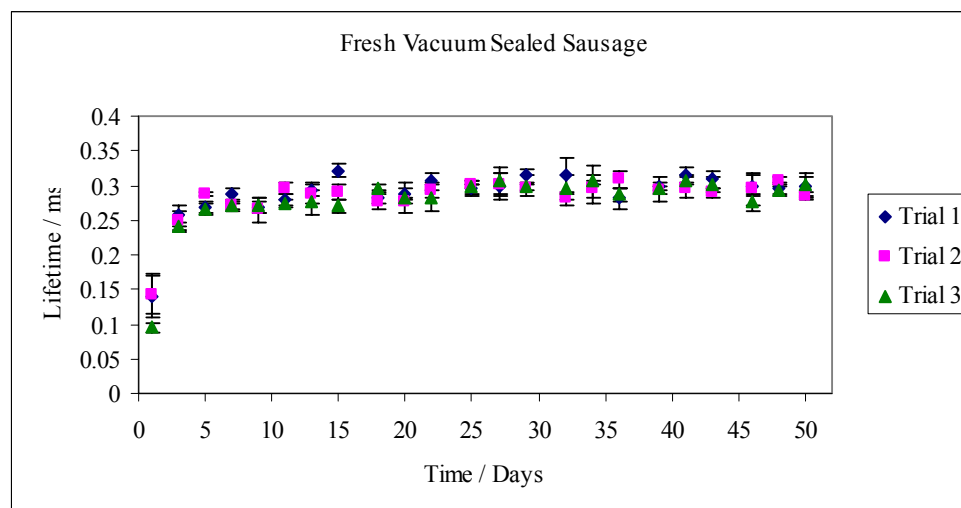
a)
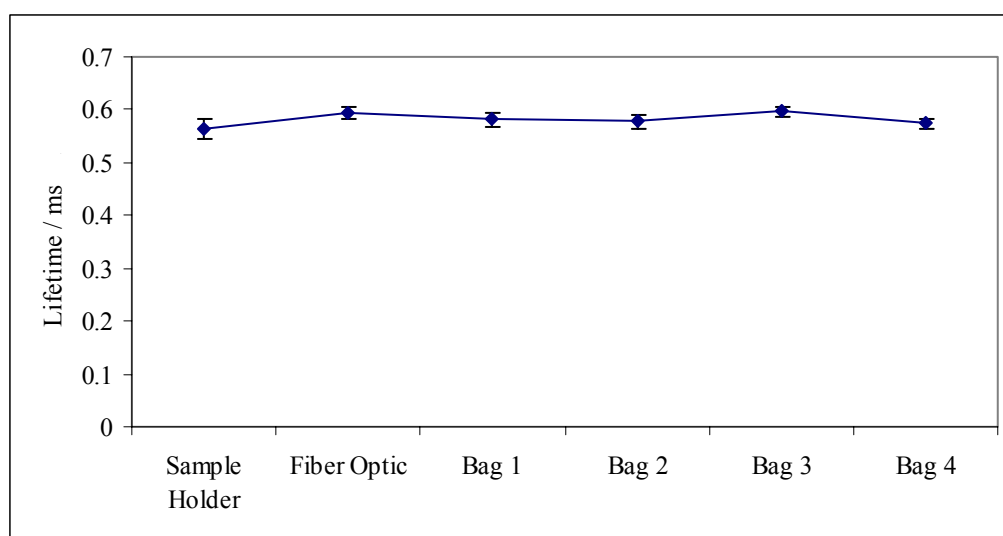
b)
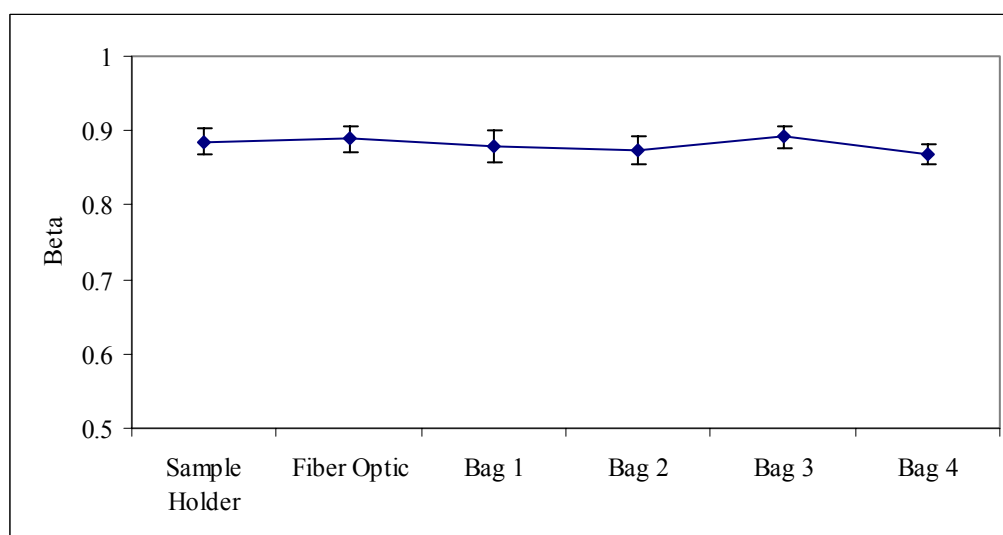
Figure VII-2: Lifetime values for sausages stuffed into Ery B doped collagen casings. Each data point is the average of three measurements, and under each storage parameter, three trials were tested. Figure VII-2a represents the fresh sausages with no further packaging, Figure VII-2b the fresh sausages vacuum sealed and stored under refrigeration, and Figure VII-2c the frozen vacuum sealed sausages.
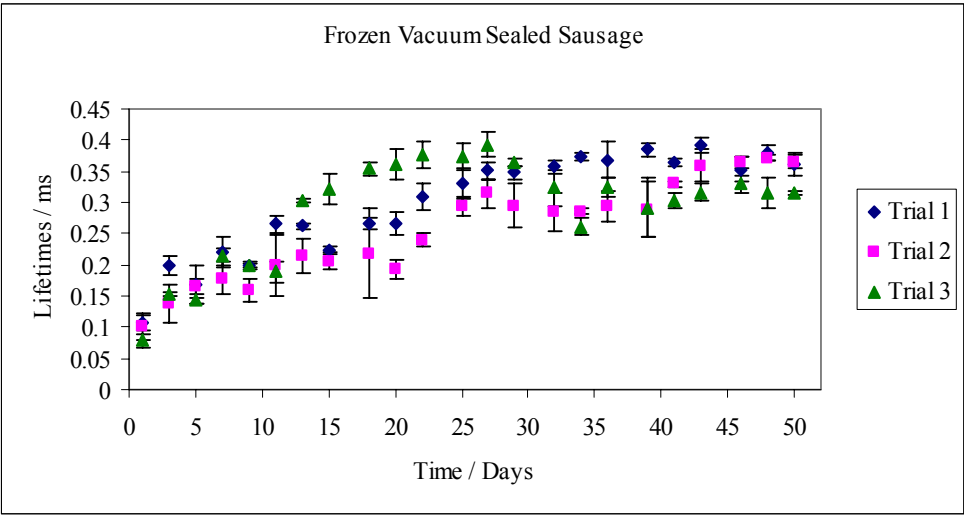
a)

b)

c)

Frozen Vacuum Sealed Sausage

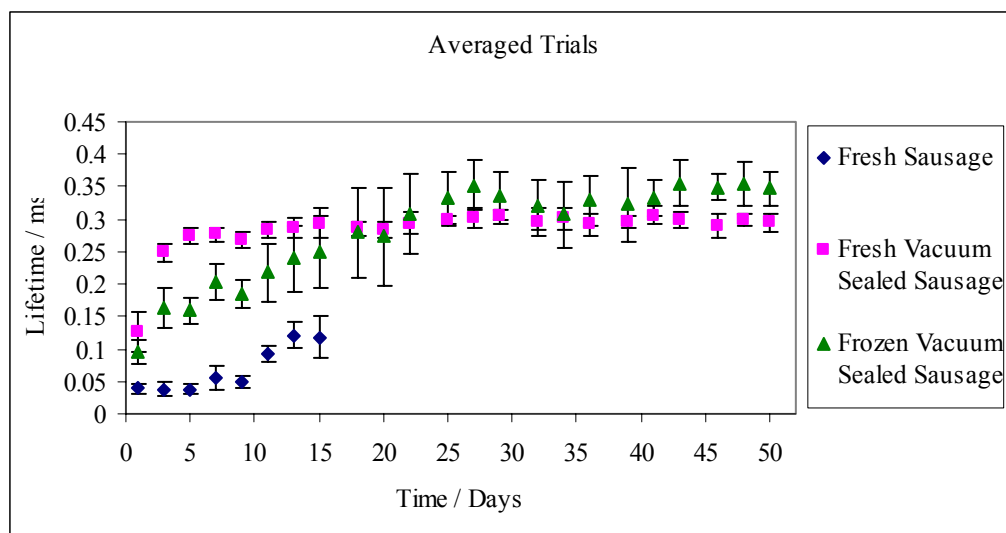Figure VII-3: Averaged lifetime values for each of the storage conditions. For each data point n=9.

Figure VII-4: Beta values for sausages stuffed into Ery B doped collagen casings. Each data point is the average of three measurements, and under each storage parameter, three trials were tested. Figure VII-4a represents the fresh sausages with no further packaging, Figure VII-4b the fresh sausages vacuum sealed and stored under refrigeration, and Figure VII-4c the frozen vacuum sealed sausages.
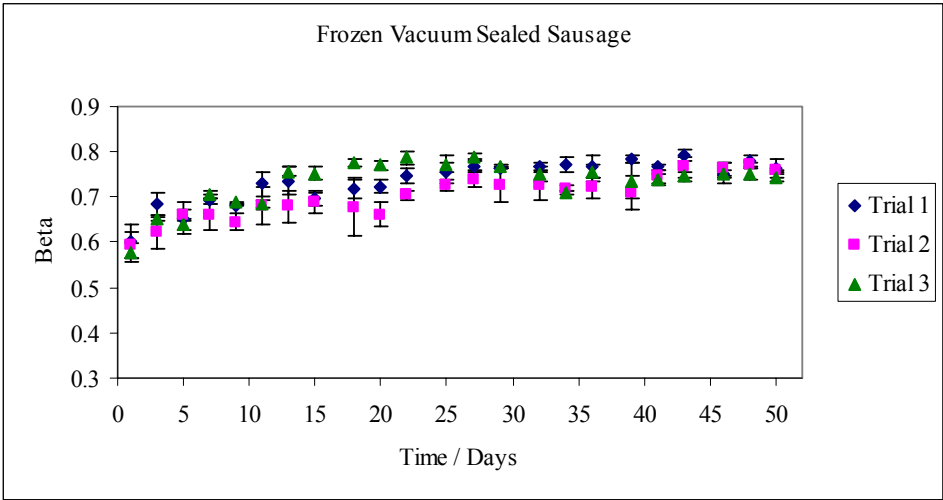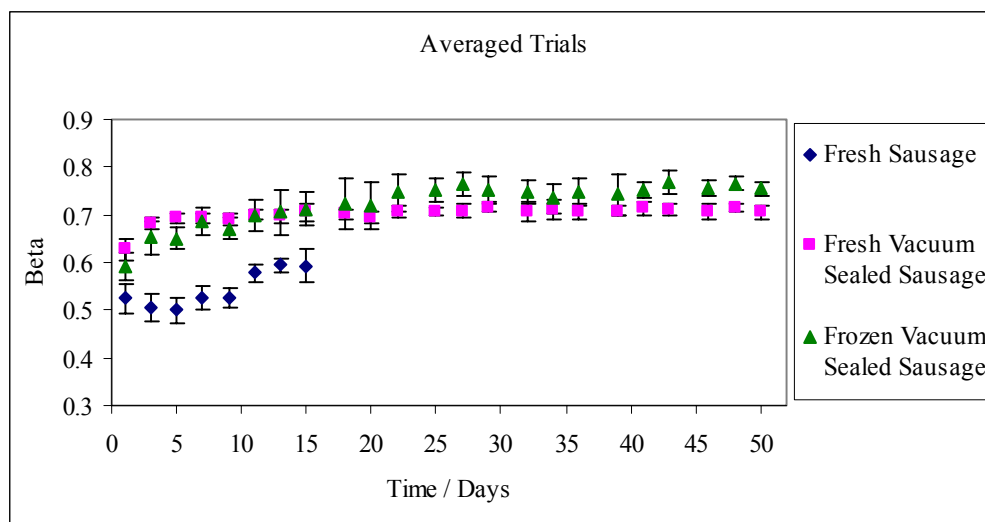
a)

b)

c)

Frozen Vacuum Sealed Sausage
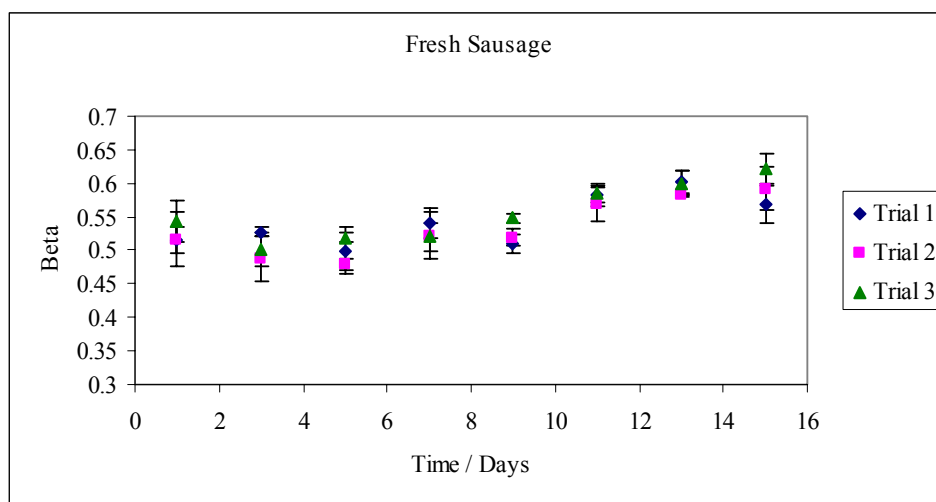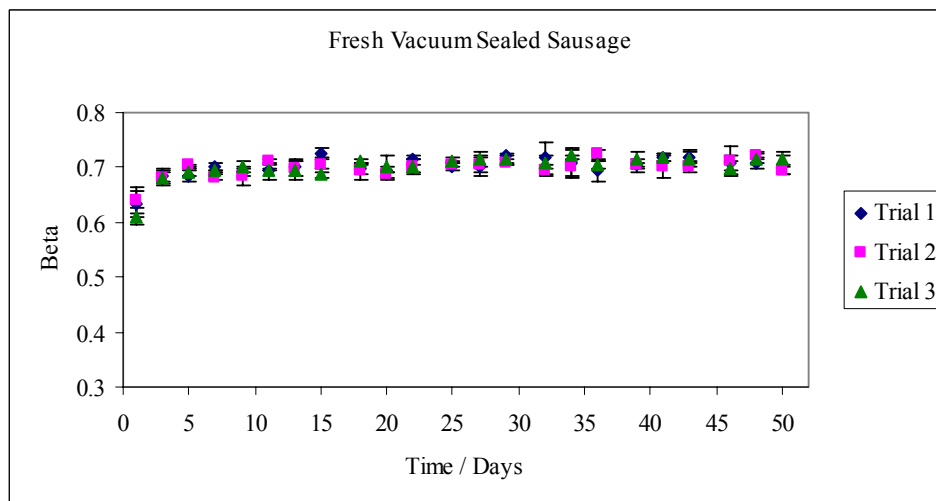
Figure VII-5: Averaged beta values for each of the storage conditions. For each data point n=9.

Chapter 7 References

Canabate-Diaz, B., Carretero, A. S., Cruces-Blanco, C., and Fernandez-Gutierrez, A. (2003). Determination of the amino acid tryptophan and the biogenic amine tryptamine in foods by the heavy atom induced-room temperature phosphorescence methodology. *Analyst* **128**, 411-415.

Champion, D., Le Meste, M., and Simatos, D. (2000). Towards an improved understanding of glass transition and relaxations in foods: molecular mobility in the glass transition range. *Trends in Food Science & Technology* **11**, 41-55.

Chen, R. (2003). Apparent stretched-exponential luminescence decay in crystalline solids. *Journal of Luminescence* **102-103**, 510-518.

Cutter, C. N. (2002). Microbial control by packaging: A review. *Critical Reviews in Food Science and Nutrition* **42**, 151-161.

FDA (2002). Part 74- Listing of Color Additives Subject to Certification. Food and Drug Administration.

Fitzgerald, M., Papkovsky, D. B., Smiddy, M., Kerry, J. P., O'Sullivan, C. K., Buckley, D. J., and Guilbault, G. G. (2001). Nondestructive monitoring of oxygen profiles in packaged foods using phase-fluorimetric oxygen sensor. *Journal of Food Science* **66**, 105-110.

Gill, C. O. (1996). Extending the storage life of raw chilled meats. *Meat Science* **43**, S99-S109.

Gill, C. O., and Jones, T. (1994). The Display of Retail Packs of Ground-Beef after Their Storage in Master Packages under Various Atmospheres. *Meat Science* **37**, 281-295.

Gill, C. O., and Mcginnis, J. C. (1995). The Use of Oxygen Scavengers to Prevent the Transient Discoloration of Ground-Beef Packaged under Controlled, Oxygen-Depleted Atmospheres. *Meat Science* **41**, 19-27.

Lam, S. K., Chan, M. A., and Lo, D. (2001). Characterization of phosphorescence oxygen sensor based on erythrosin B in sol-gel silica in wide pressure and temperature ranges. *Sensors and Actuators B: Chemical* **73**, 135-141.

Lee, K. C. B., Siegel, J., Webb, S. E. D., Leveque-Fort, S., Cole, M. J., Jones, R., Dowling, K., Lever, M. J., and French, P. M. W. (2001). Application of the Stretched Exponential Function to Fluorescence Lifetime Imaging. *Biophys. J.* **81**, 1265-1274.

Lesch, H., Schlichter, J., Friedrich, J., and Vanderkooi, J. M. (2004). Molecular Probes: What Is the Range of Their Interaction with the Environment? *Biophys. J.* **86**, 467-472.

Nack, T. J., and Ludescher, R. D. (2006). Molecular mobility and oxygen permeability in amorphous bovine serum albumin films. *Food Biophysics* **1**, 151-162.

O'Mahony, F. C., O'Riordan, T. C., Papkovskaia, N., Kerry, J. P., and Papkovsky, D. B. (2006). Non-destructive assessment of oxygen levels in industrial modified atmosphere packaged cheddar cheese. *Food Control* **17**, 286-292.

O'Mahony, F. C., O'Riordan, T. C., Papkovskaia, N., Ogurtsov, V. I., Kerry, J. P., and Papkovsky, D. B. (2004). Assessment of oxygen levels in convenience-style muscle-based Sous Vide products through optical means and impact on shelf-life stability. *Packaging Technology and Science* **17**, 225-234.

O'Riordan, T. C., Voraberger, H., Kerry, J. P., and Papkovsky, D. B. (2005). Study of migration of active components of phosphorescent oxygen sensors for food packaging applications. *Analytica Chimica Acta* **530**, 135-141.

Papkovsky, D. B., Ponomarev, G. V., Trettnak, W., and Oleary, P. (1995). Phosphorescent Complexes of Porphyrin Ketones - Optical-Properties and Application to Oxygen Sensing. *Analytical Chemistry* **67**, 4112-4117.

Papkovsky, D. B., Smiddy, M. A., Papkovskaia, N. Y., and Kerry, J. P. (2002). Nondestructive measurement of oxygen in modified atmosphere packaged hams using a phase-fluorimetric sensor system. *Journal of Food Science* **67**, 3164-3169.

Pravinata, L. C., You, Y., and Ludescher, R. D. (2005). Erythrosin B Phosphorescence Monitors Molecular Mobility and Dynamic Site Heterogeneity in Amorphous Sucrose. *Biophys. J.* **88**, 3551-3561.

Richert, R. (1997). Evidence for dynamic heterogeneity near Tg from the time-resolved inhomogeneous broadening of optical line shapes. *Journal of Physical Chemistry B* **101**, 6323-6326.

Richert, R., and Heuer, A. (1997). Rate-memory and dynamic heterogeneity of first-order reactions in a polymer matrix. *Macromolecules* **30**, 4038-4041.

Shah, N. K., and Ludescher, R. D. (1995). Phosphorescence Probes of the Glassy State in Amorphous Sucrose. *Biotechnology Progress* **11**, 540-544.

Slavic, J. (1994). "Fluorescent probes in cellular and molecular biology," CRC Press, Inc., Boca Raton.

Smiddy, M., Fitzgerald, M., Kerry, J. P., Papkovsky, D. B., O'Sullivan, C. K., and Guilbault, G. G. (2002a). Use of oxygen sensors to non-destructively measure the oxygen content in modified atmosphere and vacuum packed beef: impact of oxygen content on lipid oxidation. *Meat Science* **61**, 285-290.

Smiddy, M., Papkovskaia, N., Papkovsky, D. B., and Kerry, J. P. (2002b). Use of oxygen sensors for the non-destructive measurement of the oxygen content in modified atmosphere and vacuum packs of cooked chicken patties; impact of oxygen content on lipid oxidation. *Food Research International* **35**, 577-584.

Strambini, G. B., and Gonnelli, M. (1985). The indole nucleus triplet-state lifetime and its dependence on solvent microviscosity. *Chemical Physics Letters* **115**, 196-200.

Sundaresan, K. V., and Ludescher, R. D. (2007). Molecular mobility and oxygen permeability in amorphous Beta-lactoglobulin films. *Food Hydrocolloids* **In Press**.

You, Y. M., and Ludescher, R. D. (2006). Phosphorescence of erythrosin B as a robust probe of molecular mobility in amorphous solid sucrose. *Applied Spectroscopy* **60**, 813-819.

CURRICULUM VITA

Thomas J. Nack

Education
University of Wisconsin, Stevens Point
Major: Environmental Engineering
September 1998-May 2000
Degree: N/A

University of Wisconsin, Madison
Major: Food Science
September 2000-May 2003
Degree: BS, Food Science, May 2003

Rutgers, The State University of New Jersey
September 2003-December 2007
Major: Food Science with an emphasis in Protein Chemistry
Degree: Ph.D., Food Science, January 2008

Occupations held between the conferral of the baccalaureate and doctorate
Con Agra Foods, Downers Grove, IL
Summer Intern
May 2003-August 2003

Publications
Nack, T.J., Ewoldt, K.A., Ingham, S.C. (2002) "Potential use of Staphylococci as indicators of post-heating contamination of hot smoked fish." *Dairy, Food & Environmental Sanitation.* 22(7) 526-533.

Nack, Thomas J. & Ludescher, Richard D. (2006) "Molecular Mobility and Oxygen Permeability in Amorphous Bovine Serum Albumin Films." *Food Biophysics*. 1 (3) 151-162.